Fluctuations in Perceptual Decisions

Cortical microcircuit dynamics mediating alternations in conscious visual perception

Panagiota Theodoni

TESI DOCTORAL UPF / 2014

Director de la tesi

Prof. Dr. Dr. phil. Dr. rer.nat.habil Gustavo Deco
Department of Information and Communication Technologies

Barcelona, March 2014

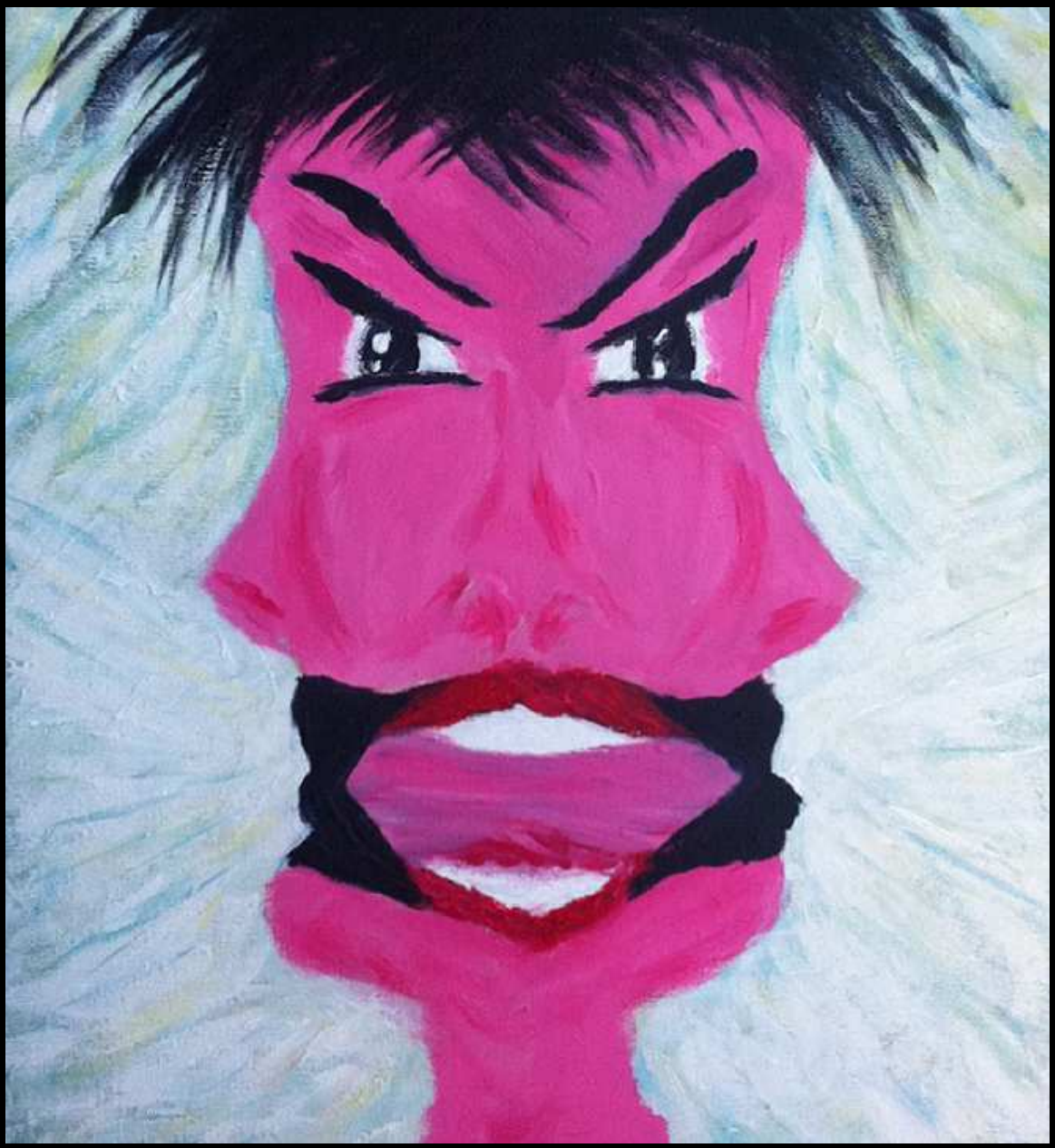

Fluctuations in Perceptual Decisions

Inspired at the dawn of the current global financial and social crisis, the cover image exhibits the perceptual ambiguity between altruism and egoism. Egoism is represented by two separate faces, while altruism by their union. It symbolizes that solidarity is the only way out of this crisis.

στους πολυαγαπημένους μου γονείς,
Γεώργιο & Μαρία Θεοδώνη

J'ai toujours pensé que le monde est comme mes rêves,
où je peux voler, changer la realité
et c'est comme ça que je veux continuer à rêver

Acknowledgements

Since my studies in physics I was curious about how the brain works. I am, therefore, deeply grateful to my Ph.D. supervisor Gustavo Deco for introducing me into the world of neuroscience, as well as for his constant support, both scientific and personal, during this exciting journey.

My special thanks to Nikos K. Logothetis, Rubén Moreno-Bote and Nava Rubin for constituting the Ph.D. committee of the current thesis, as well as to their substitutes Jaime de la Rocha and Albert Compte for their interest.

I am very happy to have had the opportunity to collaborate with Theofanis I. Panagiotaropoulos, Vishal Kapoor, Nikos K. Logothetis, Guyla Kovács, and Mark W. Greenlee.

I consider myself fortunate to have met and enjoyed inspiring discussions with many researchers, not only in Barcelona, but also during my multiple lab visits, summer courses, and conferences. Throughout this Ph.D. journey I honestly met many extraordinary people who enriched it. I am also very happy to have been a member of the CODDE family, as I used to call the Marie Curie training network Coordination for Optimal Decisions in Dynamic Environments, of which I formed part as an early stage researcher. I had great time in each of our meetings.

My special thanks also to Xiao-Jing Wang and Haim Sompolinsky for the inspiring and fruitful discussions while they supervised the projects I worked on, in the Computational and Cognitive Neurobiology, and Methods in Computational Neuroscience summer course, respectively. I am grateful to my former Professor Efstratios Manousakis for the inspiring conversations, his precious advices, and for his support through recommendation letters. I thank Pascal Mamassian for introducing me into the design of

psychophysical experiments during my visit at his lab, as well as Rainer Goebel for inviting me to attend one of his courses. I also thank Rainer Goebel, Christian Keysers, Pierre Kornprobst, Olivier Faugeras, and Biyu Jade He for inviting me to their labs to give a talk and discuss possible future collaborations. Finally, I thank Alex Roxin for giving me the opportunity to continue this exciting journey as postdoc in his lab.

I want to thank all my friends in Barcelona -specially Larissa, Joana, Marina, Adrian, Mario, Ernest, Miguel, Tristan, Andrea, Laura, Tim, Pedro, Johan, Andres, Etienne, Murat, Rikkert, Mohit, Gorka, Bea, Katha, Romain, Adrià, Ruggero, Nils from the lab, and Anna, Chiara, Deniz, Karla, Gabriela, Arguiris, Eric, Belén, Nikos, Elena outside the lab- for supporting me in difficult times and for making this journey even more pleasant, as well as my family and my best friends in Greece Eirini, Stavroula, Christos, Avgoustinos for being always there for me, despite my long disappearances.

Last, but not least, I couldn't avoid mentioning the difficult times large populations of people have gone through the last years, and are still going through today, due to the ongoing crisis. I am grateful to all those people -the antifascists all over the world- who maintain dreams alive with their solidarity, and creativity.

yotta

Abstract

Fluctuations in perceptual decisions emerge when our brain confronts with ambiguous sensory stimuli. For instance, our perception alternates between two conflicting images when presented dichoptically to our eyes, allowing a dissociation of the sensory stimulation from the conscious visual perception, and therefore providing a gateway to consciousness. How does the brain work when it deals with such ambiguous sensory stimuli? We addressed this question theoretically by employing a biophysically realistic attractor network, by consistently reducing it to a four-variable rate- based model, and by extracting analytical expressions for second- order statistics. We considered human behavioral and macaque neurophysiological data collected when subjects were confronting with such ambiguities. Our results show the relevance of neuronal adaptation in perceptual decision making, as well as that it contributes to the speed- accuracy trade- off. Furthermore, our findings affirm that both noise and neural adaptation operate in balance during the fluctuating states of visual awareness and suggest that while adaptation in inhibition is not relevant for the perceptual alternations, it contributes to the brain dynamics at rest. Finally, we explain the observed neuronal noise- decorrelation during visual consciousness and provide insights on the long-standing question: where in the brain rivalry is resolved.

Resum

Les fluctuacions en les decisions perceptives sorgeixen quan el nostre cervell s'enfronta a estímuls sensorials ambigus. Per exemple, la nostra percepció alterna entre dues imatges contradictòries quan es presenten de forma dicòptica als nostres ulls, cosa que permet una dissociació de l'estimulació sensorial de la percepció visual conscient, i per tant proporciona una porta d'entrada a la consciència. Com funciona el cervell quan es tracta d'aquest tipus d'estímuls sensorials ambigus? Hem tractat aquesta qüestió de forma teòrica mitjançant l'ús d'una xarxa d'atractors biofísicament realista, reduint-la de forma consistent a un model de quatre variables basat en la freqüència, i extraient expressions analítiques pels estadístics de segon ordre. Hem emprat dades neurofisiològiques de comportament d'humans i macacos recollides quan els subjectes s'enfrontaven a aquest tipus d'ambigüitats. Els nostres resultats mostren la importància de l'adaptació neuronal en la presa de decisions perceptives i mostren la seva contribució a l'equilibri velocitat-precisió. D'altra banda, els nostres resultats confirmen que tant el soroll com l'adaptació neural operen en equilibri durant els estats fluctuants de consciència visual i suggereixen que, si bé l'adaptació en la inhibició no és rellevant per a les alternances de percepció, contribueix a la dinàmica del cervell en repòs. Finalment, expliquem la decorrelació del soroll neuronal observada durant la consciència visual i proporcionem noves idees en relació a l'antiga qüestió de en quin lloc del cervell es resol la rivalitat visual.

Contents

Abstract vii

Resum ix

List of figures xiii

List of tables xiv

1 Introduction
1.1 Multistable perception 2
1.2 Experimental paradigms 3
1.3 Temporal dynamics of multistable perception 8
1.4 Neural correlates of subjective visual perception 12
1.5 Outline of the thesis 16

2 Theoretical basis of multistable perception
2.1 Introduction 17
2.2 Biophysically plausible spiking model 20
2.3 Consistently derived rate model 28
2.4 Analytical expressions for second- order statistics 42

3 Microcircuit dynamics mediating binocular rivalry
3.1 Introduction 53
3.2 Methods 55
3.2.1 Experimental paradigm & results 55
3.2.2 Model description 56
3.3 Results 56
3.3.1 Spike- frequency adaptation to all neurons of the network 57
a. Bifurcation diagrams 57
b. Replicating experimental data 59
3.3.2 Spike- frequency adaptation only to excitatory pyramidal neurons of the network 63
a. Bifurcation diagrams 63
b. Replicating experimental data 65
3.3.3 Levelt's second revised and fourth proposition 68
3.4 Discussion 71

4 Neuronal adaptation effects in decision- making
4.1 Introduction 75
4.2 Methods 76
4.2.1 Experimental paradigm & results 76
4.2.2 Model description 78
4.2.3 Stimulation protocols 79
4.3 Results 85
4.3.1 Model analysis: bifurcation diagrams 88
4.3.2 Simulations in comparison with psychophysical data 90
4.3.3 Parameter search supporting the results 92
4.3.4 Decision making and decision certainty 94
4.4 Discussion 99

5 Noise- decorrelation during visual consciousness
5.1 Introduction 105
5.2 Methods 107
5.2.1 Experimental paradigm & results 108
5.2.2 Model description 111
5.2.3 Stimulation protocols 113
5.3 Results 116
5.3.1 A mechanistic analysis underlying the experimental noise- correlations 116
5.3.2 What provokes the noise- correlation reduction in BFS of the dominant neural ensemble? 119
5.3.3 What provokes the noise- correlation stability in BFS of the suppressed neural ensemble? 121
5.3.4 Analysis with the moments method 123
5.4 Discussion 129

General Discussion 133

Bibliografia 145

List of Abbreviations 173

List of figures

Fig. 1.1 Ambiguous figures in Art 3
Fig. 1.2 Ambiguous figures, monocular rivalry & structure- from- motion 4
Fig. 1.3 Binocular rivalry 5
Fig. 1.4 Binocular flash suppression, physical alternation, generalized flash suppression & motion- induced blindness 6
Fig. 1.5 High-level Adaptation-related aftereffects with ambiguous stimuli 7
Fig. 1.6 Intermittent presentation 7
Fig. 1.7 Tristable perception, auditory, tactile, olfactory & verbal rivalry .. 8
Fig. 1.8 Distribution of dominance durations 10
Fig. 1.9 Singe-cell recordings during rivalry 13
Fig. 1.10 Human & non-human primate brain 15

Fig. 2.1 Architecture of the biophysically plausible spiking network 21
Fig. 2.2 Consistently derived rate model 28
Fig. 2.3 Mean firing rate of the non- selective population 32
Fig. 2.4 Input – output function of an interneuron 35
Fig. 2.5 Mean gating variable Ca_I 36
Fig. 2.6 Input – output function of one selective population 42
Fig. 2.7 Augmented method of moments: network descripition 43
Fig. 2.8 Input and transfer function 48
Fig. 2.9 Mean firing rate and adaptation 48
Fig. 2.10 Mean firing rate and adaptation variances 48
Fig. 2.11 Mean covariance between pairs of neurons within and across ensembles for the activity and adaptation variables 49
Fig. 2.12 Comparison of analytical results with direct simulations 51

Fig. 3.1 Spike- frequency adaptation to all neurons of the network 58
Fig. 3.2 Spike- frequency adaptation to all neurons of the network: Replicating the experimental data (1) 60
Fig. 3.3 Spike- frequency adaptation to all neurons of the network: Replicating the experimental data (2) 62
Fig. 3.4 Spike- frequency adaptation only to the excitatory pyramidal neurons of the network. 64
Fig. 3.5 Spike- frequency adaptation only to the excitatory pyramidal neurons of the network: Replicating the experimental data 67
Fig. 3.6 Mean time dominance and coefficient of variation as a function of neuronal adaptation 68
Fig. 3.7 Levelt´s propositions 70

Fig. 4.1 Experimental design and behavioral results of the high- level adaptation- related aftereffects task 77
Fig. 4.2 Stimulation protocol: adaptation- related aftereffects 81
Fig. 4.3 Dynamical regimes in the g_{AHP} - w_+ space, in the absence of external stimulus 84

Fig. 4.4 Schematic representation of noise- driven and adaptation- driven landscapes 87
Fig. 4.5 Bifurcation diagram as a function of the level of neuronal adaptation 89
Fig. 4.6 Bifurcation diagram as a function of the external stimulus 90
Fig. 4.7 Replicating the experimental data 91
Fig. 4.8 Parameter search 93
Fig. 4.9 Decision making without preceding adaptor 97
Fig. 4.10 Decision making with and without preceding adaptor 98
Fig. 4.11 Mean dominance time and coefficient of variation for different levels of adaptation 102

Fig. 5.1 Experimental desing 109
Fig. 5.2 Recording stie: Inferior convexity of prefrontal cortex 109
Fig. 5.3 Experimental results 111
Fig. 5.4 Biophysically realistic spiking networks 112
Fig. 5.5 Stimulation protocols: PA & BFS 114
Fig. 5.6 Competition increases noise- correlations 117
Fig. 5.7 Correlated variability in PA & BFS 118
Fig. 5.8 Mean firing rates in PA & BFS 118
Fig. 5.9 BFS followed by BR 119
Fig. 5.10 Decrease of input noise to the dominant population ($\beta' < \beta$) 120
Fig. 5.11 Increase of input noise to the suppressed population ($\beta' > \beta$) 122
Fig. 5.12 Stimulation protocol 124
Fig. 5.13 Network without competition 125
Fig. 5.14 The effect of competition to noise- correlations 126
Fig. 5.15 Network with competition 127
Fig. 5.16 Near the bifurcation 128
Fig. 5.17 Bifurcation points 129

Fig. A. Modeling social decision making 142

List of tables

Table 2.1 Tabular description of the spiking model: summary 25
Table 2.2 Tabular description of the spiking model: population 26
Table 2.3 Tabular description of the spiking model: connectivity 26
Table 2.4 Tabular description of the spiking model: neurons & synapses . 26
Table 2.5 Default values of the fixed parameters of the spiking model 27
Table 2.6 Default values of the free parameters of the spiking model 27

CHAPTER 1

Introduction

ἔτι δὲ καὶ πολλοῖς τῶν ἄλλων ζῴων τἀναντία
[περὶ τῶν αὐτῶν] φαίνεσθαι καὶ ἡμῖν,
καὶ αὐτῷ δὲ ἑκάστῳ πρὸς αὑτὸν
οὐ ταὐτὰ κατὰ τὴν αἴσθησιν ἀεὶ δοκεῖν.
ποῖα οὖν τούτων ἀληθῆ ἢ ψευδῆ, ἄδηλον:
οὐθὲν γὰρ μᾶλλον τάδε ἢ τάδε ἀληθῆ,
ἀλλ᾽ ὁμοίως. διὸ Δημόκριτός
γέ φησιν ἤτοι ο ὐθὲν εἶναι ἀληθὲς
ἢ ἡμῖν γ᾽ ἄδηλον.
Αριστοτέλης, Μεταφυσικά Γ.1009β [1]

The ultimate, still unanswered, human query is the nature of consciousness. Until relatively recently, consciousness was a "forbidden" word in science. How could we study subjectivity objectively? This was the main obstacle, since *objectivation* is a "pillar" of science, although debatable ***(Schrödinger 1967)***. The bridge to this gap came, in the second half of 19th century, from Franz Brentano who suggested three different forms of consciousness: *the consciousness of a primary object (e.g. a human face) presented, for example in an act of seeing, the conscious experience of this act (which represents a secondary object) and the consciousness of the first order mental act (e.g. that we are conscious of the fact that we see a face) (adapted from* ***Panagiotaropoulos & Logothetis 2013)***. We could, therefore, study with rigorous scientific

[1] *And further they say that many of the animals as well get from the same things impressions which are contrary to ours, and that the individual himself does not always think the same in matters of sense-perception. Thus it is uncertain which of these impressions are true or false; for one kind is no more true than another, but equally so. And hence Democritus says that either there is no truth or we cannot discover it.* Aristotle, Metaphysics 4.1009b. ***(Taylor 1999)***

techniques, at least the first form of consciousness. The most prominent way was, and still is, to study phases of perceptual dominance and suppression of an unchangeable sensory stimulus, usually visual. While, many behavioural studies were held, almost a century later the first experimental study of neural correlates of subjective visual perception was presented ***(Logothetis & Schall 1989)***, and a year later this methodological approach was supported by Crick and Koch ***(Crick & Koch 1990)***.

Successive phases of perceptual dominance and suppression of an unchanged sensory stimulus form the so called multistable perception (MP). In the current thesis we study its underlying neural mechanisms, via theoretical / computational investigation driven by different types of experimental data, employing numerical and analytical tools, models based on known neuronal properties.

In the following paragraphs of this chapter, we introduce multistable perception (§1.1), along with its most common, and the ones we consider in the current thesis, experimental paradigms (§1.2), as well as outcomes from macroscopic (§1.3), mesoscopic and microscopic studies (§1.4). Finally, the outline of the current thesis is presented (§1.5).

1.1 Multistable perception

Multistable perception is thought to be a gateway to visual consciousness because it dissociates perception from sensory stimulus. The first signs that humans were aware of this phenomenon have been found in art from the classical period in ancient Greece (Figure 1.1A). Reappeared in Renaissance (Figure 1.1B), and later (Figures 1.1C,D).

Here, we focus in one paradigm of multistable perception: Perceptual bistability (or else bistable perception (BP)). Perceptual bistability emerges when an ambiguous stimulus, usually visual, under continuous constant stimulation is perceived as the alternation of two mutually exclusive perceptual states. While this perceptual phenomenon can emerge with ambiguous figures (Figures 1.1, 1.2) it can also arise when each eye is presented with a different image (Figure 1.3). The latter is called Binocular Rivalry (BR) and was first mentioned by **della Porta**

(**1593**), supported later by **Le Clerc**'s observations (**1712**), but the first clearest early description of BR came from **Du Tour** (**1761**) ***(Wade 1998)***. However, the first systematic study was made by Sir Charles Wheatstone ***(Wheatstone 1838)*** using the, invented by him, mirror stereoscope *(For reviews see* ***Logothetis 1998, 1999, 2006; Blake & Logothetis 2002; Sterzer et al. 2009; Panagiotaropoulos & Logothetis 2013; Panagiotaropoulos et al. 2014*** *and for a full BR bibliography up to 2001 see the one provided online by* ***O'Shea***[2]*)*.

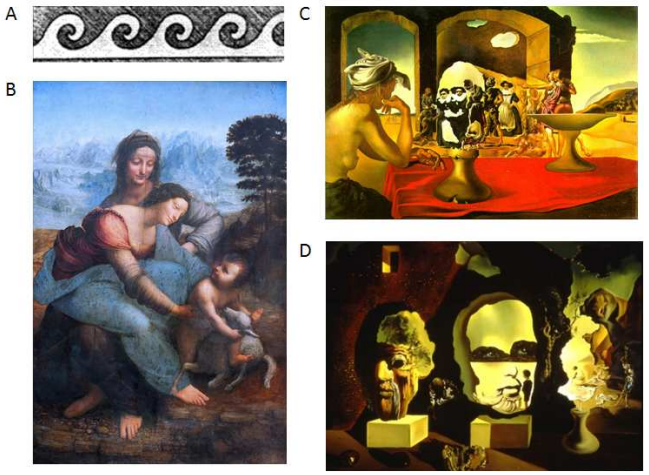

Figure 1.1 Ambiguous figures in Art
A. *The Greek key. A decorative repeated motif appeared in many arquitectural friezes and in bands on the pottery of ancient Greece from Geometric Period onwards. It can be perceived as either a series of white waves or black hanging tentacles* ***B.*** *The Virgin and Child with St. Anne - Leonardo Da Vinci, ~1508. The garment of the Virgin can also be perceived as a vulture* ***C.*** *Slave Market with the Disappearing Bust of Voltaire - Salvador Dalí, 1940. The face of Voltaire can also be perceived as a gathering of people* ***D.*** *Old age, Adolescence, Infancy (The Three Ages) - Salvador Dalí, 1940. The faces of the old, the adolescent and the infant can also be perceived as complex scenes. (Adapted from* ***Panagiotaropoulos & Logothetis 2013*** *(A,B))*

1.2 Experimental paradigms

Ambiguous figures, since the ancient and old times (Figure 1.1), have been a common way to induce perceptual conflict. Some of the most

[2] sites.google.com/site/oshearobertp/publications/binocular-rivalry-bibliography

famous examples are presented in Figure 1.2A-E. When one views each of these images, although the visual sensory stimulus he receives remains unchanged, his perception alternates between its two conflicting interpretations. We find such visual stimuli in many studies of multistable perception. Another way to induce such perceptual alternations is by superimposing patterns of dissimilar colour and orientation, known as monocular rivalry *(**Andrews & Purves 1997**)* (Figure 1.2F,G). In addition, ambiguous stimuli can also be constructed with the structure- from motion imaging technique, where three- dimensional randomly speckled rotating objects are orthographically projected provoking subjective changes in the direction of rotation upon reversal or illusionary depth *(**Wallach et al. 1953**)* (Figure 1.2H), as well as with moving plaids *(**Hupé & Rubin 2003**)* (Figure 1.2I), among others.

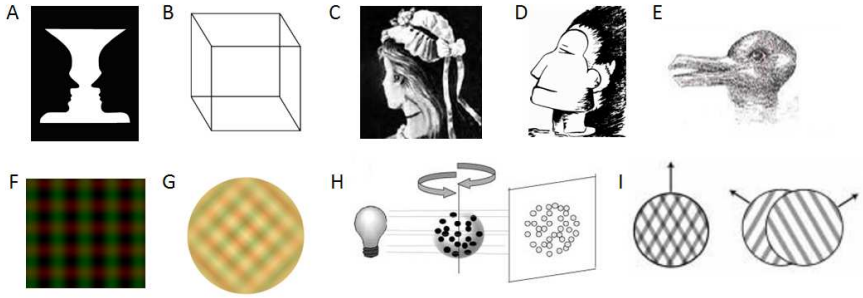

Figure 1.2 Ambiguous figures, monocular rivalry &structure- from- motion
A. *Rubin's face - vase figure (**Rubin 1984**)* ***B.*** *The Necker Cube (**Necker 1832**).* ***C.*** *Old lady - young woman (**Boring 1930**)* ***D.*** *The Indian - Eskimo* ***E.*** *The duck - rabbit (adapted by Weisstein, from the Wolfram MathWorld)* ***F.G*** *Monocular rivalry (MR) figures (adapted from **Maier 2004** (F), and **Blake & Logothetis 2002** (G)* ***H.*** *Structure- from- motion (SFM): The rotating sphere (RS) (adapted from **Maier et al. 2003**)* ***I.*** *Moving plaids (adapted from **Rubin & Hupé 2005**)*

The most extensively studied, though, psychophysical paradigm that generates perceptual alternations is Binocular rivalry. BR occurs when incompatible images are dichoptically presented simultaneously and independently to the two eyes, such as vertical stripes to one eye and horizontal stripes to the other (Figure 1.3). Stereomatching fails *(**Blake & Boothroyd 1985**)* and the observer perceives only one of the two images at a time while the other is suppressed from awareness *(**Levelt 1968; Blake 1989, 2001; Blake & Logothetis 2002**)*. Perception, therefore, alternates between the two visual patterns allowing a dissociation of sensory

stimulation from conscious visual perception. There have been various visual stimuli used in BR, from sinusoidal gratings of different orientations ***(Lee & Blake 1999)***, images of a face and a house ***(Tong et al. 1998)***, as well as geometrical patterns and images of animate objects ***(Sheinberg & Logothetis 1997)***, among others.

Visual stimuli in BR can be presented in different ways: e.g. with goggles of different colours (Figure 1.3A), acting as colour filters; with prism goggles (Figure 1.3B) or with mirror stereoscope (Figure 1.3C) ***(Carmel et al. 2010a)***. Since the invention of the stereoscope by **Sir Charles Wheatstone (1838)**, and his first systematic description of the phenomenon, there has been a plethora of both experimental and theoretical studies**.** In the current thesis, in one of our studies we considered human behavioural data obtained during BR, employing the mirror stereoscope, in order to study the underlying mechanism of PB (Chapter 3).

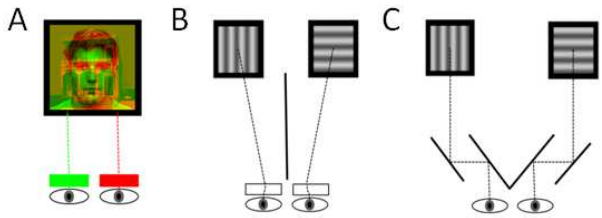

Figure 1.3 Binocular rivalry
A. *Red green goggles* ***B.*** *prism goggles* ***C.*** *mirror stereoscope. (Adapted from* ***Carmel et al. 2010a)***

Reversals in perception can not only be generated spontaneously, but they can also be externally induced. A way to control which of the two conflicting perceptions will arise first to awareness, is Binocular Flash Suppression (BFS) ***(Wolfe 1984; Sheinberg & Logothetis 1997; Kreiman et al. 2002; Keliris et al. 2010; Panagiotaropoulos et al. 2012)*** (Figure 1.4A). In BFS subjects are presented with one image to one eye and after a short time period (of the order of a second) a conflicting image is flashed to the collateral eye. Subjects perceive the new image until it is suppressed and the previous image arises to awareness, i.e. a perceptual reversal occurs. BFS is a common way to find neural correlates of visual awareness when compared to physical alternation (PA), where the same perception emerges without visual competition ***(Keliris et al. 2010;***

Panagiotaropoulos et al. 2012) (Figure 1.4B). In the current thesis, in one of our studies, we consider electrophysiological data from macaque later Prefrontal Cortex (LPFC) obtained during BFS and PA, in order to study the underlying mechanisms of the differences of the noise-correlations of neurons in the dominant and suppressed state in BFS, compared to PA (Chapter 5).

An other way to study perceptual suppression is the Generalized Flash Suppression (GFS) ***(Wilke et al. 2003, 2009; Tsuchiya & Koch 2005)*** (Figures 1.4C,D). In GFS, a salient target stimulus is perceptual suppressed due to a sudden presentation of a surrounding pattern. In addition, when a moving pattern, e.g. a RS, is superimposed on high-contrast stationary or slowly moving stimuli, the latter disappear and reappear alternately for periods of several seconds, a "visual disappearance" phenomenon known as motion induced- blindness (MIB) ***(Bonneh et al. 2001)*** (Figure 1.4E).

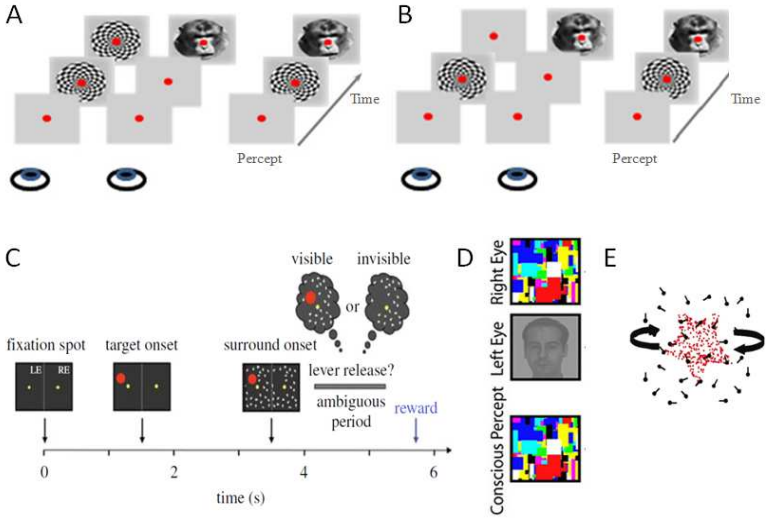

Figure 1.4 Binocular flash suppression, physical alternation, generalized flash suppression & motion induced- blindness
A. *Binocular Flash Suppression (BFS)* ***B.*** *Physical Alternation (PA) (Adapted from* ***Panagiotaropoulos & Logothetis 2013*** *(A,B))* ***C. D.*** *Generalized Flash Suppression (GFS)(adapted from* ***Wilke et al. 2009*** *(A) and* ***Carmel et al. 2010a*** *(B))* ***E.*** *motion induced- blindness (MIB) (adapted from* ***Leopold et al. 2002****)*

A similar to BFS experimental paradigm, yet not the same, is the so called adaptation- related aftereffects. It is known that prolonged exposure of a

complex stimulus, e.g. an image of a face, biases perceptual decisions toward non- adapted dissimilar stimuli ***(Leopold et al. 2001; Webster et al. 2004)***. In a recent study, a similar procedure was followed having as test stimuli ambiguous face/hand composite stimuli ***(Cziraki et al. 2010)*** (Figure 1.5). The behavioral data of this study showed that adaptation to a face or hand stimulus biased the categorization of subsequent ambiguous face/hand composite stimuli toward the opposite category. In the current thesis, in one of our studies, we consider human behavioural data from this experiment, in order to study the neuronal adaptation effects in perceptual decisions (Chapter 4).

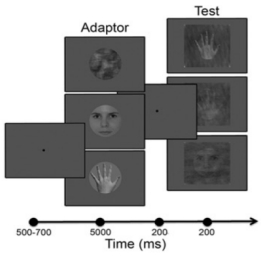

Figure 1.5 High-level adaptation-related aftereffects with ambiguous stimuli
*A high contrast face, or hand, or their Fourier phase randomized version, is used as adaptor, while test stimuli are composite images of faces and hands other than adaptors. (Adapted from **Cziraki et al. 2010**)*

A striking experimental finding, in the context of MP, is the freeze of perception in one of the two images in BR, or perceptual interpretations of an ambiguous stimulus, when the visual input is provided intermittently in time ***(Orbach et al. 1963a, 1963b, 1966; Leopold et al. 2002)*** (Figure 1.6).

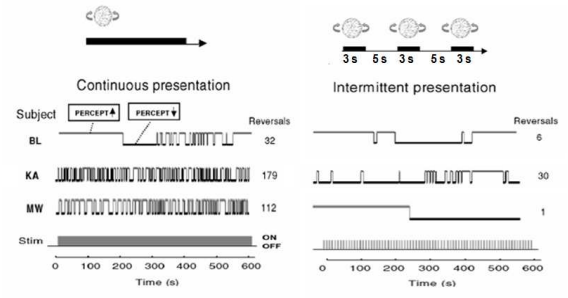

Figure 1.6 Intermittent presentation
Up. *Stimuli are presented either continuously (left), or intermittently (right) in time (adapted from **Maier et al. 2003**)* ***Down.*** *Behavioral reports over the perceived direction of rotation of a RS (adapted from **Leopold et al. 2002**)*

So far we have focused on BP emerging with visual stimuli. Nevertheless, it has been shown that BP is not the only manifestation of MP. Depending on the stimuli, tristable perception (TP) can also emerge ***(Naber et al. 2010; Wallis & Rigelhan 2013)*** (Figure 1.7A-D). In addition, PB does not only emerge with visual stimuli. It has been shown that auditory ***(Warren & Gregory 1958; Van Noorden 1975; Pressnitzer & Hupé 2006; Sterzer et al. 2009)*** (Figure 1.8E), as well as tactile ***(Carter et al. 2008; Sterzer et al. 2009)*** (Figure 1.8F), olfactory ***(Zhou & Chen 2009)*** (Figure 1.7G), and verbal ***(Warren & Gregory 1958)*** (Figure 1.7H) rivalry may occur.

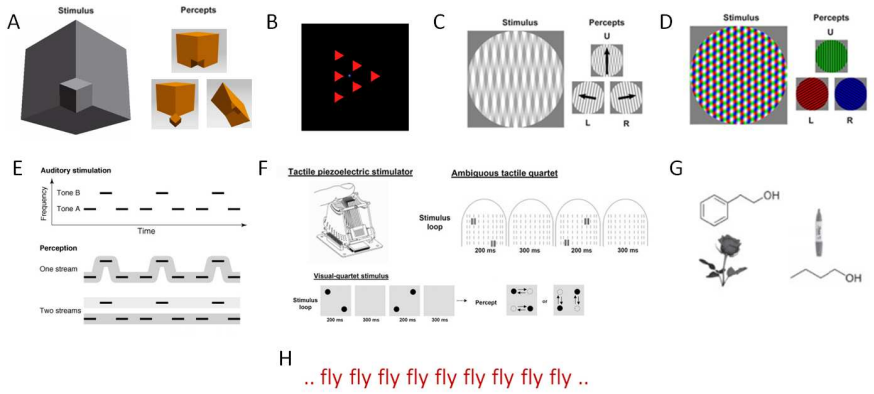

Figure 1.7 Tristable perception, auditory, tactile, olfactory & verbal rivalry
A - D. *Tristable perception (TB) (adapted from* ***Wallis & Rigelhan 2013*** *(A,B) and* ***Naber et al. 2010*** *(C,D))* ***D.*** *Auditory rivalry (AR) (adapted from* ***Sterzer et al. 2009****)* ***E.*** *Tactile rivalry (TR). The tactile stimulus is similar to the visual stimulus: quartet dots (QD, down) (adapted from* ***Carter et al. 2008****)* ***F.*** *Olfactory rivalry (OR) (adapted from* ***Zhou & Chen 2009****)* ***H.*** *verbal rivalry*

We have introduced MP and the basic experimental paradigms which allow its rigorous scientific study. We proceed with well known experimental findings, using various techniques, from macroscopic to microscopic, which have shed some light towards the answer of the initially presented query.

1.3 Temporal dynamics of multistable perception

The term psychophysics refers to the macroscopic experimental way to extract information from human and/or animal behaviour. It has been the initial and traditional way for studying MP. As technological advances

were held, mesoscopic and microscopic experimental techniques appeared and scientists were able to contribute in extracting information related to the neural correlates of subjective perception. Here, we focus on the main measures and results obtained via psychophysics.

When observers are presented continuously in time with ambiguous figures, or two conflicting images dichoptically, they experience perceptual alternations and they are asked, by the experimentalist, to report them. The durations of successive phases of dominance and suppression are thus recorded. A typical characteristic of these durations is their non-chaotic (***Lehky 1995)*** stochastic behaviour ***(Fox & Hermann 1967; Borsellino et al. 1972; Walker 1975)***. However, nonzero serial correlations have also been reported ***(van Ee 2009)***. In addition, cumulative history effects ***(Pastukhov & Braun 2011)***, as well as stochastic resonance ***(Gammaitoni et al. 1998)*** has also been shown to be present in BP ***(Kim et al. 2006, Garcia-Rodriguez 2012)***.

Distribution of time dominances

One of the most common characteristics of the dominance durations, regardless the kind of ambiguous stimulation (in BP), is the shape of their distribution, which is unimodal, right skewed with a long tail (Figure 1.8). Traditionally the distribution of time dominances is fitted by a gamma function ***(Fox & Hermann 1967; Levelt 1967; Logothetis et al. 1996; Kovacs et al. 1996; Rubin & Hupé 2004)***, but log-normal distribution ***(Lehky 1995)*** and Weibull function ***(Zhou et al. 2004)*** have also been used to fit it.

Along with the distribution of time dominances, the coefficient of variation ranges also in a small range of parameters, usually between 0.4 and 0.6 ***(Shpiro et al. 2009)***. It has been shown that the standard deviation and the mean of the dominance durations are related by a factor 2 in average ***(Levelt 1967; Walker 1975)***, and that the parameters of the gamma distribution can be expressed as a function of the mean dominance durations ***(Borsellino et al. 1972; Walker 1975)*** or be equal upon normalization by the mean dominance duration ***(Levelt 1967)***. The distribution of dominance times has been one of the main experimental evidences used to validate theoretical approaches (Chapter 3).

Apart from the distribution of dominance durations to describe the temporal dynamics of the perceptual alternations, the distribution of the reversal rates have also been reported ***(Brascamp et al. 2005)***, and fitted by beta' distribution (a two-parameter distribution related to the gamma distribution, and similar in shape).

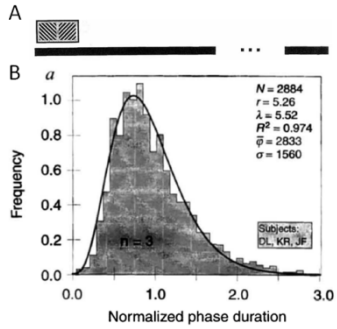

Figure 1.8 Distribution of dominance durations
A. *Stimulation protocol: two orthogonal sinusoidal gratings are presented dichoptically to subjects, continuously in time* ***B.*** *Distribution of dominance durations, fitted by a gamma function. (Adapted from* ***Logothetis et al. 1996****)*

Successive phases of perceptual dominance and suppression can be interrupted by periods of -complete or partial (piecemeal transitions, ***Bossink et al. 1993***)- merged perception of the two conflicting percept, depending on the the rival stimuli. Finally, these transitions periods could be followed by return to the previous perceptual dominance (return or failed transitions ***Mueller & Blake 1989; Brascamp et al. 2006***).

Levelt's propositions

An additional set of experimental evidences, widely used to test theoretical approaches (Chapters 3), have been provided in four propositions by Levelt ***(Levelt 1968),*** and verified experimentally multiple times. Levelt's four propositions denote how stimulus parameters affect the duration of perception of the two conflicting images. Levelt's second proposition has been recently revised ***(Brascamp et al. 2006),*** and all four of them are the followings *(adapted from* ***Klink et al. 2008b****)*:

1. *Increasing the stimulus strength of one perceptual interpretation of a bistable stimulus increases the predominance of this perceptual interpretation*

2. *(Revised) Manipulations of stimulus strength of one perceptual interpretation of a bistable stimulus will mainly influence the average dominance duration of the perceptual interpretation corresponding to the strongest stimulus*
3. *Manipulating the stimulus strength of one perceptual interpretation of a bistable stimulus will influence the average rivalry reversal rate*
4. *Increasing the general stimulus strength of a bistable stimulus will increase the average rivalry reversal rate*

Levelt´s four propositions have been validated for ambiguous figures as well as for conflicting images in BR ***(Klink et al. 2008b; Moreno-Bote et al. 2010)***. In addition, it has been shown that alternation rate in BP is maximal at and symmetric around equi-dominance (***Moreno-Bote et al. 2010)***.

Psychophysical studies apart from revealing the temporal dynamics they can give insights on the underlying neural mechanisms mediating MP. Since the beginnings of MP studies the dominant theory suggests that two neural assemblies that compete in time for perceptual dominance are responsible for the successive phases of perceptual dominance and suppression. In the framework of this theory, nevertheless, there has been a long- standing debate on whether this competition is resolved in the primary, sensory, visual cortex and therefore is held between monocular neurons or is held between binocular neurons, i.e. neurons that encode the neural representation of the stimuli. The answer to this question has been vacillated between the two alternatives as new experimental findings were reported. Initial psychophysical experiments favoured the interocular competition, i.e. competition between monocular neurons ***(Blake et al. 1979, 1980; Blake 1989, Blake & fox 1974; Blake & Lema 1978)***. Other studies though favoured the second explanation ***(Diaz-Caneja 1928; Weitzman 1963; Whittle 1968; Wong & Weisstein 1982; Logothetis et al. 1996; Kovács et al. 1996; Treue 1997)***. Nowadays, all experimental evidences, combining various experimental techniques, suggest that what compete in MP are neural representations of the stimuli, not necessarily bound to monocular input.

In the following paragraph we summarize the experimental mesoscopic and microscopic evidences related to the neural correlates of subjective

visual perception. For more details we refer to the recent thorough reviews by **Panagiotaropoulos & Logothetis** (**2013**), and **Panagiotaropoulos et al.** (**2014**).

1.4 Neural correlates of subjective visual perception

As we pointed out in the begining of this introductory chapter, the current way to approach the problem of subjective visual perception -or else visual awareness, or else visual consciousness- is to find the neural mechanisms that take place in the brain and give rise to the observed behaviour exhibited by humans and non-human primates during phenomena of perceptual dominance and perceptual suppression. Two of the main questions, therefore, are:

1. What are the computations performed by the neurons engaged in such phenomena, and
2. Where in the brain these phenomena are manifested?

These questions are not independent, since the answer of the first question is dependent on the answer of the second question. In order to answer them, both experimental techniques -psychophysics, magnetic resonance imaging (MRI), positron emission tomography (PET), functional magnetic resonance imaging (fMRI), diffusion tensor imaging (DTI), electroencephalography (EEG), magnetoencephalography (MEG), transcranial magnetic stimulation (TMS), electrocorticography (ECoG), deep brain stimulation (DBS), neuroelectrophysiology (intracortical extracellular single-cell recordings)-, as well as theoretical approaches based on experimental evidences can be employed in order to provide insights towards answering these questions.

While macroscopic (physchophysics), as well as mesoscopic non-invasive (MRI, PET, fMRI, DTI, EEG, MEG, TMS) experimental techniques can be applied to both human and non-human primates, it is not always easy to employ mesoscopic and microscopic invasive (ECoG, DBS, single-cell recordings) techniques to humans. This problem has been overcome by finding that non-human primates exhibit similar behaviour with human-primates and that their visual system (Figure 1.10A) is evolutionary similar to that of human-primates (Figure

1.10B,C). Nevertheless, single-neuron recordings in humans have also been performed in epileptic human patients in the context of MP ***(Kreiman et al. 2002)*** and a clearer comparison between humans and non-human primates has been possible.

Under ambiguous conditions, the subjective perceptual dominance of a visual stimulus is conceptualized to be physiologically supported by an assembly of neurons with similar stimulus preference that dominates over a competing, perceptually suppressed, population through the dominance of its averaged firing rate ***(Crick & Koch 2003; Logothetis 1998)***. Indeed, neurophysiological findings in studies combining rivalrous stimulation with extracellular recordings in monkeys and humans suggest that perceptual competition involves two rivaling stimuli representations embedded in two distinct neuronal assemblies that are tuned to each visual pattern and battle for activity dominance ***(Gail et al. 2004; Keliris et al. 2010; Kreiman et al. 2002; Leopold & Logothetis 1996; Logothetis & Schall 1989; Panagiotaropoulos et al. 2012; Sheinberg & Logothetis 1997)*** (Figure 1.9).

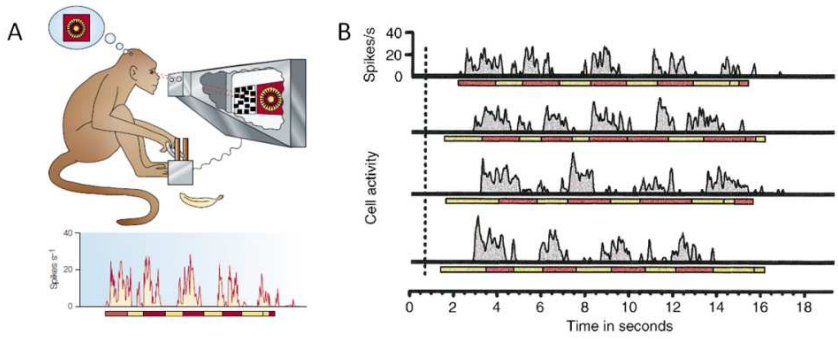

Figure 1.9 Single-cell recordings during rivalry
A. *Up: Monkey trained to report, via a lever, its dominant perception. Down. Activity recorded from a single cell correlated with the animal's perceptual reports (adapted from* ***Blake & Logothetis 2002)*** ***B.*** *Activity of a single cell correlated with the animal's perceptual reports in four observation periods (adapted from* ***Leopold & Logothetis 1999****)*

Where in the brain rivalry is resolved?

Nowadays, it is widely known that neural correlates of subjective visual perception can be detected in multiple sites across the visual cortical hierarchy; from primary visual (V1) to the lateral prefrontal cortex

(LPFC). Nevertheless, they are more likely to reflect the outcome of visual competition, and thus the content of conscious visual perception, in the higher-order association cortical areas (the temporal and prefrontal cortex ***(Leopold 2012; Panagiotaropoulos et al. 2012; Sheinberg & Logothetis 1997)*** and thalamic nuclei; the pulvinar ***(Wilke et al. 2009)***.

As we enter higher areas in visual hierarchy the percentage of neurons activated in agreement with the reported perception increases (Figure 1.10B). More specifically, extracellular electrophysiological recordings in the non-human primate brain, have shown that in early visual processing stages V1 and V2 only 14% of multi-unit spiking activity (MUA) and 20-25% of single-unit activity (SUA) are perceptual modulated during rivalrous perception ***(Leopold & Logothetis 1999; Grunewald et al. 2002; Gail et al. 2004; Keliris et al. 2010)***, while they were not modulated during GFS ***(Wilke et al. 2006; Maier et al. 2008)*** or MIB ***(Libedinsky et al. 2009)***. In hierarchically intermediate cortical areas V4 and middle temporal (MT or else V5) 25-40% of the recorded neurons were perceptual modulated during BR, BFS, SFM ***(Logothetis & Schall 1989; Leopold & Logothetis 1996; Bradley et al. 1998; Dodd et al. 2001; Maier et al. 2007)***. Further in the visual processing hierarchy, in the superior temporal sulcus (STS) and in the inferior temporal (IT), 90% of the recorded neurons were perceptually modulated during BR, BFS ***(Sheinberg & Logothetis 1997)***, while in the human medial temporal lobe (MTL) ~70% are perceptually modulated during BFS ***(Kreiman et al. 2002)***. Finally, in the lateral prefrontal cortex (LPFC) ~60-90% of SUA and ~75-95% of MUA reflect the perceptual dominance and suppression in BFS ***(Panagiotaropoulos et al. 2012)***. In addition, 40% of the recorded sites in the ventral pulvinar and 60% of the recorded sites in the dorsal pulvinar reflect perceptual suppression. In summary, prefrontal, temporal areas and the pulvinar reflect much more robustly perceptual dominance and suppression. Therefore, a cortico - thalamocortical network is suggested to represent the content of subjective visual perception ***(Panagiotaropoulos et al. 2014)*** (Figure 1.10C).

On the other hand, fMRI studies have shown different results regarding the neural correlates of subjective visual perception. In contrast to electrophysiological findings, they have shown significant perceptual modulation of the blood-oxygen-level dependent (BOLD) signal in LGN

and VI during BR ***(Polonsky et al. 2000; Tong & Engel 2001; Lee & Blake 2002; Haynes & Rees 2005; Heynes et al. 2005; Lee et al. 2007; Wang et al. 2013)***. The reason of this discrepancy could be that the BOLD signal reflects changes in relative concentration of the oxygenated and deoxygenated blood that depend more on the local field potentials (LFP's) than neuronal discharges ***(Logothetis et al. 2001; Logothetis 2002, 2003; Logothetis & Wandell 2004; Goense & Logothetis 2008)*** and LFP's are thought to reflect synaptic input ***(Mitzdorf et al. 1999; Logothetis 2003)*** which is different than the spiking activity (measured with single-cell recordings). Nevertheless, fMRI studies have also shown higher cortical areas to be perceptually modulated during BR ***(Lumer et al. 1998; Sterzer et al. 2002; Sterzer & Kleinschmidt 2007; Knapen et al. 2011; Zaretskaya et al. 2010; Wang et al. 2013)***. Therefore, also fMRI studies suggest that early visual processing areas are not sufficient for visual awareness, supporting the pattern competition theory, as well as that interaction between multiple sites across the visual hierarchy are present (***Wang et al. 2013)***.

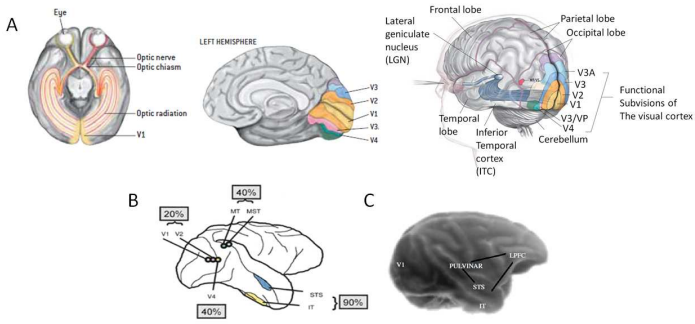

Figure 1.10 Human & non-human primate brain
A. *Human brain (Adapted from* ***Logothetis 1999)*** ***B.*** *Macaque brain (adapted from* ***Leopold & Logothetis 1999)*** ***C.*** *Suggested cortico-thalamic network based on experimental evidences. The pulvinar is depicted on the surface of the cortex for illustration purposes (adapted from* ***Panagiotaropoulos & Logothetis 2013)***

Finally, together with single-cell recordings and fMRI studies, EEG, MEG and TMS studies suggest global functional networks engaged in subjective visual perception in MP ***(Tononi et al. 1998; Srinivasan et al. 1999; Cosmelli et al. 2004; Doesburg et al. 2009; Gaillard et al. 2009; Carmel et al. 2010b; Kanai et al. 2010; Zaretskaya et al. 2010; Hipp et al. 2011)***.

1.5 Outline of the thesis

All the previously presented experimental evidences have shed some light to the problem of visual awareness. In addition, theoretical approaches, based on known experimental evidences, have also contributed in the understanding of the underlying mechanisms during MP. In the current thesis, after a brief review of the theoretical approaches for perceptual mutlistability (§2.1), we study the underlying neural mechanism that generate the spontaneous alternations in BR (Chapter 3), employing a biophysically realistic spiking network (§2.2) and its consistently derived base-rate model (§2.3). Furthermore, we employ biophysically realistic networks, as well as we derive analytical expressions for the second- order statistics (§2.4), to study recent experimental evidences of noise decorralation during visual consciousness (Chapter 5). In addition, we study the effects of neuronal adaptation on perceptual decision making when the sensory stimuli are ambiguous in an adaptation- related aftereffects paradigm (Chapter 4). Finally, the current thesis ends with a general discussion.

CHAPTER 2

Theoretical basis of Multistable Perception[3]

2.1 Introduction

In the beginning of MP's studies, two alternative views were in debate. The first was that perceptual alternations are caused by shifts in attention under conscious control (Hermann von Helmhotz, William James, Sir Charles Sherrington) and the second that perceptual rivalry is caused at the low levels of the visual hierarchy, e.g. due to retinal adaptation (Ewald Hering) ***(Lehky 1988; Blake & Logothetis 2002)***. The first view was initially expressed with an attentional theory of rivalry ***(Walker 1978)***, while the second with an oscillator based on cross-inhibition in the primary visual cortex ***(Fox & Rasche 1969, Lehky 1988).*** Nowadays, and after a plethora of experimental studies, both views are merged together since it is well known that rivalry emerges across multiple sites throughout the visual hierarchy.

[3] Some theoretical approaches presented in this chapter are published: P. Theodoni, T. I. Panagiotaropoulos*, V. Kapoor*, N. K. Logothetis, and G. Deco, (2011), Cortical Microcircuit Dynamics mediating Binocular Rivalry: the role of adaptation in inhibition, *Frontiers in Human Nueroscience, 5, 145, 1-19* & P. Theodoni, G. Kovács, M. W. Greenlee, and G. Deco (2011), Neuronal Adaptation Effects in Decision Making, *The Journal of Neuroscience 31, 1, 234-246*, and others are *in preparation for submission*: T. I. Panagiotaropoulos*, P. Theodoni*, V. Kapoor*, G. Deco, and N. K. Logothetis (2014), Decorrelated noise in dominant prefrontal microcircuits during visual consciousness. (*equal contribution)

Since the invention of the stereoscope by Sir Charles **Wheatstone** (**1838**), BR is the most extensively studied paradigm of MP, both experimentally and theoretically**.** The beauty in BR is the capacity of the phenomenon to offer insights into conscious perception, rather than on the earlier notion that rivalry is strictly a "binocular phenomenon" which optimizes unified stereoscopic vision and is utterly unrelated to other multistable perceptual phenomena. When a subject is dichoptically presented with two conflicting images, only one image is perceived at a time while the other is suppressed from awareness (Chapter 1).

Theoretical studies are mostly based on competition models consisting of two selective neuronal populations whose activity encodes one of the two conflicting images in BR (or perceptual interpretation of an ambiguous figure). Most theoretical approaches so far are based on abstract rate models. Abstract refers to non- biologically plausible, and rate to the main variable of the system of equations which is the mean firing rates of each neural population. Few studies have considered biologically inspired spiking networks (***Laing & Chow 2002; Moreno-Bote 2007;*** Chapters 3, 5), as well as consistent derivations of them to a rate model (***Laing et al. 2010***, Chapter 3). Rate models that have been studied in the context of MP, can be divided into two big categories: Single- stage rate models ***(Fox & Rasche 1969, Sugie 1982; Wolfe 1986; Cogan 1987; Lehky 1988; Blake 1989; Mueller 1990; Lumer 1998; Kalarickal & Marshall 2000; Lago-Fernandez & Deco 2002; Laing & Chow 2002; Stollenwerk & Bode 2003; Moldakarimov et al. 2005; Kim et al. 2006; Wilson 2007; Shpiro et al. 2007; Curtu et al. 2008; Shpiro et al. 2009; van Ee 2009; Curtu 2010; Moreno-Bote 2010; Seely & Chow 2011; Pastukhov et al. 2013)*** and multi- stage rate models ***(Matsuoka 1984; Lumer 1998; Dayan 1998; Nguyen et al. 2001; Wilson 2003; Freeman 2005; Grossberg et al. 2008; Lehky 2011; Said & Heeger 2013)***. Most of the rate models are single- stage, which means that correspond to one area in the brain. Nevertheless, the widespread activity of cortical areas involved in multistable perception makes apparent the need of multi- stage, hierarchical, models ***(Blake & Logothetis 2002; Wang et al. 2013)***.

These rate- based models are mainly characterized by cross-inhibition, which generates competition ***(Seely & Chow 2011)***, between two neuronal populations that encode e.g. each conflicting image in BR, with main

component a slow fatiguing process that produces oscillations *(**Lehky 1988; Lago-Fernández & Deco 2002; Laing & Chow 2002; Wilson 2003, Shpiro et al. 2007).*** Cross-inhibition leads to the suppression of one of the two images, while a fatiguing process, such as spike-frequency adaptation, or synaptic depression, eventually weakens inhibition, and causes the previously suppressed neuronal population to win the competition. This mechanism generates anti- phase oscillations of the mean firing rates of the two neuronal populations believed to represent perceptual alternations between the two conflicting visual patterns. Alternatively, alternations in perception have also been represented as switches between two attractors due to noise in noise- driven attractor models *(**Salinas 2003; Freeman 2005; Kim et al. 2006; Moreno-Bote et al. 2007)*. **Shpiro et al. (2009)** implemented both noise and adaptation mechanisms in a common theoretical framework, and showed that both mechanisms operate in balance during perceptual bistability. In addition, similar result has been shown taking into account cumulative history effects *(**Pastukhov et al. 2013)***, as well as in order to explain the pattern of neural discharges observed in the macaque prefrontal cortex during rivalrous stimulation *(**Panagiotaropoulos et al. 2013)***, while it was recently proposed that noisy adaptation signals could represent one of the physiological mechanisms resulting in BR dynamics *(**van Ee 2009; Alais et al. 2012)***. In Chapter 3, we affirm that noise and adaptation operate in balance during BP by employing a biophysically realistic one- stage spiking network, as well as its consistently derived rate model, and by considering human behavioural data.

Interestingly, many studies with various theoretical approaches -such as neural fields *(**Hock et al. 2003; Wilson 2009; Kilpatrick & Bressloff 2010; Bressloff & Webber 2011; Diekman et al. 2012; Rankin et al. 2013)***, synergetics *(**Ditzinger & Haken 1989, 1990, 1995, 1997**), as well as* solitons *(**Loxley & Robinson 2007, 2009)***, Ising model *(**Riani & Simonotto 1995)*** Bayesian *(**Bialek & DeWeese 1995; Mamassian et al. 2002; Hohwy et al. 2008; van Ee et al. 2003; Wilson 2009; Moreno-Bote et al. 2011),*** in the framework of energy well models *(**Moreno-Bote et al. 2007, 2010, 2011),*** and quantum formalism *(**Atmanspacher et al. 2004; Manousakis 2009, 2012),*** statistics *(**van der Ven et al. 2005)***, chaotic attractor *(**Fürstenau 2004)***, winnerless competition *(**Ashwin & Lavric 2010)***- have been held. Apparently, there is a plethora of theoretical

studies and approaches on MP, and it would be interesting to see a thorough review on them, currently missing from the literature.

In the current thesis, we employed a biologically plausible spiking network to study BR, BFS and perceptual decision making (§2.2, Chapter 3, 4, 5). We also consistently derived a rate model from the biologically inspired network to study the underlying neural mechanisms of BP (§2.3.2, Chapter 3). Finally, expanding the consistently derived rate model to two populations, we extracted analytical expressions for second- order statistics (means, variances, cross-correlations) to study the observed neural noise- decorrelation in BFS (§2.3.4, Chapter 5).

2.2 Biophysically plausible spiking model

Model description

The biophysically realistic spiking model with integrate- and- fire neurons that we employ in the current thesis, was first introduced for working memory ***(Brunel & Wang 2001)*****,** later for decision making ***(Wang 2002)***, and attention ***(Deco et al. 2005)***. Implementing into the model firing- rate adaptation mechanism ***(Liu & Wang 2001)*** has also been employed for adaptation- related aftereffects (Chapter 4) and perceptual bistability ***(Moreno-Bote et al. 2007****;* Chapter 3). It is attractor- based ***(Amit 1995)*** and implements competition and cooperation mechanisms among neurons belonging to two neural groups of pyramidal cells that encode the two conflicting percepts (in a binary decision- making task) or percepts of two dissimilar images of an ambiguous stimulus (in a visual perceptual bistability situation). The essential aspects and components of the model are presented in a compact way in Tables 2.1 - 2.6 (as proposed by ***Nordlie et al. 2009)***, and they are described below. Cooperation mechanisms arise from high recurrent connectivity among neurons belonging to the same neuronal population. Competition between two selective neuronal populations is mediated by a feedback inhibition from interneurons in the network.

Model composition

The network is divided into different populations (Figure 2.1) where neurons belonging to one particular population share the same statistical properties and single- cell parameters, as well as inputs and connectivity. There is a total number of neurons, N, where $N_E = 0.8N$ are excitatory pyramidal cells and $N_I = 0.2N$ are inhibitory interneurons, consistent with the neurophysiologically observed proportion of 80% pyramidal cells versus 20% interneurons ***(Abeles 1991)***. The inhibitory neurons form one population to which we will refer as pool I. The excitatory neurons form three distinct populations. Populations 1 and 2 consist of neurons selective to one or the other conflicting images in BR. The third population (labeled as ns) comprises neurons that are non- selective to the stimulus features. Non- selective neurons are included for biophysical realism and computationally to increase the stability of the network at the spontaneous state; they do not play a particular role in the decision process per se. The union of these three excitatory populations of neurons is named pool E. Each of the two selective pools consists of fN_E neurons. The non-selective one consists of $(1 - 2f)N_E$.

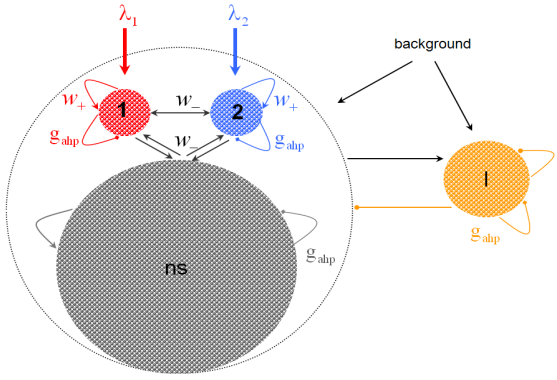

Figure 2.1 Architecture of the biophysically plausible spiking network
The sizes of neuronal populations are proportional to their number of neurons ($N_E = N_1 + N_2 + N_{ns} = 4NI$, $N_{ns} = 0.7N_E$, and $N_1 = N_2 = 0.15N_E$, when $f = 0.15$). There are four neuronal populations: one inhibitory (orange, I), one excitatory comprised of non- selective neurons (gray, ns), and two excitatory populations (red, 1 and blue, 2) within which neurons have similar stimulus selectivity. Arrows denote excitatory connections; lines ending to circles, inhibitory connections whereas lines ending to squares, after hyperpolarizing currents with peak conductance g_{ahp}. All neurons receive background input and selective populations receive an additional external stimulus λ_1, λ_2.

Connectivity

The connectivity architecture of the network can be seen graphically in Figure 2.1. The connections of the neurons and their strengths between and within the populations are determined by dimensionless weights w_j, corresponding to the synaptic efficacies. Within the selective neuronal populations, 1 and 2, excitatory synapses are potentiated by a factor $w_j \equiv w_+ \geq 1$ according to the "Hebbian" rule, according to which cells that fire together are strongly connected. In the text we refer to this factor as recurrent connectivity. Excitatory synapses between the two selective neuronal populations, and excitatory synapses between the non-selective to each selective population are modified by $w_j \equiv w_- = 1 - f(w_+-1)/(1-f) < 1$, so that the spontaneous activity of all excitatory cells is at the same level ***(Amit & Brunel 1997)***. The remaining connections are all set to $w_j = 1$. There is all- to- all connectivity, meaning that each neuron in the network receives N_E excitatory and N_I inhibitory synaptic contacts. Within each population we assume homogeneity of connections for simplicity. The introduction of inhomogeneities (e.g. sparse random connectivity) does not affect the attractor landscape of the dynamics but only increases the noise (finite-size effects, see ***Mattia & Del Giudice 2002)***.

Dynamics of neurons, synapses and channels

All neurons in the network are modeled as being leaky integrate- and- fire neurons. Integrate- and- fire (IF) neurons are point- like elements, meaning that the whole neural membrane is taken as equipotential. Its dynamical state is described by a single variable, the instantaneous value of its membrane potential, $V(t)$. Under normal conditions, the potential inside the cell is lower than the potential outside, which is zero by convention. Membrane voltage changes are due to different ionic concentrations found on both sides of the membrane. Synaptic inputs to an IF neuron are basically described by a capacitor, C_m, connected in parallel with a resistor, R_m. The capacitor corresponds to the membrane capacitance and the resistor to the membrane conductance through which currents are injected into the neuron by its synapses (I_{syn}). In addition, a spike- frequency adapting mechanism is taken into account, which has been observed experimentally ***(Madison & Nicolle 1984)***. It is implemented in the network by including a slow Ca^{2+}- activated K^+

current, I_{AHP}, into the dynamical equation of the membrane potential of each neuron. This afterhyperpolarization current I_{AHP} is given by the following equation:

$$I_{AHP}(t) = -g_{AHP}\mathrm{Ca}(t)\left(V(t) - V_K\right) \tag{2.1}$$

where V_K = -80 mV is the reversal potential of potassium channels. The gating variable Ca, emulating the cytoplasmic Ca^{2+} concentration, is initially set to 0 and between spikes is modeled as a leaky integrator with a decay time constant τ_{Ca} ***(Liu & Wang 2001)***. The g_{AHP}Ca is the effective K^+ conductance and the g_{ahp} defines the level of neuronal adaptation or adaptation strength. Hence, the dynamics of the subthreshold membrane potential of each neuron, excitatory (E) or inhibitory (I), in the network is given by the following system of equations:

$$C_m \frac{dV(t)}{dt} = -g_m\left(V(t) - V_L\right) - I_{syn}(t) + I_{AHP}(t) \tag{2.2}$$

$$\frac{d\mathrm{Ca}(t)}{dt} = -\frac{\mathrm{Ca}(t)}{\tau_{Ca}} + \rho\sum_i \delta(t - t_i) \tag{2.3}$$

where C_m = 0.5 nF for excitatory neurons and C_m = 0.2 nF for inhibitory, $g_m = 1/R_m$ is the membrane leak conductance with the values g_m = 25 nS for pyramidal cells and g_m = 20 nS for interneurons, V_L = -70 mV is the resting potential, I_{syn} is the synaptic current entering the neuron, and sum over i is sum over spikes of the same neuron up to time t.

When the membrane potential of an excitatory or inhibitory neuron reaches a certain threshold, $V_{thr} \equiv \theta$ = -50 mV, a spike is emitted and transmitted to other neurons. In addition, the membrane potential is reset to V_{reset} = -55 mV after a refractory time, τ_{ref} = 2 ms for excitatory neurons and τ_{ref} = 1 ms for inhibitory ones, during which the neuron is unable to produce further spikes. In addition, the cytoplasmic Ca^{2+} concentration increases by a small amount, ρ ***(Liu & Wang 2001)***. Therefore, if $V(t) = V_{thr}$, a spike is emitted and

$$\begin{aligned} V &\rightarrow V_{reset} \\ \mathrm{Ca} &\rightarrow \mathrm{Ca} + \rho \end{aligned} \tag{2.4}$$

The default values of the fixed parameters used in the simulations are displayed in Table 2.5, and they are equal to the ones used in the network introduced by **Brunel and Wang** (**2001**).

Ion channels are modeled as having three types of receptors mediating the synaptic currents flowing into them: AMPA and NMDA glutamatergic and $GABA_A$ GABAergic receptors. The total synaptic current of a neuron is given by the sum of the recurrent EPSCs, mediated by slow NMDA and fast AMPA receptors (I_{NMDA} and I_{AMPA}, respectively), and the IPSCs, mediated by $GABA_A$ receptors (I_{GABA}). External cells contribute to the current through AMPA receptors ($I_{AMPA,ext}$). External EPSCs were mediated exclusively by AMPA receptors to keep the external stimulus as simple as possible. Recurrent EPSCs include NMDA receptors because it is helpful to maintain the system in an asynchronous state. Hence, the total synaptic current is given by $I_{syn}(t) = I_{AMPA,ext}(t) + I_{AMPA}(t) + I_{NMDA}(t) + I_{GABA}(t)$, where:

$$I_{\mathrm{AMPA,ext}} = g_{\mathrm{AMPA,ext}}\left(V(t) - V_{\mathrm{E}}\right)\sum_{j=1}^{N_{\mathrm{ext}}} S_j^{\mathrm{AMPA,ext}}(t) \tag{2.5}$$

$$I_{\mathrm{AMPA}} = g_{\mathrm{AMPA}}\left(V(t) - V_{\mathrm{E}}\right)\sum_{j=1}^{N_{\mathrm{E}}} w_j S_j^{\mathrm{AMPA}}(t) \tag{2.6}$$

$$I_{\mathrm{NMDA}} = \frac{g_{\mathrm{NMDA}}\left(V(t) - V_{\mathrm{E}}\right)}{1 + \gamma e^{-\beta V(t)}}\sum_{j=1}^{N_{\mathrm{E}}} w_j S_j^{\mathrm{NMDA}}(t) \tag{2.7}$$

$$I_{\mathrm{GABA}} = g_{\mathrm{GABA}}\left(V(t) - V_{\mathrm{I}}\right)\sum_{j=1}^{N_{\mathrm{I}}} S_j^{\mathrm{GABA}}(t) \tag{2.8}$$

where sums over j are over presynaptic neurons. The reversal potentials for excitatory post synaptic current (EPSCs) are V_E = 0 mV and for inhibitory ones (IPSCs) V_I = -70 mV. The dimensionless parameters w_j of the excitatory connections are the synaptic weights. The peak conductances for excitatory synapses are $g_{AMPA,ext}$ = 2.08 nS, $g_{AMPA,rec}$ = 104/N nS, $g_{NMDA,rec}$ = 370/N nS, and g_{GABA} = 1250/N nS, where N is the total number of neurons in the network and divides the recurrent conductances to keep the mean recurrent input constant if N is varied in the network. The peak conductances for inhibitory synapses are $g_{AMPA,ext}$ = 1.62 nS, $g_{AMPA,rec}$ = 81/N nS, $g_{NMDA,rec}$ = 258/N nS, and g_{GABA} = 973/N nS.

The NMDA currents are voltage-dependent and they are modulated by extracellular magnesium concentration $[Mg^{2+}] = 1$ mM, with parameters $\gamma = [Mg^{2+}]/(3.57 \text{ mM})$ and $\beta = 0.062$ $(\text{mV})^{-1}$. The functions $S_j(t)$ are the synaptic gating variables, representing the fractions of open channels of neurons and they are given by the following:

$$\frac{dS_j^{\text{AMPA,ext}}(t)}{dt} = -\frac{S_j^{\text{AMPA,ext}}(t)}{\tau_{\text{AMPA}}} + \sum_k \delta\left(t - t_j^k\right) \tag{2.9}$$

$$\frac{dS_j^{\text{AMPA}}(t)}{dt} = -\frac{S_j^{\text{AMPA}}(t)}{\tau_{\text{AMPA}}} + \sum_k \delta\left(t - t_j^k\right) \tag{2.10}$$

$$\frac{dS_j^{\text{NMDA}}(t)}{dt} = -\frac{S_j^{\text{NMDA}}(t)}{\tau_{\text{NMDA}\downarrow}} + \alpha x_j(t)\left(1 - S_j^{\text{NMDA}}(t)\right) \tag{2.11}$$

$$\frac{dx_j(t)}{dt} = -\frac{x_j(t)}{\tau_{\text{NMDA}\uparrow}} + \sum_k \delta\left(t - t_j^k\right) \tag{2.12}$$

$$\frac{dS_j^{\text{GABA}}(t)}{dt} = -\frac{S_j^{\text{GABA}}(t)}{\tau_{\text{GABA}}} + \sum_k \delta\left(t - t_j^k\right) \tag{2.13}$$

where sums over k are over spikes emitted by the presynaptic neuron j at time $t_{j,}^k$, $a = 0.5$ ms^{-1} and $\delta(t)$ is the Dirac delta function. The rise time for the NMDA synapses is $\tau_{\text{NMDA}\uparrow} = 2$ ms. The rise times of both AMPA and GABA synaptic currents are neglected because they are extremely short (< 1 ms). The decay time for AMPA synapses is $\tau_{\text{AMPA}} = 2$ ms, for NMDA synapses is $\tau_{\text{NMDA}\downarrow} = 100$ ms, and for GABA synapses is $\tau_{\text{GABA}} = 10$ ms.

Populations	Four: three excitatory, one inhibitor
Topology	-------
Connectivity	Full, no synaptic delay
Neuron model	Leaky integrate- and- fire, fixed voltage threshold, fixed absolute refractory time
Channel model	-------
Synapse model	Conductance- based AMPA, $GABA_A$, and conductance- based and voltage- depènded NMDA
Plasticity	-------
Input	Time- dependent, fixed- rate Poisson spike trains to all neurons: $\nu = \nu_{ext} + \lambda$, one generator per neuron
Measurements	Spike activity, mean firing rates of the populations (calculated in a 50 ms time window shifted by 5 ms step)

Table 2.1 Tabular description of the spiking model: summary

Name	Elements	Size
N_{ext}	Poisson generator	$N_{ext} = 800$
I	IF neuron	$N_I = 0.2N$
$E = N_{rs} \cup E_1 \cup E_2$	IF neuron	$N_E = 0.8N = 4N_I$
E_1	IF neuron	$E_1 = f \cdot N_E$
E_2	IF neuron	$E_2 = f \cdot N_E$
N_{rs}	IF neuron	$N_{rs} = (1-2f) \cdot N_E$

Table 2.2 Tabular description of the spiking model: population

Source	Target	Pattern
N_{ext}	I, N_{ext}, E_1, E_2	full connected, weight 1, receptors AMPA, NMDA
I	I, N_{ext}, E_1, E_2	full connected, weight w_I, receptors GABA
N_{rs}, E_1, E_2	I	full connected, weight 1, receptors AMPA, NMDA
N_{rs}, E_1, E_2	N_{rs}	full connected, weight 1, receptors AMPA, NMDA
E_1	E_2	full connected, weight w_-, receptors AMPA, NMDA
E_2	E_2	full connected, weight w_+, receptors AMPA, NMDA
N_{rs}	E_1, E_2	full connected, weight w_-, receptors AMPA, NMDA
E_1	E_1	full connected, weight w_+, receptors AMPA, NMDA
E_2	E_1	full connected, weight w_-, receptors AMPA, NMDA

Table 2.3 Tabular description of the spiking model: connectivity

Type	Leaky integrate- and- fire
Subthreshold dynamics	If $t > t^* + \tau_{rp}$ $C_m \frac{dV(t)}{dt} = -g_m (V(t) - V_{reset}) - I_{syn}(t) - I_{AHP}(t)$ $\tau_{Ca} \frac{d\mathrm{Ca}}{dt} = -\mathrm{Ca}$ Else $V(t) = V_{reset}$ Where $I_{syn}(t) = I_{AMPA,ext}(t) + I_{AMPA}(t) + I_{NMDA}(t) + I_{GABA}(t)$
Spiking	If $V(t) = V_{thr}$ 1. Set $t^* = t$ 2. Emit a spike with time stamp t^* 3. $\mathrm{Ca} = \mathrm{Ca} + a$

Table 2.4 Tabular description of the spiking model: neurons & synapses

Excitatory & Inhibitory neurons		Excitatory neurons		Inhibitory neurons	
N_{ect}	800 neurons	N_E	$0.8N$	N_I	$0.2N$
ν_{ect}	3 Hz	V_E	0 mV	V_I	−70 mV
V_L	−70 mV	C_m	0.5 nF	C_m	0.2 nF
V_{thr}	−50 mV	g_m	25 nS	g_m	20 nS
V_{reset}	−55 mV	$g_{AMPA,ect}$	2.08 nS	$g_{AMPA,ect}$	1.62 nS
τ_{AMPA}	2 ms	g_{AMPA}	$104/N$	g_{AMPA}	$81/N$
$\tau_{NMDA\uparrow}$	2 ms.	g_{NMDA}	$327/N$	g_{NMDA}	$258/N$
$\tau_{NMDA\downarrow}$	100 ms	g_{GABA}	0.625 nS	g_{GABA}	0.4865 nS
τ_{GABA}	10 ms				

Table 2.5 Default values of the fixed parameters of the spiking model

Excitatory & Inhibitory neurons					
N	2000 neurons	f	0.15	g_{AHP}	40 nS
E_i	$f \cdot N_E$	w_+	1.68	ρ	0.005
N_{ns}	$(1-2f)N_E$	w_I	1	τ_{Ca}	600 ms

Table 2.6 Default values of the free parameters of the spiking model

Inputs and outputs

Each neuron in the network receives a background input E_{ext}. In order to simulate the background input, each neuron in the network receives input through C_{ext} = 800 excitatory connections, each one receiving an uncorrelated Poisson spike train with rate 3 Hz. Hence, the excitatory and the inhibitory neurons of the network receive an independent Poisson train of spikes with rate ν_{ext} = 2.4 kHz. In addition, to simulate the sensory stimulus, the neurons within the two selective populations receive an additional Poisson spike train with invariant time rates λ_1 and λ_2, which define the stimuli strength, respectively. Therefore, the total input that each neuron of the selective pools receives is $\nu_{1,2} = \nu_{ext} + \lambda_{1,2}$. Output of the model is the mean spike activity of the neuronal populations of the network, as are raster plots and firing rates.

Simulations

To integrate the system of coupled differential equations that describe the dynamics of all cells and synapses, we used a second order Runge–Kutta routine ***(Press et al. 2007)*** with time step of 0.02 ms. In each trial, the mean firing rate of each neuronal population was calculated by dividing the number of spikes emitted in a 50ms window by its number of neurons and by the window size. The time window was sliding with a time step of

5 ms. The spiking neural model was programmed with C++ programming initially by Marco Loh, Daniel Martí, Gustavo Deco and extended adequately to the needs of the current thesis by the author of this thesis. For analyzing the outputs of the spiking simulations, scripts in Matlab R2007b were written and used.

2.3 Consistently derived rate model

Here, we consistently derive a four-variable reduced rate model from the previously described biophysically plausible spiking network (§2.2, Figures 2.1, 2.2A), following the simplified mean field approach of **Wong and Wang (2006)**. This approach is based on the mean field approximation derived by Brunel and Wang ***(Brunel & Wang, 2001)*** which analyses networks of neurons that have conductance- based synaptic inputs when the network of integrate and fire neurons is in a stationary state. In the mean field approximation, it is considered the diffusion approximation according to which the sums of the synaptic gating variables (Equations 2.5 - 2.8) are replaced by a DC component and a fluctuation term. Moreover, due to the different synaptic time constants, the only noise term that remains is that of the external synaptic gating variable which is considered as Gaussian.

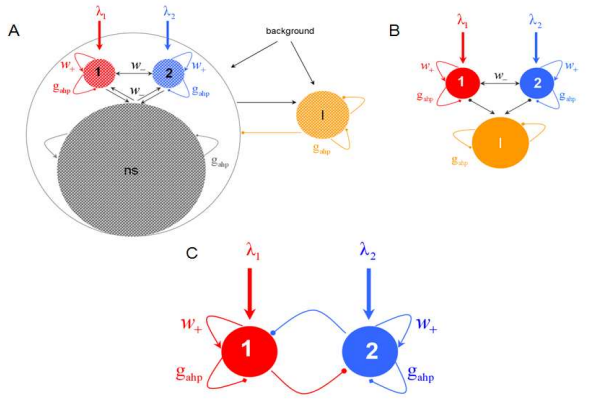

Figure 2.2 Consistently derived rate model
(A) *Biophysically plausible spiking network, same as in Figure 2.1* ***(B)*** *Assuming that the mean firing rate of the non- selective neuronal population is constant, the network is reduced into three neuronal populations: two excitatory (1, 2), and one inhibitory (I).* ***(C)*** *Four- variable reduced rate model of two populations with recurrent excitation, cross- inhibition, and neuronal adaptation.*

Using this approach, the original network of thousands of spiking neurons can be reduced into a set of coupled self- consistent non- linear equations. This describes the average firing rate of each neuronal population as a function of the average input current, which in turn is a function of its average firing rate. This mean field approximation has been extended for spiking networks including Ca^{2+}- activated K^+ hyperpolarizing currents ***(Deco & Rolls 2005)***, such as the one described in the previous paragraph (§2.2). Here, we extend the two-variable reduced model of **Wong and Wang** (**2006**) by considering this spike-frequency adaptation mechanism in neurons.

The transfer function of a LIF neuron receiving a noisy input, I_{total}, is given y the first-passage time formula ***(Renart et al. 2003)***:

$$r = \phi(I_{\text{total}}) = [\tau_{\text{ref}} + \tau_{\text{m}}\sqrt{\pi}\int_{\frac{V_{\text{reset}}-V_{ss}}{s}}^{\frac{V_{\text{thr}}-V_{ss}}{s}} e^{u^2}(1+erf(u))\mathrm{d}u]^{-1} \qquad (2.14)$$

Where s is the amplitude of the fluctuations of the synaptic input, i.e. of the noise, $V_{ss} = (V_L + I_{\text{total}}/g^{E,I}{}_m)$, and *erf*(*u*) is the error function. The remaining parameters have been defined in the description of the spiking network in the previous paragraph (§2.2). In the simplified mean field approach, it is assumed that the driving force of the synaptic currents is constant and that the variance of the membrane potential does not vary significantly and it can be considered fixed as constant. Furthermore, instead of using Equation 2.14, the input-output function of Abbott and Chance ***(Abbott & Chance 2005)*** is considered:

$$\phi(I_{\text{total}}) = \frac{c_i I_{\text{total}} - I_i}{1 - e^{-g_i(c_i I_{\text{total}} - I_i)}}, \quad i = \text{E}, \text{I} \qquad (2.15)$$

where c_i (c_E = 310 (Hz/nA) for excitatory neurons, c_I = 615 (Hz/nA) for inhibitory neurons) is the gain factor, g_i (g_E = 0.16 s for excitatory neurons, g_I = 0.087 s for inhibitory neurons) is a noise factor determining the shape of the "curvature" of φ, and I_i/c_i (I_E = 125 Hz, I_I = 177 Hz) is the threshold current when φ acts as a linear/threshold function for high g_i. The values of these parameters are calculated after fitting Equation 2.15 to the first-passage time formula (Equation 2.14) of a LIF excitatory (E) and

of an inhibitory (I) neuron, which receives AMPA receptor-mediated external Gaussian noise ***(Wong & Wang, 2006)***.

The initial spiking network can be reduced in this way into a system with 11 + 4 variables, where the 11 are the mean firing rates of the four neuronal populations with their average synaptic gating variables. The remaining 4 are the average cytoplasmic Ca^{2+} concentration gating variables of the neuronal populations. While, by solving the mean field equations, one can only determine the fixed points of the system i.e. the stationary firing rates of the four neuronal populations describing the firing rates by the Wilson-Cowan type equations ***(Wilson & Cowan 1973)*** with time constant τ_r = 2 ms, one can calculate their temporal dynamics. Then, the system of the 11 + 4 variables is given by the following equations:

$$\tau_r \frac{dr_i}{dt} = -r_i + \varphi(I_{\text{total},i}) \tag{2.16}$$

$$\tau_r \frac{dr_I}{dt} = -r_I + \varphi(I_{\text{total,I}}) \tag{2.17}$$

$$\frac{dS_i^{\text{ampa}}}{dt} = -\frac{S_i^{\text{ampa}}}{\tau_{\text{ampa}}} + \tilde{r}_i \tag{2.18}$$

$$\frac{dS_i^{\text{nmda}}}{dt} = -\frac{S_i^{\text{nmda}}}{\tau_{\text{nmda}}} + \left(1 - S_i^{\text{nmda}}\right) F(\psi_i) \tag{2.19}$$

$$\frac{dS_I^{\text{gaba}}}{dt} = -\frac{S_I^{\text{gaba}}}{\tau_{\text{gaba}}} + \tilde{r}_I \tag{2.20}$$

$$\frac{d\text{Ca}_i}{dt} = -\frac{\text{Ca}_i}{\tau_{\text{Ca}}} + \rho\tilde{r}_i \tag{2.21}$$

$$\frac{d\text{Ca}_I}{dt} = -\frac{\text{Ca}_I}{\tau_{\text{Ca}}} + \rho\tilde{r}_I \tag{2.22}$$

Where, i = 1, 2, ns accounts for the two selective and the non- selective to stimulus features excitatory neuronal populations, and I accounts for the inhibitory neuronal population. In Equations 2.16 and 2.17, r_i and r_I (expressed in Hz) are the presynaptic mean firing rate of the excitatory and inhibitory populations respectively. In Equations 2.18, 2.20 – 2.22, $\tilde{r}_i$

= $r_i/1000$ and $\tilde{r}_I = r_I/1000$, in order to be consistent with the units since the time constants are expressed in ms. $S^{ampa}{}_i$, $S^{nmda}{}_i$ and $S^{gaba}{}_I$ stand for the average synaptic gating variables of the AMPA, NMDA and GABA receptors respectively, and τ_{ampa}, τ_{nmda}, τ_{gaba}, for their corresponding decay time constants. Ca_i and Ca_I stand for the cytoplasmic Ca^{2+} concentration gating variable of the three excitatory (i = 1, 2, ns), and the one inhibitory (I) population respectively. $\psi_i = \gamma\tau_{nmda}\,\tilde{r}_i/(1 + \gamma\tau_{nmda}\,\tilde{r}_i)$ is the steady state of $S^{nmda}{}_i$, γ = 0.641 and $F(\psi_i) = \psi_i/(\tau_{nmda}(1 - \psi_i)) = \gamma\tilde{r}_i$ ***(Brunel & Wang 2001; Wong & Wang 2006)***.

Furthermore, the model can be reduced to a 4- variable system if we: 1. assume constant activity of the non- selective neurons, 2. consider only the slow dynamics of NMDA gating variable and of the Ca^{2+}- activated K^+ channels, 3. linearize the input- output relation of the interneurons, and 4. consider the Ca^{2+} concentration gating variable of inhibitory interneurons constant. We will discuss this in more details in the following sections.

Constant activity of non- selective excitatory neurons

When there is no adaptation in the network (g_{ahp} = 0 nS), the firing rate of the non selective neurons does not change much under different conditions. This allows us to assume that they fire at a constant rate of 2 Hz, as in **Wong and Wang (2006)**. We further assume the same when there is neuronal adaptation in the network ($g_{ahp} \neq 0$ nS) in order for our four variable reduced model to coincide with the two-variable reduced of **Wong and Wang (2006)** at g_{ahp} = 0 nS. Implementing spike- frequency adaptation to all excitatory and inhibitory neurons, the mean firing rate of the non selective population increases as a function of the level of neuronal adaptation (Figure 2.3). The mean firing rate was calculated by averaging the last 5 s of each 10 s- trial. and by averaging over 100 trials. In Figure 2.3A, we show this dependence at different recurrent connectivities for an additional external stimulus to neurons belonging to the two selective populations of 40 Hz (a stimulus strength used in the simulations in Chapter 3). We see that, for a given stimulus, recurrent connectivity does not change much the mean firing rate of the non-selective population as a function of the level of adaptation strength. This result stands for different stimuli (not shown here).

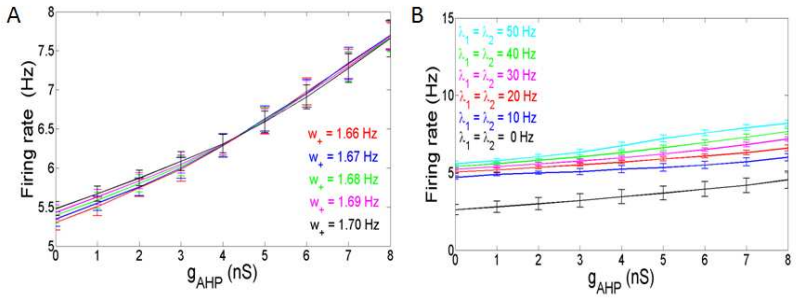

Figure 2.3 Mean firing rate of the non- selective population
(A) *Average firing rate of the non- selective neuronal population as a function of the level of adaptation at different recurrent connectivities for external input* $\lambda_1 = \lambda_2 = 40$ *Hz.* ***(B)*** *Average firing rate of the non- selective neuronal population as a function of the level of neuronal adaptation at different external stimuli for recurrent connectivity* $w_+ = 1.68$.

In Figure 2.3B, we show the mean firing rate of the non selective population as a function of the level of adaptation at different external inputs for a recurrent connectivity of $w_+ = 1.68$ (the recurrent connectivity used in the simulations in Chapter 3). It is apparent that there is an increase, both as a function of level of neuronal adaptation for a given stimulus, and as a function of stimulus for a given neuronal adaptation. Nevertheless, for simplicity we decided to neglect this increase and considered that the mean firing rate of the non selective population is constant at 2 Hz for all conditions (i.e. also when there is neuronal adaptation in the network). As a consequence of this assumption, we further neglected the extra inhibition on the selective populations evoked through the interneurons. Nevertheless, as we show in Figures 3.2C, 3.2D, 3.5C, and 3.5D, that the adopted assumptions do not change the results much. By assuming that the mean firing rate of the non- selective population is constant, the system is reduced to three neuronal populations as it is shown in Figure 2.2B.

Slow dynamics of NMDA gating variable and cytoplasmic Ca^{2+} concentration

The membrane time constant of LIF neurons can be neglected since they respond instantaneously to a stimulus ***(Brunel et al. 2001; Fourcaud & Brunel 2002)***. In addition, the fast dynamics of the synaptic gating variables of AMPA and $GABA_A$ receptors, compared to the slow synaptic

gating variable of NMDA receptors, may also be neglected as they reach their steady states much faster. Their average values can thus be written as proportional to the mean firing rate of presynaptic cells ***(Brunel & Wang 2001; Wong & Wang 2006)***. In this work, we also consider the slow dynamics of the cytoplasmic Ca^{2+} concentration that cannot be neglected. Therefore, Equations 2.19, 2.21 and 2.22 remain as they were, while Equations 2.16-2.18 and 2.20 become:

$$r_i = \phi(I_{\text{total},i}) \tag{2.23}$$

$$r_{\text{I}} = \phi(I_{\text{total,I}}) \tag{2.24}$$

$$S_i^{\text{ampa}}(t) = \tau_{\text{ampa}} \tilde{r}_i(t) \tag{2.25}$$

$$S_{\text{I}}^{\text{gaba}}(t) = \tau_{\text{gaba}} \tilde{r}_{\text{I}}(t) \tag{2.26}$$

where i = 1, 2. The total currents in the selective populations (1, 2) and in the inhibitory (I), resulting from the simplified mean field approach, are given by the following equations:

$$\begin{aligned}
I_{\text{total},1} &= I_{\text{syn},1} + I_{\text{ahp},1} = I_{\text{ampa,ext},1} + I_{\text{stim},1} + I_{\text{ampa},1} + I_{\text{nmda},1} + I_{\text{gaba},1} + I_{\text{ahp},1} \\
&= -g^{\text{E}}_{\text{ampa,ext}} \langle V_{\text{E}} \rangle \tau_{\text{ampa}} C_{\text{ext}} \tilde{r}_{\text{ext}} - g^{\text{E}}_{\text{ampa,ext}} \langle V_{\text{E}} \rangle \tau_{\text{ampa}} \tilde{\lambda}_1 \\
&\quad - g^{\text{E}}_{\text{ampa}} \langle V_{\text{E}} \rangle \tau_{\text{ampa}} f C_{\text{E}} w_+ \tilde{r}_1 - g^{\text{E}}_{\text{ampa}} \langle V_{\text{E}} \rangle \tau_{\text{ampa}} f C_{\text{E}} w_- \tilde{r}_2 \\
&\quad - g^{\text{E}}_{\text{ampa}} \langle V_{\text{E}} \rangle \tau_{\text{ampa}} (1-2f) C_{\text{E}} w_- \tilde{r}_{\text{ns}} \\
&\quad - g^{\textit{eff},\text{E}}_{\text{nmda}} \langle V_{\text{E}} \rangle f C_{\text{E}} w_+ S_1 - g^{\textit{eff},\text{E}}_{\text{nmda}} \langle V_{\text{E}} \rangle f C_{\text{E}} w_- S_2 \\
&\quad - g^{\textit{eff},\text{E}}_{\text{nmda}} \langle V_{\text{E}} \rangle (1-2f) C_{\text{E}} w_- \psi_{\text{ns}} \\
&\quad - g^{\text{E}}_{\text{gaba}} (\langle V_{\text{E}} \rangle - V_{\text{I}}) \tau_{\text{gaba}} C_{\text{I}} \tilde{r}_{\text{I}} - \tilde{g}_{\text{ahp}} (\langle V_{\text{E}} \rangle - V_{\text{K}}) Ca_1
\end{aligned} \tag{2.27}$$

$$\begin{aligned}
I_{\text{total},2} &= I_{\text{syn},2} + I_{\text{ahp},2} = I_{\text{ampa,ext},2} + I_{\text{stim},2} + I_{\text{ampa},2} + I_{\text{nmda},2} + I_{\text{gaba},2} + I_{\text{ahp},2} \\
&= -g^{\text{E}}_{\text{ampa,ext}} \langle V_{\text{E}} \rangle \tau_{\text{ampa}} C_{\text{ext}} \tilde{r}_{\text{ext}} - g^{\text{E}}_{\text{ampa,ext}} \langle V_{\text{E}} \rangle \tau_{\text{ampa}} \tilde{\lambda}_2 \\
&\quad - g^{\text{E}}_{\text{ampa}} \langle V_{\text{E}} \rangle \tau_{\text{ampa}} f C_{\text{E}} w_- \tilde{r}_1 - g^{\text{E}}_{\text{ampa}} \langle V_{\text{E}} \rangle \tau_{\text{ampa}} f C_{\text{E}} w_+ \tilde{r}_2 \\
&\quad - g^{\text{E}}_{\text{ampa}} \langle V_{\text{E}} \rangle \tau_{\text{ampa}} (1-2f) C_{\text{E}} w_- \tilde{r}_{\text{ns}} \\
&\quad - g^{\textit{eff},\text{E}}_{\text{nmda}} \langle V_{\text{E}} \rangle f C_{\text{E}} w_- S_1 - g^{\textit{eff},\text{E}}_{\text{nmda}} \langle V_{\text{E}} \rangle f C_{\text{E}} w_+ S_2 \\
&\quad - g^{\textit{eff},\text{E}}_{\text{nmda}} \langle V_{\text{E}} \rangle (1-2f) C_{\text{E}} w_- \tilde{\psi}_{\text{ns}} \\
&\quad - g^{\text{E}}_{\text{gaba}} (\langle V_{\text{E}} \rangle - V_{\text{I}}) \tau_{\text{gaba}} C_{\text{I}} \tilde{r}_{\text{I}} - \tilde{g}_{\text{ahp}} (\langle V_{\text{E}} \rangle - V_{\text{K}}) Ca_2
\end{aligned} \tag{2.28}$$

$$
\begin{aligned}
I_{\text{total,I}} &= I_{\text{syn,I}} + I_{\text{ahp,I}} = I_{\text{ampa,ext,I}} + I_{\text{ampa,I}} + I_{\text{nmda,I}} + I_{\text{gaba,I}} + I_{\text{ahp,I}} \\
&= -\mathrm{g}^{\mathrm{I}}_{\text{ampa,ext}} \left\langle V_{\mathrm{I}} \right\rangle \tau_{\text{ampa}} \mathrm{C}_{\text{ext}} \tilde{r}_{\text{ext}} \\
&\quad - \mathrm{g}^{\mathrm{I}}_{\text{ampa}} \left\langle V_{\mathrm{I}} \right\rangle \tau_{\text{ampa}} f \, \mathrm{C}_{\mathrm{E}} \, \tilde{r}_1 - \mathrm{g}^{\mathrm{I}}_{\text{ampa}} \left\langle V_{\mathrm{I}} \right\rangle \tau_{\text{ampa}} f \, \mathrm{C}_{\mathrm{E}} \, \tilde{r}_2 \\
&\quad - \mathrm{g}^{\mathrm{I}}_{\text{ampa}} \left\langle V_{\mathrm{I}} \right\rangle \tau_{\text{ampa}} (1-2f) \mathrm{C}_{\mathrm{E}} \tilde{r}_{\text{ns}} \\
&\quad - \mathrm{g}^{\mathit{eff},\mathrm{I}}_{\text{nmda}} \left\langle V_{\mathrm{I}} \right\rangle f \, \mathrm{C}_{\mathrm{E}} \, S_1 - \mathrm{g}^{\mathit{eff},\mathrm{I}}_{\text{nmda}} \left\langle V_{\mathrm{I}} \right\rangle f \, \mathrm{C}_{\mathrm{E}} \, S_2 \\
&\quad - \mathrm{g}^{\mathit{eff},\mathrm{I}}_{\text{nmda}} \left\langle V_{\mathrm{I}} \right\rangle (1-2f) \mathrm{C}_{\mathrm{E}} \, \tilde{\psi}_{\text{ns}} \\
&\quad - \mathrm{g}^{\mathrm{I}}_{\text{gaba}} \left(\left\langle V_{\mathrm{I}} \right\rangle - \mathrm{V}_{\mathrm{I}} \right) \tau_{\text{gaba}} \mathrm{C}_{\mathrm{I}} \tilde{r}_{\mathrm{I}} - \tilde{\mathrm{g}}_{\text{ahp}} \left(\left\langle V_{\mathrm{I}} \right\rangle - \mathrm{V}_{\mathrm{K}} \right) \mathrm{Ca}_{\mathrm{I}}
\end{aligned}
\tag{2.29}
$$

Where $g^{eff,E,I}_{nmda} = g^{E,I}_{nmda}/(1 + \gamma e^{-\beta<V_{E,I}>})$, E stands for excitatory, I for inhibitory, and S_1, S_2 are the average synaptic gating variables of the NMDA receptors of the two selective populations. To the external excitatory input currents to the two selective populations, $I_{ampa,ext,1}$, $I_{ampa,ext,2}$, we included the contribution of the external stimuli $\tilde{\lambda}_1 = \lambda_1/1000$ (1/ms) and $\tilde{\lambda}_2 = \lambda_2/1000$ (1/ms) respectively. $\tilde{g}_{ahp} = g_{ahp}/1000$ (μS), and the values of the fixed averaged membrane potentials for the excitatory and inhibitory neurons are $<V_E>$ = -53.4 mV, $<V_I>$ = -52.1 mV respectively, the same as the ones considered in **Wong and Wang** (**2006**).

Linearization of the input-output relation of interneurons

The mean firing rate of the inhibitory neurons lies in the range of 8 - 15 Hz when there is no spike- frequency adaptation encoded in the neurons of the network. However when spike- frequency adaptation in all neurons in the network, the mean firing rate of the inhibitory neurons increases slightly and up to 20 Hz. Within the range 8 - 20 Hz, the single- cell input-output relation is still almost linear (Figure 2.4) and is fitted by:

$$
r_{\mathrm{I}} = \phi\left(I_{\text{total,I}}\right) = \frac{1}{\mathrm{g}_{\mathrm{I2}}} \left(\mathrm{c}_{\mathrm{I}} I_{\text{total,I}} - \mathrm{I}_{\mathrm{I}} \right) + r_0 \tag{2.30}
$$

where g_{12} = 1.7876, and r_0 = 11.3721 Hz. c_I = 615 (Hz/nA) and I_I = 177 Hz are the same as in Equation 2.15. By substituting $I_{total,I}$ (Equation 2.29) in Equation 2.30 we find:

$$
\begin{aligned}
r_{\mathrm{I}} = & -\frac{\mathrm{c_I}}{\eta \mathrm{g_{I2}}} \mathrm{g}^{\mathrm{I}}_{\mathrm{ampa,ext}} \left\langle V_{\mathrm{I}} \right\rangle \tau_{\mathrm{ampa}} \mathrm{C_{ext}} \tilde{r}_{\mathrm{ext}} \\
& -\frac{\mathrm{c_I}}{\eta \mathrm{g_{I2}}} \begin{pmatrix} \mathrm{g}^{\mathrm{I}}_{\mathrm{ampa}} \left\langle V_{\mathrm{I}} \right\rangle \tau_{\mathrm{ampa}} \mathrm{C_E} f \tilde{r}_1 + \mathrm{g}^{\mathrm{I}}_{\mathrm{ampa}} \left\langle V_{\mathrm{I}} \right\rangle \tau_{\mathrm{ampa}} \mathrm{C_E} f \tilde{r}_2 \\ + \mathrm{g}^{\mathrm{I}}_{\mathrm{ampa}} \left\langle V_{\mathrm{I}} \right\rangle \tau_{\mathrm{ampa}} \mathrm{C_E} \left(1-2f\right) \tilde{r}_{\mathrm{ns}} \end{pmatrix} \\
& -\frac{\mathrm{c_I}}{\eta \mathrm{g_{I2}}} \begin{pmatrix} \mathrm{g}^{\mathit{eff},\mathrm{I}}_{\mathrm{nmda}} \left\langle V_{\mathrm{I}} \right\rangle \mathrm{C_E} f S_1 + \mathrm{g}^{\mathit{eff},\mathrm{I}}_{\mathrm{nmda}} \left\langle V_{\mathrm{I}} \right\rangle \mathrm{C_E} f S_2 \\ + \mathrm{g}^{\mathit{eff},\mathrm{I}}_{\mathrm{nmda}} \left\langle V_{\mathrm{I}} \right\rangle \mathrm{C_E} \left(1-2f\right) \psi_{\mathrm{ns}} \end{pmatrix} \\
& -\frac{\mathrm{c_I}}{\eta \mathrm{g_{I2}}} \tilde{\mathrm{g}}_{\mathrm{ahp}} \left(\left\langle V_{\mathrm{I}} \right\rangle - \mathrm{V_K} \right) \mathrm{Ca_I} - \frac{\mathrm{I_I}}{\eta \mathrm{g_{I2}}} + \frac{r_0}{\eta}
\end{aligned}
\tag{2.31}
$$

where $\eta = 1 + (\mathrm{c_I}/\mathrm{g_{12}})\mathrm{g}^{\mathrm{I}}_{\mathrm{gaba}}(\langle V_{\mathrm{I}} \rangle - \mathrm{V_I})\tau_{\mathrm{gaba}}\mathrm{C_I}/1000$. Finally, by substituting r_{I} (Equation 2.31) in the expressions of $I_{\mathrm{total,1}}(t)$, $I_{\mathrm{total,2}}(t)$ (Equations 2.27 and 2.28), the system is reduced to two populations (Figure 2.2C).

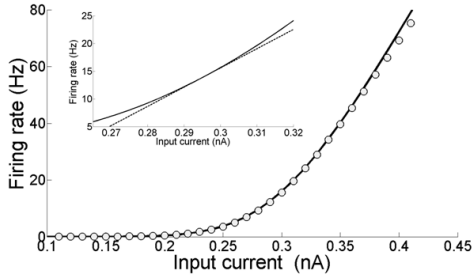

Figure 2.4 Input – output function of an interneuron
The line is plot of the first- passage time formula of a LIF model with σ = 4.2 (Equation 2.14), while the circles correspond to the fit of Equation 2.15. In the inset, a close up is drawn (solid line) and the line an approximation using Equation 2.30 (dashed line).

Ca^{2+} concentration of interneurons as a function of the level of neuronal adaptation

If we consider spike- frequency adaptation to the inhibitory interneurons, the model consists of five variables, two average synaptic gating variables, $S_{1,2}$, of the selective populations, two average Ca^{2+} concentration gating variables of the selective populations, $\mathrm{Ca}_{1,2}$, and one of the inhibitory population, $\mathrm{Ca_I}$. In order to further reduce the system of equations, we assume that the Ca^{2+} concentration of the inhibitory population is constant in time at different levels of neuronal adaptation, since it changes only by a modest amount. The dependence of $\mathrm{Ca_I}$ on the level of neuronal adaptation is found by simulating the full biophysically

plausible network, as we did in section *Constant activity of non- selective excitatory neurons* for the mean firing rate of the non- selective population. More specifically, the Ca_I was calculated by averaging the last 5 s of each 10 s- trial, and then by averaging over 100 trials. In Figure 2.5A, we present Ca_I as a function of the level of neuronal adaptation at different recurrent connectivities for an additional external stimulus to both selective populations of 40 Hz (a stimulus strength used in the simulations in Chapter 3). In Figure 2.5B, we present Ca_I as a function of the level of neuronal at different external inputs for a recurrent connectivity of $w_+ = 1.68$ (the recurrent connectivity used in the simulations in Chapter 3). After fitting a quadratic function to the plot $Ca_I = f(g_{ahp})$ for recurrent connectivity $w_+ = 1.68$, and without external stimulus (black line in Figure 2.5B), we find:

$$Ca_I = 2.1\times10^{-5} g_{gahp}^2 + 8.4\times10^{-4} g_{ahp} + 0.025 \qquad (2.32)$$

In Figures 2.5A and 2.5B, it is apparent that the shape of this function does not change significantly under different conditions, but it is shifted to higher values at higher stimuli. Nevertheless, for simplicity, we neglected this increase and we considered Equation 2.32 approximated by the value 0.025 for all g_{AHP}, i.e. $Ca_I = 0.025$ for all conditions. The consequence of this assumption is that we consider higher inhibition to the selective populations. However in Figures 3.2C, 3.2D, 3.5C, and 3.5D where we compare the reduced model with the spiking model, we show that both models behave similarly.

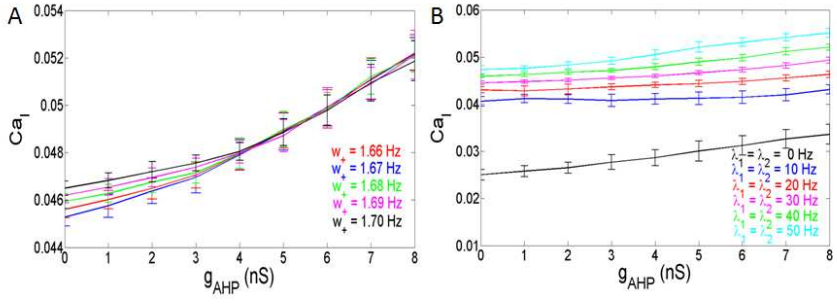

Figure 2.5 Mean gating variable Ca_I
(A) *Average gating variable Ca_I emulating the Ca^{2+} concentration of the inhibitory population as a function of the level of adaptation at different recurrent connectivities for external stimulus $\lambda_1 = \lambda_2 = 40$ Hz.* ***(B)*** *The average gating variable Ca_I as a function of the level of neuronal adaptation at different external stimuli for recurrent connectivity $w_+ = 1.68$.*

Reduced four-variable model

As described in the previous sections, we consistently reduced a full biophysically plausible spiking network, with spike-frequency adaptation mechanism implemented, to a four-variable reduced rate model (Figure 2.2C). The dynamical equations characterizing this system are:

$$r_1 = \phi\left(I_{\text{total},1}\right) = \frac{\mathrm{c_E} I_{\text{total},1} - \mathrm{I_E}}{1 - e^{-\mathrm{g_E}\left(\mathrm{c_E} I_{\text{total},1} - \mathrm{I_E}\right)}} \tag{2.33}$$

$$r_2 = \phi\left(I_{\text{total},2}\right) = \frac{\mathrm{c_E} I_{\text{total},2} - \mathrm{I_E}}{1 - e^{-\mathrm{g_E}\left(\mathrm{c_E} I_{\text{total},2} - \mathrm{I_E}\right)}} \tag{2.34}$$

$$\frac{dS_1}{dt} = -\frac{S_1}{\tau_{\text{nmda}}} + \left(1 - S_1\right)\gamma\, \tilde{r}_1 \tag{2.35}$$

$$\frac{dS_2}{dt} = -\frac{S_2}{\tau_{\text{nmda}}} + \left(1 - S_2\right)\gamma \tilde{r}_2 \tag{2.36}$$

$$\frac{d\,\mathrm{Ca}_1}{dt} = -\frac{\mathrm{Ca}_1}{\tau_{\mathrm{Ca}}} + \rho\, \tilde{r}_1 \tag{2.37}$$

$$\frac{d\,\mathrm{Ca}_2}{dt} = -\frac{\mathrm{Ca}_2}{\tau_{\mathrm{Ca}}} + \rho \tilde{r}_2 \tag{2.38}$$

The total inward currents to the populations are given by

$$\begin{aligned} I_{\text{total},1} = {} & J_{\mathrm{N},11} S_1 - J_{\mathrm{N},12} S_2 + J_{\mathrm{A},11} r_1 - J_{\mathrm{A},12} r_2 - \lambda \mathrm{Ca}_1 + \kappa \mathrm{Ca}_1 \\ & + I_0 + I_{\text{stim},1} + I_{\text{noise},1} \end{aligned} \tag{2.39}$$

$$\begin{aligned} I_{\text{total},2} = {} & J_{\mathrm{N},22} S_2 - J_{\mathrm{N},21} S_1 + J_{\mathrm{A},22} r_2 - J_{\mathrm{A},21} r_1 - \lambda \mathrm{Ca}_2 + \kappa \mathrm{Ca}_{\mathrm{I}} \\ & + I_0 + I_{\text{stim},2} + I_{\text{noise},2} \end{aligned} \tag{2.40}$$

where

$$\begin{aligned} J_{\mathrm{N},11} = {} & g^{\mathrm{E}}_{\text{gaba}} \left(\left\langle V_{\mathrm{E}} \right\rangle - \mathrm{V_I}\right) \frac{\tau_{\text{gaba}}}{1000} \mathrm{C_I} \frac{\mathrm{c_I}}{\eta \mathrm{g_{I2}}} g^{\mathit{eff},\mathrm{I}}_{\text{nmda}} \left\langle V_{\mathrm{I}} \right\rangle f\, \mathrm{C_E} \\ & - g^{\mathit{eff},\mathrm{E}}_{\text{nmda}} \left\langle V_{\mathrm{E}} \right\rangle f\, \mathrm{C_E}\, w_+ \end{aligned} \tag{2.41}$$

$$J_{\mathrm{N},22} = J_{\mathrm{N},11} \tag{2.42}$$

$$J_{\mathrm{N},12} = g^{eff,\mathrm{E}}_{\mathrm{nmda}} \langle V_{\mathrm{E}} \rangle f \mathrm{C}_{\mathrm{E}} w_{-} - g^{\mathrm{E}}_{\mathrm{gaba}} \left(\langle V_{\mathrm{E}} \rangle - \mathrm{V}_{\mathrm{I}} \right) \frac{\tau_{\mathrm{gaba}}}{1000} \mathrm{C}_{\mathrm{I}} \frac{\mathrm{c}_{\mathrm{I}}}{\eta \mathrm{g}_{\mathrm{I2}}} g^{eff,\mathrm{I}}_{\mathrm{nmda}} \langle V_{\mathrm{I}} \rangle f \mathrm{C}_{\mathrm{E}} \tag{2.43}$$

$$J_{\mathrm{N},21} = J_{\mathrm{N},12} \tag{2.44}$$

$$J_{\mathrm{A},11} = g^{\mathrm{E}}_{\mathrm{gaba}} \left(\langle V_{\mathrm{E}} \rangle - \mathrm{V}_{\mathrm{I}} \right) \frac{\tau_{\mathrm{gaba}}}{1000} \mathrm{C}_{\mathrm{I}} \frac{\mathrm{c}_{\mathrm{I}}}{\eta \mathrm{g}_{\mathrm{I2}}} g^{\mathrm{I}}_{\mathrm{ampa}} \langle V_{\mathrm{I}} \rangle \frac{\tau_{\mathrm{ampa}}}{1000} f \mathrm{C}_{\mathrm{E}} - g^{\mathrm{E}}_{\mathrm{ampa}} \langle V_{\mathrm{E}} \rangle \frac{\tau_{\mathrm{ampa}}}{1000} f \mathrm{C}_{\mathrm{E}} w_{+} \tag{2.45}$$

$$J_{\mathrm{A},22} = J_{\mathrm{A},11} \tag{2.46}$$

$$J_{\mathrm{A},12} = g^{\mathrm{E}}_{\mathrm{ampa}} \langle V_{\mathrm{E}} \rangle \frac{\tau_{\mathrm{ampa}}}{1000} f \mathrm{C}_{\mathrm{E}} w_{-} - g^{\mathrm{E}}_{\mathrm{gaba}} \left(\langle V_{\mathrm{E}} \rangle - \mathrm{V}_{\mathrm{I}} \right) \frac{\tau_{\mathrm{gaba}}}{1000} \mathrm{C}_{\mathrm{I}} \frac{\mathrm{c}_{\mathrm{I}}}{\eta \mathrm{g}_{\mathrm{I2}}} g^{\mathrm{I}}_{\mathrm{ampa}} \langle V_{\mathrm{I}} \rangle \frac{\tau_{\mathrm{ampa}}}{1000} f \mathrm{C}_{\mathrm{E}} \tag{2.47}$$

$$J_{\mathrm{A},21} = J_{\mathrm{A},12} \tag{2.48}$$

$$\lambda = \lambda' \tilde{g}_{\mathrm{ahp}}, \quad \text{where } \lambda' = \left(\langle V_{\mathrm{E}} \rangle - \mathrm{V}_{\mathrm{K}} \right) \tag{2.49}$$

$$\kappa = \kappa' \tilde{g}_{\mathrm{ahp}}, \quad \kappa' = g^{\mathrm{E}}_{\mathrm{gaba}} \left(\langle V_{\mathrm{E}} \rangle - \mathrm{V}_{\mathrm{I}} \right) \frac{\tau_{\mathrm{gaba}}}{1000} \mathrm{C}_{\mathrm{I}} \frac{\mathrm{c}_{\mathrm{I}}}{\eta \mathrm{g}_{\mathrm{I2}}} \left(\langle V_{\mathrm{I}} \rangle - \mathrm{V}_{\mathrm{K}} \right) \tag{2.50}$$

$$I_0 = l \cdot r_{\mathrm{ext}} + m \cdot r_{\mathrm{ns}} + n \cdot \psi_{\mathrm{ns}} + g^{\mathrm{E}}_{\mathrm{gaba}} \left(\langle V_{\mathrm{E}} \rangle - \mathrm{V}_{\mathrm{I}} \right) \frac{\tau_{\mathrm{gaba}}}{1000} \mathrm{C}_{\mathrm{I}} \left(\frac{\mathrm{I}_{\mathrm{I}}}{\eta \mathrm{g}_{\mathrm{I2}}} - \frac{\mathrm{r}_0}{\eta} \right) \tag{2.51}$$

$$l = g^{\mathrm{E}}_{\mathrm{gaba}} \left(\langle V_{\mathrm{E}} \rangle - \mathrm{V}_{\mathrm{I}} \right) \frac{\tau_{\mathrm{gaba}}}{1000} \mathrm{C}_{\mathrm{I}} \frac{\mathrm{c}_{\mathrm{I}}}{\eta \mathrm{g}_{\mathrm{I2}}} g^{\mathrm{I}}_{\mathrm{ampa,ext}} \langle V_{\mathrm{I}} \rangle \frac{\tau_{\mathrm{ampa}}}{1000} \mathrm{C}_{\mathrm{ext}} - g^{\mathrm{E}}_{\mathrm{ampa,ext}} \langle V_{\mathrm{E}} \rangle \frac{\tau_{\mathrm{ampa}}}{1000} \mathrm{C}_{\mathrm{ext}} \tag{2.52}$$

$$m = g^{\mathrm{E}}_{\mathrm{gaba}} \left(\langle V_{\mathrm{E}} \rangle - \mathrm{V}_{\mathrm{I}} \right) \frac{\tau_{\mathrm{gaba}}}{1000} \mathrm{C}_{\mathrm{I}} \frac{\mathrm{c}_{\mathrm{I}}}{\eta \mathrm{g}_{\mathrm{I2}}} g^{\mathrm{I}}_{\mathrm{ampa}} \langle V_{\mathrm{I}} \rangle \frac{\tau_{\mathrm{ampa}}}{1000} (1-2f) \mathrm{C}_{\mathrm{E}} - g^{\mathrm{E}}_{\mathrm{ampa}} \langle V_{\mathrm{E}} \rangle \frac{\tau_{\mathrm{ampa}}}{1000} (1-2f) \mathrm{C}_{\mathrm{E}} w_{-} \tag{2.53}$$

$$n = g^{\mathrm{E}}_{\mathrm{gaba}}\left(\langle V_{\mathrm{E}}\rangle - \mathrm{V_I}\right)\frac{\tau_{\mathrm{gaba}}}{1000}\mathrm{C_I}\frac{\mathrm{c_I}}{\eta \mathrm{g_{I2}}}g^{eff,\mathrm{I}}_{\mathrm{nmda}}\langle V_{\mathrm{I}}\rangle(1-2f)\mathrm{C_E} - g^{eff,\mathrm{E}}_{\mathrm{nmda}}\langle V_{\mathrm{E}}\rangle(1-2f)\mathrm{C_E}w_{-} \tag{2.54}$$

$$I_{\mathrm{stim},1} = J_{\mathrm{A,ext}}\cdot\lambda_1 = -g^{\mathrm{E}}_{\mathrm{ampa,ext}}\langle V_{\mathrm{E}}\rangle\frac{\tau_{\mathrm{ampa}}}{1000}\lambda_1 \tag{2.55}$$

$$I_{\mathrm{stim},2} = J_{\mathrm{A,ext}}\cdot\lambda_2 = -g^{\mathrm{E}}_{\mathrm{ampa,ext}}\langle V_{\mathrm{E}}\rangle\frac{\tau_{\mathrm{ampa}}}{1000}\lambda_2 \tag{2.56}$$

$$\eta = 1 + \frac{\mathrm{c_I}}{\mathrm{g_{I2}}}g^{\mathrm{I}}_{\mathrm{gaba}}\left(\langle V_{\mathrm{I}}\rangle - \mathrm{V_I}\right)\frac{\tau_{\mathrm{gaba}}}{1000}\mathrm{C_I} \tag{2.57}$$

$$g^{eff,\mathrm{E,I}}_{\mathrm{nmda}} = \frac{g^{\mathrm{E,I}}_{\mathrm{nmda}}}{1+e^{-0.062\langle V_{\mathrm{E,I}}\rangle}/3.57} \tag{2.58}$$

$$\psi_{\mathrm{ns}} = \frac{\gamma\tau_{\mathrm{nmda}}r_{\mathrm{ns}}/1000}{1+\gamma\tau_{\mathrm{nmda}}r_{\mathrm{ns}}/1000} \tag{2.59}$$

where N is the total number of neurons in the spiking network, $\mathrm{C_E} = 0.8N$, $\mathrm{C_I} = 0.2N$ are the numbers of the excitatory (E) and inhibitory (I) neurons, $\mathrm{C_{ext}} = 800$ is the external excitatory connections, and $f = 0.15$. The rest of the parameters are: $\mathrm{c_E} = 310$ (Hz/nA), $\mathrm{g_E} = 0.16$ s, $\mathrm{I_E} = 125$ Hz, $\mathrm{c_I} = 615$ Hz/nA, $\mathrm{I_I} = 177$ Hz, $\gamma = 0.641$, $\tau_{\mathrm{nmda}} = 100$ ms, $\tau_{\mathrm{Ca}} = 600$ ms, $\alpha = 0.005$, $\langle V_{\mathrm{E}}\rangle = -53.4$ mV, $\langle V_{\mathrm{I}}\rangle = -52.1$ mV, $\mathrm{V_I} = -70$ mV, $\mathrm{V_K} = -80$ mV, $r_{\mathrm{ext}} = 3$ Hz, $r_{\mathrm{ns}} = 2$ Hz, $\tau_{\mathrm{ampa}} = 2$ ms, $\tau_{\mathrm{gaba}} = 10$ ms, $\mathrm{g_{12}} = 1.7876$, $\mathrm{r_0} = 11.3721$ Hz, $\mathrm{g^{ext,E}_{ampa}} = 0.0021$ μS, $\mathrm{g^{E}_{ampa}} = 0.1/N$ (μS), $\mathrm{g^{E}_{nmda}} = 0.3/N$ (μS), $\mathrm{g^{E}_{gaba}} = 1.3/N$ (μS), $\mathrm{g^{ext,I}_{ampa}} = 0.00162$ μS, $\mathrm{g^{I}_{ampa}} = 0.086/N$ (μS), $\mathrm{g^{I}_{nmda}} = 0.258/N$ (μS), $\mathrm{g^{I}_{gaba}} = 1/N$ (μS), $\tilde{g}_{\mathrm{ahp}} = \mathrm{g_{ahp}}/1000$ (μS), and $\mathrm{Ca_I} = 0.025$. In e.g. Chapter 3, we used $w_+ = 1.68$ ($w_- = 0.88$) while $\mathrm{g_{ahp}}$ (nS) defines the level of neuronal adaptation, one of the parameters that we mainly vary.

Noise, $I_{\mathrm{noise},i}$ where $i = 1, 2$ stands for neuronal population 1 and 2, is modeled as white noise**,** filtered by the fast time constant of AMPA synapses, and described by an Ornestein-Uhlenbeck process ***(Uhlenbeck & Ornstein 1930)***

$$\tau_{\mathrm{ampa}}\frac{dI_{\mathrm{noise},i}(t)}{dt} = -I_{\mathrm{noise},i}(t) + \eta(\mathrm{t})\sqrt{\tau_{\mathrm{ampa}}\sigma^2_{\mathrm{noise}}} \tag{2.60}$$

where η(t) is a Gaussian white noise with zero mean and unit variance and σ^2_{noise} is the variance of the noise. Here, $n \equiv \sigma_{noise}$ defines the level of noise, and is the other parameter that we mainly varied.

Effective transfer function

It is not trivial to solve Equations 2.33 - 2.40 since the mean firing rates are given by their inputs through the transfer function (Equations 2.33 and 2.34), and the inputs are themselves dependent on the mean firing rates (Equations 2.39 and 2.40). To overcome this difficulty of self- consistency calculations, we found (as in ***Wong & Wang 2006***), an effective transfer function $\Lambda(I_{total})$. We start by defining four variables:

$$x_1 = J_{N,11}S_1 - J_{N,12}S_2 + I_0 + I_{stim,1} \tag{2.61}$$

$$x_2 = J_{N,22}S_2 - J_{N,21}S_1 + I_0 + I_{stim,2} \tag{2.62}$$

$$x_3 = \lambda Ca_1 - \kappa Ca_I \tag{2.63}$$

$$x_4 = \lambda Ca_2 - \kappa Ca_I \tag{2.64}$$

Then, according to Equations 2.39 and 2.40, in the noise-free case, Equations 2.33 and 2.34 can be written as:

$$r_1 - \frac{c_E(x_1 - x_3 + J_{A,11}r_1 - J_{A,12}r_2) - I_E}{1 - e^{-g_E\left(c_E(x_1 - x_3 + J_{A,11}r_1 - J_{A,12}r_2) - I_E\right)}} = 0 \tag{2.65}$$

$$r_2 - \frac{c_E(x_2 - x_4 + J_{A,22}r_2 - J_{A,21}r_1) - I_E}{1 - e^{-g_E\left(c_E(x_2 - x_4 + J_{A,22}r_2 - J_{A,21}r_1) - I_E\right)}} = 0 \tag{2.66}$$

Equations 2.65 and 2.66 define a system which we can numerically solve for different sets of the variables x_1, x_2, x_3 and x_4. We then fit r_1 and r_2 with an equivalent transfer function, which depends on the new variables:

$$\begin{aligned} r_1 &= \Lambda_1(x_1, x_2, x_3, x_4) \\ &= \frac{a(J_{A,11})x_1 - f_A(J_{A,12}, x_2 - x_4) - e(J_{A,11})x_3 - b(J_{A,11})}{1 - e^{-d(J_{A,11})\left(a(J_{A,11})x_1 - f_A(J_{A,12}, x_2 - x_4) - e(J_{A,11})x_3 - b(J_{A,11})\right)}} \end{aligned} \tag{2.67}$$

$$r_2 = \Lambda_2\left(x_1, x_2, x_3, x_4\right)$$
$$= \frac{a\left(J_{A,22}\right)x_2 - f_A\left(J_{A,21}, x_1 - x_3\right) - e\left(J_{A,22}\right)x_4 - b\left(J_{A,22}\right)}{1 - e^{-d\left(J_{A,22}\right)\left(a\left(J_{A,22}\right)x_2 - f_A\left(J_{A,21}, x_1 - x_3\right) - e\left(J_{A,22}\right)x_4 - b\left(J_{A,22}\right)\right)}} \quad (2.68)$$

where $J_{A,11} = J_{A,22}$, $J_{A,12} = J_{A,21}$ and

$$a = 239400 \cdot J_{A,11} + 270 \quad \text{(Hz/nA)} \quad (2.69)$$

$$b = 97000 \cdot J_{A,11} + 108 \quad \text{(Hz)} \quad (2.70)$$

$$d = -30 \cdot J_{A,11} + 0.154 \quad \text{(s)} \quad (2.71)$$

$$e = 301000 \cdot J_{A,11} + 270 \quad \text{(Hz/nA)} \quad (2.72)$$

$$f_A(J_{A,12}, y) = J_{A,12}\left(-276y + 106\right)\theta(y - 0.4) \quad \text{(Hz)} \quad (2.73)$$

where $\theta(x)$ is the Heaviside function. Note that the parameters a, b, d and the function f_A are the same as in the two-variable reduced model of **Wong and Wang** (**2006**, supplementary information D) where there is no spike- frequency adaptation in the neurons ($x_3 = x_4 = 0$). In that case, our four- variable reduced model coincides with the two- variable reduced model of **Wong and Wang** (**2006**). In order to also consider spike-frequency adaptation, we included parameter e, which we approximated as linearly dependent on $J_{A,11}$ with parameters chosen to fit the numerical solutions. In Figure 2.6A, the average firing rate of population 1 is plotted as a function of x_1 by numerically solving Equation 2.65 (line), and by fitting Equation 2.67 (circles). In Figure 2.6B the average firing rate of population 1 is plotted as a function of x_1 for different couplings through AMPA synapses (from right to left: $J_{A,11} = J_{A,22} = 0$, 0.0005, 0.001, 0.0025 nA). As the couplings $J_{A,11}$, $J_{A,22}$ increase, the gain of the effective transfer function also does. The effective transfer functions Λ_1, Λ_2 do not change no matter how the network parameters (recurrent connectivities, synaptic conductances, stimulus strength) change. Finally, our four-variable reduced rate model is given by Equations 2.67, 2.68, 2.61 - 2.64, 2.35 - 2.38 and 2.60. The noise terms $I_{noise,1}$, $I_{noise,2}$ were included in the variables x_1, x_2 respectively.

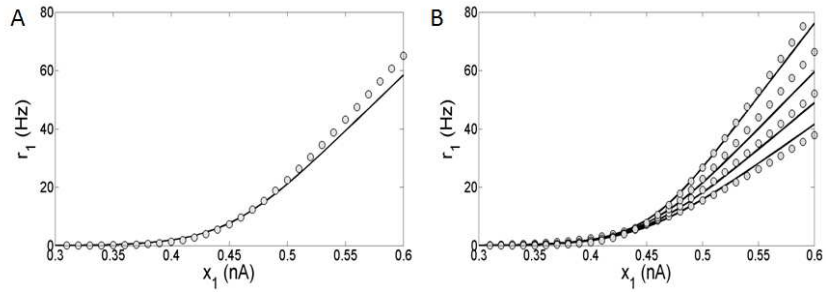

Figure 2.6 Input-output function of one selective population
(A) *The line is numerical solution of Equation 2.65 and the circles are fit of the effective transfer function Equation 2.67.* ***(B)*** *Numerical solutions (lines) and fits (circles) as in A for different couplings through AMPA synapses: from right to left* $J_{A,11} = J_{A,22} = 0, 0.0005, 0.001, 0.0015$ *nA/Hz.*

2.4 Analytical expressions for second- order statistics

Single neuron discharges in association cortices represent reliably the content of visual consciousness. However, it is unknown if emergent functional ensemble properties like the structure of interneuronal firing correlations constrain the population coding accuracy during subjective perception. In Chapter 5 we study the observed decorraled discharges during subjective perceptual dominance of a preferred stimulus, in the macaque LPFC, compared to significantly correlated fluctuations in the same population during perception of the same pattern without competition. Theoretically, the most adequate model to employ in order to study second- order statistics is a spiking network model. Nevertheless, it can sometimes be computationally expensive to employ a large scale network when it comes to parameter search in order to investigate the different dynamical regimes of the network. The mean field reduction, presented previously, is not an appropriate alternative candidate, because the activity of the whole population is described by one variable; its mean firing rate.

We overcome this obstacle by expanding the mean field reduction, considering N neurons, in each population, modeled as dynamic mean-field based rate models. We then can use the augmented method of moments ***(Hasegawa 2003a, 2033b, 2004a, 2004b, 2008, 2009; Deco & Marti 2007a, 2007b; Martinez-Cancino & Sotero 2011; Ponce-Alvarez***

et al., 2013). The augmented method of moments provides an analytical way to calculate the first three moments of a system of stochastic equations: the mean firing rate, μ, of each neuronal ensemble, the averaged firing rate fluctuations, γ, of each population and the average covariance between pairs of neurons, within each population or across populations.

Here, we extend this method to two populations of N neurons each, modeled as dynamic mean- field based rate models, with spike- frequency adaptation (Figure 2.7); neural population E1, where neurons are selective to one visual stimulus and neural population E2, where neurons are selective to a different visual stimulus. There is all- to- all connectivity and neurons within each ensemble are connected with self- excitation w_+ (arrows), between ensembles with cross- inhibition w_- (dashed lines ending to circles) and have spike-frequency adapting mechanism based on Ca2+-activated K+ hyperpolarizing currents (lines ending to circles, where g_{AHP} is the level of neural adaptation). Each neuron is modeled according to the consistent derivation, presented previously (§2.3), from the biophysically realistic network, presented previously (§2.2). Here, we do not consider AMPA synapses, for simplicity. Each neuron receives a background input, and an external input which represents the presentation of a visual stimulus (λ_1 (or λ_2) in Figure 2.7, where β_1 (or β_2) is the level of noise)

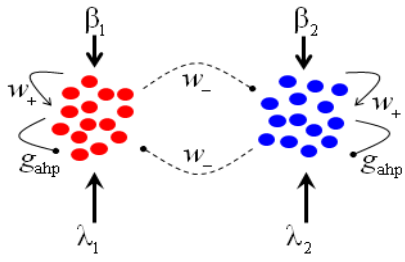

Figure 2.7 Augmented method of moments: Network description
Network of two neural ensembles with self- excitation w_+ (arrows) and cross inhibition w_- (dashed lines ending to circles) and neuronal adaptation g_{AHP} (lines ending to circles). Each ensemble is consisted of N neurons selective to the same stimulus.

Dynamics of neuron *i* in a given ensemble *m*, is described by

$$\frac{dx_{ki}^{m}(t)}{dt} = -\frac{x_{ki}^{m}(t)}{\tau_k} + \left(1 - x_{ki}^{m}(t)\right)\gamma\Phi\left(u_i^m\right) + \xi_i \tag{2.74}$$

$$\frac{dx_{li}^{m}(t)}{dt} = -\frac{x_{li}^{m}(t)}{\tau_l} + \rho\Phi\left(u_i^m\right) \tag{2.75}$$

where $i = 1, \ldots, N$, m = E1, E2, x^m_{kl} is the synaptic gating variable (fraction of open channels) of the neuron i in the ensemble m and it is analogous to the firing rate. x^m_{li} is the the gating variable emulating the cytoplasmic Ca^{2+} concentration in neuron i of the ensemble m. ξ_i denotes additive independent Gaussian white noise source which satisfies $< \xi_i(t) > = 0$ and $< \xi_i(t)\xi_j(t') > = \beta^2\delta(t - t')\delta_{ij}$, where we define β as the level of noise. $\tau = 2$ ms, is the decay time constant of AMPA mediated synaptic currents and $\gamma = 6.41\times10^{-4}$. Φ, is the gain function given by

$$\Phi\left(u_i^m\right) = \frac{cu_i^m - d}{1 - e^{-g(cu_i^m - d)}} \tag{2.76}$$

where c = 310 Hz/nA, d = 125 Hz, g = 0.16 s and the input to neural population i is

$$u_i^m = \frac{w_+}{N_m}\sum_j^{N_m} x_{kj}^m - \frac{w_-}{N_n}\sum_j^{N_n} x_{kj}^n - \lambda x_{lj}^m + I \tag{2.77}$$

where $I = I_0 + J_{A,ext}\lambda$, I_0 is the background input, λ is the external input and $J_{A,ext} = 0.0025$.

Given the local variables x^m_{pi} ($p = k$, l and m = 1, 2) we define global variables for each assembly m as

$$X_p^m(t) = \frac{1}{N}\sum_i x_{pi}^m(t) \tag{2.78}$$

their means, variances and covariances are

$$\mu_p^m(t) = \left\langle X_p^m(t)\right\rangle_{trials} = \frac{1}{N_m}\sum_i \left\langle x_{pi}^m(t)\right\rangle_{trials} \tag{2.79}$$

$$\gamma_{kl}^m(t) = \frac{1}{N_m}\sum_i \left\langle \delta x_{ki}^m(t)\delta x_{li}^m(t)\right\rangle_{trials} \tag{2.80}$$

$$\rho_{kl}^{mn}(t) = \left\langle \delta X_k^m(t) \delta X_l^n(t) \right\rangle_t = \frac{1}{N_m N_n} \sum_i \sum_j \left\langle \delta x_{ki}^m(t) \delta x_{lj}^n(t) \right\rangle_{trials} \tag{2.81}$$

where $\delta X_p^m(t) = X_p^m(t) - \mu_p^m(t)$ and $\delta x_{pi}^m(t) = x_{pi}^m(t) - \mu_p^m(t)$.

Assuming that the noise intensity β is small, we express Equation 2.74 in a Taylor expansion of δx^m_{ki}, and Equation 2.75 of δx^m_{li}, as

$$\frac{dx_{ki}^m}{dt} = f^{mk}\left(u_m^*\right) + \sum_j^{N_m} \frac{\partial f^{mk}}{\partial x_{kj}^m} \delta x_{kj}^m + \sum_j^{N_n} \frac{\partial f^{mk}}{\partial x_{kj}^n} \delta x_{kj}^n + \frac{\partial f^{mk}}{\partial x_{li}^m} \delta x_{li}^m + \xi_i^m \tag{2.82}$$

$$\frac{dx_{li}^m}{dt} = f^{ml}\left(u_m^*\right) + \sum_j^{N_m} \frac{\partial f^{ml}}{\partial x_{kj}^m} \delta x_{kj}^m + \sum_j^{N_n} \frac{\partial f^{ml}}{\partial x_{kj}^n} \delta x_{kj}^n + \frac{\partial f^{ml}}{\partial x_{li}^m} \delta x_{li}^m \tag{2.83}$$

where

$$u_m^* = w_{mm}\mu_k^m - w_{mn}\mu_k^n - \lambda\mu_l^m + I \tag{2.84}$$

The differential equations (DEs) for the two first order moments are

$$\frac{d\mu_p^m}{dt} = \frac{1}{N_m} \sum_i^{N_m} \frac{d\left\langle x_{pi}^m \right\rangle}{dt} = f^{mp}\left(u_m^*\right) \tag{2.85}$$

where $p = k, l$. From equations 2.82, 2.85 and 2.83, 2.85 we get DEs for $d\delta x^m_{ki}$ and for $d\delta x^m_{li}$ as

$$\begin{aligned} \frac{d\delta x_{ki}^m}{dt} &= \frac{dx_{ki}^m}{dt} - \frac{d\mu_k^m}{dt} \\ &= \sum_j^{N_m} \frac{\partial f^{mk}}{\partial x_{kj}^m} \delta x_{kj}^m + \sum_j^{N_n} \frac{\partial f^{mk}}{\partial x_{kj}^n} \delta x_{kj}^n + \frac{\partial f^{mk}}{\partial x_{li}^m} \delta x_{li}^m + \xi_{ki}^m \end{aligned} \tag{2.86}$$

$$\begin{aligned} \frac{d\delta x_{li}^m}{dt} &= \frac{dx_{li}^m}{dt} - \frac{d\mu_l^m}{dt} \\ &= \sum_j^{N_m} \frac{\partial f^{ml}}{\partial x_{kj}^m} \delta x_{kj}^m + \sum_j^{N_n} \frac{\partial f^{ml}}{\partial x_{kj}^n} \delta x_{kj}^n + \frac{\partial f^{ml}}{\partial x_{li}^m} \delta x_{li}^m \end{aligned} \tag{2.87}$$

From Equations 2.80, 2.86, and 2.87, we get DEs for $d\gamma^m_{kl}/dt$ as

$$
\begin{aligned}
\frac{d\gamma^m_{kl}}{dt} &= \frac{1}{N_m}\sum_i^{N_m}\left\langle \frac{d\delta x^m_{ki}}{dt}\delta x^m_{li}\right\rangle + \frac{1}{N_m}\sum_i^{N_m}\left\langle \delta x^m_{ki}\frac{d\delta x^m_{li}}{dt}\right\rangle \\
&= \gamma^m_{k\neq l,l}\frac{\partial f^{mki}}{\partial x^m_{k\neq l,i}} + \left(N_m\rho^{mm}_{k\neq l,l} - \gamma^m_{k\neq l,l}\right)\frac{\partial f^{mki}}{\partial x^m_{k\neq l,j}} \\
&\quad + N_{p\neq m}\rho^{p\neq m,m}_{k\neq l,l}\frac{\partial f^{mki}}{\partial x^{p\neq m}_{k\neq l,j}} + \gamma^m_{l\neq k,l}\frac{\partial f^{mki}}{\partial x^m_{l\neq k,i}} \\
&\quad + \gamma^m_{k,k\neq l}\frac{\partial f^{mli}}{\partial x^m_{k\neq l,i}} + \left(N_m\rho^{mm}_{k,k\neq l} - \gamma^m_{k,k\neq l}\right)\frac{\partial f^{mli}}{\partial x^m_{k\neq l,j}} \\
&\quad + N_{p\neq m}\rho^{m,p\neq m}_{k,k\neq l}\frac{\partial f^{mli}}{\partial x^{p\neq m}_{k\neq l,j}} + \gamma^m_{k,l\neq k}\frac{\partial f^{mli}}{\partial x^m_{l\neq k,i}} + \delta_{k\neq l,l}\beta^2
\end{aligned}
\tag{2.88}
$$

From Equations 2.81, 2.86, and 2.87, we get DEs for $d\rho^{mm}{}_{kl}/dt$ as

$$
\begin{aligned}
\frac{d\rho^{mn}_{kl}}{dt} &= \frac{1}{N_m N_n}\sum_i^{N_m}\sum_j^{N_n}\left\langle \frac{d\delta x^m_{ki}}{dt}\delta x^n_{li}\right\rangle + \frac{1}{N^2}\sum_i^{N_m}\sum_j^{N_n}\left\langle \delta x^m_{ki}\frac{d\delta x^n_{li}}{dt}\right\rangle \\
&= \rho^{mn}_{k\neq l,l}\frac{\partial f^{mki}}{\partial x^m_{k\neq l,i}} + \left(N_m - 1\right)\rho^{mn}_{k\neq l,l}\frac{\partial f^{mki}}{\partial x^m_{k\neq l,j}} \\
&\quad + N_{p\neq m}\rho^{p\neq m,n}_{k\neq l,l}\frac{\partial f^{mki}}{\partial x^{p\neq m}_{k\neq l,j}} + \rho^{mn}_{k\neq l,l}\frac{\partial f^{mki}}{\partial x^m_{l\neq k,i}} \\
&\quad + \rho^{mn}_{k,k\neq l}\frac{\partial f^{nli}}{\partial x^n_{k\neq l,i}} + \left(N_n - 1\right)\rho^{mn}_{k,k\neq l}\frac{\partial f^{nli}}{\partial x^n_{k\neq l,j}} \\
&\quad + N_{p\neq n}\rho^{m,p\neq n}_{k,k\neq l}\frac{\partial f^{nli}}{\partial x^{p\neq m}_{k\neq l,j}} + \rho^{mn}_{k,l\neq k}\frac{\partial f^{nli}}{\partial x^n_{l\neq k,i}} + \delta^{mn}_{k\neq l,l}\frac{\beta^2}{N_m}
\end{aligned}
\tag{2.89}
$$

Equations 2.84, 2.85, 2.88 and 2.89 is a system of 29 coupled equations; 2.84, four equations for means ($\mu^m{}_1$, $\mu^m{}_2$, $\mu^n{}_1$, $\mu^n{}_2$), eight equations for variances ($\gamma^m{}_{11}$, $\gamma^m{}_{12}$, $\gamma^m{}_{22}$, $\gamma^m{}_{21}$, $\gamma^n{}_{11}$, $\gamma^n{}_{12}$, $\gamma^n{}_{22}$, $\gamma^n{}_{21}$) and sixteen equations for covariances ($\rho^{mm}{}_{11}$, $\rho^{mm}{}_{12}$, $\rho^{mm}{}_{22}$, $\rho^{mm}{}_{21}$, $\rho^{nn}{}_{11}$, $\rho^{nn}{}_{12}$, $\rho^{nn}{}_{22}$, $\rho^{nn}{}_{21}$, $\rho^{mn}{}_{11}$, $\rho^{mn}{}_{12}$, $\rho^{mn}{}_{22}$, $\rho^{mn}{}_{21}$, $\rho^{nm}{}_{11}$, $\rho^{nm}{}_{12}$, $\rho^{nm}{}_{22}$, $\rho^{nm}{}_{21}$).

Finally, the correlated variability of the neural activity inside an ensemble, m, is given by ***(Hasegawa 2004b, 2009; Ponce-Alvarez et al. 2013)***

$$
S^m_{kk}(t) = \frac{N\rho^{mm}_{kk}/\gamma^m_{kk} - 1}{N-1} \tag{2.90}
$$

which is 0 for completely asynchronous state and 1 for completely synchronous state.

In Chapter 5, we employ the augmented method of moments also for the network without cross- inhibition, $w_- = 0$. In this case Equations 2.74 - 2.76 are the same but Equation 2.77 becomes

$$u_i^m = \frac{w_+}{N_m}\sum_j^{N_m} x_{kj}^m - \lambda x_{lj}^m + I_0 \tag{2.91}$$

where m = E1 (or E2). The DEs for means, variances and covariances of each neural population are

$$\frac{d\mu_p^m}{dt} = f^{mp}\left(u_m^*\right) \tag{2.92}$$

where $p = k, l$ and

$$u_m^* = w_{mm}\mu_k^m - \lambda\mu_l^m + I \tag{2.93}$$

$$\begin{aligned}\frac{d\gamma_{kl}^m}{dt} &= \gamma_{k\neq l,l}^m \frac{\partial f^{mki}}{\partial x_{k\neq l,i}^m} + \left(N_m\rho_{k\neq l,l}^{mm} - \gamma_{k\neq l,l}^m\right)\frac{\partial f^{mki}}{\partial x_{k\neq l,j}^m} \\ &+ \gamma_{l\neq k,l}^m \frac{\partial f^{mki}}{\partial x_{l\neq k,i}^m} + \gamma_{k,k\neq l}^m \frac{\partial f^{mli}}{\partial x_{k\neq l,i}^m} + \left(N_m\rho_{k,k\neq l}^{mm} - \gamma_{k,k\neq l}^m\right)\frac{\partial f^{mli}}{\partial x_{k\neq l,j}^m} \\ &+ \gamma_{k,l\neq k}^m \frac{\partial f^{mli}}{\partial x_{l\neq k,i}^m} + \delta_{k\neq l,l}\beta^2\end{aligned} \tag{2.94}$$

$$\begin{aligned}\frac{d\rho_{kl}^{mm}}{dt} &= \rho_{k\neq l,l}^{mm} \frac{\partial f^{mki}}{\partial x_{k\neq l,i}^m} + \left(N_m - 1\right)\rho_{k\neq l,l}^{mm}\frac{\partial f^{mki}}{\partial x_{k\neq l,j}^m} + \rho_{k\neq l,l}^{mm}\frac{\partial f^{mki}}{\partial x_{l\neq k,i}^m} \\ &+ \rho_{k,k\neq l}^{mm}\frac{\partial f^{mli}}{\partial x_{k\neq l,i}^m} + \left(N_m - 1\right)\rho_{k,k\neq l}^{mm}\frac{\partial f^{mli}}{\partial x_{k\neq l,j}^m} + \rho_{k,l\neq k}^{mm}\frac{\partial f^{mli}}{\partial x_{l\neq k,i}^m} \\ &+ \delta_{k\neq l,l}^{mm}\frac{\beta^2}{N_m}\end{aligned} \tag{2.95}$$

Equations 2.92 - 2.95 is a system of eleven equations for each population; 2.93, two equations for means ($\mu^m{}_1$, $\mu^m{}_2$), four equations for variances ($\gamma^m{}_{11}$, $\gamma^m{}_{12}$, $\gamma^m{}_{22}$, $\gamma^m{}_{21}$) and four equations for covariances ($\rho^{mm}{}_{11}$, $\rho^{mm}{}_{12}$, $\rho^{mm}{}_{22}$, $\rho^{mm}{}_{21}$).

Equations 2.85, 2.88 and 2.89 are written in a highly compact way. For simplification, when $w_- \neq 0$, and $m = \mathrm{E1} \equiv \mathrm{a}$, they are presented in Figures 2.8 - 2.11.

$$u_a^* = w_{aa}\mu_k^a - w_{ab}\mu_k^b - \lambda\mu_l^a + I_a$$

$$\Phi_a = \frac{cu_a^* - d}{1 - e^{-g(cu_a^* - d)}}$$

$$\Phi_a' = \frac{c}{1 - e^{-g(cu_a^* - d)}} - \frac{cg\left(cu_a^* - d\right)e^{-g(cu_a^* - d)}}{\left(1 - e^{-g(cu_a^* - d)}\right)^2}$$

Figure 2.8 Input and transfer function

$$\frac{d\mu_k^a}{dt} = -\frac{\mu_k^a}{\tau_k} + \left(1 - \mu_k^a\right)\gamma\Phi_a$$

$$\frac{d\mu_l^a}{dt} = -\frac{\mu_l^a}{\tau_l} + \rho\Phi_a$$

Figure 2.9 Mean firing rate and adaptation

$$\frac{d\gamma_{kk}^a}{dt} = -2\gamma_{kk}^a\left(\frac{1}{\tau_k} + \gamma\Phi_a\right) + \left(1 - \mu_k^a\right)\gamma\Phi_a'\left[2w_{aa}\rho_{kk}^{aa} - w_{ab}\left(\rho_{kk}^{ba} + \rho_{kk}^{ab}\right) - \lambda\left(\gamma_{lk}^a + \gamma_{kl}^a\right)\right] + \beta_a^2$$

$$\frac{d\gamma_{ll}^a}{dt} = -\frac{2\gamma_{kk}^a}{\tau_l} + \rho\Phi_a'\left[w_{aa}\left(\rho_{kl}^{aa} + \rho_{lk}^{aa}\right) - w_{ab}\left(\rho_{kl}^{ba} + \rho_{lk}^{ab}\right) - 2\lambda\gamma_{ll}^a\right]$$

$$\frac{d\gamma_{kl}^a}{dt} = -\gamma_{kl}^a\left(\frac{1}{\tau_k} + \frac{1}{\tau_l} + \gamma\Phi_a\right) + \left(1 - \mu_k^a\right)\gamma\Phi_a'\left[w_{aa}\rho_{kl}^{aa} - w_{ab}\rho_{kl}^{ba} - \lambda\gamma_{ll}^a\right] + \rho\Phi_a'\left[w_{aa}\rho_{kk}^{aa} - w_{ab}\rho_{kk}^{ab} - \lambda\gamma_{kl}^a\right]$$

$$\frac{d\gamma_{lk}^a}{dt} = -\gamma_{lk}^a\left(\frac{1}{\tau_k} + \frac{1}{\tau_l} + \gamma\Phi_a\right) + \left(1 - \mu_k^a\right)\gamma\Phi_a'\left[w_{aa}\rho_{lk}^{aa} - w_{ab}\rho_{lk}^{ab} - \lambda\gamma_{ll}^a\right] + \rho\Phi_a'\left[w_{aa}\rho_{kk}^{aa} - w_{ab}\rho_{kk}^{ba} - \lambda\gamma_{lk}^a\right]$$

Figure 2.10 Mean firing rate and adaptation variances

$$\frac{d\rho_{kk}^{aa}}{dt} = -2\rho_{kk}^{aa}\left(\frac{1}{\tau_k} + \gamma\Phi_a\right)$$
$$+ \left(1-\mu_k^a\right)\gamma\Phi_a'\left[2w_{aa}\rho_{kk}^{aa} - w_{ab}\left(\rho_{kk}^{ba}+\rho_{kk}^{ab}\right) - \lambda\left(\rho_{kk}^{aa}+\rho_{kl}^{aa}\right)\right] + \frac{\beta_a^2}{N}$$

$$\frac{d\rho_{ll}^{aa}}{dt} = -2\frac{\rho_{ll}^{aa}}{\tau_l} + \rho\Phi_a'\left[w_{aa}\left(\rho_{kl}^{aa}+\rho_{lk}^{aa}\right) - w_{ab}\left(\rho_{kl}^{ba}+\rho_{lk}^{ab}\right) - 2\lambda\rho_{ll}^{aa}\right]$$

$$\frac{d\rho_{kk}^{ab}}{dt} = -\rho_{kk}^{ab}\left(\frac{2}{\tau_k} + \gamma\Phi_a + \gamma\Phi_b\right) + \left(1-\mu_k^a\right)\gamma\Phi_a'\left[w_{aa}\rho_{kk}^{ab} - w_{ab}\rho_{kk}^{bb} - \lambda\rho_{lk}^{ab}\right]$$
$$+ \left(1-\mu_k^b\right)\gamma\Phi_b'\left[w_{bb}\rho_{kk}^{ab} - w_{ba}\rho_{kk}^{aa} - \lambda\rho_{kl}^{ab}\right]$$

$$\frac{d\rho_{ll}^{ab}}{dt} = -2\frac{\rho_{kk}^{ab}}{\tau_l} + \rho\Phi_a'\left[w_{aa}\rho_{kl}^{ab} - w_{ab}\rho_{kl}^{bb} - \lambda\rho_{lk}^{ab}\right]$$
$$+ \rho\Phi_b'\left[w_{bb}\rho_{lk}^{ab} - w_{ba}\rho_{lk}^{aa} - \lambda\rho_{ll}^{ab}\right]$$

$$\frac{d\rho_{kl}^{aa}}{dt} = -\rho_{kl}^{aa}\left(\frac{1}{\tau_k} + \frac{1}{\tau_l} + \gamma\Phi_a\right) + \left(1-\mu_k^a\right)\gamma\Phi_a'\left[w_{aa}\rho_{kl}^{aa} - w_{ab}\rho_{kl}^{ba} - \lambda\rho_{ll}^{aa}\right]$$
$$+ \rho\Phi_a'\left[w_{aa}\rho_{kk}^{aa} - w_{ab}\rho_{kk}^{ab} - \lambda\rho_{kl}^{aa}\right]$$

$$\frac{d\rho_{lk}^{aa}}{dt} = -\rho_{lk}^{aa}\left(\frac{1}{\tau_k} + \frac{1}{\tau_l} + \gamma\Phi_a\right) + \left(1-\mu_k^a\right)\gamma\Phi_a'\left[w_{aa}\rho_{lk}^{aa} - w_{ab}\rho_{lk}^{ab} - \lambda\rho_{ll}^{aa}\right]$$
$$+ \rho\Phi_a'\left[w_{aa}\rho_{kk}^{aa} - w_{ab}\rho_{kk}^{ba} - \lambda\rho_{lk}^{aa}\right]$$

$$\frac{d\rho_{kl}^{ab}}{dt} = -\rho_{kl}^{ab}\left(\frac{1}{\tau_k} + \frac{1}{\tau_l} + \gamma\Phi_a\right) + \left(1-\mu_k^a\right)\gamma\Phi_a'\left[w_{aa}\rho_{kl}^{ab} - w_{ab}\rho_{kl}^{bb} - \lambda\rho_{ll}^{ab}\right]$$
$$+ \rho\Phi_b'\left[w_{bb}\rho_{kk}^{ab} - w_{ba}\rho_{kk}^{aa} - \lambda\rho_{kl}^{ab}\right]$$

$$\frac{d\rho_{lk}^{ab}}{dt} = -\rho_{lk}^{ab}\left(\frac{1}{\tau_k} + \frac{1}{\tau_l} + \gamma\Phi_b\right) + \left(1-\mu_k^b\right)\gamma\Phi_b'\left[w_{bb}\rho_{lk}^{ab} - w_{ba}\rho_{lk}^{aa} - \lambda\rho_{ll}^{ab}\right]$$
$$+ \rho\Phi_a'\left[w_{aa}\rho_{kk}^{ab} - w_{ab}\rho_{kk}^{bb} - \lambda\rho_{lk}^{ab}\right]$$

Figure 2.11 Mean covariance between pairs of neurons within and across ensembles for the activity and the adaptation variables

For m = E2 ≡ b the system of equations 2.84, 2.85, 2.88, 2.89 are the same as in Figures 2.8 - 2.11 replacing where a with b, and where b with a. When w_- = 0 the system of equation 2.92 – 2.95, for m = E1 ≡ a, are the same as in Figures 2.8 - 2.11 for $w_{ab} = w_{ba} = 0$, and for m = E2 ≡ b, are the same as in Figures 2.8 - 2.11 for $w_{ab} = w_{ba} = 0$ and replacing where a with b and where b with a.

Finally, we followed a simple stimulation protocol were only one neural ensemble is stimulated (e.g. red, Figure 2.7) and we computed the mean correlated variability over one second, via both directly simulating the stochastic equations, and solving the analytically derived equations with the method of moments, in order to validate the correctness of the derived analytical equations.

More specifically, the stimulation protocol we used was

$$\left.\begin{aligned} \nu_{E1}(t) &= I_0 + \beta_0 \cdot g(t) \\ \nu_{E2}(t) &= I_0 + \beta_0 \cdot g(t) \end{aligned}\right\} \text{ for } \quad 0 \le t < 300\,\text{ms} \tag{2.96}$$

$$\left.\begin{aligned} \nu_{E1}(t) &= I_0 + \lambda' + \beta \cdot g(t) \\ \nu_{E2}(t) &= I_0 + \beta_0 \cdot g(t) \end{aligned}\right\} \text{ for } \quad 300 \le t \le 1300\,\text{ms} \tag{2.97}$$

The parameters we used were: N = 20, g_{AHP} = 22 nS, I_0 = 0.1915, $\lambda' = J_{A,ext}\lambda$, $J_{A,ext}$ = 0.0025, λ = 90 Hz, $\beta_0 = \beta = 9\times10^{-10}$, w_+ = 0.161 and w_- = 0.45 for the network with competition, w_- = 0 for the network without competition. We calculated the mean correlated variability of pool E1 over the time interval 300 ≤ t ≤ 1300 ms, employing both networks (Equations 2.84, 2.85, 2.88, 2.89, 2.90 for the network with competition and Equations 2.90, 2.92 - 2.95 for the network without competition). Varying one of the parameters, while keeping the rest of the parameters constant, we plot the correlated variability (Figure 2.12, lines). We then simulated directly the systems of stochastic equations (Equations 2.74-2.77 for the network with competition and Equations 2.74-2.76, 2.91 for the network without competition) using the Euler's method with time step 0.1 ms, and computed the mean pair-wise correlation (Equation 2.90) of pool E1 over the time interval 300 ≤ t ≤ 1300 ms, using the same parameters as previously and added them in the plots (Figure 2.12, black dots correspond to 100 trials and green dots correspond to 200 trials).

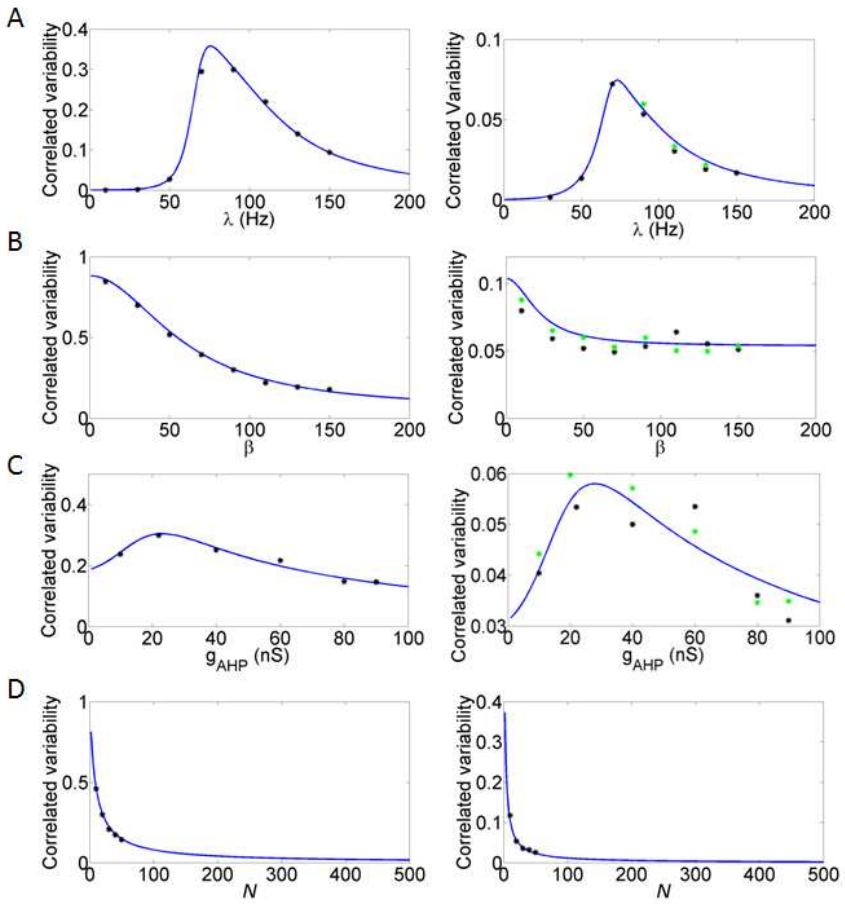

Figure 2.12 Comparison of analytical results with direct simulations
Left: *Network with competition* ***Right:*** *Network without competition* ***A.*** *Correlated variability as a function of the stimulus λ* ***B.*** *Correlated variability as a function of noise intensity β* ***C.*** *Correlated variability as a function of neuronal adaptation* g_{AHP}. ***D.*** *Correlated variability as a function of number of neurons N. Black points are simulated results from the full networks, means over 100 trials, respectively and green points are simulated results from the full networks, means over 200 trials, respectively.*

Note that in Figure 2.12B the noise intensity β is large which may seem contradictory to the initial assumption that noise should be small in order to apply the augmented method of moments to our system of stochastic equations. Actually, the values of β shown in Figure 2.12B are the ones used when solving the analytical expression of the correlated variability, while when we simulated directly the system of the stochastic equations the correspondend values of β were the same as the ones shown in Figure

2.12B multiplied by a factor of 10^{-10}, consistently with our assumption. In addition, the results obtained by solving the analytical equation for the correlated variability do not change when all noises are multiplied by the same factor. In Figure 2.12 we show that the analytically derived equations for second- order statistics are correct since they give same results as the direct simulations of the system of stochastic equations.

Note that how second- order statistics change by stimulus strength (as for example we see in Figure 2.12A) depends on network dynamical state ***(Ponce-Alvarez et al. 2013)***. Finally, our analytical expressions presented in this paragraph provide a useful tool for studying second- order statistics not only in BP, but also in other phenomena of binary perceptual decision making where neural adaptation is relevant, or not.

CHAPTER 3

Microcircuit dynamics mediating Binocular Rivalry[4]

3.1 Introduction

Most of the computational models proposed to account for BR are rate-based models. Biophysically plausible spiking networks have also been put forward *(**Moreno-Bote et al. 2007**; **Laing & Chow, 2002**)*, as well as reduced rate models *(**Laing et al. 2010**)*. Nevertheless, the reduced models presented in **Laing et al. (2010)** for BR were derived heuristically from the spiking network of **Laing and Chow (2002)**. Here, we present, instead, a four-variable reduced model consistently derived from a spiking neuronal network *(**Deco & Rolls 2005; Moreno-Bote et al. 2007**)* with biophysically realistic AMPA, NMDA and GABA receptor-mediated synaptic dynamics, as well as spike-frequency adaptation mechanisms based on Ca^{2+}- activated K^{+} after- hyperpolarization currents *(**Wang 1998; Liu & Wang 2001**)*, using mean field techniques *(**Brunel & Wang 2001; Deco & Rolls 2005; Wong & Wang, 2006**)*. Here, we further reduce the extended mean- field model *(**Deco & Rolls 2005**)* of Brunel and Wang (**2001**) by using a simplified mean field approach introduced by **Wong**

[4] Main results presented here were published in: P. Theodoni, T. I. Panagiotaropoulos*, V. Kapoor*, N. K. Logothetis, and G. Deco (2011), Cortical Microcircuit Dynamics mediating Binocular Rivalry: the role of adaptation in inhibition, *Frontiers in Human Nueroscience, 5, 145, 1-19*. (*equal contribution)

and Wang (**2006**). We thus reduced the original full spiking network of thousands of neurons to a four- variable rate- like model of two neuronal populations each one encoding one of two competing percepts in BR.

Both the spiking network and our four- variable reduced network consider noise and adaptation mechanisms. Our goal was to find out which of them is responsible for the perceptual alternations in BR. We based our study on behavioral data collected from human subjects experiencing BR between orthogonal sinusoidal gratings, which were presented continuously in time. The experimental data used to constrain our model consisted of dominance durations of both percepts, coefficients of variation, and parameters of gamma distribution fits to the distribution of dominance durations. When varying the strength of neuronal adaptation in the absence of noise, different dynamical regimes appear. At low levels of neuronal adaptation the system resides in a bistability regime where switches could happen only due to noise. As adaptation strength is increased, perceptual alternations are possible without noise because the system has entered an oscillatory regime. The transition regime separating the bistability from the oscillatory regime is through a regime of coexistence of stable and unstable limit cycles. By emulating the experimental paradigm for different adaptation strengths and levels of noise, we searched for parameters where our model would replicate the experimental data. In addition, we tested two extreme conditions where all inhibitory interneurons in the original spiking network are adapted or not. We found that, in order to account for the experimental data, and in both conditions, the system operates in the bistability regime near the boundary between noise- driven switches and adaptation- driven oscillations. In addition we show that in this case the model also satisfies Levelt's second revised and fourth propositions.

Interestingly, spike- frequency adaptation of interneurons, apart from decreasing the overall adaptation necessary for the bifurcation to occur when the same stimulus is applied, also influences the system behavior in the absence of a stimulus. When interneurons are not adapted, the two neuronal populations fire asynchronously and at low rates in the spontaneous state. On the contrary, adapted inhibitory interneurons lead the two neuronal populations to a higher firing and oscillatory activity in the absence of stimulus.

3.2 Methods

In the followings, we describe the experimental protocol and results (§3.2.1), designed and obtained by Theofanis I. Panagiotaropoulos, Vishal Kapoor and Nikos K. Logothetis at the Max Plank Institute, Biological Cybernetics in Tübingen. Then, we describe the networks we employed (§3.2.2).

3.2.1 Experimental paradigm & results

During the psychophysical experiment, subjects were presented with flickering (at 18 Hz) orthogonal sinusoidal gratings to the two eyes. The gratings (spatial frequency 2.5 cycles per degree, contrast 20%) were foveally presented on independently linearized monitors facing each other (resolution 1024 x 768 at 72 Hz). The subjects viewed the gratings through a set of angled front-surfaced silver-coated mirrors in a black shielded setup (viewing distance: 118 cm). Typically, subjects underwent 5 - 10 observation periods. Each observation period consisted of a rivalrous stimulation that lasted 100 seconds, with an interval of about 20 seconds between each observation period. During the rivalry period, subjects responded by pressing buttons to report the perceived orientation of the grating or released the buttons when a piecemeal pattern was perceived. Sometimes, multiple datasets were collected on different days from the same subject. From the data collected in each observation period, we calculated the mean dominance time, the coefficient of variation and gamma's distribution parameters λ and r after fitting to the distribution of dominance periods:

$$f(x) = \frac{\lambda^{\mathrm{r}}}{\Gamma(\mathrm{r})} x^{\mathrm{r}-1} e^{-\lambda x}, \quad \Gamma(\mathrm{r}) = \int_0^\infty t^{\mathrm{r}-1} e^{-t} dt \tag{3.1}$$

Where, r is positive real number. Then, for each subject we averaged over all its observation periods. Mean time dominances (Td) ranged between 2.01 and 3.56 s. Coefficient of variations (CV) ranged between 0.418 and 0.704 and the gamma parameter r ranged between 2.251 and 5.446. The range of these values is what we took into account to constrain our model.

3.2.2 Model description

The biophysically inspired spiking model that we employ in this chapter has been described in Chapter 2 (§2.2). In the simulations in the Results, the recurrent connectivity weight used was $w_+ = 1.68$, and, hence, from Equations 2.41 - 2.59, we find $\lambda' = 26.6$ mV, $\kappa' = 31.11$ mV, $I_0 = 0.3553$ nA, $J_{A,11} = J_{A,22} = 9.5402\times10^{-4}$ nA/Hz, $J_{A,12} = J_{A,21} = 7.1258\times10^{-5}$ nA/Hz, $J_{N,11} = J_{N,22} = 0.1497$ nA, $J_{N,12} = J_{N,21} = 0.0276$ nA and $J_{A,ext} = 2.2428\times10^{-4}$ nA/Hz. The only parameter that we slightly changed is the external background input I_0 i.e. we used $I_0 = 0.3536$ nA in order to amplify the basin of attraction of the two unstable fixed points in the absence of stimulus and zero neuronal adaptation strength.

The mean firing rate of each competing population was calculated by averaging r_1 (or r_2) over a time window of 50 ms, which was sliding every 5 ms. For the numerical integration of the differential equations, we used the Euler method with a time step of 0.5 ms. The analysis of the output of the simulations is described in the Results. For the spiking simulations, we used C++ programming, for the four- variable reduced model simulations MATLAB, and for the bifurcation diagrams XPPAUT ***(Ermentrout 1990)***.

3.3 Results

In a recent study, and in order to reproduce experimental data of perceptual bistability, both noise and adaptation mechanisms were implemented in a common framework. It was shown that the working point of the model is at the edge of the bifurcation where the system transits from noise- driven switches to adaptation- driven oscillations ***(Shpiro et al. 2009)***. Here, we come to the same conclusion with our biologically realistic reduced rate model, and we study the effect of adaptation in inhibition.

We started by considering spike- frequency adaptation to all neurons, excitatory pyramidal and inhibitory interneurons. We found that the model replicates the experimental data in a parametric region, where both noise and neuronal adaptation contribute almost in balance. Then, we tested the same for the case where there is no spike- frequency adaptation to the

inhibitory interneurons of the network. Our results show that the system still operates near the bifurcation. However, when interneurons are not adapted, a stronger level of adaptation to the excitatory neurons is necessary for the bifurcation to occur. Furthermore, adaptation of interneurons has a striking effect on the spontaneous state in the absence of stimulus. We found that in the absence of stimulus, if interneurons are adapted, the system transits to an oscillatory regime, while if interneurons are not adapted, it does not. Finally, for the parameters for which the model replicates the experimental data we show that it reproduces Levelt's fourth and second revised proposition.

3.3.1 Spike- frequency adaptation to all neurons of the network

a) Bifurcation diagrams

In the original biologically realistic spiking neuronal network presented in the methods, all excitatory pyramidal neurons and inhibitory interneurons include spike- frequency adaptation. The reduction to the four- variable rate model was derived considering this condition. In Figures 3.1A and 3.1B, we show the bifurcation diagrams where the steady states of the average synaptic gating variable of one of the two neuronal populations are plotted, in the noise- free case, as a function of the level of spike-frequency adaptation, in the absence of stimulus and upon stimulus respectively. The same bifurcation diagrams stand for the other neuronal population due to symmetry in the network. Equations 2.39 and 2.40 indicate that when interneurons include spike-frequency adaptation, there is an additional input to the selective populations due to the term:

$$\kappa Ca_I = g_{gaba}^{E}\left(\langle V_E\rangle - V_I\right)\frac{\tau_{gaba}}{1000}C_I\frac{c_I}{\eta g_{I2}}\left(\langle V_I\rangle - V_K\right)\tilde{g}_{ahp}Ca_I \qquad (3.2)$$

In the absence of external stimulus via a supercritical Hopf- bifurcation, this additional input brings the system to a transition (at g_{ahp} = 11.2 nS) from a stable low firing rate regime to an oscillatory one. At a higher level of adaptation (g_{ahp} = 52.5 nS) the system returns to a new steady state of higher firing rate via another supercritical Hopf- bifurcation. At low levels of adaptation the steady state coexists with two stable and two unstable steady states which disappear in a fold bifurcation at g_{ahp} = 1.4 nS (not shown). In the bifurcation diagrams, stable steady states are represented

by thick lines, and unstable ones by thin lines. The branched curves of circles show the maximum and the minimum oscillation amplitudes of one of the two selective populations when circles are filled. Open circles correspond to unstable oscillations.

In Figures 3.1C and 3.1D, the nullclines $dS_1(t)/dt = 0$, $dS_2(t)/dt = 0$ (whose intersections are the steady states of the system) are plotted in the (S_1,S_2) phase - space of the model, for zero spike- frequency adaptation (g_{ahp} = 0 nS). When neurons do not include spike- frequency adaptation, the phase-spaces of the model resemble the one of the two- variable reduced model ***(Wong & Wang 2006)***.

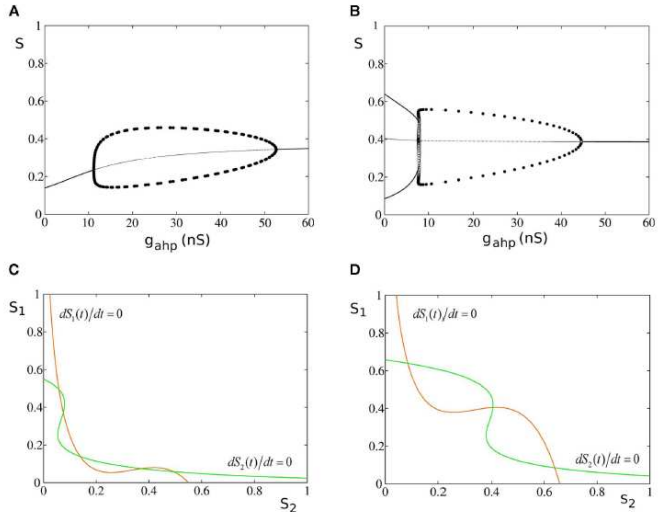

Figure 3.1 Spike – frequency adaptation to all neurons of the network.
A. *Bifurcation diagram in the absence of stimulus. Stable steady states are represented by thick lines while unstable ones by thin lines. Filled circles are the maximum and the minimum amplitudes of stable oscillations. Open circles correspond to unstable oscillations.* ***B.*** *Bifurcation diagram in the presence of stimulus $\lambda_1 = \lambda_2 = 40$ Hz.* ***C.*** *(S_1, S_2) phase - space in the absence of neuronal adaptation and in the absence of stimulus. The nullclines of the synaptic gating variables S1 and S2 are the green and orange lines respectively, and their intersections define the stable and unstable steady states.* ***D.*** *(S_1, S_2) phase- space in the absence of neuronal adaptation but in the presence of stimulus.*

In the absence of stimulus, there are five fixed points (three stable and two unstable) and the system lies in the lower left fixed point where neurons fire at the same low rates (Figure 3.1C). When external stimulus is applied to both populations, the phase- space and the bifurcation diagram (at g_{ahp} =

0 nS) reconfigure (Figure 3.1D). The input here is $\lambda_1 = \lambda_2 = 40$ Hz. The two asymmetrical attractors are separated by an unstable steady state (saddle node), and the system is in a bistability regime. In Figure 3.1B, as the level of adaptation increases, the system first transits to a regime of coexistence of stable and unstable limit cycles ***(Curtu 2010)*** at $g_{ahp} = 7.7$ nS and later to a stable one via two subcritical Hopf- bifurcations at $g_{ahp} = 7.8$ nS. Finally, at $g_{ahp} = 44.5$ nS, the system transits to a stable steady state via a supercritical Hopf- bifurcation.

b) Replicating experimental data

Keeping in mind the bifurcation diagrams, we simulated our reduced four-variable rate model by applying the same stimulation protocol as in the experiment. The input to both populations was $\lambda_1 = \lambda_2 = 40$ Hz. For each level of neuronal adaptation i.e. peak conductance of the Ca^{2+}- activated K^+ channels, g_{ahp}, we applied this stimulus for 100 s. We then calculated the mean time dominance of the two percepts, and the coefficient of variation. After fitting the distribution of time dominances to a gamma distribution, we calculated the parameter r (Equation 3.1). In order to mimic the experimental protocol that each subject underwent, for each g_{ahp}, we performed 10 such trails, and computed the average values of mean time dominance, the coefficient of variation and the r parameter from the gamma distribution fit over these trials. Finally, we did the same with different levels of noise. One dominance period was defined as the time starting when the difference in the firing rates of the two populations was 5 Hz and ended when it became zero. In Figure 3.2A, we present the mean time dominance, and the coefficient of variation for five levels of noise as a function of neuronal adaptation, g_{ahp}. In Figure 3.2B, the r parameter from the gamma distribution fit is plotted as a function of level of neuronal adaptation and for the same levels of noise. The horizontal lines denote the range that the experimental data define. Vertical lines in Figures 3.2A and 3.2B are drawn at the bifurcation points where the system transits from a bistable dynamical regime to an oscillatory one, as presented in the corresponding bifurcation diagram (Figure 3.1B). We are looking for the level of noise and of adaptation at which the model results reside in the range of values defined by the experimental data. The green big circle denotes such levels ($g_{ahp} = 6.2$ nS, $n = 0.016$), and in Figure 3.2C, we plot the mean firing rates of both populations at these levels in

the absence (black and green plots) and upon (blue and red plots) stimulus. For these parameters, the mean time dominance is Td = 3.24 s, the coefficient of variation is CV = 0.457, and r = 2.841.

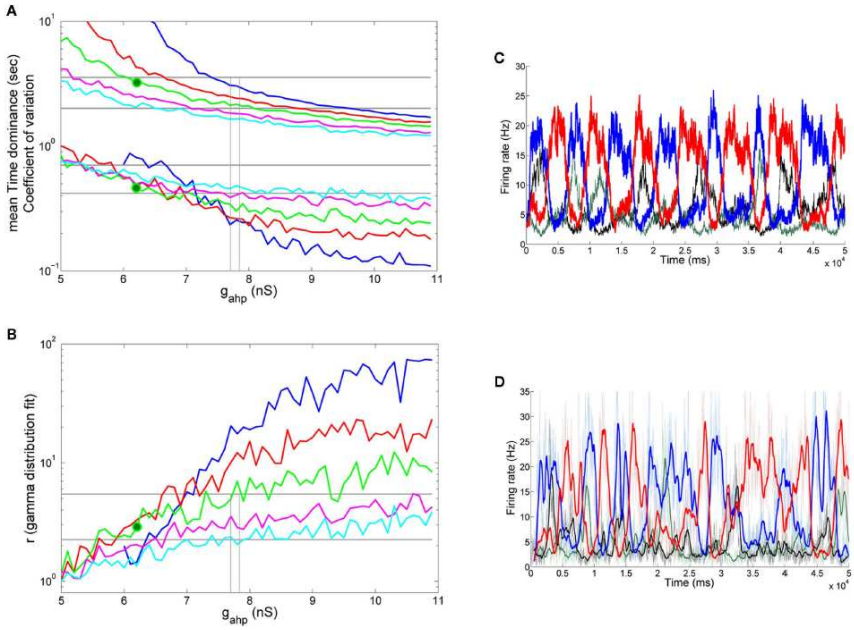

Figure 3.2 Spike- frequency adaptation to all neurons of the network: Replicating the experimental data (1)

A. *Mean time dominance and coefficient of variation as a function of neuronal adaptation for different levels of noise (blue: n = 0.01, red: n = 0.014, green: n = 0.016, magenta: n = 0.018 and celestial: n = 0.019) for* $\lambda_1 = \lambda_2 = 40$ *Hz.* ***B.*** *Parameter r of gamma distribution fit to the distribution of dominance times as a function of neuronal adaptation for the same noise levels as in (A). In both (A, B), horizontal lines denote the range that the experimental data define. Vertical lines are drawn at the bifurcation points where the system transits from a bistable dynamical regime to a regime of coexistence of stable and unstable limit cycles and to an oscillatory regime. Green big circles at the levels* $g_{AHP} = 6.2$ *nS, n = 0.016 indicate a case where the model replicates the experimental data. We find that the model replicates the experimental data in the noise- driven regime and close to the bifurcation.* ***C.*** *The mean firing rate of the selective populations for gahp = 6.2 nS and n = 0.016 in the absence of stimulus (black and green plots) and upon stimulus (blue and red plots).* ***D.*** *The mean firing rate of the selective neuronal populations by simulating the spiking network (with N = 500 neurons) with the same parameters as the ones used simulating the reduced model (C). Thin lines are plots from a trial and thick lines are the same after smoothing. We see that both models exhibit similar behavior in both the presence (blue and red plots) and absence (black and green plots) of the stimulus.*

From our results, it is apparent that both noise and adaptation are the driving forces for the alternations in BR. The working point of our model is in the bistability regime and close to the bifurcation towards the oscillatory. Noise and adaptation contribute almost in balance to the perceptual alternations. At this point, we should note that the level of noise necessary for the model to replicate the experimental data is high enough to drive the system into the oscillatory regime (Figure 3.1A) in the absence of stimulus as one can see in Figure 3.2C (black and green plots).

Moreover, in Figure 3.2D, we plot the mean firing rates of the selective neuronal populations as we compute them by simulating the spiking network with $N = 500$ total neurons, and with the same parameters we used to plot Figure 3.2C. Thin red and blue plots correspond to the activity of the selective populations upon stimulus, and thin black and gray plots to their activity in the absence of stimulus, while thick plots are the corresponding activity after smoothing with a time window of 500 ms (sliding every 50 ms). We see that both the spiking and the reduced model exhibit similar behavior in the presence, as well as in the absence, of the stimulus. This means that the approximations we considered for the derivation of our four-variable reduced rate model (§2.3) are accurate. In addition, for these parameters, we ran 10 trials of 100 s- stimulation. From the smoothed mean firing rates, we computed the average mean time dominance, coefficient of variation and r parameter from the gamma distribution fit to the distribution of the time dominances at each of the 10 trials, as we did with the reduced model. We found mean time dominance Td = 2.82 s, mean coefficient of variation CV = 0.582 and r = 3.137. These values reside in the range defined by the experimental data, similarly as we found with the reduced model. Finally we computed the bifurcation point, where the model transits to the mix-mode oscillatory regime, employing the spiking network. The total number of neurons used was $N = 20000$ in order to decrease the noise in the network as much as possible. The bifurcation point is at $g_{ahp,bif,spiking} = 6$ nS, close to the bifurcation point found with the reduced model ($g_{ahp,bif,reduced} = 7.7$ nS). The $g_{ahp,bif,reduced}$ is higher than the $g_{ahp,bif,spiking}$ due to the assumptions adopted in the Methods but mostly to the advantage of the reduced model to eliminate noise which cannot be done in the spiking network.

Furthermore, we tested the effect of increasing the external stimulus strength ($\lambda_1 = \lambda_2 = 50$ Hz) which would correspond to an increase of the stimulus contrast in the experiment. The rest of the parameters were the same as before, as well as the stimulation protocol and analysis.

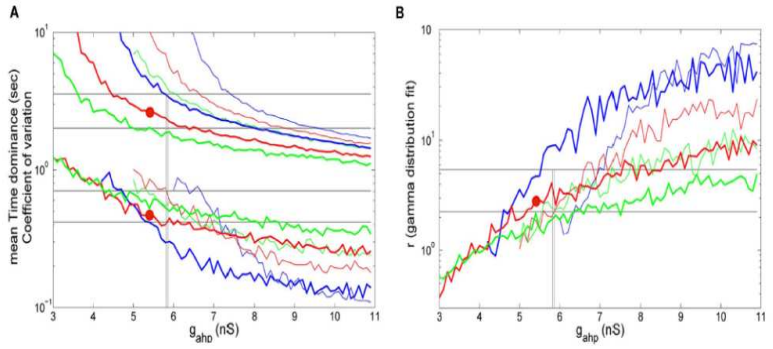

Figure 3.3 Spike- frequency adaptation to all neurons of the network: Replicating the experimental data (2)
A. *Mean time dominance and coefficient of variation as a function of neuronal adaptation for different levels of noise (blue: n = 0.01, red: n = 0.014 and green: n = 0.016) for $\lambda_1 = \lambda_2 = 40$ Hz (thin lines) and $\lambda_1 = \lambda_2 = 50$ Hz (thick lines).* ***B.*** *Parameter r of gamma distribution fit to the distribution of dominance times as a function of neuronal adaptation for the same levels of noise as in (A). In both (A, B), horizontal lines denote the range that the experimental data define. Vertical lines are drawn at the bifurcation points where the system transits from a bistable dynamical regime to a regime of coexistence of stable and unstable limit cycles and to an oscillatory regime. Red big circles at gahp = 5.4 nS, n = 0.014 indicate a case for which the model replicates the experimental data.*

In Figures 8A and 8B (thick lines), we present the results for the same levels of noise, as in Figures 3.2A and 3.2B. We also plot the results for $\lambda_1 = \lambda_2 = 40$ Hz (thin lines) for comparison. Levelt's fourth proposition indicates that increasing the stimulus contrast results in an increase of the average rivalry reversal rate ***(Levelt, 1968)***, which corresponds to a decrease in the average dominance duration. This is apparent in Figure 3.3A for all levels of neuronal adaptation and of noise. In addition, by increasing the strength of the external stimulation, the bifurcation points (vertical lines) shift to lower values, while the regime of coexistence of stable and unstable limit cycles narrows. Nevertheless, the model's results (Td =2.49 s, CV = 0.457 and r = 2.825) reside again in the ranges defined by the experimental data, while working in the bistable regime (big red circle: $g_{ahp} = 5.4$ nS, $n = 0.014$) and close to the bifurcation point

$g_{ahp,bif,reduced}$ = 5.8 nS. Once more, for the same parameters, we simulated the spiking network (with N = 1000 neurons), and found Td = 3.298 s, CV = 0.462 and r = 3.975. These values are close to the ones computed with the reduced model and inside the range of the experimental data. The bifurcation point as calculated by simulating the spiking network with N = 20000 total neurons, is at $g_{ahp,bif,spiking}$ = 4.3 nS.

3.3.2 Spike- frequency adaptation only to excitatory pyramidal neurons of the network

a) Bifurcation diagrams

We removed neuronal adaptation from interneurons by setting $\kappa = 0$ in Equations 2.63 and 2.64. The rest of the parameters of the model remained the same. We note that when interneurons are not adapted, the mean firing rate of the non- selective population and the mean firing rate of the inhibitory population decrease for higher adaptation strengths. Here, we again assume that the mean firing rate of the non- selective population is constant in all conditions, as we had assumed in the case of adapted interneurons (§2.3: *Constant activity of non-selective excitatory neurons*). In addition, and for simplicity, we kept the same parameters of the linearization of the input-output formula (Equation 2.30) as in the case of adapted interneurons. In the following we show that these assumptions do not change the results much.

In Figure 3.4, we present the bifurcation diagram of one of the two neuronal populations in the absence and in the presence of an external stimulus employing our four- variable reduced rate model. The same bifurcation diagrams also stand for the other population due to symmetry. While in the presence of a stimulus, the bifurcation diagram (Figure 3.4B) is qualitatively similar as in the case where we included spike-frequency in interneurons (Figure 3.1B), the bifurcation diagram is qualitatively different in the absence of external stimulus (Figure 3.4A compared to Figure 3.1A). Here, there is no additional input (Equations 2.39, 2.40) to the excitatory populations and the system remains in a stable steady state of low firing rate which decreases as level of neuronal adaptation increases (Figure 3.4A). We note that, as in the case where all neurons are adapted, at low levels of adaptation the steady state coexists with two

stable and two unstable steady states which disappear in a fold bifurcation at $g_{ahp} = 0.36$ nS (not shown).

In Figure 3.4B, stable steady states are represented by thick lines, and unstable ones by thin lines. Filled circles correspond to the maximum and minimum values of stable oscillations, while open circles correspond to unstable oscillations. Upon stimulus presentation, $\lambda_1 = \lambda_2 = 50$ Hz, and at $g_{ahp} = 0$, the system transits from a stable steady state of low firing rate to a winner- take- all regime, where one of the populations fires at high rate while the other fires at low rate. The system reaches the attractor and lies in a bistability regime. Without noise, the system would remain in this attractor, being unable to transit to its anti- symmetrical (i.e. switches in perception are not possible).

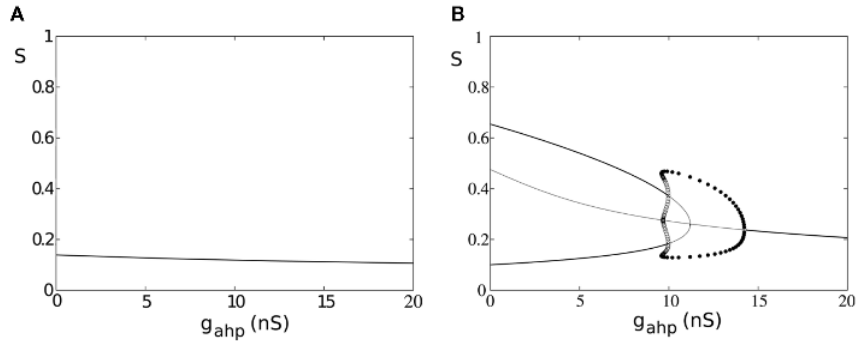

Figure 3.4 Spike- frequency adaptation only to the excitatory pyramidal neurons of the network
A. *Bifurcation diagram in the absence of stimulus, stable steady states are represented by thick lines while unstable ones by thin lines. Filled circles are the maximum and the minimum amplitudes of stable oscillations. Open circles correspond to unstable oscillations.* ***B.*** *Bifurcation diagram in the presence of stimulus $\lambda_1 = \lambda_2 = 50$ Hz.*

As adaptation increases, the basin of attraction decreases, and switches are more likely to occur upon noise introduction. Nevertheless, higher levels of adaptation drive the system into an oscillatory regime where, even in the absence of noise, alternations from one percept to the other are inevitable. More specifically, starting at high values of g_{ahp}, the system lies in a stable steady state where both populations fire at low firing rate. As g_{ahp} decreases, the system transits to a stable oscillatory regime via a supercritical Hopf- bifurcation at $g_{ahp} = 14.2$ nS. At $g_{ahp} = 9{,}96$ nS, the

system transits into a regime of coexistence of stable and unstable limit cycles ***(Curtu, 2010)*** via two subcritical Hopf- bifurcations. The unstable limit cycle and the stable limit cycle annihilate at g_{ahp} = 9.57 nS, via a double saddle-node of limit cycles bifurcation, and the system transits to the bistability regime where two anti-symmetric attractors are separated by a saddle node fixed point. At g_{ahp} = 11.2 nS, the trajectories of the three unstable fixed points coalesce into an unstable fixed point via a subcritical pitch- fork bifurcation. This cumbersome dynamics of the regime of coexistence of stable and unstable limit cycles, although very interesting, is beyond the scope of the present study. The dynamics of our model has similar characteristics as described in ***(Shpiro et al. 2007; Curtu et al. 2008; Curtu 2010)***. A point to note is that, in our case, we also have recurrent excitation resulting in an asymmetry between regimes of release and escape mechanisms with the release regime being small due to the recurrent connectivity in the network ***(Shpiro et al. 2007; Seely & Chow 2011)***.

b) Replicating experimental data

We saw previously that when inhibitory interneurons are adapted, both noise and adaptation are responsible, almost in balance, for the perceptual alternations. Here, we follow the same stimulation protocol and analysis, as in §3.3.1, for the case where inhibitory interneurons are not adapted. With the bifurcation diagram (Figure 3.4B) in mind, we applied the same fixed external stimulus to both populations, $\lambda_1 = \lambda_2$ = 50 Hz. We then computed the mean time dominance, the coefficient of variation and the r-parameter of the gamma distributions fit to the distributions of dominance times, as a function of neuronal adaptation, at different levels of adaptation and of noise. The rest of the parameters are the same except for the exclusion of spike- frequency adaptation from interneurons by setting $\kappa = 0$ in Equations 2.63 and 2.64. The results are presented in Figure 3.5. Different lines correspond to different noise levels. Horizontal lines denote the range that the experimental data define. Vertical lines are drawn at the bifurcation points which define the different dynamical regimes.

In Figures 3.5A and 3.5B, big blue (g_{ahp} = 9.7 nS, n = 0.01), red (g_{ahp} = 9 nS, n = 0.014), green (g_{ahp} = 8.8 nS, n = 0.016), and celestial (g_{ahp} = 8.2

nS, n = 0.019) circles are sets of parameters for which all three mean time dominance, coefficient of variation, and r- parameter reside in the range defined by the experimental data. We find that, in all these cases, the model is in the bistability regime and near to the bifurcation point. We note that it is also possible that for a given noise-level (n = 0.01, blue big circle), experimental data are replicated inside the regime of coexistence of stable and unstable limit cycles. In Figure 3.5C, we plot the mean firing rates of the two neuronal populations when level of noise is n = 0.014, and adaptation strength is g_{ahp} = 9 nS (red big circle in Figures 3.5A and 3.5B) in two conditions: in the absence of stimulus (black and green plots) and upon stimulus (blue and red plots). We see that when interneurons are not adapted neuronal populations fire at low rates and in an asynchronous state in the absence of stimulus.

Moreover, in Figure 3.5D, we plot the mean firing rates of the two selective neuronal populations, as we compute them by simulating the spiking network with N = 500 total neurons, and with the same parameters we used to plot Figure 3.5C. As in the case where we considered adapted inhibitory interneurons (Figures 3.2C and 3.2D), both models behave similarly in the presence and in the absence of the stimulus, indicating that the assumptions adopted for the reduction are accurate. In addition, we computed the mean time dominance, the coefficient of variation and the r-parameter from the gamma distribution fit to the distribution of the time dominances simulating the spiking network (as we did in §3.3.1). We found that the results were in the range defined by the experimental data. More specifically, we found Td = 2.64 ms, CV = 0.463 and r = 5.147, similar to the ones we attained with the reduced model for the same parameters (Td = 3.29 ms, CV = 0.581 and r = 4.992). Finally, we computed the bifurcation point by simulating the spiking network with N = 20000 neurons, and we found that the bifurcation point is at $g_{ahp,bif,spiking}$ = 8.3 nS, close to the bifurcation point we observed with the reduced model ($g_{ahp,bif,reduced}$ = 9.57 nS). As in the case where inhibitory interneurons are also adapted, the $g_{ahp,bif,reduced}$ is higher than the $g_{ahp,bif,spiking}$. This is a consequence of the assumptions adopted for the derivation of the reduced model, as well as of the noise in the spiking network which cannot be totally eliminated.

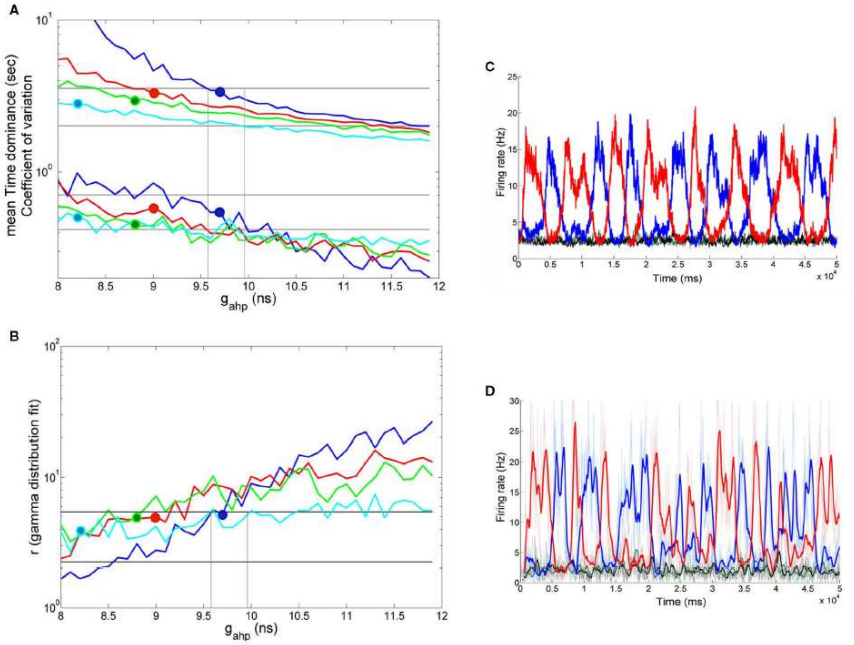

Figure 3.5 Spike- frequency adaptation only to the excitatory pyramidal neurons of the network: Replicating the experimental data
A. *Mean time dominance and coefficient of variation as a function of neuronal adaptation for different levels of noise (blue: n = 0.01, red: n = 0.014, green: n = 0.016, and celestial: n = 0.019) for* $\lambda_1 = \lambda_2 = 50$ *Hz.* ***B.*** *Parameter r of gamma distribution fit to the distribution of dominance times as a function of neuronal adaptation for the same levels of noise as in (A). In both (A, B), horizontal lines denote the range that the experimental data define. Vertical lines are drawn at the bifurcation points where the system transits from a bistable dynamical regime to a regime of coexistence of stable and unstable limit cycles and to an oscillatory regime. Blue, red, green, and celestial big circles at gahp = 9.7 nS, gahp = 9nS, gahp = 8.8 nS, and gahp = 8.2 nS, respectively indicate sets of parameters for which the model replicates the experimental data. We find that the model operates in the bistability regime close to the bifurcation as well as in the regime of coexistence of stable and unstable limit cycles (blue big circle).* ***C.*** *The mean firing rate of the populations for gahp = 9 nS and n = 0.014 in the absence of stimulus (black and green plots) and upon stimulus (blue and red plots).* ***D.*** *The mean firing rate of the selective neuronal populations by simulating the spiking network (with N = 500 neurons) with the same parameters as the ones used in (C). Thin lines are plots from a trial, and thick lines are the same after smoothing. We see that both models exhibit similar behavior in both the presence (blue and red plots) and in the absence (black and green) of the stimulus.*

Furthermore, in Figure 3.6, we plot the mean Td and the coefficient of variation for the two extreme cases, i.e. all interneurons are all (gray lines) or none (black lines) adapted. We plot the results from the simulations

where in both cases the stimulus strength is $\lambda_1 = \lambda_2 = 50$ Hz and the level of noise is $n = 0.014$. We see that by removing spike- frequency adaptation mechanism from interneurons, mean dominance duration and its coefficient of variation increase for the same level of neuronal adaptation to the excitatory neurons. The bifurcation points, where the model transits from noise- driven switches to adaptation driven oscillations, shifts to higher values of g_{ahp}. At the same time, the level of adaptation for which the model replicates the experimental data also increases but resides in both cases within the bistability regime and close to the bifurcation.

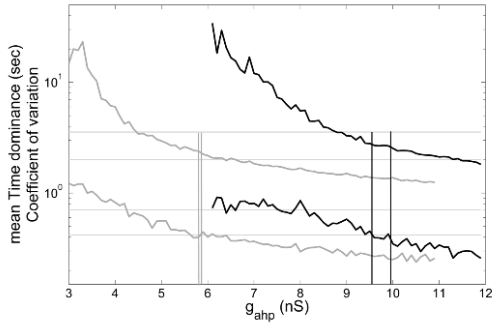

Figure 3.6 Mean time dominance and coefficient of variation as a function of neuronal adaptation
Mean time dominance and coefficient of variation as a function of neuronal adaptation for level of noise n = 0.014, when inhibitory interneurons are adapted (gray lines) and when they are not adapted (black lines) for stimulus strength $\lambda_1 = \lambda_2 = 50$ Hz. Gray and black vertical lines de fine the bifurcation points when inhibitory interneurons are adapted and when they are not, respectively.

3.3.3 Levelt's second revised and fourth proposition

Levelt's four propositions in BR ***(Levelt 1968)*** exemplify how stimulus parameters affect the duration of perception of two conflicting images. These propositions define additional constrains to computational models candidates to explain BR. Most of the times, computational models were tested with Levelt's second and fourth proposition. Recently, Levelt's second proposition has been revised ***(Brascamp et al. 2006)*** and states that, when the contrast of one image changes the average dominance duration of the image with higher contrast is mainly affected. Levelt's fourth proposition states that when the contrast of both images increases,

the average rivalry reversal rate increases, meaning that the mean time dominance of both images decreases.

Here, we tested Levelt's second revised proposition for four sets of noise and neuronal adaptation levels (big blue, red, green and celestial circles in Figures 3.5A and 3.5B) for which the model's results reside in the ranges defined by the experimental data, when inhibitory interneurons are not adapted. The results are shown in Figures 3.7A - 3.7C. In the insets, we tested the same for the case where inhibitory interneurons are adapted with the same level of noise and stimulus strength (big red circle, Figures 3.3A and 3.3B), as when they are not adapted. We first applied equal stimulus for 100 s to both populations of low strength, $\lambda_1 = \lambda_2 = 45$ Hz. We then computed the mean dominance durations of each population and we averaged over 10 such trials. Then, we kept the stimulus to one of the populations fixed, $\lambda_1 = 45$ Hz, and we increased the other. The results are shown in Figure 3.7A. In Figure 3.7B, we applied equal stimulus of intermediate strength to both populations, $\lambda_1 = \lambda_2 = 47.5$ Hz, and we computed the mean time dominance as previously. Then, we kept the stimulus to one population fixed, $\lambda_1 = 47.5$ Hz, and we manipulated the other. Finally, we applied equal stimulus of high strength to both populations, $\lambda_1 = \lambda_2 = 50$ Hz, and computed the mean dominance periods. Then, we kept the stimulus to one of the populations fixed at this high level, $\lambda_1 = 50$ Hz, while we decreased the other (Figure 3.7C). In Figures 3.7A - 3.7C, the dashed lines are plots of the mean time dominance of the population receiving fixed stimulus (λ_1) while solid lines are plots of the mean time dominance of the population receiving variable stimulus (λ_2). Vertical lines denote the stimulus strength when it is equal to both populations. We see that Levelt's second revised proposition is satisfied by all four levels of neuronal adaptation and noise for which our model replicates the experimental data when inhibitory interneurons are not adapted as well as when they are (insets in Figures 3.7A - 3.7C). We should mention though that from **Moreno-Bote et. al** (**2010**), we know that alternation rate is higher and symmetric around equi-dominance, i.e. when external stimulus is equal to both neuronal populations. This would be an additional constrain for the model. In Figure 3.7B, we see that this is not always the case. Nevertheless, in the study by **Moreno-Bote et al.** (**2010**), it is shown that models best replicate this result when normalized stimuli are applied, which is not the case here.

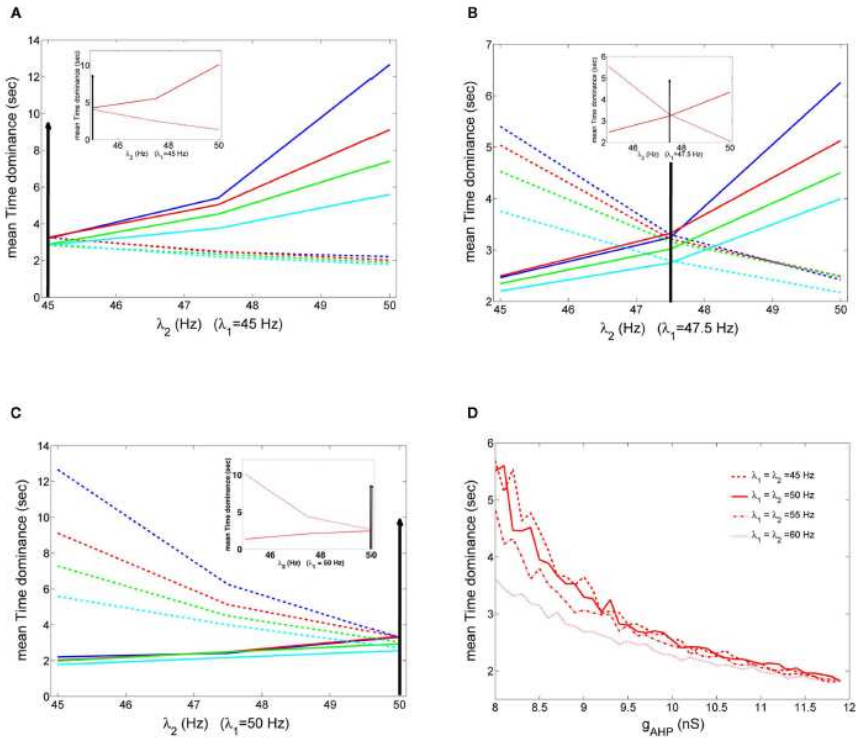

Figure 3.7 Levelt´s propositions
A - C. *Mean time dominance of one of the two neuronal populations of the model receiving fixed stimulus λ_1 (dashed lines) and of the neuronal population receiving variable stimulus λ_2 (solid line), as a function of the variable external stimulus λ_2, for the four noise- adaptation points for which the model replicates the experimental data when interneurons are not adapted (big circles in Figures 3.5A, 3.5B). Arrows denote the starting point where both populations receive the same stimulus, $\lambda_1 = \lambda_2$. In the insets the same are plotted for the case where inhibitory interneurons are adapted (red big circle in Figures 3.3A, 3.3B). A: when $\lambda_1 = 45$ Hz, B: when $\lambda_1 = 47.5$ Hz and C: when $\lambda 1 = 50$ Hz.* ***D.*** *Mean time dominance of both populations for different stimulus strengths when inhibitory interneurons are not adapted and n = 0.014.*

In §3.3.1, we tested Levelt's fourth proposition for two different stimulus strengths in the case where inhibitory interneurons are adapted. Here, we test Levelt's fourth proposition for the case where inhibitory interneurons are not adapted for applied stimulus strengths $\lambda_1 = \lambda_2 = 45, 50, 55, 60$ Hz (Figure 3.7D). Each stimulation lasted 100 s, and at each trial we computed the mean dominance durations of both populations. Finally, we averaged over 10 trials. The level of noise was $n = 0.014$. In Figure 3.7D we see that as stimulus strength increases mean dominance duration

decreases. Thus our model accounts for Levelt's fourth proposition. Note that this decrease is more prominent at low levels of neuronal adaptation and at higher levels of neuronal adaptation mean time dominance is similar across different stimulus strengths.

3.4 Discussion

In this chapter, we present a theoretical approach which could provide novel insights into the microcircuit dynamics responsible for multistable perception. We consistently derived a four- variable reduced rate model from a biologically plausible spiking neuronal network, and we tested it considering experimental behavioral data of BR. We calculated the mean dominance duration of the percepts, the coefficient of variation, and the parameters of the gamma distribution fit to the distribution of dominance durations. We emulated the experiment by simulating our reduced model for different sets of noise and neuronal adaptation levels, and we looked for the optimal ones for which the model replicates the experimental data. In the noise- free condition, the range of adaptation strength defines different dynamical regimes where our model can operate. There is a bistability regime, where switches can only arise due to the implementation of noise. There is a regime of coexistence of stable and unstable limit cycles which is the transition regime of the model from the bistability to the oscillatory regime. Finally, there is an adaptation- driven oscillatory regime where alternations can happen even without noise. By testing different levels of noise and adaptation strengths, we came to the same conclusion as **Shpiro et al.** (**2009**). In order to satisfy the experimental data, the system must operate in the noise- driven regime close to the boundary with the adaptation driven regime. Thus, both mechanisms are responsible in balance for the perceptual alternations.

It is not the first time that a reduced spiking model is used to explain BR. **Laing et al.** (**2010**) recently presented reduced rate- like models derived from a fine scale spiking model consisting of two populations, one excitatory and one inhibitory, of Hodgkin - Huxley type neurons ***(Laing & Chow 2002)***. Neurons are orientation selective, include both spike-frequency adaptation and synaptic depression, and each population can be thought of as lying on a ring. Nevertheless, their reduction is not derived

consistently from the spiking network. Instead it is based on both intuition based on observations of the spiking network, and on data- mining tools to select appropriate variables. By processing the results of simulations, the authors determined functions that govern the dynamics of these variables. Our reduced model, on the other hand, is consistently derived from a spiking network using mean field techniques. In addition, we studied the underlying mechanism responsible for perceptual alternations as **Shpiro et al.** (**2009**), and we extended the results by studying the effect of adapting inhibitory interneurons.

The biophysically realistic spiking network, from which we derived the reduced model, has been previously studied for perceptual bistability ***(Moreno et al. 2007)***. Their spiking network is very similar to ours, but the main difference is that they only include spike- frequency adaptation to excitatory pyramidal cells. Their interesting results show the effect of noise and stimulus strength in the behavior of the network. The novelty of our work is that we implemented a four- variable reduced rate- like model which we derived consistently from a similar biophysically realistic spiking network of thousands of neurons using mean field techniques. More specifically, we performed a further reduction of the extended mean field model ***(Deco & Rolls 2005)***. This helps us understand the dynamics of the full original spiking network, which in turn can provide us with numerous data such as realistic synaptic dynamics, spiking time series, local field potentials, etc.

Moreover, we were able to study two extreme cases by including spike-frequency adaptation in all or in none of the network's inhibitory interneurons. Interestingly, we found that, in both cases, our model replicates the experimental data in the boundary between noise and adaptation. We thus conclude that spike- frequency adaptation of inhibitory interneurons is not relevant to the cause of perceptual alternations observed in BR. However, we demonstrate that adaptation of interneurons has an effect on the parametric space where the bifurcation is observed. When interneurons are not adapted, stronger adaptation is necessary in the remaining components of the network to induce a bifurcation. As a result, more adaptation is necessary to obtain the optimal working point of the system.

Additionally, we found that spike- frequency adaptation in interneurons generates different types of spontaneous dynamics. When the interneurons in the spiking network are not adapted, the selective neuronal populations fire asynchronously and at low rates during the spontaneous state. On the other hand, when interneurons are adapted, the model exhibits an oscillatory regime even during the spontaneous state. This type of oscillatory regime has been reported in an attractor memory network ***(Lundqvist et al., 2010)***. Here, for the set of parameters for which the model replicates the experimental data, noise is high enough to drive the system into the oscillatory regime in the absence of stimulus, when interneurons are adapted.

Furthermore, adapted inhibitory interneurons affect the reaction time at the onset of a stimulus. In Chapter 4, we show that neuronal adaptation accelerates decisions in an adaptation- related aftereffects decision making paradigm. The spiking model studied in that work is similar to the one presented here (when all inhibitory interneurons are adapted). From our four- variable reduced model, we found that when interneurons include spike- frequency adaptation, an additional input to both selective populations is implemented which increases with adaptation strength. This results in a faster ramping activity at higher adaptation strengths, which in turn leads to faster reaction times at the onset of a stimulus. We expect that when interneurons are not adapted, we would have the opposite effect.

We would like to note that we examined two extreme conditions. Either all the inhibitory interneurons of the network are adapted or none of them. Nevertheless, for example in the prefrontal cortex, where neuronal activity follows phenomenal perception ***(Panagiotaropoulos et al. 2012)***, we know that there are three types of interneurons. Half of them are dendritic-targeting, and the others are divided into interneurons targeting, and perisoma targeting ***(Conde et al. 1994; Gabbott et al. 1996)***. Perisoma targeting interneurons do not include spike- frequency adaptation while the rest do include ***(Wang et. al 2004)***. In our network neurons are not considered as multi- compartmental, and we cannot distinguish the inhibitory interneurons among these three types. Nevertheless, a more biophysically plausible condition would be to consider a percentage of adapted inhibitory interneurons.

Levelt's propositions show how mean dominance durations are affected as a function of stimulus strength to both or to one eye. They refer to BR but it has been shown that there is a general validity in other paradigms of visual rivalry, revealing common computational mechanisms ***(Klink et al. 2008b)***. Levelt's propositions, especially the second and the fourth, have been a usual constrain for computational models of BR ***(Wilson 2007; Laing & Chow 2002; Moreno-Bote et al. 2007; Brascamp et al. 2006; Moreno-Bote et al. 2010; Seely & Chow 2011)***. Here, we tested Levelt's fourth proposition in both conditions, where interneurons are all or none adapted. In both conditions, we found that the reduced model satisfies this law. In addition we tested Levelt's second revised proposition ***(Brascamp et al. 2006)***, and found that the model also satisfies this law. We would like to mention that our study was not in full accordance with the recent study of **Moreno-Bote et al.** (**2010**). They showed that competition models like ours better reproduce experimental findings based on Levelt's revised second proposition when the stimuli applied to the populations are normalized, which was not the case in the present work.

In addition, we note that, in this study, we did not check for serial correlations in percept durations. Interestingly, non- zero serial correlations were reported recently in both BR and structure- from motion ambiguity paradigms ***(van Ee 2009)***. Experimental findings in their work were replicated by implementing noise in adaptation of percept- related neurons. It would be interesting to see whether our reduced model can reproduce such serial correlations, and in what conditions. Furthermore, an open and interesting question is the freezing of perception during intermittent presentation of ambiguous stimuli ***(Orbach et al. 1963a, 1963b, 1966; Leopold et al. 2002; Maier et al. 2003)***. Using a reduced model consistently derived from a biologically realistic spiking network one could study the underlying dynamics, and may unravel mechanisms underlying such a phenomenon.

CHAPTER 4

Neuronal Adaptation effects in Decision- Making[5]

4.1 Introduction

Perceptual decision making is a relevant process in daily life and, during the last few decades, there has been an increased interest in understanding its underlying neural mechanisms ***(Shadlen & Newsome 1996; Kim & Shadlen 1999; Wang 2002, 2008; Smith & Ratcliff 2004; Deco & Rolls 2006; Gold & Shadlen 2007; Deco et al. 2009; Wang 2012)***. Several theoretical models have been proposed and used, such as diffusion models ***(Smith & Ratcliff 2004)*** and neuronal models ***(Wang 2002; Deco & Rolls 2006; Wong & Wang 2006; Deco et al. 2009)***. From these studies, we learn that, in multistable systems, decisions are taken due to noise- driven transitions between attractor states, where noise arises from the random spiking of the neurons.

In this chapter, we study a categorical decision process where an ambiguous target stimulus appears with a temporal delay after the presentation of an adaptor stimulus. To this purpose, we consider behavioral data from a high- level, adaptation- related aftereffects experiment ***(Cziraki et al. 2010)***. The behavioral data show that prolonged adaptation to a complex stimulus leads to category- specific aftereffects during the presentation of ambiguous stimulus composites. Hypothesizing

[5] Main results presentated here were published in: P. Theodoni, G. Kovács, M. W. Greenlee, and G. Deco, "Neuronal Adaptation Effects in Decision Making", 2011, *The Journal of Neuroscience 31(1): 234-246*

that neuronal adaptation is relevant for the perceptual judgment, we studied the interaction between noise and neuronal adaptation in this perceptual decision making paradigm. Neuronal adaptation implemented by spike- frequency adaptation reduces the activity of the dominant neuronal population, selective to the adaptor stimulus, leading the nonadapted neuronal population to win the competition when the ambiguous stimulus appears. In contrast, noise- driven fluctuations in the firing rates of the neuronal populations could lead to a switch from one percept to the other. We consider both mechanisms within the same theoretical framework using a spiking neuronal model. We show that neuronal adaptation is the main driving force for the transition from the adaptor category to the novel, opposite category, indicating that the working point of the system is in the oscillatory regime. We thus predict that, if the target ambiguous composite stimulus is presented previously, it will lead to oscillation in perception between the two dissimilar categories. Preliminary experimental evidence confirms our prediction.

Furthermore, we consider, for the first time, the effects of neuronal adaptation in perceptual decision making. To this purpose, we mimic a perceptual task where the same ambiguous composite stimulus ***(Cziraki et al. 2010)*** appears with and without a preceding adaptor. We simulate this task for different levels of sensory evidence in favor of one of the two dissimilar images and for different levels of neuronal adaptation. We show that, at each level of sensory evidence, neuronal adaptation accelerates the decision process.

4.2 Methods

In the followings, we describe the experimental protocol and results (§4.2.1), designed and obtained by Csaba Cziraki, Mark W. Greenlee, and Gyula Kovács at the University of Regensburg, published in **Cziraki et al.** (**2010**). Then, we describe the network we employ (§4.2.2), the stimulations protocols and analysis we used (§4.2.3).

4.2.1 Experimental paradigm & results

In the **Cziraki et al.** (**2010**) study of high- level adaptation- related aftereffects, 13 humans (8 females) were presented with an adaptor

stimulus consisting of a high- contrast female face (face adaptation), a female hand (hand adaptation), or a Fourier randomized version (control condition) for 5 s. After a 200 ms gap (blank screen), an ambiguous, noisy stimulus composite, constructed from an overlapping human face and hand with varying Fourier phase coherences, was shown for 200 ms. Finally, subjects reported which image they perceived (Figure 4.1A).

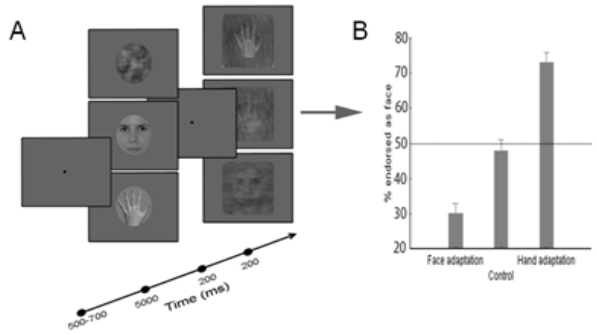

Figure 4.1 Experimental design and behavioral results of the high- level adaptation- related aftereffects task
A*. Experimental design: Subjects were presented with an adaptor stimulus (face or hand adaptation) for 5 s and, after a 200 ms gap (blank screen), with a test stimulus (ambiguous composite image of a face and a hand other than the adaptors) for 200 ms. Subjects reported which image (face or hand) they perceived.* ***B.*** *Behavioral results: Mean ratio of face responses after face, hand, and control (composite image of face and hand) adaptation for ambiguous face/hand composite test stimuli. (Adapted from* ***Cziraki et al. 2010****)*

The experimental data indicated that prolonged exposure to complex stimuli, e.g., adaptation to a face or a hand stimulus, biases perceptual decisions toward the nonadapted, dissimilar stimulus category. The simultaneously observed functional magnetic resonance imaging adaptation (fMRIa) effects in the face- sensitive fusiform face area (FFA) and in the body- sensitive extrastriate body area (EBA) were sorted according to the subject's behavioral responses. The fMRIa data indicated that adaptation to the preferred complex stimulus of the given area led to larger signal reduction on trials when it biased category decisions behaviorally than on trials when it was not effective. Figure 4.1B shows the percentage of trials endorsed as faces for ambiguous face/hand composite test stimuli after face, hand, and control (composite image of face and hand) adaptation. In a control condition, the ambiguous target

stimuli were judged 49% as faces and the remaining times as hands, whereas more trials were judged as faces after hand adaptation (73%). The opposite is true after face adaptation (27%) (Figure 4.1B). This shows that prolonged adaptation to a complex stimulus leads to category-specific aftereffects during the perception of ambiguous stimulus composites. fMRI measurements in the areas of interest (FFA and EBA) ***(Cziraki et al. 2010)*** supported the behavioral data.

4.2.2 Model description

In our model (§2.2), the competing neuronal populations are a hand selective neuronal population corresponding to the high- level body sensitive cortical area EBA ***(Downing et al. 2001)*** and a face- selective one corresponding to the fusiform face- sensitive cortical area FFA ***(Kanwisher et al. 1997)***.

The inhibitory neurons form one population to which we will refer as pool I. The excitatory neurons form three distinct populations. Two of them consist of neurons that encode one or the other complex image. Hence, there is a pool H with neurons, which are selective to the hand images. This neuronal population represents the body - sensitive EBA. There is also a pool F with neurons selective to the face images. This neuronal population represents the face - sensitive FFA.

However, we should not necessarily assume that the selective neuronal pools correspond to the cortical areas FFA and EBA. In fact, the process studied with our model could happen in another brain region and then project the result to the FFA and EBA so that top - down interaction effects could also account for **Cziraki et al.'s** (**2010**) findings.

In addition, to represent the sensory stimulus, meaning presentation of the hand and/or face stimuli, the neurons belonging to the two selective populations (H and F) receive an additional Poisson spike train with invariant time rates λ_H and λ_F, respectively. Input λ_H corresponds to activation of the neurons of the cortical area EBA due to presentation of the hand image and λ_F corresponds to activation of the neurons of the cortical area FFA due to presentation of the face image. Therefore, the total input that each neuron of the selective pools receives is $\nu_{H,F} = \nu_{ext} + \lambda_{H,F}$. To simulate the presentation of the ambiguous composite image of a

hand and a face, the same external input is applied to the two selective neuronal populations: $\lambda_H = \lambda_F \equiv \lambda \leftrightarrow \nu_H = \nu_F$. Throughout this work, λ = 50 Hz unless otherwise stated. To simulate the adaptor stimulus, we add an external input to one of the selective pools, e.g., for H pool: $\lambda_H = \lambda_{adaptor}$, whereas the competitive one receives only background input ν_{ext}. Throughout this study, $\lambda_{adaptor}$ = 200 Hz unless otherwise stated. We followed various stimulation protocols, which are described in detail below.

4.2.3 Stimulation protocols

A: bifurcation diagrams

The spiking model used in this chapter exhibits distinct regimes depending on the free parameters. To gain intuition about how the system transits from one regime to the other, we calculated the firing rate of one selective population first as a function of neuronal adaptation and later as a function of external stimulus. For this purpose, we simulated a task where an ambiguous stimulus [like **Cziraki et al.'s 2010** ambiguous composite image of a hand and a face] is presented continuously in time. Here the number of total neurons of the network is 4000 to eliminate the noise of the system. In this model, noise cannot be explicitly excluded since it arises from the finite number of neurons in the network. Therefore, we performed the same simulation, increasing the total number neurons with a 500 neurons step and in the range of $500 \leq N \leq 4500$, each time defining the bifurcation point, g_{bif}. We saw that for $N > 3000$, the value of g_{bif} did not change > 1%.The neurons of selective pools H and F, for this task, receive a Poisson spike train with an invariant firing rate of: $\nu_H = \nu_F = \nu_{ext}$ + 0 Hz for $0 \leq t \leq 500$ ms and $\nu_H = \nu_F = \nu_{ext} + \lambda$ Hz for $500 \leq t \leq 10{,}000$ ms.

We performed this simulation for different levels of adaptation corresponding to the conductance g_{AHP}, ranging from 0 to $g_{AHP,max}$ = 12 nS for w_+ = 1.65 and λ = 50 Hz, to show how the system transits from bistability to an oscillatory regime. In addition, we simulated the same task for different levels of external stimulus λ (neuronal adaptation $g_{AHP,max}$ = 10 nS and recurrent connectivity w_+ = 1.65) to show how the system transits from a spontaneous state to an oscillatory regime.

Spontaneous state is defined as the state when the firing rates of both selective pools are < 10 Hz. The parameter space of w_+ and g_{AHP} for which the system remains in the spontaneous state in the absence of external input (Figure 4.3) is described in detail in *Parameter range of w_+ and g_{AHP}*, below. This parameter space also describes the dependence of the upper limit of the level of neuronal adaptation, $g_{AHP,max}$, on the recurrent synaptic weight, w_+, of the selective populations.

B: replication of the experiment

To replicate the experimental design under discussion, during the first 500 ms the external input to both pools is $\lambda_H = \lambda_F = 0$ Hz, representing the absence of competing stimuli in the first stage of the experimental task. During this period, the network exhibits spontaneous activity of 3 Hz for excitatory pools and 9 Hz for the inhibitory pool. For the next 4500 ms, which is the period of presentation of adaptor stimulus, we set the value of external stimulus to the pool corresponding to the hand image equal to $\lambda_H = \lambda_{adaptor} = 200$ Hz and set the external input to pool F as $\lambda_F = 0$ Hz. Then both external inputs are set to 0Hz ($\lambda_H = \lambda_F \equiv \lambda = 0$ Hz) for a period of 200 ms and to 50 Hz for the last 200 ms of the cue ($\lambda_H = \lambda_F \equiv \lambda = 05$ Hz), which corresponds to the presentation of the ambiguous composite image of a hand and a face. Summarizing the stimulation protocol in this case (Figure 4.2) is as follows:

$$
\begin{aligned}
& v_H = v_F = v_{ext} && \text{for} \quad 0 \le t \le 500 \ \text{ms} \\
& \left.\begin{aligned} v_H &= v_{ext} + \lambda_{adaptor} \\ v_F &= v_{ext} \end{aligned}\right\} && \text{for} \ 500 \le t \le 5000 \ \text{ms} \\
& v_H = v_F = v_{ext} && \text{for} \, 5000 < t \le 5200 \, \text{ms} \\
& v_H = v_F = v_{ext} + \lambda && \text{for} \, 5200 < t \le 5400 \, \text{ms}
\end{aligned}
$$

The total number of neurons of the network is 2000 to take into account the noise of the network. The recurrent synaptic connectivity is $w_+ = 1.65$. We performed 100 trials and calculated the mean ratio of face and hand responses after hand adaptation in the EBA for each value of the level of adaptation, g_{AHP}. We did the same for 10 series of 100 trials and calculated the mean percentage performance at each. We averaged over the 10 series and calculated the standard deviations (SDs). A face response occurs when the firing rate of selective pool F at $t = 5400$ ms is >

10 Hz (because spontaneous state is typically below this value) and surpasses the firing rate of selective pool H at the same time by at least 5 Hz. Hand responses were defined as non- face responses, i.e., total number of trials minus number of face responses.

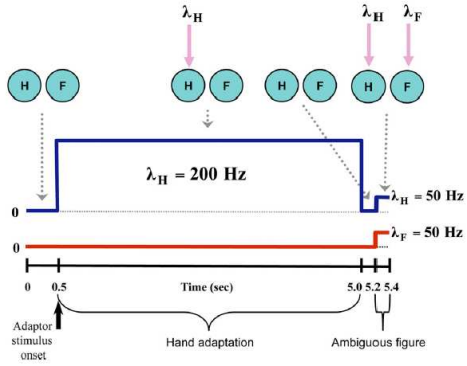

Figure 4.2 Stimulation protocol: adaptation- related aftereffects
During the first 500 ms, the external input to both pools is $\lambda_H = \lambda_F = 0$ Hz to represent the absence of competing stimuli in the first stage of the psychophysical task. During this period, the network exhibits spontaneous activity (3 Hz for the excitatory pools and 9 Hz for the inhibitory pools). For the next 4500 ms, we set the value of the external stimulus to the pool corresponding to the hand stimulus equal to $\lambda_H = 200$ Hz and $\lambda_F = 0$ Hz, corresponding to the hand adaptation process. For a period of 200 ms, both external stimuli are set to zero, $\lambda_H = \lambda_F = 0$ Hz, which corresponds to the post- adaptation blank period used by ***Cziraki et al. (2010)****. For the last 200 ms, both are set to 50 Hz, $\lambda_H = \lambda_F = 50$ Hz, which corresponds to the presentation of the ambiguous test stimulus (composite image of a hand and a face). The colored circles represent the different neural populations.*

C: decision making, reaction time

In this part of our study, we examined the effects of neuronal adaptation in a binary decision- making task. To this purpose, we simulated an experiment similar to **Cziraki et al. (2010)** with and without a preceding adaptor. The proposed experiment corresponds to the presentation of an ambiguous composite image of a hand and face that is gradually changed over trials to one of the two interpretations by increasing the contrast of one image (e.g., the face) in different blocks of trials. We simulated this by introducing a bias between the external inputs to selective pools H and F by increasing the level of sensory evidence to pool F and decreasing it to pool H at each set of simulations. Decision- making, without adaptor, is shown as:

$$
\begin{aligned}
&v_H = v_F = v_{ext} && \text{for} \quad 0 \le t \le 3000 \text{ ms} \\
&\left.\begin{aligned} v_H &= v_{ext} + \lambda - \Delta\lambda \\ v_F &= v_{ext} + \lambda + \Delta\lambda \end{aligned}\right\} && \text{for } 3000 < t \le 6500 \text{ ms}
\end{aligned}
$$

We refer to this stimulation protocol as decision making without adaptor because there is no stimulation of one selective pool preceding the decision- making task. We also examined the model with an adaptor stimulus preceding the target [i.e., where pool H is stimulated initially as in **Cziraki et al.'s** (**2010**) experiment]. Decision- making, with adaptor, is shown as:

$$
\begin{aligned}
&v_H = v_F = v_{ext} && \text{for} \quad 0 \le t \le 500 \text{ ms} \\
&\left.\begin{aligned} v_H &= v_{ext} + \lambda_{adaptor} \\ v_F &= v_{ext} \end{aligned}\right\} && \text{for} \quad 500 \le t \le 5000 \text{ ms} \\
&v_H = v_F = v_{ext} && \text{for } 5000 \le t \le 5200 \text{ ms} \\
&\left.\begin{aligned} v_H &= v_{ext} + \lambda - \Delta\lambda \\ v_F &= v_{ext} + \lambda + \Delta\lambda \end{aligned}\right\} && \text{for } 5200 \le t \le 6500 \text{ ms}
\end{aligned}
$$

We performed 1000 simulations for the decision- making task without adaptor, and 100 simulations for the decision- making task with adaptor. In both cases, we calculated the mean firing rates of both selective populations, the mean time needed for pool F to win the competition with pool H, and the percentage of correct performance on correct trials (when pool F won pool H) as a function of ΔI, where $\Delta I = 2\,\Delta\lambda$. In addition, we performed the same simulations varying the level of adaptation. In the decision- making task without a preceding adaptor, neuronal adaptation is varied within the range $0 \le g_{AHP} \le 12$ nS, whereas $w_+ = 1.65$ and $\lambda = 50$ Hz. In the decision- making task with a preceding adaptor, we studied three different levels of neuronal adaptation, where for each level the remaining free parameters were the same as those used in the model coinciding with the **Cziraki et al.** (**2010**) experiment ($w_+ = 1.65$, $\lambda = 50$ Hz, $\lambda_{adaptor} = 300$ Hz for $g_{AHP} = 9$ nS, $\lambda_{adaptor} = 200$ Hz for $g_{AHP} = 10$ nS, and $\lambda_{adaptor} = 160$ Hz for $g_{AHP} = 11$ nS). When the system is in the bistable region, a correct trial is defined as the trial in which the firing rate of pool F is > 10 Hz and surpasses the mean firing rate of pool H by at least 5 Hz. In this case, the network eventually falls into the attractor that represents

percept of the face image. When the system is in the oscillatory region, a correct trial is defined as the trial in which the firing rate of pool F is > 10 Hz and surpasses first the firing rate of pool H by at least 5 Hz. Decision times are defined as the times for which these criteria are first fulfilled minus the onset time of 3000 ms in the without adaptor case and minus the first 5200 ms in the with-adaptor case. When the system is in the bistable region, the firing rates are defined as the maximum value of the winning population's neural activity and minimum value of the losing population's neural activity, averaged over correct trials for each level of adaptation and sensory evidence. When the system is in the oscillatory region, the firing rates are the maxima and the minima of the neural activity of the winning and losing population, respectively, in the period that the first win occurs, averaged over correct trials for each level of adaptation and sensory evidence.

D: prediction, time dominance, CV

In this part, the time dominance and its coefficient of variation (CV) were examined after various levels of neuronal adaptation. This study presents an experimental prediction that can be tested to verify our findings. For this purpose, we calculated the mean time dominance of the percept of the hand and face images when an ambiguous composite image of both is presented for 5 min to subjects. We simulated this proposed experiment, having the same parameters for which the model coincides with the **Cziraki et al.** (**2010**) experiment, and defined the expected mean dominance time of perceiving the images and its coefficient of variation. The stimulation protocol is then given by $v_H = v_F = v_{ext}$ for $0 \leq t \leq 500$ ms and $v_H = v_F = v_{ext} + \lambda$ for $500 \leq t \leq 300{,}000$ ms, where $\lambda = 50$ Hz.

We did the same for other values of λ ($\lambda = 30$ Hz and 40 Hz) for which the model coincided with the behavioral data of **Cziraki et al.** (**2010**) for same recurrent connectivity $w_+ = 1.65$. The mean dominance time is defined as the mean of periods of time starting when the firing rate of the winning neural population is < 10 Hz and surpasses the firing rate of the losing one by at least 5 Hz, until the difference between them becomes < 5 Hz. The result arises from one trial that we run for 5 min. We repeat this protocol for different levels of adaptation, g_{AHP}, and we concentrate our

interest in its values for which the model coincides with **Cziraki et al.'s (2010)** experiment.

Parameter range of w_+ and g_{AHP}

To define the parameter space of recurrent connectivity weights w_+ and afterhyperpolarization conductance g_{AHP}, we investigated the behavior of the network when zero additional external input is given to its neuronal selective populations. In this case, neurons receive only background input and the firing rate of the neuronal populations should stay at low levels by increasing level of adaptation. The constraint taken into account was that the network should remain in a spontaneous state, defined as the state when mean firing rates of neuronal pools do not surpass the threshold of 10 Hz. The resulting parameter space is shown in Figure 4.3.

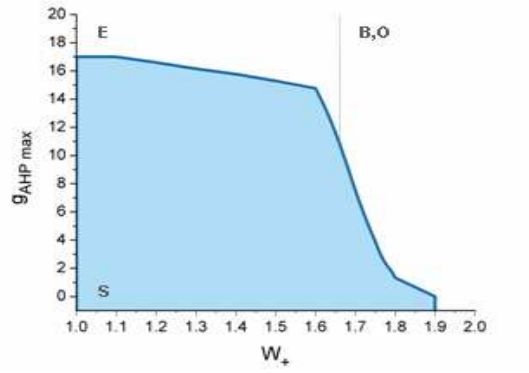

Figure 4.3 Dynamical regimes in the g_{AHP} - w_+ space, in the absence of external stimulus
Parameter space of recurrent connectivity w_+ weights and afterhyperpolarization conductance g_{AHP} when no additional external input is given to the selective neuronal populations of the network, except the background input, with the constraint that the network should stay in the spontaneous state. The parameter space is separated into two regions by the thick line. The shaded region shows where the network remains in the spontaneous state (S) and the unshaded area shows where it does not. The thin line divides the parameter space in two smaller regions. The excitation region (E), where both pools are excited and no decisions can be taken, and the bistability (B)/oscillatory (O) region where recurrent connectivity is big enough that low levels of adaptation excite the network to decisions or oscillatory states, even without additional external input. These regions are not acceptable and thus these values were not taken into account in the parameter search.

4.3 Results

We present a biologically inspired neural model of leaky integrate- and-fire neurons with spike- frequency adapting mechanism implemented to investigate the role of neuronal adaptation in decision making. We start our theoretical/computational investigation with the examination of and comparison with the behavioral data of a high- level, adaptation- related aftereffects experiment ***(Cziraki et al. 2010)*** to understand the driving force of the perceptual decision process. Adaptation- related aftereffects refer to the impact of the previous presentation of the adaptor stimulus on the perceptual decision related to a subsequently presented stimulus. The experimental data show that prolonged exposure to complex high- level stimuli, such as faces or hands, biases the perceptual decisions of a subsequent ambiguous face - hand composite stimulus away from the adaptor category, indicating that adaptation exists at a high- level of the visual processing hierarchy. Here, we hypothesize that neural frequency adaptation underlies this adaptation-related aftereffect. Even more, our simulation results support the hypothesis that neural frequency adaptation in this task is large enough so that the dynamical working regime of the network is in the oscillatory regime, indicating that the underlying model is not just a bistable model, as usual in the decision- making modeling literature.

We propose the hypothesis that the mechanism underlying the decision process in the adaptation- related aftereffect experiments should also be relevant and generally observable during decision making without any initial adaptor. For this purpose, we simulated a typical binary decision-making experiment without previous adaptor stimulus, using the same parameters for which the model coincides with the experimental data of **Cziraki et al.** (**2010**). We found that decision times are shorter for higher levels of neuronal adaptation, a finding that corresponds to the behavioral findings of the original study. We therefore conclude that a high level of neural adaptation in the network leads to a more efficient performance by accelerating the decision. In addition, we found that if an adaptor precedes the presentation of the composite-target stimulus, decision times are even shorter. Our results are consistent with an ecological relevance of

adaptation for the prompt reactions, when a sudden change occurs in the environment to which a subject is adapted.

We considered two scenarios to understand the mechanism underlying the decision process in the adaptation- related aftereffect experiment ***(Cziraki et al., 2010)***. One is noise- driven switch due to probabilistic spiking times of neurons and the other is adaptation- driven transition arising from spike-frequency adaptation due to afterhyperpolarizing (AHP) $Ca2^{+}$- activated K^{+} currents. Both noise and adaptation mechanisms are implemented in the neuronal network. With increasing level of adaptation (AHP conductance), the network shifts from a noise- driven to an adaptation- driven modus when both neuronal selective populations are stimulated. Our initial goal is to learn which of the two mechanisms is the main driving force responsible for the perceptual switch from one percept (adaptor stimulus) to the novel percept, when the ambiguous stimulus is presented at cue's end of the high- level adaptation- related aftereffects task.

Within the theoretical framework of the network that we use, each of the two competing percepts of the ambiguous stimulus can be viewed as a stable state of the neuronal dynamics (i.e., an attractor) (Figure 4.4A, where percept A represents the percept of hand and percept B represent the percept of face). Noise in our model is considered to be the source of Poisson spikes inputs amplified by the fact that the network has a limited number of neurons. Fluctuations arise in its time course and in the system's outcome on each trial. Due to the finite size effect, noise plays a crucial role in decision-making tasks by destabilizing the network's stable states, leading to the transition to other state (Figure 4.4A, percept B). The escape from one basin of attraction to the other could be described as a Kramers' escape problem, which is applied in many problems in physics and which deals with noise-activated escape ***(Kramers, 1940)***. The mechanisms of spike- frequency adaptation is thought to be related to a slow Ca^{2+}- activated K^{+} current, called afterhyperpolarization current (I_{AHP}) because it changes after hyperpolarization of each spike. It is implemented in the network by adding an I_{AHP} current into the dynamical equation of the neuronal membrane potential, resulting in a gradual decrease of the firing rate of the dominant neuronal population. This effect is shown schematically in Figure 4.4B. Higher levels of neuronal

adaptation result in destabilizing the initially stable states (percepts A and B) leading eventually to an oscillation between the two different network states. The adaptation mechanism may coexist with the noise but when adaptation is high, noise contributes only to the randomness of the oscillations due to the fluctuations arising from the finite- size effect, whereas when there is no adaptation, noise is the underlying mechanism.

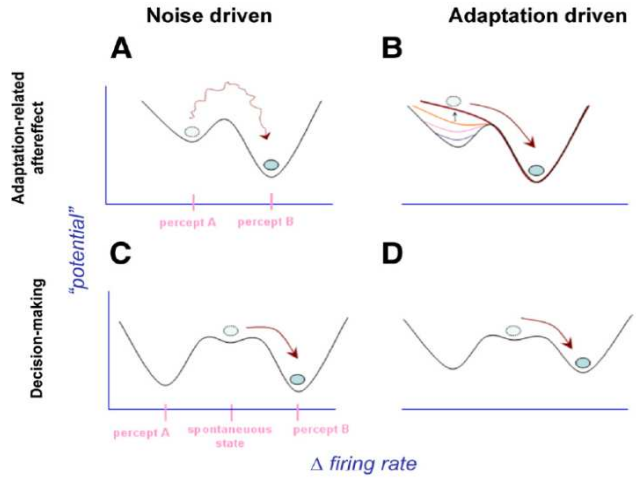

Figure 4.4 Schematic representation of noise- driven and adaptation- driven landscapes
A, B. *Adaptation- related aftereffect* ***A****. Transition between the two different percepts of an ambiguous stimulus is viewed as noise- driven transition between two basins of attractors of the neural network.* ***B.*** *Adaptation- driven, noise-sensitive fluctuations lead to oscillations.* ***C, D.*** *Decision- making* ***C****. Noise-driven decision taken in a typical decision- making task of two choices.* ***D****. Same procedure, but with adaptation implemented in the network, resulting in shallower basins of attractors.*

Figures 4.4A and 4.4B correspond to the model with an adaptor stimulus preceding one of the target stimuli (for instance, A). In this case, there are only the two stable states in the system corresponding to each percept with shallower basin of the attractor corresponding to the category of the adaptor (i.e., A). In Figures 4.4C and 4.4D, a typical binary decision-making task is captured schematically. In this case, there is no adaptor stimulus presented prior the target. The system is initially in its spontaneous state. When both selective pools, corresponding to the two interpretations (or conflicting percepts of an ambiguous stimulus), are simultaneously stimulated, the competition between them leads eventually

to one of them winning. In Figure 4.4C, the decision is taken due to noise in the network. In Figure 4.4D, the same is shown but with adaptation added to the system, resulting in shallower basins of attractors for both selective pools.

4.3.1 Model analysis: bifurcation diagrams

When the model replicates the presentation of an ambiguous stimulus, noise- driven fluctuations lead to switches between the two competitive interpretations of an ambiguous stimulus and adaptation- driven fluctuations lead to oscillations of the system, depending on the magnitude of the afterhyperpolarization conductance (level of adaptation). To define the underlying driving mechanism of decision making during adaptation- related aftereffects, we first examined the bifurcation diagram of the system in the noise- free model (when N is large). The bifurcation diagram (Figure 4.5) displays the behavior of the mean firing rate of one of the two selective populations (for instance, the H pool) as a function of the level of adaptation in the network. We distinguish two regimes, the bistable regime, in which transitions from one percept to the other are noise- driven, and the oscillatory regime, in which transitions are adaptation- driven. The bifurcation point is where the model passes from one regime to the other.

Therefore, after determining the parameter space for w_+ and g_{AHP} for which the system remains in the spontaneous state in the absence of external input (Figure 4.3), we followed stimulation protocol A (§4.2.3). This parameter space also constrains the upper limit of the level of adaptation. In Figure 4.5, two regions are delineated by the bifurcation point g_{bif} = 3.35 nS. Before the bifurcation point, the mean firing rate of the dominant perceived population at the end of the task, t = 10,000 ms, is plotted (circles). After the bifurcation, bistability vanishes and an oscillatory regime appears. The maximum (upward- pointing triangles) and minimum (downward- pointing triangles) values of the mean firing rate of pool H are plotted. The maxima and minima are obtained after smoothing the firing rate of the population in a 500 ms period, using 50 ms sliding windows. In the noise- free model, or, to be more precise, in the model of low noise such that does not change significantly the result, and in the bistable regime, the system cannot escape from the stable state

and therefore cannot switch from one state to the other. In contrast, in the oscillatory regime, there are no stable states at all. Transitions from one state to the other arise in a periodic rhythm depending on the level of adaptation. When the number of active neurons is small, finite- sized noise effects are relevant and therefore switches in the bistable regime are possible, becoming gradually more probable as approaching the bifurcation point. In the oscillatory region, noise induces randomness in the frequency of the oscillations.

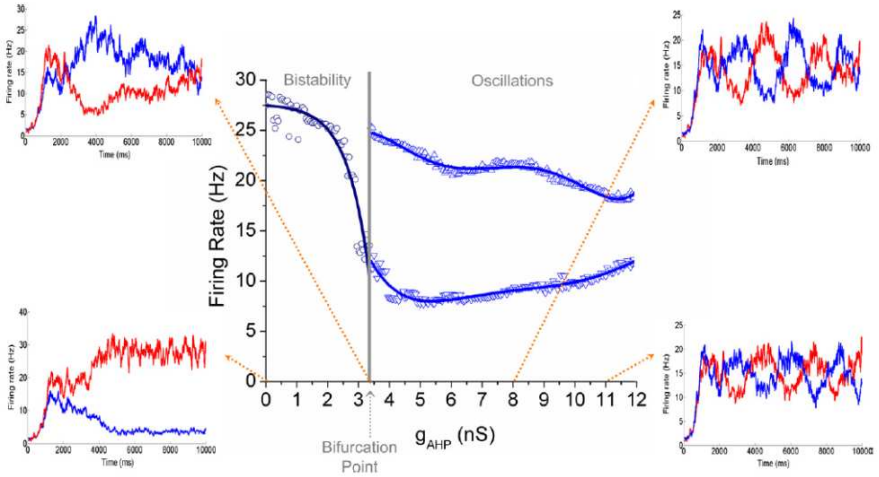

Figure 4.5 Bifurcation diagram as a function of the level of neuronal adaptation

Bifurcation diagram for the noise- free model (N = 4000 neurons) as a function of level of adaptation. The system passes from bistability to an oscillatory regime at the bifurcation point g_{bif} = 3.35 nS. Center graph, left: The firing rate of the dominant population at the end of the simulation is plotted for each g_{AHP} (circles). Center graph, right: The mean maximum (upward- pointing triangles) and minimum (downward- pointing triangles) values of the same population's oscillatory activity are plotted. The lines are fits of the spiking simulations. Small graphs: The mean firing rates of pools F (blue) and H (red) are plotted as a function of time for g_{AHP} = 0, g_{bif}, 8, and 11 nS.

In addition, we performed simulations for different levels of external stimulus λ, to show how the system transits from a spontaneous state to an oscillatory regime. Recurrent connectivity was w_+ = 1.65 and neuronal adaptation was g_{AHP} = 10 nS. In Figure 4.6, two regions are delineated by the bifurcation point λ_{bif} = 5 Hz. In the spontaneous regime, the mean firing rate of one selective population is plotted (circles). In the oscillatory

regime, the maximum (upward- pointing triangles) and minimum (downward- pointing triangles) values of the first winning population's firing rate are plotted.

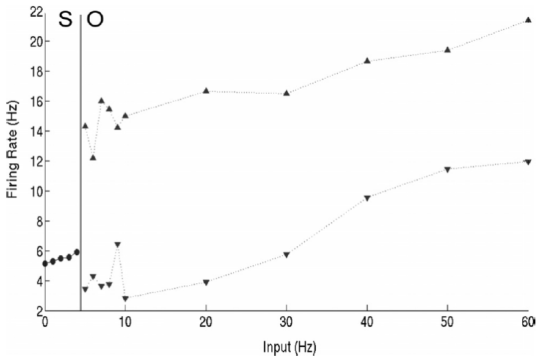

Figure 4.6 Bifurcation diagram as a function of the external stimulus
Bifurcation diagram for the noise- free model (N = 4000 neurons) as a function of external stimulus. The level of neural adaptation is $g_{exp} = g_{AHP} = 10$ nS. The system passes from a spontaneous state (S) to an oscillatory regime (O) when $\lambda = \lambda_{bif} = 5$ Hz. Left, Mean firing rate of one selective population (circles). Right, Maximum (upward- pointing triangles) and minimum (downward- pointing triangles) values of the first winning population's firing rate.

4.3.2 Simulations in comparison with psychophysical data

Our next step was to find the level of adaptation for which the modeling results from the spiking- neuron simulations coincide with the behavioral data (Figure 4.1B). To replicate **Cziraki et al.'s** (**2010**) experiment, we used an attractor network of leaky integrate- and- firing neurons with spike- frequency adaptation implemented using stimulation protocol B (§4.2.3). In our model, two selective pools are thought to represent populations of neurons in high- level cortical areas FFA and EBA. Having the bifurcation diagram (Figure 4.5) as a reference, we calculated the mean ratio of face and hand responses after hand adaptation in EBA for different values of level of adaptation g_{AHP}. Switch in this case is the percept of the novel image when both stimuli are presented to the subject via their composite ambiguous image after adaptation. The result is demonstrated in Figure 4.7A. More trials were judged as faces after hand adaptation, with mean percentage being 73% when the level of adaptation is $g_{exp} = g_{AHP} = 10$ nS. Since $g_{exp} > g_{bif}$, we conclude that the working point

of the network is in the oscillatory regime. The mean ratio of face responses after hand adaptation is equivalent to hand responses after face adaptation since our network is symmetric.

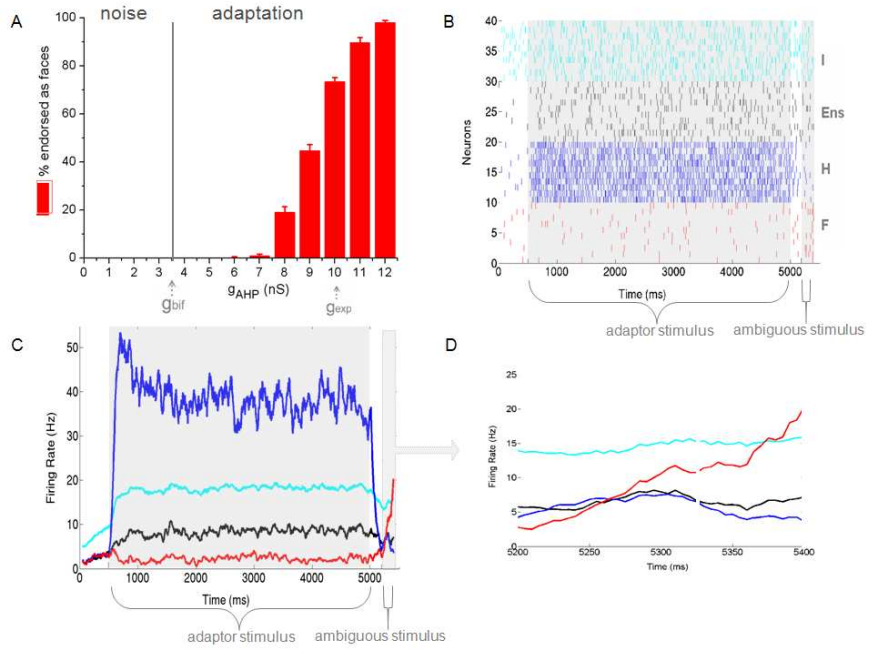

Figure 4.7 Replicating the experimental data
A. *Simulations mimicking high- level, adaptation- related aftereffects experiment* ***(Ziraki et al. 2010)****. Mean ratio of face responses after hand adaptation in the EBA as a function of the level of adaptation averaged over 10 series of 100 trials. The model coincides with the behavioral data when* $g_{exp} \equiv g_{AHP} = 10\ nS > g_{bif}$*, meaning that the working point of the system is in the oscillatory regime. The error bars are SDs.* ***B****, Raster histogram. Spiking times of 10 neurons from each of the four neural populations of the network (I, Ens, H, and F) in one trial in which the model coincides with the experiment,* g_{exp}*, when pool F wins the competition at* $5200 \leq t \leq 5400$*.* ***C****, Time course of the mean firing rate of all four populations of neurons in one trial in which the model coincides with the experiment,* g_{exp}*, when pool F wins the competition at* $5200 \leq t \leq 5400$*.* ***D****, Zoom in of Figure 4.7C for* $5200 \leq t \leq 5400$*.*

The rastergram (Fig. 4.7B) shows the spiking times of 10 neurons from each of the four neural populations during one trial when the results of the model coincided with that of the behavioral data, g_{exp}. Interestingly, this level of adaptation is close to the value g_{AHP} = 7.5 nS used in **Liu and Wang** (**2001**) and **Deco and Rolls** (**2005**), where the same parameters of $[Ca^{2+}]$ dynamics were used to study the dynamics of one IF neuron ***(Liu &***

Wang 2001) and a network of spiking neurons ***(Deco & Rolls 2005)***. In Figure 4.7C, the time course of the mean firing rates is plotted for all four neuronal populations on one trial in which pool F wins the competition at $5200 \leq t \leq 5400$ ms. The system initially reaches a stable state and then, when both pools are stimulated, competition will eventually lead to oscillations due to high level of neuronal adaptation. We thus predict that if the target ambiguous composite stimulus is persistently presented, in time subjects will experience rivalry, revealed as an oscillation in perception from one type to the other.

4.3.3 Parameter search supporting the results

The results demonstrated in Figure 4.7 arise from a specific set of the three main free parameters: $w_+ = 1.65$, $\lambda_{adaptor} = 200$ Hz, and $\lambda = 50$ Hz. This set is only one example from a variety of parameter sets for which the results of the spiking simulations coincide with the behavioral data. It was found after performing an analytical parameter search while keeping the total number of neurons in the network constant and equal to $N = 2000$ neurons. The range of values of recurrent connectivity weight w_+ was $1.6 \leq w_+ \leq 1.8$, defined by both the region for which there can be decision states when stimulus is applied to selective pools ***(Martí et al. 2008)*** and the region where the network remains at the spontaneous state when no additional external stimulus is applied to the selective pools determining, in parallel, the upper limit of level of adaptation, g_{AHP} (Figure 4.3). The range of external input to the two selective pools H and F in the second part of stimulation protocol B was $10 \leq \lambda \leq 60$ Hz, defined by the constraint that decision states and/or oscillations exist depending on adaptation, g_{AHP}. As for $\lambda_{adaptor}$, the range of values was $\lambda \leq \lambda_{adaptor} \leq 60$ Hz. The adaptor was a high- contrast hand or face and the test stimulus was a composite image of a hand and a face different from the adaptors and of lower contrast. In our simulations, we started from the point where both the adaptor and the test stimuli are equally excited by λ and $\lambda_{adaptor}$, respectively. We continued by studying the response of the system by manipulating the $\lambda_{adaptor}$. We chose a frequency of 60 Hz as an upper limit, but afterward examined the effect of an increase in the adaptor's stimulus amplitude.

From the parameter search, with the above- defined constraints, we found that the model coincides with the behavioral results for $1.6 \leq w_+ \leq 1.65$ and, whenever this happened for different test stimuli λ and adaptor stimuli $\lambda_{adaptor}$, the underlying mechanism was adaptation- driven. By varying input λ, the bifurcation point changes for a given value of the w_+. From the cases for which the model coincides with the experiment, we found that by increasing λ while keeping w_+ and $\lambda_{adaptor}$ constant, the g_{exp} decreases but so does also g_{bif}, although the difference g_{exp} - g_{bif} remains constant with g_{exp} being always in the oscillatory region ($g_{exp} >> g_{bif}$). By increasing w_+ while keeping λ and $\lambda_{adaptor}$ constant, the g_{bif} increases but so does g_{exp}. Again, the difference g_{exp} - g_{bif} remains constant with g_{exp} being always in the oscillatory region. We also investigated the effect of increasing noise by decreasing the number of total neurons in the network, resulting in stronger, finite- sized noise. For fewer neurons in the network, g_{bif} is constant and g_{exp} is smaller; thus, the difference g_{exp} - g_{bif} decreases, meaning that the role of noise increases. However, noise never becomes the main driving force. The working point of the system remains g_{exp} in the oscillatory regime.

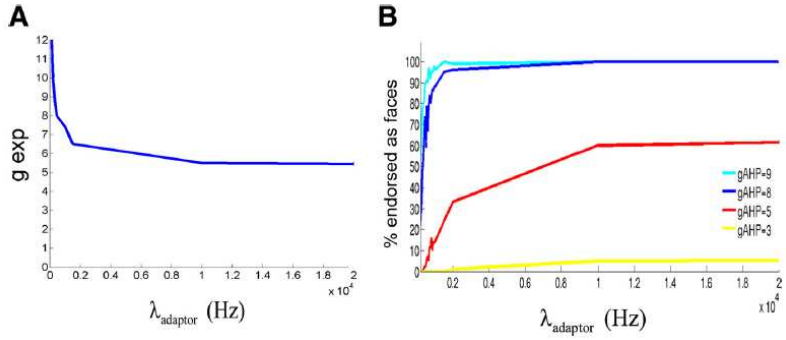

Figure 4.8 Parameter search
A. *Value of the adaptation parameter for which the results of the model coincide with the experimental behavioral data, g_{exp}, as a function of the initial external input,$\lambda_{adaptor}$, to the neuronal pool H. The total number of neurons in the network is 2000 and recurrent connectivity is $w_+ = 1.65$. The stimulus to both pools, F and H, during the last 200 ms of the cue, representing the presentation of the ambiguous stimulus, is $\lambda = 50$ Hz. The g_{exp} never reaches the bifurcation point $g_{bif} = 3.35$ nS even for extreme values of $\lambda_{adaptor}$* ***B****. The ratio of face responses after hand adaptation is plotted for different levels of adaptation, g_{AHP}, as a function of the initial input, $\lambda_{adaptor}$.*

Finally, we studied the effect of the adaptor's stimulus strength ($\lambda_{adaptor}$). We saw that by increasing $\lambda_{adaptor}$ while keeping constant w_+, λ, and N, the difference g_{exp} - g_{bif} gradually decreased. Since the upper limit of $\lambda_{adaptor}$ was selectively chosen without any specific constraint, this decrease would probably lead to $g_{exp} \leq g_{bif}$, which means that the decision making is driven by noise. Hence, Figure 4.8A shows the decrease of g_{exp} as a function of adaptor stimulus, $\lambda_{adaptor}$, with all other parameters equal to the ones used for Figure 4.7. We can clearly see that the g_{exp} never reaches the bifurcation point g_{bif} = 3.35 nS even for extreme values of $\lambda_{adaptor}$. In Figure 4.8B, the same point is demonstrated. The percentage performance of face responses after hand adaptation is plotted for different levels of adaptation as a function of the initial external input to pool H, $\lambda_{adaptor}$. From the previous discussion and this last study, we can be sure that in this high level, adaptation- related aftereffects experiment, the underlying mechanism of the decision- making process when the composite ambiguous image is presented at the end of the cue is adaptation- driven and the working point of the system is in the oscillatory regime.

4.3.4 Decision making and decision certainty

Decision making in binary choices has been studied extensively, both experimentally and theoretically, to understand its underlying mechanisms. Lately, there has been an increased interest in the confidence in decisions and it has been seen that reaction times of the decisions are shorter on easy than on difficult trials ***(Kim & Shadlen 1999)***. In addition, it has been shown that when the input to the selective- neuron pool of the network in the adaptation- free model is increased, decision times are also shorter for high- input versus for low- input situations ***(Martí et al. 2008)***. Nevertheless, the effect of the firing-rate adaptation mechanism in decision- making processes has not yet been studied. Next, we studied this effect by using the same spiking network with the same parameters as we used to define the underlying mechanism in the high-level adaptation-related aftereffects task of **Cziraki et al. (2010)**.

We followed stimulation protocol C (§4.2.3) for different levels of adaptation. We began our study without having any adaptor in the task, meaning that the experimental task was to present an ambiguous face–hand composite stimulus ***(Cziraki et al. 2010)*** that changes over trials to

either the face or the hand image, therefore increasing sensory evidence available about one of the interpretations of the stimulus and decreasing its ambiguity. Psychophysically, the measure would be the ratio of trials endorsed as faces. Neurophysiologically, it would be the neural activity of the cortical areas EBA and FFA and the decision times (i.e., the times needed for perceiving the stimulus as hand or face) as a function of the level of sensory evidence (i.e., the increase of the amount of the sensory evidence of one interpretation of the composite image). We simulated this task by externally increasing the input to neurons of selective population F by $\Delta\lambda$ while simultaneously decreasing the external input to neurons of selective populations H by $\Delta\lambda$ over trials. We calculated the mean firing rate of both pools as a function of the total external input to the network, ΔI, averaged on correct trials from 1000 simulations. The total external input ΔI is the difference in spikes per second summed across all synapses to each neuron between the external input $\lambda + \Delta\lambda$ to pool F and $\lambda - \Delta\lambda$ to pool H. Correct trials are defined as the trials when the mean firing rate of pool F surpasses first and adequately the mean firing rate of pool H (§4.2.3, C). Then we ran 1000 trials for different levels of adaptation, $0 \leq g_{AHP} \leq 12$.

Figure 4.9A shows the neural activity (mean firing rate ± 1⁄2 × SD) of pools F (solid lines) and H (dashed lines) on correct trials. In Figure 4.9B, the percentage performance ± 1⁄2 × estimated error over 1000 trials (estimated error = sqrt(performance/1000)) for different levels of adaptation is plotted. Figure 4.9C shows the mean decision times for different levels of adaptation ± 1⁄2 × SD on correct trials and the activities of the neuronal population in one single trial in the most difficult decision case ($\Delta I = 0$) and in the most easy one ($\Delta I = 60$) without adaptation ($g_{AHP} = 0$ nS) and for the level of adaptation for which the model coincides with **Cziraki et al.'s (2010)** experiment ($g_{AHP} \equiv g_{exp} = 10$ nS).

The first important conclusion from Figure 4.9 is that all levels of adaptation show the same behavior as a function of the level of sensory evidence: Neural activity of the F pool increases monotonically as a function of level of sensory evidence and its variability decreases. The variability in the firing rates is higher in difficult trials, reflecting that the system is noisier since there is less available sensory evidence. The difference between the neural activity of the winning and the losing neural

population increases with the level of sensory evidence, reflecting the increase in certainty as the task gets easier. In difficult trials, low certainty in the decision is also reflected in the performance. The percentage of correct choices, which starts from chance level (50%) showing the ambiguity of the stimulus when there is equal level of sensory evidence applied to the selective neuronal populations, increases as the task gets easier (Figure 4.9B). The performance increases monotonically as a function of the level of sensory evidence.

Second and more interestingly, we observed that, for higher levels of adaptation, the decision times are shorter for all the range of ΔI (Figure 4.9C). Furthermore, the variability in decision times caused by the random spiking of the neurons in the network is high in difficult decision cases and decreases as certainty increases. The activity of the winning neuronal population is decreasing as adaptation increases and the activity of the losing population increases, indicating that the certainty decreases but decision times are smaller. In addition, the rate of increase of the performance curve depends on the level of adaptation. In conclusion, these results show that adaptation in the context of decision making could serve to the speed- accuracy trade- off.

Our findings show that neuronal adaptation in the firing rate of the competitive neuronal population lead to faster discrimination among them. After calculating the balance of the excitation-inhibition of the selective populations, we found that higher levels of neural adaptation lead the system to become more imbalanced, resulting in shorter decision times. This result can also be explained schematically if we consider the representation of the two percepts seen as basins of attractors in a bistable system (Figure 4.4). In the network, noise arising from the probabilistic spiking times exists with and without neural adaptation. If there is no adaptation in the system, then a certain time is needed for the system to move from one state to the other. When adaptation is added into the system having the same level of noise, there is a higher probability that the system will move from one state to the other because the basin of attraction of the dominant perceptual state is becoming shallower in parallel and the other interpretation can win the competition earlier.

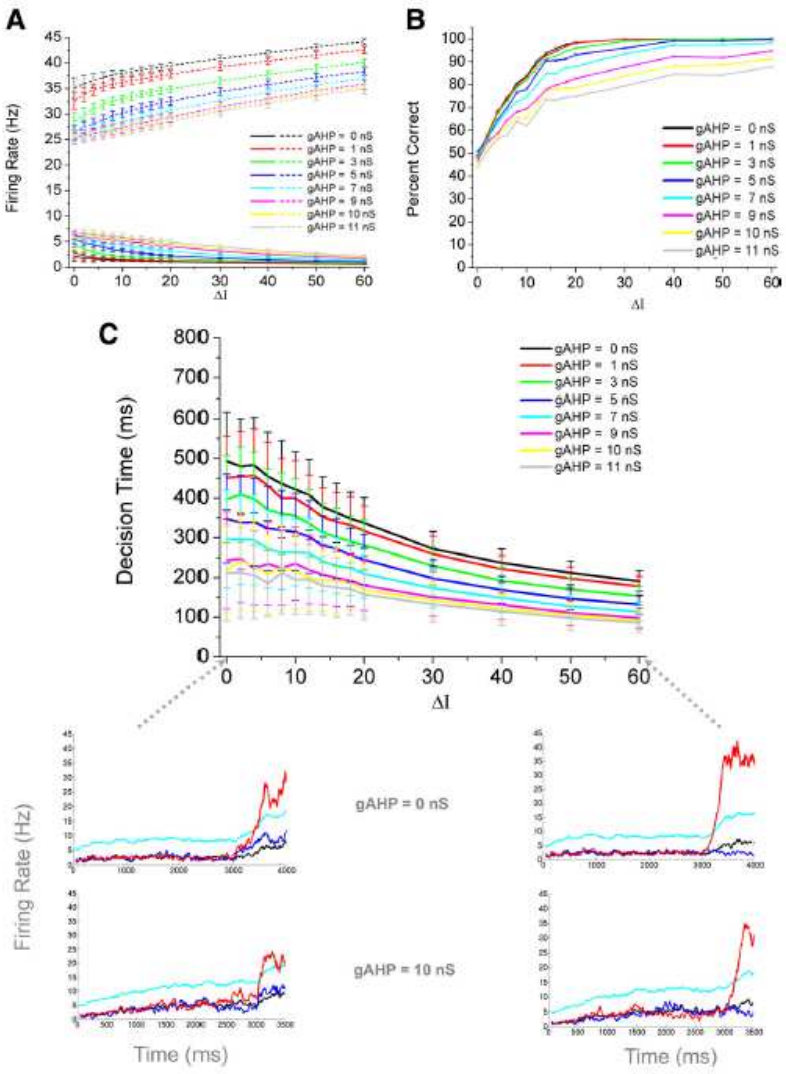

Figure 4.9 Decision making without preceding adaptor

Decision making without an adaptor preceding the decision- making task, for different levels of adaptation ***A.*** *Mean firing rates of the winning pool (solid lines) and of the loosing pool (dashed lines) averaged on correct trials over 1000 simulations.* ***B.*** *Percentage of correct trials as a function of the level of sensory evidence.* ***C.*** *Decision times when the selective neuronal pool receiving increased level of sensory evidence wins competition, averaged over correct trials. Bottom left, Mean firing rate of all pools in the adaptation-free and in high- level adaptation case, both in a single trial of the most difficult case for decision making (ΔI = 0 Hz). Bottom right, The same plots from one single trial for the easiest case (ΔI = 60 Hz).*

Higher levels of neural adaptation lead to even shallower basins of the dominant attractor and the transition is even faster. When one neuron receives a Poisson spike train input, its firing rate decreases with increasing adaptation, which also increases the variability of its output spike trains ***(Liu and Wang, 2001)***. In a neural network, this output spike train with higher variability when adaptation is implemented is an additional noise into the postsynaptic neurons, resulting in an increase in the noise and eventually to a faster transition.

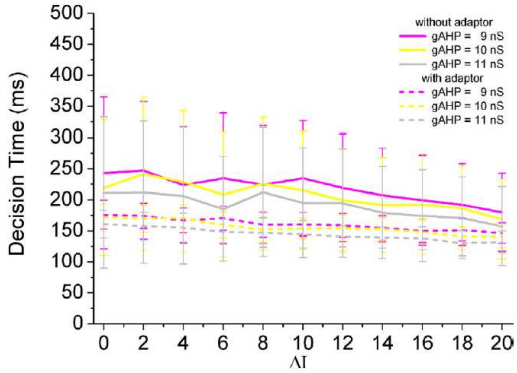

Figure 4.10 Decision making with and without preceding adaptor
Decision making with (dashed lines) and without (solid lines) an adaptor preceding the decision- making task, for different values of neural adaptation around the g_{exp} value. With adaptor, the behavior is the same as without adaptor, but decision times are faster.

Next, we applied the same adaptor stimuli to the current system as in **Cziraki et al.'s** (**2010**) experiment (§4.2.3, C). We were interested in the effect of adaptation on the decision times. Figure 4.10 shows decision times for the adapted (dashed lines) and unadapted (solid lines) conditions for various levels of adaptations ($g_{exp} - 1 \leq g_{AHP} \leq g_{exp} + 1$). For the adapted case, the behavior is the same as in the unadapted case. Decision times decrease analogous to the level of sensory evidence for all levels of adaptation, with a smaller slope than in the unadapted case. In addition, decision times decrease as magnitude of adaptation increases. Interestingly, although Figure 4.10 shows that when a subject is adapted to a perceptual interpretation of an ambiguous composite stimulus, the percept of the other interpretation occurs faster ($\Delta I = 0$) than when there is no adaptor. From an ecological point of view, it is extremely important to be able to react as fast as possible to a sudden change in the environment.

As we increase the magnitude of adaptation over trials, a novel percept (in this case, the opposite interpretation of the target stimulus) is more likely to occur. Our results suggest that it also happens faster. It is also logical from a theoretical point of view since the activity of the adapted neuronal population is suppressed and it is easier for the competitive neuronal population to win the competition, leading to faster reaction times.

4.4 Discussion

In this chapter, we investigated the role of the spike- frequency adaptation in the context of decision making. We used a biophysically realistic competition model of decision making with an implemented spike-frequency adaptation mechanism. Decision making and its underlying mechanisms is a common field of interest among neuroscientists during the last few decades but the role of neural adaptation in this context is still unknown. Our work addresses some fundamental aspects of adaptation effects in decision making.

We began our study by considering behavioral data from a high- level adaptation- related aftereffects experiment ***(Cziraki et al. 2010)***. In this experiment, it was shown that prolonged adaptation to a complex stimulus (e.g. an image of a hand) leads to category- specific aftereffects during the perception of ambiguous stimulus composites (a composite image of a hand and a face). From a theoretical point of view, we studied the dynamics of the perceptual switch from the adaptor category to the novel, opposite category by comparing two scenarios: noise- and adaptation-driven transition. When an ambiguous stimulus is presented, noise- driven fluctuations lead to switches from one percept to the other. These fluctuations arise in the network due to the probabilistic spike time of the neurons amplified by finite- sized effects. Adaptation- driven transitions, on the other hand, lead to oscillations between the two different percepts, with random frequency while noise- driven fluctuations still exists in the network. We investigated the dynamical regime for which the competition model is consistent with the behavioral data. The behavioral result and our detailed parameter study, in the accepted parameter space, constrain the adaptation- driven regime to be the working point of the network.

Since we find that spike- frequency adaptation is the underlying mechanism in high- level, decision- making tasks like the high- level, adaptation- related aftereffects, we extended our study to typical binary decision- making tasks. We simulated an experiment of decision making where an ambiguous figure, like the one presented in **Cziraki et al.** (**2010**), is presented to subjects. In this experiment, the contrast of one of the two competing percepts is increased over different sets of trials. Simulating this experiment for different levels of adaptation, we found that when neuronal adaptation is high, decision becomes faster while the rate of increase of the performance curve decreases, indicating the role of neuronal adaptation in the speed- accuracy trade- off. With increasing levels of neural adaptation, the balance between excitatory and inhibitory currents received at the synapses of the selective populations decreases, resulting in shorter decision times. In addition, when an adaptor precedes the decision making task, decision is even faster for the same level of adaptation. The output of the spiking model we use could be tested in psychophysical and neurophysiological experiments. Our results are also consistent with an ecological point of view, since it is important to be able to react quickly when new environmental information is presented.

Finally, we integrate our work by presenting testable predictions via experimental tasks that may verify our findings. For the decision- making task presented above, an increase in the reaction times should be observed if the Ca^{2+}- activated K^{+} channels can be gradually blocked. We also propose another task. The composite ambiguous figure of a hand and a face ***(Cziraki et al. 2010)*** is presented to subjects continuously for 5 min and the psychophysically mean time dominance and coefficient of variation are measured. We mimic this task by having the same parameters as those in **Cziraki et al.** (**2010**). We calculate the mean dominance time of perceiving the hand or the face and its coefficient of variation (§4.2.3, D). The result is shown in Figure 4.11. In Figure 4.11, the green line corresponds to $\lambda = 50$ Hz, which is the external stimulus mainly used in this chapter, but calculations were also performed for $\lambda =$ 30 Hz and $\lambda = 40$ Hz (with same recurrent connectivity), for which the model coincided with the behavioral data of **Cziraki et al.'s** (**2010**) experiment. Hence, psychophysically, we expect to measure a mean dominance time, $\langle T \rangle$, approximately in the range of $2 \leq \langle T \rangle \leq 6$ s and its coefficient of variation in the range of $0.5 \leq CV \leq 1$. We therefore

conclude that the ambiguous composite stimulus is indeed a rivalrous stimulus. Preliminary experimental data further confirm our prediction. The same ambiguous composite stimulus was presented for 30 s and subjects (n = 3) were asked to report which image they perceived by pressing a button. Subjects experienced alternations in their perception with a mean time dominance of T_{exp} = 4.5 sec and coefficient of variation CV = 0.52. Naturally, more subjects are needed to be quantitatively more precise but qualitatively we can conclude that the composite stimulus of our study is indeed rivalrous, since the experimental time dominance and coefficient of variation is within the typical range of rivalrous figures ***(Levelt 1968)***. This result is also in line with previous experiments where adaptation led to unambiguous percepts of such ambiguous stimuli as the Necker cube ***(Long & Moran 2007)***. In this study, previous exposure to an unambiguous version of the Necker cube for several minutes produced an immediate bias to perceive the ambiguous figure in the opposite configuration and led to decreased number of reversals. We note that the experimental data are also within the predicted range by our study. We therefore conclude that our hypotheses that neuronal adaptation should be relevant in **Cziraki et al.'s** (**2010**) experiment, which led to the conclusion that our model can account for modeling perceptual bistability.

Perceptual bistability emerges when an ambiguous stimulus with two mutually exclusive interpretations is perceived as the frequent alternation of these states during long- term stimulus presentation. This visual phenomenon arises in many domains of perception, such as ambiguous figures as the well known face- vase stimulus, the Necker cube, or monocular rivalry, but the most extensively studied domain is binocular rivalry (for review, see ***Blake & Logothetis 2002***). Neurodynamical models proposed for binocular rivalry are based on a competition between two populations of excitatory neurons whose activities encode the two conflicting percepts. This competition is mediated through inhibitory neurons that lead the dominant neuronal population to suppress the activity of the competitive one, such that at a given time only one has high activity corresponding to one of the interpretations.

Moreover, theoretical studies show that random alternations in perception in such tasks can be achieved by two mechanisms: adaptation- driven and noise- driven transitions. Neuronal adaptation implemented by spike-

frequency adaptation and/or synaptic depression results in reducing the activity of the dominant neuronal population or in weakening the inhibition between the two populations of neurons, leading the nonadapted population to win the competition. In this case, even in the absence of noise, adaptation generates alternations between the competing percepts with perfect periodicity, the reason these models are called oscillator models *(**Lehky 1988; Lago-Fernández & Deco 2002; Laing & Chow 2002; Shpiro et al. 2007**)*. In contrast, noise- driven fluctuations in the firing rates of the neuronal populations in a bistable attractor network lead to random switches between two stable attractors representing the two dissimilar percepts *(**Salinas 2003; Freeman 2005; Kim et al. 2006; Moreno-Bote et al. 2007**)*. In these models, called noise driven attractor models, a switch in perception cannot exist without noise. Both mechanisms have recently been studied jointly in a common neuronal competition- rate model *(**Shpiro et al. 2009**)*. **Shpiro et al. (2009)** show that the working point of the models, considering both noise- driven and adaptation- driven mechanisms, should be at the edge of the bifurcation.

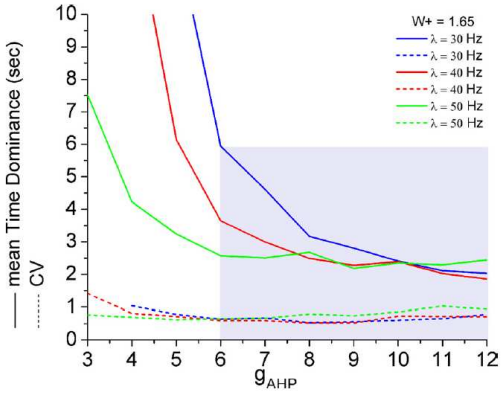

Figure 4.11 Mean dominance time and coefficient of variation for different levels of adaptation
*Mean dominance time and coefficient of variation for different levels of adaptation when the ambiguous composite figure of the hand and the face is presented, having the same parameters as the ones coinciding with the behavioral data from **Cziraki et al.'s (2010)** experiment.*

In this chapter, we considered both mechanisms within the same theoretical framework, using a spiking neuronal model to study the underlying mechanism in a high- level adaptation- related aftereffects task

*(**Cziraki et al. 2010**)*. We found that neuronal adaptation is high enough that the working point of the system is in the oscillatory regime. We therefore predict that if the target stimulus is presented continuously, subject will experience rivalry with the predicted time dominance and coefficient of variation. Preliminary experimental results confirm our prediction. Although these preliminary data are enough to qualitatively confirm our hypothesis, we understand that more subjects should be tested to provide more precise quantitatively results. The predicted dominance time calculated is inside the range of typical dominance times measured experimentally when rivalry figures are presented to subjects, but the predicted coefficient of variation can be larger than the upper bound of the typical range *(**Levelt 1968**)*.

In conclusion, our study links, for the first time, neural processes and high- level, adaptation- related aftereffects. Using a spiking neural network, including neuronal adaptation mechanism by the slow $Ca2^{+}$-activated K^{+} current, we found that neuronal adaptation is the main driving force in such high- level visual phenomena in humans. Furthermore, we have investigated the effect of this mechanism in typical binary decision-making task and found that neuronal adaptation leads to faster decisions, contributing to a speed- accuracy trade- off.

CHAPTER 5

Noise- decorrelation during Visual Consciousness[6]

5.1 Introduction

How neurons encode information and perform computations? This is one of the major questions in neuroscience. Until recently the firing activity of neurons has been the main correspondent to information coding of neurons. When researchers found that there is information encoded also in the spike count correlations of pairs of neurons, the interest of the scientific community in the correlated variability has been increased and it is still increasing. Several review articles in this context have been published ***(Salinas & Sejnowski 2001; Averbeck et al. 2006; Quiroga & Panzeri 2009; Cohen & Kohn 2011)***, and there is a plethora of studies in this scheme, both experimental and theoretical.

Intrinsic noise can be detected in the fluctuation of neuronal discharge responses to repeated presentations of the same stimulus ***(Tolhurst et al. 1983)***. The total amount of noise, or noise entropy, in a neuronal ensemble is captured in the covariance matrix where both individual and interneuronal, correlated, fluctuations are described ***(Averbeck & Lee***

[6] Main results presented in this chapter are *in preparation for submission*: T. I. Panagiotaropoulos*, P. Theodoni*, V. Kapoor*, G. Deco, and N. K. Logothetis (2014), Decorrelated noise in dominant prefrontal microcircuits during visual consciousness. (*equal contribution)

2006; Ecker et al. 2011). The latter component of noise is commonly called "noise correlation" and its impact on neuronal information processing has been studied extensively in both elementary and higher-order processes like stimulus drive *(Aertsen et al. 1989; Ahissar et al. 1992; Kohn & Smith 2005),* neuronal adaptation *(Gutnisky & Dragoi 2008; Adibi et al. 2013),* perceptual discrimination *(Romo et al. 2003; Liu et al. 2013a, 2013b)*, attention *(Cohen & Maunsell 2009; Mitchell et al. 2009; Herrero et al. 2013; Poort & Roelfsema 2009),* perceptual and associative learning *(Ahissar et al. 1992; Gutnisky & Dragoi 2008; Komiyama et al. 2010; Gu et al. 2011; Jeanne et al. 2013)* and behavioral context *(Cohen et al. 2008; Poulet & Petersen 2008; Vaadia et al. 1995)*. In these studies noise correlations were shown to be detrimental, beneficial or irrelevant to the fidelity of population codes, depending on their magnitude, structure and the assumptions employed by decoding algorithms. In general, in a so-called limited-range and stimulus-dependent correlation structure, where more similarly tuned neurons are more correlated and a preferred stimulus results in higher noise compared to a non preferred, correlated noise is detrimental for population coding, since pooling neuronal responses is unable to average out common noise fluctuations. On the other hand, opposite tuning renders correlations beneficial *(Averbeck et al. 2006; Romo et al, 2003; Abbot & Dayan 1999)*.

Under ambiguous conditions, two assemblies of neurons, with different stimulus preferences, compete for perceptual dominance (§1.4). Until now, these neurons were studied in isolation and their averaged firing rate during perceptual dominance and suppression was compared to the respective average rate during perception without any underlying competition to infer the relative contribution of a given cortical area in conscious perception. However, due to the probabilistic, noisy nature of neuronal firing, statistical features like the magnitude and structure of individual and shared discharge variability, within and between the competing neuronal pools, could influence their information capacity *(Abbot & Dayan 1999; Averbeck et al. 2006; Sompolinsky et al. 2001; Wilke & Eurich 2002; Zohary et al. 1994; Cafaro & Rieke 2010)*.

Therefore, determining the effect of perceptual dominance and suppression on intrinsic neuronal noise could evaluate the fidelity of

conscious representations in cortical microcircuits, particularly in association areas *(**Crick & Koch 1995, 1998; Panagiotaropoulos et al. 2014**)*.

In this chapter, we consider neurophysiological data collected during the study of the effect of perceptual dominance and suppression achieved through binocular flash suppression (BFS) on intrinsic noise measured in the pair-wise interneuronal correlations and individual variability in the macaque lateral prefrontal cortex (LPFC). The data show that during the perceptual dominance of a preferred stimulus the dominant population settled in a decorrelated state compared to monocular visual stimulation, that is when the same population encoded the same stimulus without any underlying competition. In striking contrast, no differences in noise correlation were found between perceptual suppression and the physical absence of the preferred stimulus. Most interestingly, correlated noise between neurons with opposite stimulus preference remained unaffected by visual rivalry, suggesting that the dynamic changes in LPFC functional connectivity occur selectively in the cortical microcircuit signaling perceptual dominance. We employed a biophysically realistic spiking network of two neural populations with and without cross- inhibition. We found, contrary to our intuition, that competition is not relevant to the noise- correlation reduction during rivalrous visual stimulation. Instead, the noise- correlation reduction is due to stimulus and noise modulation coming from preceding stages of processing. A plausible scenario is that competition is resolved in a previous stage, like IT, and neurons in LPFC are driven by IT's output.

5.2 Methods

In the followings, we describe the experimental protocol and results (§5.2.1), designed and obtained by Theofanis I. Panagiotaropoulos, Vishal Kapoor and Nikos. K. Logothetis at the Max Plank Institute, Biological Cybernetics in Tübingen. Then, we describe the networks we employed (§5.2.2), the stimulation protocols, the simulations and the analysis we used (§5.2.3).

5.2.1 Experimental paradigm & results

The dominant and suppressed states of LPFC neurons were dissected, during visual consciousness by combining BFS, a well-controlled variant of BR stimulation that dissociates subjective perception from sensory stimulation ***(Wolfe 1984; Sheinberg & Logothetis 1997; Kreiman et al. 2002; Keliris et al. 2010; Panagiotaropoulos et al. 2012),*** with extracellular tetrode recordings in awake, behaving macaques. The effects of subjective perceptual dominance and suppression of a preferred stimulus on intrinsic noise during BFS were compared to the effects of similar perceptual states during monocular physical alternation (PA) of the same stimuli, that didn't involve visual rivalry and therefore lacked any subjective component.

A schematic description of BFS and monocular PA trials is depicted in Figure 5.1. In PA (Figure 5.1A), each trial starts with the presentation of a fixation spot in both eyes that is binocularly fused and remains on until the end of the trial. After 300ms of stimulus-free fixation (t = 0 - 300 ms) a polar checkerboard is presented in one eye for 1000 ms (t = 301 - 1300 ms) and then removed and followed by the presentation of a monkey face stimulus for 1000 ms (t = 1301 - 2300 ms) in the contralateral eye. In half of the PA trials the order of stimulus presentation is reversed and the checkerboard follows visual stimulation with a face. In both PA conditions visual perception has a purely sensory component, in the sense that a unique pattern stimulates the visual system during each trial phase. In BFS trials (Figure 5.1B), one second following the first stimulus onset (i.e. at t = 1301 ms), the same disparate visual patterns -as in PA- are flashed to the corresponding part of the contralateral eye. The flashed stimuli remain on for 1000 ms (t = 1301 - 2300 ms), robustly suppressing the perception of the contra laterally presented visual patterns which are still physically present. As a result of this manipulation, in BFS trials a visual competition period dissociating sensory stimulation from subjective perception is externally induced for the last 1000 milliseconds ***(Wolfe 1984; Sheinberg & Logothetis 1997; Keliris et al. 2010; Panagiotaropoulos et al. 2012)***. During this period the newly presented pattern is perceptually dominant while the initially presented stimulus becomes perceptually suppressed. At the end of each trial and following a brief stimulus free fixation period (100 - 300 ms) a drop of juice was used

as a reward.

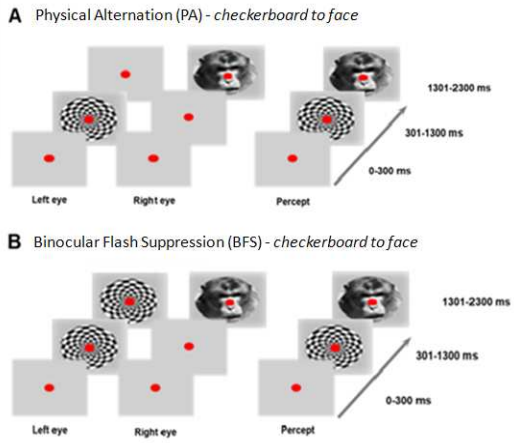

Figure 5.1 Experimental design
A. *Physical Alternation (PA)* ***B.*** *Binocular Flash Suppression (BFS). In both PA and BFS it is shown a checkerboard to face trial. Nevertheless, face to checkerboard trials were mixed with checkerboard to face trials, so that the monkey does not obtain a rule.*

The experiments were performed on three adult rhesus monkeys (*macaca mulatta*). The recording site was the inferior convexity of the prefrontal cortex (Figure 5.2). This area contains face selective cells ***(Ó Scalaidhe et al. 1997)*** and in humans the inferior frontal cortex shows neural correlates during binocular rivalry ***(Lumer et al. 1998; Lumer & Rees 1999)***.

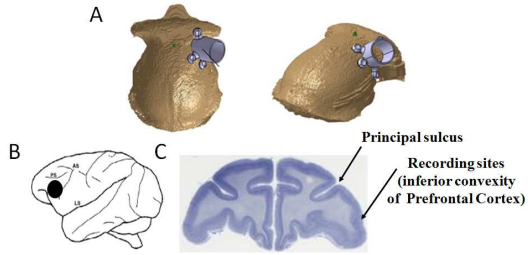

Figure 5.2 Recording site: Inferior convexity of prefrontal cortex
A. *3D sketch of a monkey's scalp showing the position of the recording chamber over the inferior convexity of prefrontal cortex* ***B****. Drawing of a monkey's brain, showing the recording sites (black dot)* ***C.*** *Sketch of a monkey's brain slice showing the recoding sites (inferior convexity of prefrontal cortex). (Figure obtained personally from* ***Theofanis I. Panagiotaropoulos****).*

Simultaneously recorded pairs of neurons in two different pools were assigned depending on the stimulus preference index of the recorded units. The first pool comprised pairs of neurons where both units had a similar stimulus preference during both PA and BFS and the second order statistics of this population was tracked during a) monocular perception of the preferred stimulus in PA, b) monocular perception of the non-preferred stimulus during the physical absence of the preferred one in PA, c) subjective perceptual dominance of the preferred stimulus in BFS and d) perception of the non-preferred stimulus inducing perceptual suppression of the preferred one in BFS. The second pool comprised pairs of neurons where the two units had opposite stimulus preference during PA and maintained this opposite preference during BFS and compared their statistics during PA and BFS to examine the effect of visual competition.

The pair-wise spike count correlation coefficient (or else correlated variability) during t = 1301 – 2300 ms was computed similar to **Bair et al. (2001)**. Specifically, for each pair of simultaneously recorded neurons consisted of units i and j and for each of the four conditions separately, the total number of spike counts across all trials was first normalized, by converting them into z-scores and then for each pair the Pearson correlation coefficient was computed for the two vectors. In addition, for each neuron and for each condition separately the individual variability across trials during t = 1301 - 2300 ms was estimated, by computing the Fano factor.

The experimental data show a decrease in correlated variability across pairs of neurons sharing similar stimulus preferences, when their preferred stimulus is perceived during rivalrous visual stimulations, compared to the magnitude of correlation when the same stimulus is perceived without competition (Figure 5.3B).

Here, we focus on the mean firing rates, correlated variability and Fano factor of the dominant and suppressed populations during the last second of the PA and BFS trials: The mean firing rate of the dominant population in BFS is slightly smaller than in PA. The mean firing rate of the suppressed population is similar to the mean firing rate of the suppressed population in PA (Figure 5.3A). The correlated variability of the dominant population in PA is 0.1 and decreases to 0.05 in BFS. The correlated

variability of the suppressed population in PA is 0.05 and remains 0.05 in BFS (Figure 5.3B). The Fano factor of the dominant population and of the suppressed is not different in BFS compared to PA.

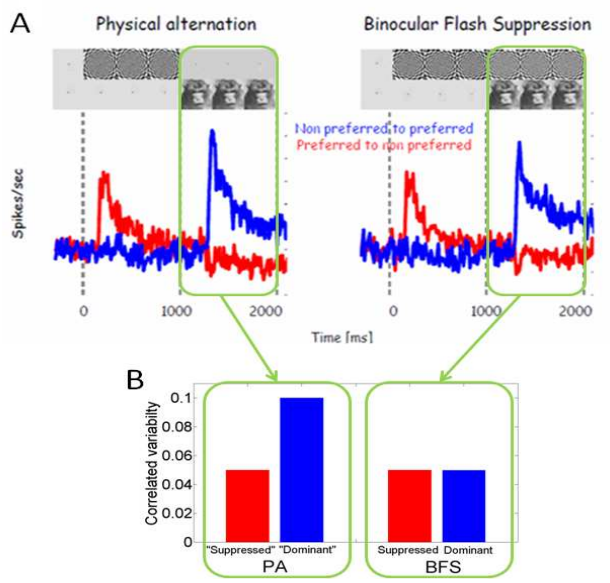

Figure 5.3 Experimental results
A. *Mean firing rates of the finally suppressed (red) neural assembly and of the finally dominant (blue) neural assembly, during the last second of PA and BFS (figure obtained personally from* ***Theofanis I. Panagiotaropoulos) B.*** *Pair- wise correlated variability of the suppressed neural assembly and of the dominant, during the last second of PA and BFS. We call the neuronal population that is suppressed in BFS, also suppressed in PA, for the sake of convenience. The same stands for the dominant population in BFS. Here we write "suppressed" and "dominant" just to emphasize it.*

5.2.2 Model description

We considered two biophysically realistic networks with different architectures. One network is consisted of three neuronal populations (two excitatory and one inhibitory, Figure 5.4A), and the other network is consisted of two neuronal populations (one excitatory and one inhibitory, Figure 5.4B). The first network is characterized by cross-inhibition, and hence competition, between the two excitatory neuronal populations. Details of the network are presented in Chapter 2 (§2.2). Here we do not include a non- selective neuronal population, in order to better compare this network with the network without cross- inhibition in terms of the

effect of the competition. One of the excitatory neuronal populations, E1, is consisted of neurons selective to one of the images in PA and BFS, e.g. the face image, and the other excitatory neuronal population, E2, is consisted of neurons selective to the other image in PA and BFS, i.e. the polar image. The second network is similar to the first one, with the difference that there is not cross- inhibition, and hence competition, since there is only one excitatory neuronal population. We consider two such networks (without competition) for convenience in the description of our results.

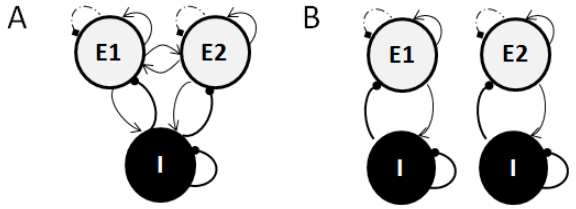

Figure 5.4 Biophysıcally realistic spiking networks
A. *Network with competition: Two excitatory neuronal populations, E1and E2, with self- excitation (arrows), neuronal adaptation (dashed lines), connected with each other (arrows) and with an inhibitory population, I.* ***B.*** *Network without competition: One excitatory population, E1 or E2, with self- excitation (arrows), neuronal adaptation (dashed lines), connected with an inhibitory population, I.*

Model input and output

All excitatory neurons receive background input, through C_{ext} = 800 excitatory connections, each one receiving an independent Poisson spike train with rate λext = 3 Hz, and noise $\beta_{ext} \cdot g(t)$, where g is being drawing, at each time step, from a Gaussian distribution with mean 0 and standard deviation 1, and β_{ext} is the so called background input noise. The presentation of an image in the experiment is simulated by additional to the background input Poison spike train of rate λ, and total input noise β, to the excitatory neurons. Inhibitory neurons in all times and all conditions receive background input, through C_{ext} = 800 excitatory connections , each one receiving an independent Poisson spike train with rate λext = 3 Hz.

5.2.3 Stimulation protocols

Physical alternation (PA)

The first 300 ms all excitatory neurons receive only background input. In the following 1000 ms, neurons of one of the selective populations, E1, receive additional external input of rate λ and total input noise β, while neurons of E2 receive only background input. The last 1000 ms, neurons of E2 receive additional external input of rate λ and total input noise β, while neurons of E1 receive only background input (Figure 5.5, PA). In Summary, the inputs to the selective populations, v_{E1} and v_{E2}, are given by the following equations:

$$\left.\begin{aligned} v_{E1}(t) &= \lambda_{ext} + \beta_{ext} \cdot g(t) \\ v_{E2}(t) &= \lambda_{ext} + \beta_{ext} \cdot g(t) \end{aligned}\right\} \text{for} \quad 0 \le t \le 300\,\text{ms} \tag{5.1}$$

$$\left.\begin{aligned} v_{E1}(t) &= \lambda_{ext} + \lambda + \beta \cdot g(t) \\ v_{E2}(t) &= \lambda_{ext} + \beta_{ext} \cdot g(t) \end{aligned}\right\} \text{for} \quad 300 < t \le 1300\,\text{ms} \tag{5.2}$$

$$\left.\begin{aligned} v_{E1}(t) &= \lambda_{ext} + \beta_{ext} \cdot g(t) \\ v_{E2}(t) &= \lambda_{ext} + \lambda + \beta \cdot g(t) \end{aligned}\right\} \text{for } 1300 < t \le 2300\,\text{ms} \tag{5.3}$$

Considering two networks without cross-inhibition -one where the excitatory population (E1) consists of neurons selective to one of the images, e.g. face image, and another where the excitatory population (E2) consists of neurons selective to the other image, i.e. polar image- we follow the same stimulation protocol as previously (Equations 5.1 - 5.3).

Binocular Flash Suppression (BFS)

The first 300 ms all excitatory neurons receive only background input. For the next 1000 ms, neurons of one of the selective populations (E1) receive additional external input of rate λ and noise β. The last 1000 ms, neurons of the same selective population receive additional external input of rate λ_1 and noise β_1 while of the other selective population (E2) receive additional external input of rate λ_2 and noise β_2 (Figure 5.5, BFS). In Summary, the inputs to the selective populations, v_{E1} and v_{E2}, are given by the following equations:

$$\left.\begin{aligned} v_{E1}(t) &= \lambda_{ext} + \beta_{ext} \cdot g(t) \\ v_{E2}(t) &= \lambda_{ext} + \beta_{ext} \cdot g(t) \end{aligned}\right\} \text{for} \quad 0 \le t \le 300\,\text{ms} \tag{5.4}$$

$$\left.\begin{aligned} v_{E1}(t) &= \lambda_{ext} + \lambda + \beta \cdot g(t) \\ v_{E2}(t) &= \lambda_{ext} + \beta_{ext} \cdot g(t) \end{aligned}\right\} \text{for} \quad 300 < t \le 1300\,\text{ms} \tag{5.5}$$

$$\left.\begin{aligned} v_{E1}(t) &= \lambda_{ext} + \lambda_1 + \beta_1 \cdot g(t) \\ v_{E2}(t) &= \lambda_{ext} + \lambda_2 + \beta_2 \cdot g(t) \end{aligned}\right\} \text{for} \quad 1300 < t \le 2300\,\text{ms} \tag{5.6}$$

Considering two networks without cross-inhibition -one where the excitatory population (E1) consists of neurons selective to one of the images, e.g. face image, and another where excitatory population (E2) consists of neurons selective to the other image, i.e. polar image- we follow the same stimulation protocol as previously (Equations 5.4 - 5.6).

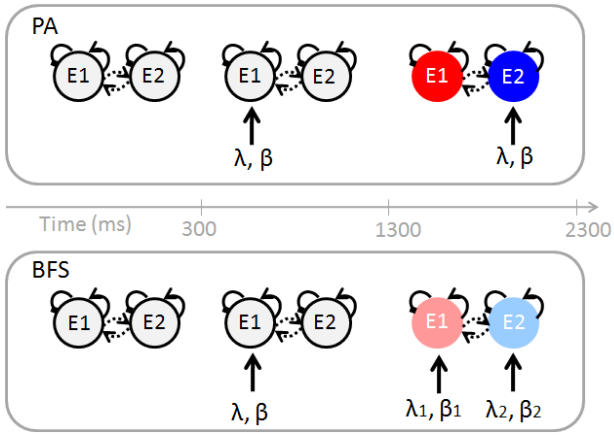

Figure 5.5 Stimulation protocol: PA & BFS
Physical Alternation (PA): *at time 300 ms stimulus of strength λ and variability β is applied to population E1 and at 1300 ms stimulus of same strength and variability is applied to population E2.* ***Binocular Flash Suppression (BFS):*** *at time 300 ms stimulus of strength λ and variability β is applied to population E1 and at 1300 ms stimulus of strength λ_1 and variability β_1 is applied to population E1, while stimulus of strength λ_2 and variability β_2 is applied to population E2. The connection between the excitatory populations E1, E2 is drawn with dashed lines, representing its existence, network with competition (Figure 5.4A) or not, network without competition (Figure 5.4B). The colors of the neuronal ensembles in the last second of the stimulation protocol correspond to the colors used throughout the presentation of the results.*

Parameters for which the networks replicate the experimental data

In both networks the parameters are the same, for the sake of comparison, and the values of the main parameters are presented in Chapter 2 (Tables 2.2, 2.5, 2.6). The rest of the parameters here are: $N = 500$, $w_+ = 1$, $w_1 = 2$, $g_{AHP} = 30$ nS, $\rho = 0.1$, $\tau_{Ca} = 2000$. The total number of neurons is the same in both networks, thus in the network without cross-inhibition the excitatory population is double in size ($N_E = 400$ neurons, $f = 1$) compared with each excitatory population in the network with cross-inhibition ($N_{E1,2} = 200$ neurons, $f = 0.5$).

The network with cross-inhibition replicates the experimental data in PA and BFS when $\beta_{ext} = 2.5\times10^{-4}$, $\lambda = 480$ Hz, $\beta = 1\times10^{-4}$, $\lambda_1 = 160$ Hz, $\beta_1 = 1.1\times10^{-4}$ and $\lambda_2 = 460$ Hz, $\beta_2 = 1\times10^{-5}$. The network without cross-inhibition replicates the experimental data in PA and BFS when $\beta_{ext} = 3.5\times10^{-4}$, $\lambda = 360$ Hz, $\beta = 1\times10^{-4}$, $\lambda_1 = 160$ Hz, $\beta_1 = 1.5\times10^{-4}$ and $\lambda_2 = 340$ Hz, $\beta_2 = 5.5\times10^{-5}$. The rest of the parameters are the same in both networks. The only difference is the number of the excitatory neurons in each population.

Analysis

Mean firing rate: In each trial, the mean firing rate of each neuronal population was calculated by dividing the number of spikes emitted in a 50ms window by its number of neurons and by the window size. The time window was sliding with a time step of 5 ms.

Noise-correlations: We recorded the spike timings of 200 neurons across 100 trials from each excitatory neuronal population of the network with cross-inhibition, and 400 neurons across 100 trials from the excitatory neuronal population of the network without cross-inhibition, in each condition (PA, BFS). Selecting randomly 50 neurons from them, we computed their spike counts during the time interval $1300 < t \leq 2300$, in each of the 100 trials. After converting them into z-scores, we computed the Pearson correlation coefficient for all pairs of the 50 neurons, as done experimentally. We followed the same procedure 100 times and finally computed the mean correlation coefficient.

Excitatory-inhibitory balance: In each trial, every 1ms, for each excitatory population, we recorded the mean synaptic currents over all its neurons.

After summing them, we calculated the mean of over the time, where we add 450 pA ***(Brunel & Wang 2001)***, and finally we averaged over 100 trials,

$$\text{Balance} = \left\langle \left\langle I_{\text{AMPA,ext}} + I_{\text{AMPA}} + I_{\text{NMDA}} + I_{\text{GABA}} + 450 \right\rangle_{1300 \le t \le 2300} \right\rangle_{100\,\text{trials}}.$$

Mean and standard deviation of the voltage: At every time step (0.02 ms), during the time interval $1300 < t \le 2300$ ms, we recorded the voltage of 50 neurons from each excitatory neuronal population, in each condition. We then calculated the mean voltage of each neuron across 500 trials, then we computed the mean voltage, for each neuron, over time and finally the mean voltage across neurons.

5.3 Results

Contrary to our intuition, we find that competition is not the reason for the noise- correlation reduction during rivalrous visual stimulations. Instead, the most plausible scenario is that competition is resolved in a previous stage, like IT and neurons in IPFC are driven by IT's output.

5.3.1 A mechanistic analysis underlying the experimental noise-correlations

The experimentally observed ecorrelated discharges during rivalrous visual stimulation compared to the strength of correlated fluctuations in the same population during perception without competition, as well as the unchanged noise-correlations in the suppressed population in BFS compared to the noise correlations in the same population during the absence of external stimulus, provide a challenge for current theoretical approaches to explain these experimental evidences. Here, we present a tentative theoretical explanation for the noise-correlation in the populations of interest.

We consider a network with mutual inhibition between two selective populations because it is well known as a mechanism, together with spike-frequency adaptation, that gives rise to successive phases of perceptual dominance and suppression in BR (Chapter 3), as well as to controlled perceptual suppression in BFS (***Panagiotaropoulos et al. 2013***) and in

adaptation- related afterrefects (Chapter 4). Therefore, our initial hypothesis was that cross-inhibition between the two neuronal ensembles that encode each visual stimulus would be responsible for the noise-correlation decrease in BFS compared to PA. To test this hypothesis, we considered a biophysically realistic spiking network comprised of two selective excitatory neural populations, each one encoding one of the visual stimuli, exhibiting competition through an inhibitory population (Figure 5.4A). We also considered a network of two selective excitatory neural populations without cross-inhibition (Figure 5.4B), in order to compare the with vs. without competition conditions.

The network with competition, for a set of parameters, accounts for the experimental trial by trial spike count correlations and mean firing rates of the neuronal populations in PA (Figure 5.7A, PA). Simulating, then, BFS, without any stimulus or noise modulation of the incoming input (Figure 5.5, BFS, where $\lambda_1 = \lambda_2 = \lambda$, $\beta_1 = \beta_2 = \beta$), we find that both noise-correlation of the dominant and of the suppressed neural population increases (Figure 5.6A). Calculating the excitatory-inhibitory balance at the synapses of the neurons we find that this is due to higher excitatory currents (Figure 5.6B), due to the external stimulus to the suppressed population. Therefore, just competition is not enough for the model to account for the experimental data.

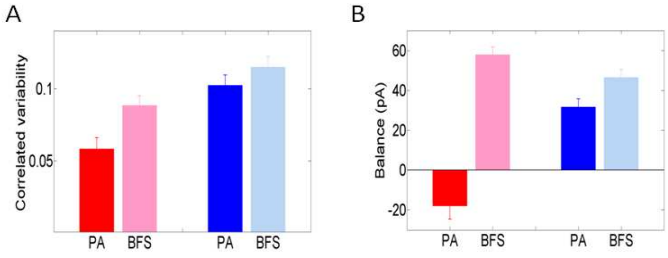

Figure 5.6 Competition increases noise- correlations
A. *Correlated variability of the dominant population in PA (blue), BFS (cyan) and of the suppressed population in PA (red), BFS (magenta) in the case where* $\lambda_1 = \lambda_2 = \lambda$, $\beta_1 = \beta_2 = \beta$ *(Figure 5.5, BFS).* ***C.*** *Excitatory-inhibitory synaptic balance of the dominant neurons in PA (blue), BFS (cyan) and of the suppressed neurons in PA (red), BFS (magenta) in the same case as in A.*

Modulating the strength and the variability of the input to the neuronal ensembles in BFS, the network with competition, successfully accounts for the experimental trial by trial spike count correlations both in PA and

BFS (Figure 5.7), as well as the experimental mean firing rates of the conflicting neuronal ensembles (Figure 5.8A). Nevertheless, the network without competition, with similar input modulations, can also account for the experimental data (Figures 5.7B, 5.8B). Therefore, our results allow us to speculate that competition is not the driving force for the noise-correlation decrease of the dominant population in BFS, nor for the insignificant differences in noise- correlation between PA and BFS of the suppressed population. Rather, strength and noise modulations of the incoming input from previous processing stages are responsible for the decorrelation during visual consciousness.

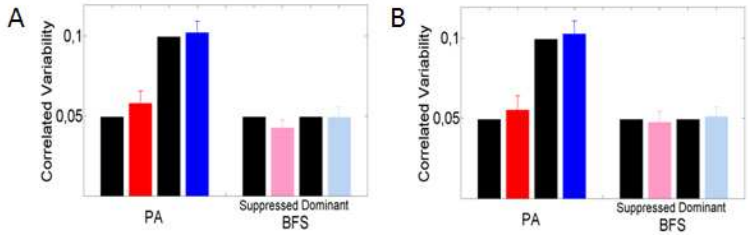

Figure 5.7 Correlated variability in PA & BFS
A. *Experimental Trial by trial spike count correlations (correlated variability) in PA and BFS for the suppressed and dominant neural population (black bars). Blue and red bars are theoretical correlated variability for the dominant and suppressed population respectively, in PA. Cyan and magenta bars are the theoretical correlated variability for the dominant and suppressed neural population respectively, in BFS* ***B.*** *Correlated variability as in A for the network without cross-inhibition*

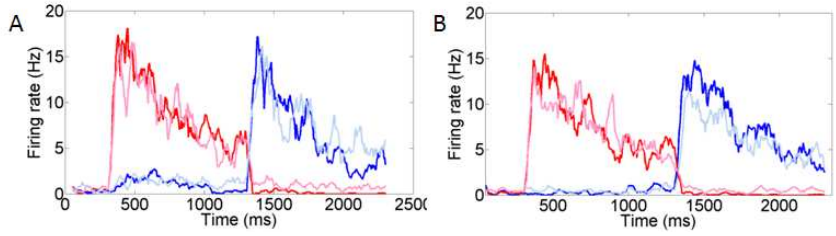

Figure 5.8 Mean firing rates in PA & BFS
A. *Mean firing rate of the dominant population in PA (blue), BFS (cyan) and of the suppressed population in PA (red), BFS (magenta) for the parameters for which the network with cross-inhibition replicates the trial by trial spike count correlations* ***B.*** *Mean firing rate as in A for the network without cross-inhibition*

Furthermore, employing the network with competition, (as well as the network without competition), and using the same parameters for which

accounts for the experimental data, we stimulated both populations for longer period of time and found that no alternations occur (Figure 5.9). It is known that alternations are maintained in binocular rivalry following a period of forced dominance ***(Blake et al. 1990)***, as well as following BFS in LPFC ***(Panagiotaropoulos et al. 2012)***. Therefore, under stimuli-driven conditions, in order for alternations to occur, our theoretical framework suggests that LPFC should be driven by previous processing stages. Given that neurons of the same selectivity in LPFC are strongly anatomically connected with neurons of the same selectivity in IT, our results suggest that IT's output is a plausible candidate for driving rivalry and BFS in LPFC. Nevertheless, we cannot exclude that spontaneous alternations in the BFS followed by BR condition, could be generated by spatiotemporal patterns of the background input in PFC.

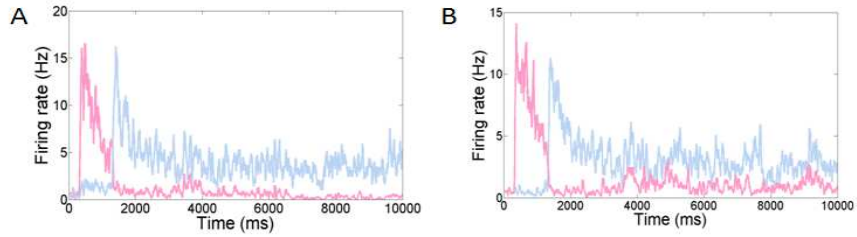

Figure 5.9 BFS followed by BR
A. *For the parameters for which the network with cross-inhibitions replicates the experimental correlated variability, a one trial of BFS followed by long constant stimulation of both populations* ***B.*** *The same as in A for the network without cross-inhibition*

5.3.2 What provokes the noise- correlation reduction in BFS of the dominant neural ensemble?

The noise- correlation of the dominant population decreases in BFS due to smaller fluctuation of the incoming stimulus rate. Calculating the mean and the standard deviation of the membrane potential of the dominant neurons, we find that decrease of input fluctuations results in reduction of the sub- threshold membrane potential fluctuation, while its mean does not change. Thus, the probability for the membrane potential to reach the spiking threshold is smaller, leading to a reduction of noise- correlation. The same stands for the network without competition.

In Figure 5.10 we plot the correlated variability of the dominant neurons (cyan lines), in BFS, as a function of stimulus strength λ for different noises β′. In Figures 5.10A, 5.10B, we consider the network with competition and in Figure 5.10C, the network without competition. In Figures 5.10A, 5.10B, we plot also the correlated variability of the suppressed neurons (magenta lines) in order to show its dependence on the stimulus strength to the dominant population. We do not show the same for the network without competition (Figure 5.10C), because the two populations are independent.

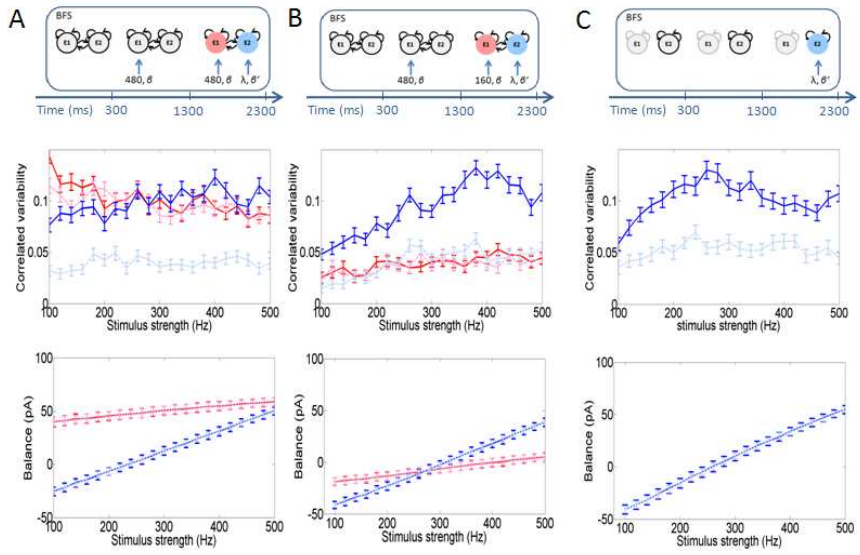

Figure 5.10 Decrease of input noise to the dominant population (β′ < β)
A. Network with competition Up: *Stimulation protocol.* ***Middle:*** *Correlated variability of the dominant population (cyan lines), and suppressed population (magenta lines), as a function of the input strength to the dominant population, λ.* ***Down:*** *Excitatory-inhibitory balance at the synapses of the dominant neurons (cyan lines) and suppressed neurons (magenta lines), as a function of the input strength to the dominant population, λ. Solid lines correspond to* $\beta' = 10^{-4}$ *and dashed lines to* $\beta' = 1\times10^{-5}$*, while* $\beta = 10^{-4}$*.* ***B. Network with competition*** *as in A, with different input strength to the suppressed population.* ***C. Network without competition Up:*** *Stimulation protocol.* ***Middle:*** *Correlated variability of the dominant population (cyan lines), as a function of the input strength to the dominant population, λ.* ***Down:*** *Excitatory-inhibitory balance at the synapses of the dominant neurons (cyan lines), as a function of the input strength to the dominant population, λ. Solid lines correspond to* $\beta' = 10^{-4}$ *and dashed lines to* $\beta' = 5\times10^{-5}$*, while* $\beta = 10^{-4}$*.*

Considering only input modulation in BFS, both networks cannot account for the experimental data of the dominant neural population. For smaller stimulus strength to the dominant population, noise-correlation decreases (Figures 5.10), but stimulus is so small that the mean firing rate of the dominant population in BFS is much smaller than in PA which is against the experimental findings. As a result, competition with only input strength modulation cannot account for the experimental results. Only noise modulation is enough to account for the trial by trial spike count correlations of the dominant population (Figure 5.10). Small stimulus decrease though is needed in order to account for the slightly smaller mean firing rate of the dominant population in BFS than PA, as found experimentally.

The Fano factor of the dominant neurons in BFS has been found to be not significantly different than the Fano factor of the dominant neurons in PA. This is because the mean firing rate of the dominant neurons in BFS slightly decreases and so does their variance. Decrease of the stimulus to the dominant population in BFS increases the Fano factor of the neurons, and decrease of the input noise to the dominant population decreases the Fano factor of the neurons. Both actions result in keeping the Fano factor of the dominant neurons in BFS similar as in PA.

5.3.3 What provokes the noise- correlation stability in BFS of the suppressed neural ensemble?

The noise- correlation of the suppressed neurons in BFS remains at the same level compared to PA, due to both stimulus decrease and noise increase coming from a preceding processing stage. Considering the network with competition and without any stimulus or noise modulation, the noise correlation of the suppressed population is higher in BFS than in PA (Figure 5.6). Decreasing the stimulus strength, noise correlation decreases, but the stimulus for which the experimental data are replicated is high leading to higher mean firing rate of the suppressed population in BFS compared to PA, contrary to the experimental data. Increasing the fluctuation of the incoming rate to the suppressed population, noise correlation increases, thus smaller stimulus strength to the suppressed population is needed in order for the network to account for experimental data.

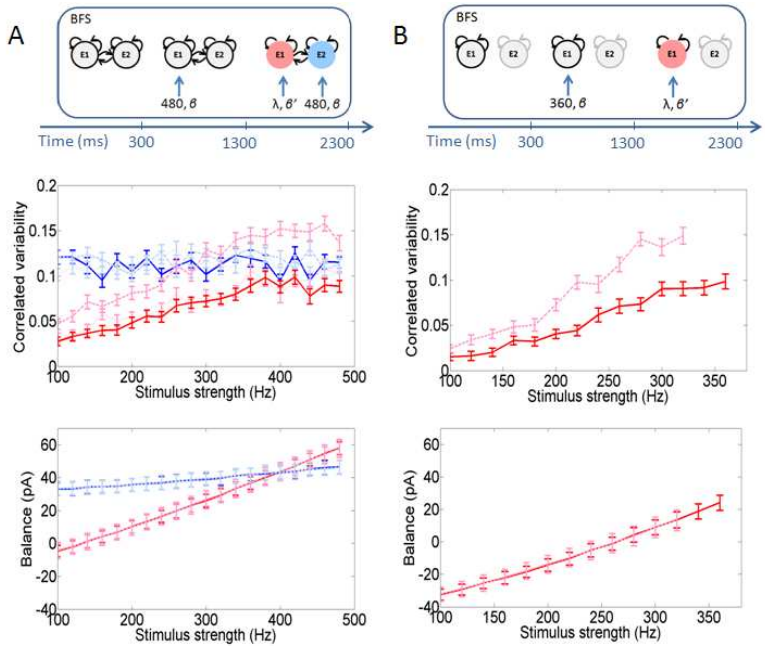

Figure 5.11 Increase of input noise to the suppressed population (β′ > β)
A. Network with competition Up: *Stimulation protocol* ***Middle:*** *Correlated variability of suppressed neurons in BFS as a function of stimulus strength, λ, when the fluctuation of the incoming input β′ is 10^{-4} (solid magenta line), 1.1×1^{-4} (dotted magenta line) and 1.5×10^{-4} (dashed magenta line), while in all conditions $\beta = 10^{-4}$. The correlated variabilities of the dominant neurons in these conditions are the cyan solid, dotted and dashed line respectively.* ***Down:*** *Excitatory-inhibitory synaptic balance at the synapses of the suppressed neurons as a function of stimulus strength, λ, when $\beta' = 10^{-4}$ (solid magenta line), $\beta' = 1.1\times10^{-4}$ (dotted magenta line) and $\beta' = 1.5\times10^{-4}$ (dashed magenta line), while in all conditions $\beta = 10^{-4}$. The excitatory-inhibitory synaptic balances of the dominant neurons in these conditions are the cyan solid line, dotted, and dashed, respectively.* ***B. Network without competition Up:*** *Stimulation protocol* ***Middle:*** *Correlated variability of suppressed neurons in BFS as a function of stimulus strength, λ, when the fluctuation of the incoming input β′ is 1×10^{-4} (solid magenta line), and 1.5×10^{-4} (dashed magenta line).* ***Down:*** *Excitatory-inhibitory synaptic balance of the suppressed neurons as a function of stimulus strength, λ, when $\beta' = 10^{-4}$ (solid magenta line) and when $\beta' = 1.5\times10^{-4}$ (dashed magenta line), while in both conditions $\beta = 10^{-4}$.*

Therefore, both modulations to the input rate and to the noise of the input rate are responsible for the non- significant differences of the trial by trial spike count correlation of the suppressed population in BFS compared to PA. The same stands for the network without competition (Figure 5.11). Calculating the mean and the standard deviation of the membrane

potential of the suppressed neurons we find that in BFS the mean voltage increases but the standard deviation decreases, compared to PA, and this is why the noise- correlations do not change significantly.

In Figure 5.11 we plot the correlated variability of the suppressed neurons (magenta lines), in BFS, as a function of stimulus strength λ for different noises β′. In Figure 5.11A we consider the network with competition and in Figure 5.11B, the network without competition. In Figure 5.11A we plot also the correlated variability of the dominant neurons (magenta lines) in order to show its dependence on the stimulus strength to the suppressed population. We do not show the same for the network without competition (Figure 5.11B), because the two populations are independent.

The Fano factor of the suppressed neurons in BFS is found to be not significantly different compared to PA. This is because the mean firing rate of the suppressed neurons slightly increases and so does their variance. The input to the suppressed population in BFS decreases the Fano factor of the suppressed neurons, compared to PA where there is no external stimulus. By increasing, though, the noise of the input rate, the Fano factor of the suppressed neurons in BFS increases and approaches the value of their Fano factor in PA.

5.3.4 Analysis with the moments method

Using the augmented method of moments presented in Chapter 2 (§2.4), we simulated PA and BFS (Figure 5.12) and replicated the experimental correlated variability, employing both networks, with and without competition. We, hence, conclude that competition is not the driving force for the noise- correlation reduction during rivalrous visual stimulations. Instead, the noise- correlation reduction is due to stimulus and noise modulation coming from previous stages. Therefore, we conclude the same result that we found by employing the biophysically realistic networks. The most plausible scenario is that competition is resolved in a previous stage, like IT, and neurons in LPFC are driven by IT's output.

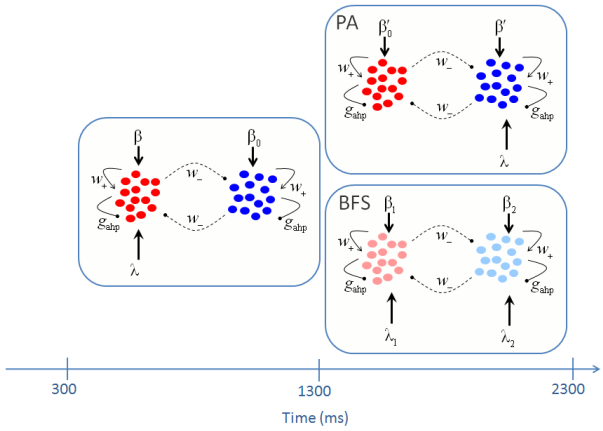

Figure 5.12 Stimulation protocol
*Network of two neural ensembles with self-excitation w_+ (arrows) and cross inhibition w_- (dashed lines ending to circles) and neuronal adaptation g_{AHP} (lines ending to circles). Each pool is consisted of N neurons selective to the same stimulus. During the first second only one pool is stimulated (e.g. red) by λ. During the 2nd second, in **PA**, neurons of the other pool (blue) receive external input λ, while in **BFS**, neurons of pools receive external stimuli, red pool is stimulated by λ_1, and blue by λ_2. β_0, β_0', β', β, β_1, β_2 are the noises of the background and the corresponding inputs. The colors of the neurons during the last second of stimulation in PA and BFS are different just to correspond to the colors used throughout the results.*

We solved the system of the DEs (§2.4) with Euler method, and time step dt = 0.1 ms. Noise intensities β_0, β, β_0', β', β_1 and β_2 in the followings are integers for simplicity, since results do not change when all are multiplied by the same factor. In the direct simulations of the system of stochastic equations we multiplied all by 10^{-9}, and as we see in Figure 2.12, the results do not change.

More specifically, we first consider the case when there is not cross inhibition between the two neuronal ensembles ($w_- = 0$), i.e. when there is not competition. We simulated PA for a given level of adaptation, g_{AHP}, and stimulus strength, λ, and found the region in the β_0'- β space where the correlated variability of both ensembles is similar to the experimental data (Figure 5.13A). Then, for a set of noise intensities taken from this region we found the region in the g_{AHP} - λ space where the simulated correlated variability of both ensembles is similar to the experimental data (Figure 5.13B).

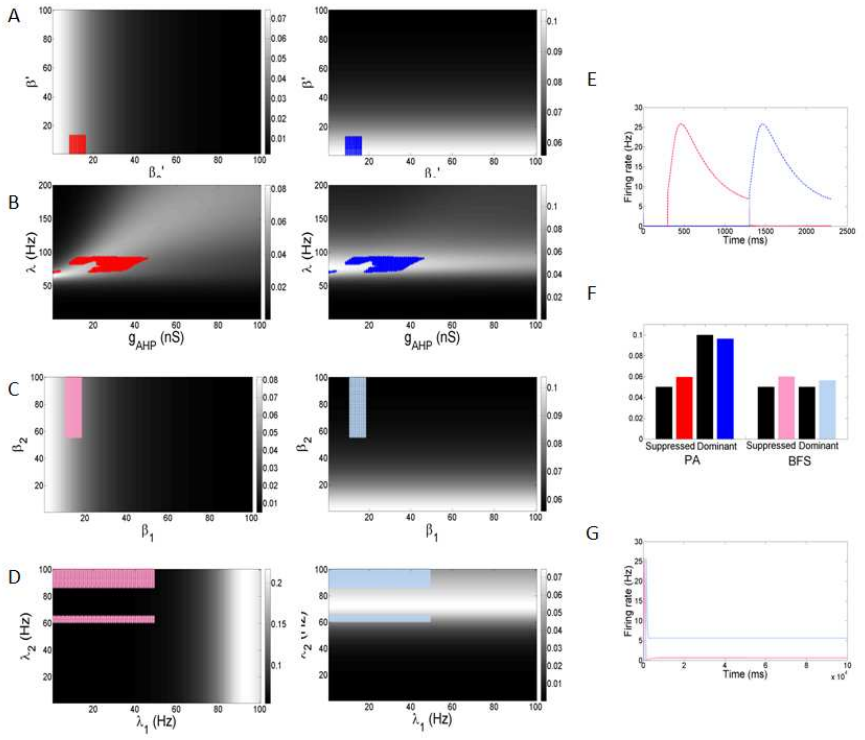

Figure 5.13 Network without competition
A. *Correlated variability of the suppressed (red) and dominant (blue) population in PA as a function of the noise intensities β_0', β', for a given level of adaptation (g_{AHP} = 22 nS) and stimulus strength (λ = 90 Hz)* ***B.*** *Correlated variability of the suppressed (red) and dominant (blue) population in PA as a function of the level of adaptation g_{AHP} and stimulus strength λ, for a set of noise intensities taken from A ($\beta_0' = \beta' = 9$)* ***C.*** *Correlated variability of the suppressed (magenta) and dominant (cyan) population in BFS as a function of the level of noise intensities β_1, β_2, for a given set of stimuli (λ = 90 Hz, λ_1 = 49 Hz, λ_2 = 90 Hz)* ***D.*** *Correlated variability of the suppressed (magenta) and dominant (cyan) population in BFS as a function of the stimuli λ_1, λ_2, for a set of noise intensities taken from C (β_1 = 11, β_2 = 90)* ***E.*** *Mean firing rate of the two ensembles in PA and BFS for g_{AHP} = 22 nS, λ = 90 Hz, $\beta_0' = \beta' = 9$, λ_1 = 49 Hz, λ_2 = 90, β_1 = 11, and β_2 = 90* ***G.*** *Correlated variabilities in PA and BFS for same parameters as in E* ***G.*** *BFS followed by BR keeping the same parameters as in E.*

Then, for a set of a level of adaptation g_{AHP} and stimulus strength, λ, from this region, and for a given set of $\lambda 1$, $\lambda 2$, we simulated BFS and found the region in the β_1 - β_2 space where the simulated correlated variability of both ensembles is similar to the experimental ones (Figure 5.13C). Finally, for a set of β_1, β_2 from this region, we find the region in the λ_1 - λ_2 space where the simulated correlated variability of both ensembles in BFS

is similar to the experimental ones (Figure 5.13D). From this region some sets of λ_1, λ_2 should be excluded because the firing rate of the ensembles are not similar to the experimental, when $\lambda_1 > \lambda_2$ and $\lambda_2 < 87$ Hz. For a set of λ_1, λ_2 from the final region in the λ_1 - λ_2 space, we plot the mean firing rates in PA and BFS (Figure 5.13E) and the correlated variabilities together with the experimental ones (Figure 5.13F). In addition, as expected, when we stimulate both pools for longer period of time, no alternations are observed, since there is no competition (Figure 5.13G).

We find that only with competition, i.e. when $\lambda_1 = \lambda_2 = \lambda$ and $\beta_1 = \beta_2 = \beta' = \beta_0'$, the experimental results in BFS are not satisfied (Figure 5.14), meaning, that competition is not enough in order to replicate the experimental data. Manipulating also the noise intensities, still it is not possible to replicate the experimental data.

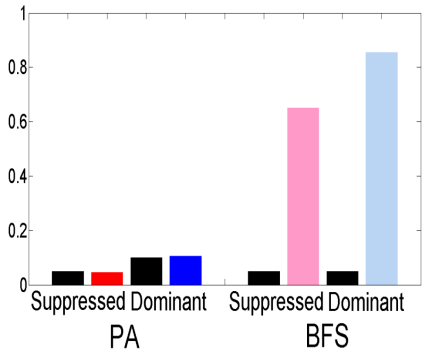

Figure 5.14 The effect of competition to noise- correlations
Correlated variability of the dominant population in PA (blue), BFS (cyan) and of the suppressed population in PA (red), BFS (magenta) in the case when $\lambda_1 = \lambda_2 = \lambda = 90$ Hz and $\beta_1 = \beta_2 = \beta' = \beta_0' = 9$.

We follow the same procedure employing the network with competition ($w_- \neq 0$, Figure 5.15). For the parameters for which we replicate the experimental data, if we stimulated both pools for longer period of time we find no alternations, even in the case when there is competition in the network (Figure 5.15G), as we found with the biophysically realistic spiking network (Figures 5.9A). Therefore our results suggest that competition is not resolved in LPFC, rather neurons in LPFC are driven by previous procession stages.

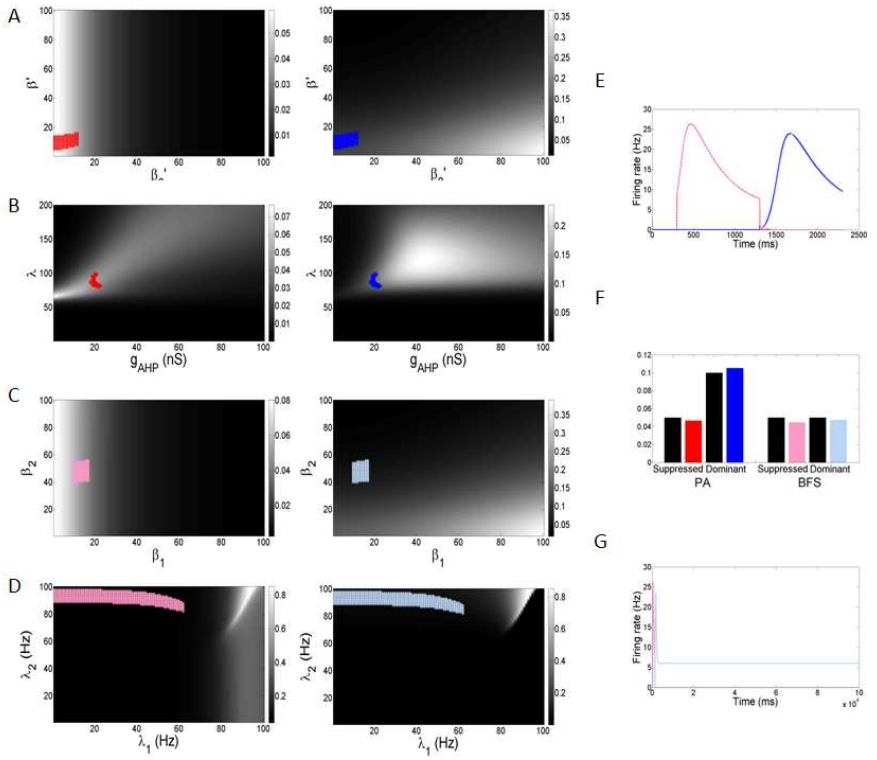

Figure 5.15 Network with competition
A. *Correlated variability of the suppressed (red) and dominant (blue) population in PA as a function of the noise intensities β_0', β', for a given level of adaptation (g_{AHP} = 2 nS) and stimulus strength (λ = 90 Hz)* ***B.*** *Correlated variability of the suppressed (red) and dominant (blue) population in PA as a function of the level of adaptation g_{AHP} and stimulus strength λ, for a set of noise intensities taken from A ($\beta_0' = \beta' = 9$)* ***C.*** *Correlated variability of the suppressed (magenta) and dominant (cyan) population in BFS as a function of the level of noise intensities β_1, β_2, for a given set of stimuli (λ = 90 Hz, λ_1 = 60 Hz, λ_2 = 90 Hz)* ***D.*** *Correlated variability of the suppressed (magenta) and dominant (cyan) population in BFS as a function of the stimuli λ_1, λ_2, for a set of noise intensities taken from C (β_1 = 11, β_2 = 40)* ***E.*** *Mean firing rate of the two ensembles in PA and BFS for g_{AHP} = 2 nS, λ = 90 Hz, $\beta_0' = \beta' = 9$, λ_1 = 60 Hz, λ_2 = 90 Hz, β_1 = 11, β_2 = 40* ***G.*** *Correlated variabilities in PA and BFS for same parameters as in E* ***G.*** *BFS followed by BR keeping the same parameters as in E.*

Our study suggests that LPFC is driven by previous processing stages because of the stimulus manipulation needed in order to account for the experimental results, but also because, as we show, if we stimulate longer both pools there are no alternations of their firing rates. This is expected for the network without competition but it is not trivial for the network

with competition. In Figures 5.15E - 5.15G we present the results of one set of λ_1, λ_2. Nevertheless, higher λ_1 lead to alternations (Figure 5.16). We calculated the correlated variability of both ensembles, in BFS, for different values of λ_2, especially near the bifurcation. We find that the experimental data are not satisfied in the oscillatory regime.

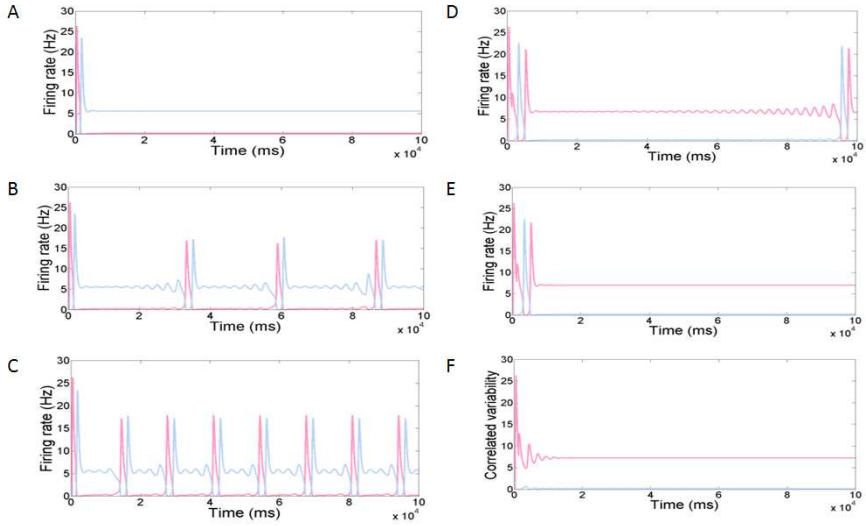

Figure 5.16 Near the bifurcation
A. *Mean firing rate of the two ensembles for λ1 = 83 and λ2 = 90 Hz.* ***B.*** *Same as A for λ1 = 84.* ***C.*** *Same as A for λ1 = 85.* ***D.*** *Same as A for λ1 = 87.* ***E.*** *Same as A for λ1 = 96 Hz* ***F.*** *Same as A for λ1 = 97 Hz.*

This result comes from a given set of g_{AHP}, λ, taken from Figure 5.15B. Therefore, for the sake of robustness, we calculated the correlated variability at the bifurcation points for all sets of g_{AHP}, λ that replicate the PA data (Figure 5.17). For these values we then computed the correlated variability as a function of β_1, β_2, and found if and when the model replicates the BFS data. There are some cases when the model with competition can replicate the experimental trial by trial spike count correlations in the oscillatory regime, i.e. right after the bifurcation, (circles, Figure 5.17). Nevertheless, the firing rate of the dominant population in BFS when the model is in the oscillatory regime, it is not similar to PA (Figure 5.17 smaller panels). As λ_1 increases the difference of the firing rate of the dominant pool in BFS compared to PA is increasing. We therefore, conclude that both the spiking and the rate

model operate in the non-oscillatory regime, in order to replicate the experimental data.

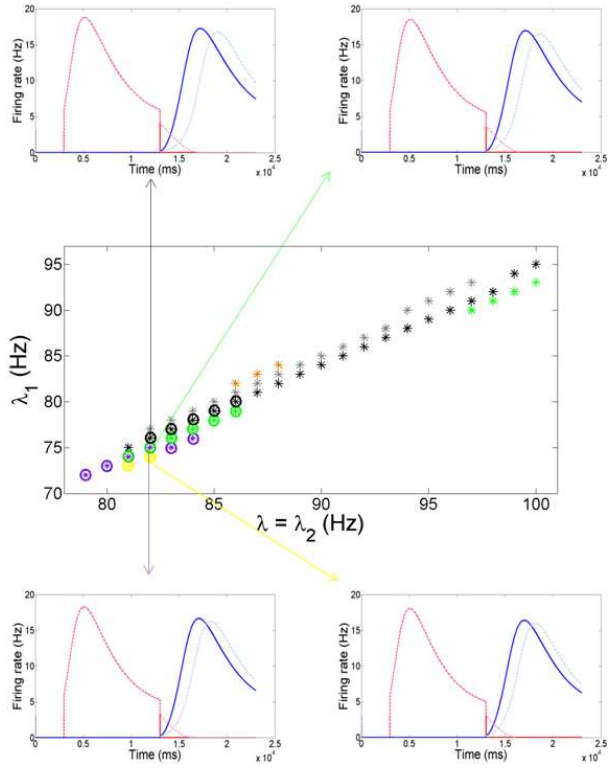

Figure 5.17 Bifurcation points
Bifurcation points λ_1, $\lambda = \lambda_2$, g_{AHP} for which the system in BFS followed by long stimulation the system transits to oscillatory regime. Orange points correspond to g_{AHP} = 18 nS, gray to g_{AHP} = 19 nS, black to g_{AHP} = 20 nS, green to g_{AHP} = 21 nS, purple to g_{AHP} =22 nS and yellow to g_{AHP} =23 nS. The λ, g_{AHP} values are taken from Figure 5.14B (red and blue regions). Circles correspond to the bifurcation points for which the system replicates the experimental data in BFS, varying the noise intensities β_1, β_2. In smaller panels we draw the firing rate of the neuronal ensembles in PA (blue, red) and BFS (cyan, magenta) for $\lambda = \lambda_2$. Qualitatively similar is the behavior for the rest of λ_1, $\lambda = \lambda_2$, g_{AHP} points.

5.4 Discussion

Although single unit recordings indicate that neurons in association cortical areas represent explicitly the content of visual consciousness ***(Panagiotaropoulos et al. 2012; Sheinberg & Logothetis 1997)***, it is unknown how features of neuronal ensemble interactions influence the

fidelity of these representations. Specifically, the direct relationship between correlated neuronal interactions and information encoding ***(Zohary et al. 1994; Abbot & Dayan 1999; Averbeck et al. 2006)*** makes necessary the study of correlations during subjective visual perception. To address this issue in the macaque LPFC, we tracked the responses of simultaneously recorded neuronal pairs with similar stimulus preference during the perceptual dominance or suppression of their preferred visual pattern under conditions of visual rivalry. Within this population and during subjective visual perception of a preferred stimulus, pair-wise noise correlations were found to be close to zero compared to the weak but significant correlated variability when the same visual pattern was perceived without competition. No differences in correlated variability were observed when the preferred stimulus was rendered invisible through perceptual suppression compared to its physical absence. Furthermore, pair-wise correlations between neurons of opposite preference were not modulated by visual competition. These findings provide the first insights into the functional interactions of neuronal ensembles mediating visual consciousness.

The experimental results indicate a dramatic alteration in the noise correlation structure of prefrontal microcircuits during subjective visual perception compared to the structure observed when perception occurred without visual competition and therefore without significant subjective factor. Specifically, under conditions of stimulus perception without any visual competition, noise correlations have a *limited-range* and *stimulus-dependent* structure. In a limited-range structure, neurons that are more similarly tuned are also more correlated (regardless of the stimulus used) while a stimulus-dependent structure implies stronger correlations for similarly tuned neurons when a preferred stimulus is presented. This is indeed what it is observed in the LPFC during purely sensory perception since noise correlations were stronger for neurons with similar tuning when the correlation values for preferred and non-preferred stimuli were combined compared to the correlations for pairs of neurons with opposite stimulus preference. In addition during PA a stimulus-dependent structure was also observed since pairs of neurons with similar stimulus preference where more correlated during perception of a preferred stimulus compared to the perception of a non-preferred.

During BFS, the limited-range and stimulus-dependent structure is not observed due to an asymmetric reduction of correlations observed specifically during the perceptual dominance of the preferred pattern. As a result both the limited-range and stimulus-dependent structure of correlations are lost.

Two recently published studies demonstrated a decrease in correlated variability across pairs of simultaneously recorded neurons in macaque area V4 as a result of attention ***(Cohen & Maunsell 2009; Mitchell et al. 2009)***. It was further estimated that the beneficial effect of the decorrelation on the signal to noise ratio of a pooled response was much larger than the respective effect of a concomitant decrease in individual variability, as assessed by the Fano factor, or an increase in the population mean firing rate. The experimental data demostrate that perceptual dominance of a preferred stimulus under conditions of BFS is accompanied by a very similar decrease in correlated variability compared to purely sensory stimulation. No difference in the mean firing rate or in the individual response variability was found when compared BFS to sensory stimulation. Therefore an enhanced signal to noise ratio is observed only at the population level as a result of decorrelated discharges. The striking similarity of decorrelation provides a link associating directly the computational processes emerging through population coding in visual awareness to those of selective attention. In that case, prefrontal microcircuits facilitate subjective visual perception most likely by exploiting the same computational strategies employed in selective attention in area V4. Active decorrelation of interneuronal discharges might thus constitute a broadly used strategy in the cortex that effectively gives rise to selection processes by increasing the signal to noise ratio and encoding capacity of a given population under conditions of visual competition.

There was no external manipulation ("cueing") of attention in one of the two experimental conditions. In both sensory and perceptual trials an identical, incoming stimulus is either replacing or perceptually suppressing, respectively, the same, disparate, visual pattern. Thus, any observed changes in the correlated state of the network should be ascribed to the impact of visual competition between disparate patterns on the network *per se* and not to any differences in exogenous attention levels. In

support of this argument, these experimental results are not completely identical to those reported during attention tasks.

The perceptually modulated neurons during BR are distributed from V1 to PFC, nonetheless where competition is resolved is still unknown. Employing two biophysically realistic spiking networks, with and without competition, we replicated the experimental correlation coefficients, and found that perceptually modulated neurons in LPFC are driven by previous processing stages, e.g. IT. Our results exclude LPFC from having an active role in the disambiguation of the conflicting percepts in BR. To our knowledge, this is the first time that a theoretical study suggests where in the cortical pathways mechanisms are resolved. We conclude the same by calculating analytically the correlation coefficients using the augmented method of moments.

Furthermore, we found which mechanisms provoke the intriguing decrease of the correlated variability of the dominant neurons in BFS compared to PHA, as well as the constancy of the correlated variability of the suppressed neurons in BFS compared to PHA. More specifically, we concluded that the dominant neurons in BFS receive smaller input noise from previous stages, compared to the input noise they receive in PHA. The steadiness of the correlated variability of the suppressed neurons, on the other hand, is due to the smaller input and higher noise input the suppressed neurons receive in BFS compared to PHA. Our results provide also a prediction about the variability of the incoming input to LPFC during BFS compared to PHA. For example, recording simultaneously from IT and LPFC during BFS and PHA, we expect that the variability of mean firing rates of the dominant neurons in IT is smaller in BFS compared to PHA.

In conclusion, it is the first time that a noise- correlation study has been conducted in the context of visual consciousness. We employed a biophysically inspired cortical network to understand the underlying mechanism of this decorrelation. The main conclusion of our study is that neurons in IPFC are driven by preceding processing stages, like IT. Then we show that competition is not relevant for the correlation decrease and we explain why. Finally we show the mechanism for the correlation decrease of the dominant population and the stability of the suppressed population.

General Discussion

Three passions,
simple but overwhelmingly strong,
have governed my life;
the longing for love,
the search for knowledge, and
unbearable pity for the suffering of mankind.
These passions, like great winds, have blown me hither and thither, in a wayward course, over a deep ocean of anguish, reaching to the very verge of despair
Bertrand Russell

When a subject is dichoptically presented with two conflicting images, only one image is perceived at a time while the other is suppressed from awareness; a paradigm of multistable perception, known as Binocular Rivalry (BR). Perception, therefore, alternates between the two visual patterns allowing a dissociation of sensory stimulation from conscious visual perception. From theoretical point of view, most of the computational models proposed to account for BR are rate- like models. It was, nevertheless, apparent the need of employing biophysically plausible neuronal network models.

Competition models based on cross-inhibition and adaptation have shown that noise is a crucial force for rivalry, and operates in balance with adaptation ***(Shpiro et al. 2009)***. In particular, noise- driven transitions and adaptation- driven oscillations define two dynamical regimes and the system explains the observed alternations in perception when it operates near their boundary. In order to gain insights into the microcircuit dynamics mediating spontaneous perceptual alternations, we used a reduced recurrent attractor- based biophysically realistic spiking network, well known for working memory, attention, and decision making, where a

spike-frequency adaptation mechanism is implemented (§2.2) to account for perceptual bistability. We then derived a consistently reduced four-variable population rate model using mean- field techniques (§2.3), and we tested it on BR data collected from human subjects (Chapter 3). Our model accounts for experimental data parameters such as mean time dominance, coefficient of variation, and gamma distribution fit. In addition, we show that our model operates near the bifurcation that separates the noise- driven transitions regime from the adaptation- driven oscillations regime, and agrees with Levelt's second revised and fourth propositions. These results demonstrate for the first time that a consistent reduction of a biophysically realistic spiking network of leaky integrate-and- fire neurons with spike- frequency adaptation could account for BR. Moreover, we demonstrate that BR can be explained only through the dynamics of competing neuronal pools, without taking into account the adaptation of inhibitory interneurons. However, the adaptation of interneurons affects the optimal parametric space of the system by decreasing the overall adaptation necessary for the bifurcation to occur, and introduces oscillations in the spontaneous state.

Furthermore, we considered recent experimental data from the macaque lateral Prefrontal Cortex collected during Binocular Flash Suppression, a paradigm of externally induced perceptual alternation. They show a decrease in correlated variability across pairs of neurons sharing similar stimulus preferences when their preferred stimulus is perceived during rivalrous visual stimulation compared to the magnitude of correlation when the same stimulus is perceived without competition. We employed a biophysically realistic spiking network (§2.2), as well as we extracted analytical expression for second-order statistics (§2.4), in order to explain these intriguing experimental evidences regarding population coding of visual consciousness (Chapter 5). Our results suggest that the source of noise- decorrelation during visual consciousness is not due to the dynamics of local competition between antagonistic ensembles but rather due to stimulus and noise modulations in preceding processing stages.

Finally, there has been an increased interest on the neural mechanisms underlying perceptual decision making. However, the effect of neuronal adaptation in this context had not been studied. We, therefore, investigated how neural adaptation can bias perceptual decisions. For this

purpose, we considered behavioral data of an experiment on high- level adaptation- related aftereffects in a perceptual decision task with ambiguous stimuli on humans (Chapter 4). To understand the driving force behind the perceptual decision process, a biologically inspired cortical network model was used (§2.2). Two theoretical scenarios arose for explaining the perceptual switch from the category of the adaptor stimulus to the opposite, nonadapted one. One is noise- driven transition due to the probabilistic spike times of neurons and the other is adaptation-driven transition due to afterhyperpolarization currents. With increasing levels of neural adaptation, the system shifts from a noise- driven to an adaptation- driven modus. The behavioral results show that the underlying model is not just a bistable model, as usual in the decision- making modeling literature, but that neuronal adaptation is high and therefore the working point of the model is in the oscillatory regime. Using the same model parameters, we studied the effect of neural adaptation in a perceptual decision- making task where the same ambiguous stimulus was presented with and without a preceding adaptor stimulus. We find that for different levels of sensory evidence favoring one of the two interpretations of the ambiguous stimulus, higher levels of neural adaptation lead to quicker decisions contributing to a speed- accuracy trade- off.

- Why "fluctuations in perceptual decisions"?

Perceptual decision making denotes the perceptual choice of a subject due to the temporal accumulation of sensory evidence. The most extensively studied paradigm is the two- alternative forced- choice experiment. In such an experiment a subject is asked to discriminate between two alternative sensory visual stimuli, as in the random- dots motion discrimination task *(**Newsome et al. 1989; Britten et al. 1992; Shadlen & Newsome 2001; Roitman & Shadlen 2002; Palmer et al. 2005**)*, or between two alternative tactile stimuli, as in the vibrotactile frequency discrimination task *(**Romo et al. 2000; Romo & Salinas 2003**) (for reviews see **Opris & Bruce 2005; Gold & Shadlen 2007; Wang 2012**)*.

Multistable perception has often been compared to cognitive processes such as attention and decision making *(**Leopold & Logothetis 1999, Stoner et al. 2005**)*. But it is only recently, that attempts have been made in order to study how these phenomena might be related *(**Braun & Mattia 2010; Kalisvaart et. al 2011**)* within a common theoretical framework. As

we see in the current thesis, recurrent attractor networks seem to be a plausible candidate.

- *But, are there attractors in the brain?*

Up to date, almost all evidences in favor of attractors in the brain come from theoretical studies that replicate experimental evidences. While this is convincing enough, they become even more convincing when they further provide predictions which are later validated by experiments. There is a large literature in this direction, mostly from studies related to perceptual decision making and working memory. Interestingly, there is one purely experimental study that provides indirect evidence of attractor dynamics in the brain, specifically in the hippocampal representation of the local environment ***(Wills et al. 2005)***. But is there a way to experimentally test the existence of attractors in multistable perception? The approach we follow, suggest that cross-inhibition between neural populations each comprised of neurons selective to e.g. one of the images in BR, along with a slow fatiguing process, e.g. neural adaptation, explain the perceptual alternations, when noise operates in balance with neural adaptation. The working point of the model is in the bistability regime, very close to the bifurcation that separates it from oscillatory dynamical regime. Is there a way to test this experimentally? Our theoretical approach suggests that if noise in the brain decreases or if the level of neural adaptation decreases, the observer would experience perceptual stabilization. While the manipulation of the level of neural adaptation could be possible via pharmacological application, naturally a question arises: is there a way to manipulate the noise in the brain? Interestingly, it has been shown that reversal rates can be slowed down via meditation (***Carter et al. 2005***). Perhaps, speculatively we could assume that meditation could result in decreasing the intrinsic noise, and this could be an indirect evidence of attractors in the brain.

- *What about attention?*

A common neural mechanism has been suggested to underlie stimulus selection processes leading to both subjective visual perception and selective attention ***(James 1890; Posner 1994)***. The visual system is resolving both problems by selecting a unique interpretation of a bistable visual pattern or a specific feature of a visual scene to be further processed

and reach awareness while suppressing competing stimuli or ignoring potential distracters, respectively, in the visual environment. Indeed, elegant psychophysics studies have previously shown significant interactions between attention and binocular rivalry ***(Lack 1978; Meng & Tong 2004; van Ee et al. 2005; Mitchell et al. 2004; Chong et al. 2005; Chong & Blake 2006; Hancock & Andrews 2007)***. Most interestingly, attentional selection of one stimulus was found to bias its predominance over the rivaling stimulus during spontaneous binocular rivalry ***(Mitchell et al. 2004)***. Such a modulatory role of attention in perceptual dominance provides direct evidence that at least a part of the neural mechanisms mediating selective processes in attention might interact with, or even be similar to, the mechanisms mediating visual awareness *(**Leopold and Logothetis 1999; Sasaki & Gyoba 2002; Ooi et al. 1999, Mitchel et al, 2004; Stoner et al. 2005)***.

- *Is adaptation really important?*

In the current thesis we show that an adapting reciprocal inhibtion model, with both noise and adaptation operating in balance, can explain the behavior in BP (Chapter 3), affirming a previous study ***(Shpiro et al. 2009)***, as well as that neural adaptation is relevant in a category of decision- making paradigms (Chapter 4). In addition, it has been suggested that noise and adaptation operate in balance in order to account cumulative history effects in BP ***(Pastukhov et al. 2013)***. Furthermore, it has been suggested that adaptation plays crucial role in explaining the freeze of perception under intermittent presentation (***Noest et al. 2007; Brascamp et al. 2008***). The effect of cross-inhibition in BR has been observed experimentally by showing that gaba shapes the dynamics of bistable perception ***(van Loo et al. 103)***. However, experiments have shown evidences both in favor and against the relevance of neural adaptation in BP ***(Hupé & Rubin 2003; Rubin & Hupé 2005; Mamassian & Goutcher 2005; van Ee 2009; Alais 2012)***, which along with theoretical approaches for BP different to the adapting reciprocal inhibition model (§2.1) renders the question still open.

- *So, what's next?*

There is an increasing interest in studying multistable perception when multiple sensori stimuli are integrated *(see the special issue **Schwartz et***

al. 2012). This means, that while a subject experiences e.g. visual rivalry an event of a different modality occurs in the dominance or the suppressed perceptual phase. Furthermore, one can experience perceptual alternations between more than two interpretations of an ambiguous stimulus (Figure 1.7). There are not yet many theoretical studies to explain this phenomenon ***(Huguet et al. 2012)***. It would be interesting to see how e.g. cross-inhibition models can account for the increasing experimental evidences in this context. In addition, perceptual multistability emerges across different modalities: visual, auditory, tactile, olfactory, and verbal (Figure 1.7). There is an increasing interest in studying the similarities and discrepancies in the temporal dynamics of MP between different modalities. It would be interesting to see what happens when two or more different rivalry modalities are emerging simultaneously, and how the results can be explained theoretically. All these new experimental paradigms and evidences challenge theoretical approaches that so far have been restricted only to bistable visual rivalry. Of course, here, the need of multistage networks, as we discussed previously, is even more apparent.

Furthermore, when subjects are presented with an ambiguous figure intermittently in time their perception freezes in one of its interpretations (Figures 1.6) ***(Orbach et al. 1963a, 1963b, 1966; Leopold et al 2002; Maier et al. 2003;*** *for review see* ***Pearson & Brascamp 2008)***. Following the initial studies, more psychophysical experiments ***(Chen & He 2004; Pearson & Clifford 2004; Zheng & Ukai 2006; Noest et al. 2007; Brascamp et al. 2008; Klink et al. 2008b; Pastukhov & Braun 2008; Brascamp et al. 2009; Klink et al. 2009; Kang & Shevell 2011; Manousakis 2012; de Jong et al. 2012; Zheng & Ukai 2013; Murphy et al. 2014)*** have been held in this context, as well as several EEG ***(Kornmeier & Bach 2005; Kornmeier et al. 2007; Sterzer & Rees 2008; Britz et al. 2009; Pitts & Britz 2011)***, fMRI ***(Wang et al. 2013),*** and electrophysiological studies ***(Maier et al. 2002; Tsuchiya et al. 2008; Tsuchiya et al. 2009; Klink et al. 2012)***. This intriguing phenomenon arises interesting questions from theoretical point of view, and several theoretical approaches have been considered ***(Noest et al. 2007; Wilson 2007; Brascamp et al. 2008; Klink et al. 2008; Pastukhov & Braun 2008; Brascamp et al. 2009; Gigante et al. 2009; Klink et al. 2009; Manousakis 2009; Manousakis 2012; Noest & van Wezel 2012; Woldman 2012)***.

The most extensively studied so far model to account for the perceptual repetitions, is Noest's model ***(Noest et al. 2007)***. It is based on cross-inhibition and slow shunting adaptation with a near-threshold facilitatory effect ***(Noest et al. 2007; Brascamp et al. 2008; Klink et al. 2008; Pastukhov & Braun 2008; Brascamp et al. 2009; Noest & van Wezel 2012)***. It distinguishes *percept-choices* at the onset of the presentation after the blank period from the *percept-switching* in continuous presentation. Shunting adaptation is the main mechanism that gives rise to the perceptual repetitions under intermittent presentation. Nevertheless, let us make a hypothetical simple experiment: a subject is presented intermittently with an ambiguous figure for some period until a continuous presentation starts and lasts for e.g. 5 minutes. The subject, as we expect, will experience *percept-choices* during the intermittent presentation, followed by *percept-switches* during the continuous presentation. How Noest's model would then change in order to account for the experimental evidences during continuous presentation? Interestingly, this question has not only not been studied yet, but neither discussed. In continuous presentation, a two-population model with cross-inhibition and a slow fatiguing process, e.g. spike-frequency adaptation, can account for the experimental evidences near the bifurcation that separates bistabilty from oscillatory regime ***(Shpiro et al. 2009;*** Chapter 3). Shouldn't there be a common theoretical framework that accounts for the previously described hypothetical experiment? It has been shown that periods of disambiguation between long continuous presentations of ambiguous stimuli do not affect the temporal dynamics of MP ***(Blake et al. 1990)***. We have no reason to expect that periods of intermittent presentations between long continuous presentations would alter the temporal dynamics of MP, but of course, this is only a speculation, and the experiment should be performed in order to test it. In any case, we think that a common theoretical framework with adequate, neurophysiologically plausible, modulations, if needed, should account for the experimental evidences of such an experiment. In addition, perceptual stabilization increases with increasing blank periods and for some subjects it can reach up to 10 minutes for long blank periods ***(Leopold et al. 2002)***. None of the models studied so far have convincingly shown that can account for this remarkable phenomenon. Neurophysiological findings have shown that differences in firing rate related to the perceptual

interpretation (disambiguation) happen faster when a macaque is experiencing perceptual stabilization *(**Tsuchiya et al. 2009; Maier A.,** personal communication)*. This could be an additional constrain to models together with other neurophysiological findings in this context *(**Maier et al. 2002; Tsuchiya et al. 2008; Klink et al. 2012**)*. It would be interesting to see whether and how a biophysically plausible network can account for this intriguing phenomenon and how it should change in order to account for the experimental evidence of the previously described experiment: intermittent periods of presentation between long continuous presentations.

Regarding all experimental evindences, from macroscopic to microscopic, apparently there is need of a multi- stage neural network. In that, both top-down and bottom-up interactions should be taken into account *(**Wang et al. 2013**)*. Such a hierarchical network needs to be biophysically realistic in order to be as more directly as possible related to microscopic evidences. Nevertheless, consistent derivations of rate-based models and analytical derivations of second-order statistics would again be necessary due to computational expensiveness. In addition, a thorough review of all theoretical approaches used, so far, to explain experimental evidences in MP is needed.

Finally, living in a socially interactive environment, our decisions are often influenced by the decisions of others, as for instance in the Asch conformity experiment. Traditionally, a framework to study social decision making is behavioral game theory.

- *Wait, did you just say social decision making?*

Perhaps, in a first glance, this appears irrelevant to the subject of the current thesis. Nevertheless, it is closely related to perceptual decision making, and as we discussed previously, perceptual decision making is not much different to subjective visual perception. Therefore, we could consider it as a possible extention of our studies.

Behavioral game theory is about predicting how agents behave when they are engaged in interactive processes *(**Camerer 2003**)*. At the same time neurobiological studies focus on revealing the underlying brain mechanisms involved in this context and together with behavioral game theory form the rapidly progressing field of neuroeconomics *(**Glimcher et***

al. 2008). Depending on the experimental paradigm, competition and cooperation mechanisms emerge such as, for instance, in the prisoner's dilemma ***(Rapoport & Chammah 1965; Axelrod 1984)***. During this game it is supposed that two individuals have been arrested for a crime. They are given the possibility to choose between defection (provide testimony against the other) or cooperation (keep silent). Each agent receives higher payoff when he chooses defection regardless of what the other player chooses. This denotes defection as the optimal strategy i.e. the Nash equilibrium for this game. Nevertheless, mutual cooperation leads to higher payoff for both agents, hence the dilemma. In the one-shot version of the game, players most of the times choose mutual defection highlighting a behavior which is driven by self-interest. On the contrary, when the game is played repeatedly, behavior deviates from the Nash equilibrium and mutual cooperation often occurs, corresponding to a more altruistic behavior ***(Lee 2008; Cooper et al. 1996)***. What are the underlying mechanisms of the mutual cooperative behavior observed during the iterated version of this game? To this purpose we could consider two decision-making networks (Figure A) and apply reinforcement learning algorithms. So far, theoretical models of reinforcement learning and a biophysically realistic spiking network have been studied by testing different strategies adopted by one or both of the agents ***(Soltani et al. 2006)***. It would be interesting to model both agents at the same time and let their behavior arise just from the learning dynamics of both of them. Furthermore one could extend the reinforcement learning algorithm by considering the hypothetical payoffs or fictive rewards ***(Lee 2008; Abe & Lee 2011)***.

In a recent study ***(Soltani et al. 2006)*** it has been shown that a biologically plausible model of decision making with plastic synapses, following a reward- dependent stochastic Hebbian learning rule, can reproduce behavioral data from a matching pennies game where monkeys are competing against a computer. In addition, the authors show that their model constitutes a biophysical implementation of reinforcement learning with the value functions of alternative actions and the learning rates encoded at the plastic synapses of the input neurons to the network.

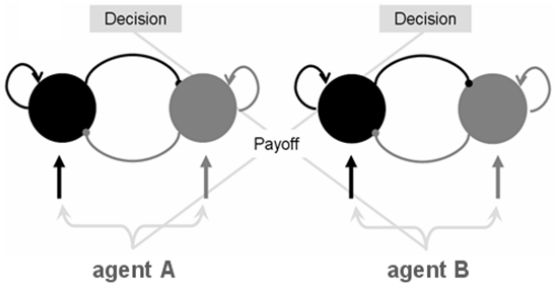

Figure A. Modeling social decision making
Two cortical microcircuit networks, for social decision making, each corresponding to each agent engaged in a game, e.g. the prisoner's dilemma. Black circles denote neuronal populations selective to defection and gray circles denote neuronal populations selective to cooperation.

For instance, we could initially consider two simple rate models with winner-take-all dynamics, where each network corresponds to one of the agents (Figure A) and be consisted of two interconnected units supposed to represent populations of neurons selective to one of the two choices: cooperation (gray circles) or defection (black circles). The inputs to both populations are equal and constant and what is altered after each trial is the synaptic strength between the input neurons and the network neurons. This modulation results in changing the effective input to the populations of the agents. Finally we could expand the payoffs to decision makers to incorporate agents' aversion to inequality ***(Lee 2008; Fehr and Camerer 2007; Tricomi et al. 2010)***. The subjective payoff of an agent for a specific choice is quantified by its utility function, which is a function of his own payoff and of the payoff differences between the two agents. In this case an agent suffers from disadvantageous inequalities with a factor a (envy), and from advantageous inequalities with a factor b (compassion) and the payoffs are modified accordingly. By changing these factors two Nash equilibria will emerge: mutual defection and mutual cooperation. Interestingly, this could render the model consistent with recent experimental evidences that show that mutual cooperation should be a possible equilibrium action in order to observe mutual cooperation ***(Dal Bo & Frechette 2011)***.

It would be, therefore, interesting to study social decision making by modeling at the same time both agents, using a double biophysically

realistic decision making network and applying reinforcement learning algorithms to both of them, letting their behavior arise from the learning dynamics of both of them. Nowadays there is an increasing interest in the field of neuroeconomics and researchers are focused on understanding the underlying brain mechanisms governing social interactions. Furthermore, new experimental techniques like fMRI and EEG hyperscanning as well as multi-dimensional recording have appeared. Neural correlates during cooperation and in particular during the prisoner's dilemma were found in ventral striatum ***(Lee 2008; Fehr & Camerer 2007)*** as well as in medial prefrontal cortex ***(Babilobi et al. 2007)***. Neural evidence for inequality-averse social preferences has been found in ventral striatum and ventromedial prefrontal cortex ***(Tricomi et al. 2010)***. Activity in striatum has been found to be influenced by both real and fictive reward prediction errors ***(Lee 2008)*** and activity in orbital and dorsolateral prefrontal cortex has been found to code actual and hypothetical outcomes ***(Abe & Lee 2011)***. There is rich information and a plethora of ongoing studies and the need for theoretical studies in this direction is apparent.

- *So, what do we learn from all these?*

In conclusion, in the current thesis, we show that a biophysically realistic attractor-based recurrent network, that was initially employed to account for working memory ***(Brunel & Wang 2001)***, decision making ***(Wang 2002)***, and attention ***(Deco & Rolls 2005)***, can account also for adaptation-related aftereffects in perceptual decisions, as well as for multistable perception. The ability of a similar theoretical approach to produce these different, but related, cognitive phenomena indicates that they could have similar underlying neural mechanisms, and a common theoretical framework for the brain could probably be possible.

Bibliografia

1593 **della Porta** G. (1593), De Refractione, Optices Parte, *Libri Novem, Naples: Carlinum and Pacem. pp. 142-143: Place a partition between the eyes, to divide one from the other, and place a book before the right eye, and read; if another book is placed before the left eye, not only ca nit not be read, but the pages cannot even be see, unless the visual virtue is withdrawn from the right eye and changed to left.*

1712 **Le Clerk** S. (1712), Système de la Vision, *Paris: Delaulme. p. 17: If one opens both eyes, the object does not appear in only one of the two places, i.e., in D or in C; that is the result of the experiment. From this I conclude that only one eye sees the object.*

1761 **Du Tour** E. F. (1761), Addition au Mémoire intitulñe. Discussion d'une question d'optique, *Académie des Sciences, Mémoires de Mathématique et de Physique Présentés pars Divers Savants 4, 499-511*

1832 **Necker** L. A. (1832), Observations on some remarkable optical phænomena seen in Switzerland; and on an optical phænomenon which occurs on viewing a figure of a crystal or geometrical solid, *Philosophical Magazine Series 3, 1, 5, 329-337*

1838 **Wheatstone** C. (1838), Contributions to the physiology of vision. Part the first. On some remarkable and hitherto unobserved, phenomena of binocular vision, *Philosophical Transactions of the Royal Society of London, 128, 371-394*

1890 **James** W. (1890), The principles of psychology (Vol1), *New York: Holt*

1928 **Diaz-Caneja** E. (1928), Sur l'alternance binoculaire, *Annales d' Oculistique, 165, 721-731*

1930 **Boring** E. G. (1930), A new ambiguous figure, *The American Journal of Psychology, 42, 445-445*

Uhlenbeck G. E., and Ornstein L. S. (1930), On the theory of brownian motion, *Physical Review, 36, 823-841*

1940 **Kramers** H. A., (1940), Brownian motion in a field of force and the diffusion model of chemical reactions, *Physica, 7, 284-304*

1953 **Wallach** H., and O'Connell D. N. (1953), The kinetic depth effect, *Journal of Experimental Psychology, 45, 205-217*

1958 **Warren** R. M., and Gregory R. L. (1958), An auditory analogue of the visual reversible figure, *The American Journal of Psychology, 71, 612-613*

1963 **Orbach** J., Ehrlich D., and Heath H. A. (1963a), Reversibility of the Necker Cube: I. An examination of the concept "Satiation of Orientation", *Perceptual and Motor Skills*, *17, 439-458*

Orbach J., Ehrlich D., and Vainstein E. (1963b), Reversebility of the Necker Cube: III. Effects of interpolation on reversal rate of the cube presented repetitively, *Perceptual and Motor Skills*, *17, 571-582*

Weitzman B. (1963), A threshold difference produced by a figure-ground dichotomy, *Journal of Experimental Psychology, 66(2), 201-205*

1965 **Rapoport** A., Chammah A. M. (1965), Prisoner's dilemma: a study in conflict and cooperation, *Ann Arbor Univ Mich Press*

1966 **Orbach** J., Zucker E., and Olson R. (1966), Reversibility of the Necker Cube: VII. Reversal rate as a function of figure-on and figure-off durations, *Perceptual and Motor Skills*, *22, 615-618*

1967 **Fox** R., and Hermann J. (1967), Stochastic properties of binocular rivalry alternations, *Perception & Psychophysics, 2(9), 432-446*

Levelt W. J. M. (1967), Note on the distribution of dominance times in binocular rivalry, *British Journal of Psychology, 58(1), 143-145*

Schrödinger E. (1967), What is Life? And Mind and Matter, *Cambridge University Press, Cambridge*

1968 **Levelt** W. J. M. (1968), On Binocular Rivalry, *The Hague: Mouton*

Whittle P., Bloor D. C., and Pocock S. (1968), Some experiments on figural effects in binocular rivalry, *Perception & Psychophysics, 4, 3, 183-188*

1969 **Fox** R., and Rasche F. (1969), Binocular rivalry and reciprocal inhibition, *Perception & Psychophysics, 5, 215-217*

1972 **Borsellino** A., De Marco A., Allazetta A., Rinesi S., and Bartolini B. (1972), Reversal time distribution in the perception of visual ambiguous stimuli, *Kybernetik, 10(3), 139-144*

1973 **Wilson** H. R., and Cowan J. D. (1973), A mathematical theory of the functional dynamics of cortical and thalamic nervous tissue. *Kybernetik, 13, 55-80*

1974 **Blake** R., and Fox R. (1974), Adaptation to invisible gratings and the site of binocular rivalry suppression, *Nature, 249(456), 488-490*

1975 **van Noorden** L. P. A. S. (1975), Temporal coherence in the perception of tone-sequences, *Doctoral Thesis, Eindhoven University of Technology, Technische Hogeschool Eindhoven*

Walker P. (1975), Stochastic properties of binocular rivalry alternations, *Perception & Psychophysics, 18(6), 467-473*

1978 **Lack** L. C. (1978), Selective attention and the control of binocular rivalry, *Mouton, The Hague Noordeinde, 41*

Walker P. (1978), Binocular rivalry: central or peripheral selective processes?, *Psychological Bulletin, 85, 376-389*

1979 **Blake** R., and Camisa J. (1979), On the inhibitory nature of binocular rivalry suppression, *Journal of Experimental Psychology: Human Perception and Performance, 5(2), 315-323*

1980 **Blake** R., Westendorf D. H., and Overton R. (1980), What is suppressed during binocular rivalry?, *Perception, 9(2), 223-231*

1982 **Sugie** N. (1982), Neural models of brightness perception and retinal rivalry in binocular vision, *Biological Cybernetics, 43, 13-21*

Wong E., and Weisstein N. (1982), A new perceptual context-superiority effect: Line segments are more visible against a figure than against a ground, *Science, 218, 4572, 587-589*

1983 **Tolhurst** D. J., Movshon J. A. and Dean A. F. (1983), The statistical reliability of signals in single neurons in cat and monkey visual cortex, *Vision Research, 23, 775-785*

1984 **Axelrod** R. M. (1984), The evolution of cooperation, *New York: Basic Books*

Madison D. V., Nicoll R. A. (1984), Control of the repetitive discharge of rat CA1 pyramidal neurons in vitro, *The Journal of Physiology, 345, 319-331*

Matsuoka K. (1984), The dynamic model of binocular rivalry, *Biological Cybernetics, 49, 201-208*

Rubin G. S. (1984), Suppression and summation in binocular pattern vision, *Dissertation Abstracts International, 44 (9-B), 2926*

Wolfe J. M. (1984), Reversing ocular dominance and suppression in a single flash, *Vision Research, 24, 471-8*

1985 **Blake** R., and Boothroyd K. (1985), The precedence of binocular fusion over binocular rivalry, *Perception & Psychophysics, 37, 2, 114-124*

1986 **Wolfe** J. M. (1986), Stereopsis and Binocular rivalry, *Psychological review, 93, 3, 269-282*

1987 **Cogan** A. I. (1987), Human binocular interaction: towards a neural model, *Vision Research, 27, 12, 2125-2139*

Mitzdorf U. (1987), Properties of the evoked potential generators: current source-density analysis of visually evoked potentials in the cat cortex, *International Journal of Neuroscience 33, 33-59*

1988 **Lehky** S. R. (1988), An astable multivibrator model of binocular rivalry, *Perception, 17, 215-228*

1989 **Aertsen** A. M., Gerstein G. L., Habib M. K., and Palm G. (1989), Dynamics of neuronal firing correlation: modulation of "effective connectivity", *Journal of Neurophysiology 61, 900-917*

Blake R. (1989), A neural theory of binocular rivalry, *Psychophysical Review 96, 145-167*

Ditzinger T., and Haken H. (1989), Oscillations in the perception of ambiguous patterns, *Biological Cybernetics, 61, 279-287*

Logothetis N. K., and Schall J. D. (1989), Neuronal correlates of subjective visual perception, *Science, 245, 761-763*

Mueller T. J., and Blake R. (1989), A fresh look at the temporal dynamics of binocular rivalry, *Biological Cybernetics, 61, 223-232*

Newsome W. T., Britten K. H., and Movshon J. A. (1989), Neuronal correlates of a perceptual decision, *Nature, 341(6237), 52-54*

1990 **Blake** R., Westendorf D., and For R. (1990), Temporal pertubations of binocular rivalry, *Perception & Psychophysics, 48, 6, 593-602*

Crick F., Koch C. (1990), Towards a neurobiological theory of consciousness, *Seminars in the Neurosciences, 2, 263-275*

Ditzinger T., and Haken H. (1990), The impact of fluctuations on the recognition of amgiguous patterns, *Biological Cybernetics, 63, 453-456*

Ermentrout B. (1990), Phase-plane: the dynamical systems tool, *Pacific Grove, CA: Brooks/Cole*

Mueller T. J. (1990), A physiological model of binocular rivalry, *Visual Neuroscience, 463-73*

1991 **Abeles** A. (1991), Corticonics, *New York: Cambridge UP*

1992 **Ahissar** E., Vaadia E., Ahissar M., Bergman H., Arieli A., and Abeles M. (1992), Dependence of cortical plasticity on correlated activity of single neurons and on behavioral context, *Science, 257, 1412-1415.*

Britten K. H., Shadlen M. N., Newsome W. T., Movshon J. A. (1992), The analysis of visual motion: a comparison of neuronal and psychophysical performance, *Journal of Neuroscience, 12, 4745-4765*

1993 **Bossink** C. J., Stalmeier P.- F., Weert C. M. D. (1993), A test of Levelt's second proposition for binocular rivalry, *Vision Research, 33, 1413-1419*

1994 **Conde** F., Lund J. S., Jacobowitz D. M., Baimbridge K. G., and Lewis D. A. (1994), Local circuit neurons immunoreactive for calretinin, calbindin D-28k or parvalbumin in monkey prefronatal cortex: Distribution and morphology, *Journal of Computational Neurology 341, 95-116*

Posner M. I. (1994), Attention: the mechanisms of consciousness, *PNAS, 91, 16, 7398-7403*

Riani M., and Simonotto E. (1994), Stochastic resonance in the perceptual interpretation of ambiguous figures: A neural network model, *Physical Review Letters, 72, 19, 3120-3123*

Zohary E., Shadlen M. N., and Newsome W. T. (1994), Correlated neuronal discharge rate and its implications for psychophysical performance, *Nature, 370, 140-143*

1995 **Amit** D. J. (1995), The hebbian paradigm reintegrated: local reverberations as internal representations, *Behavioral and Brain Sciences, 18 (4), 617-625*

Bialek W., and DeWeese M. (1995), Random switching and optimal processing in the perception of ambiguous signals. *Physical Review Letters, 74, 3077-3080*

Crick F., and Koch C. (1995), Are we aware of neural activity in primary visual cortex?, *Nature, 375, 121-3*

Ditzinger T., Haken H. (1995), A synergetic model of multistability in perception, *Springer Series in Synergetics, 64, Ambiguity in Mind and Nature, Editors: P. Kruse, M. Stadler, springer-Verlag Berlin Heidelberg*

Lehky S. R. (1995), Binocular rivalry is not chaotic, *Proceedings of the Royal Society B, 259, 71-76*

Riani M., and Simonotto E. (1995), Periodic pertubation of ambiguous figure: a neural-network model and a non-simulated experiment, Il Nuovo Cimento, 70, 7-8, 903-913

1996 **Cooper** R., DeJong D. V.m and Forsythe R. (1996), Cooperation without reputation: experimental evidence from prisoner's dilemma games, *Games and Economic Behavior 12, 187-218*

Gabbott P. L. A., and Bacon S. J. (1996), Local circuit neurons in the medial prefrontal cortex (areas 24a, b, c, 25 and 32) in the monkey: II. Quantitative areal and laminar distributions, *Journal of Comparative Neurology, 364, 609-636*

Kovács I., Papathomas T. V., Yang M., Fehér A. (1996), When the brain changes its mind: interocular grouping during binocular rivalry, *PNAS, 93, 15508-11*

Leopold D. A., and Logothetis N. K. (1996), Activity changes in early visual cortex reflect monkeys' percepts during binocular rivalry, *Nature, 379, 549-553*

Logothetis N. K., Leopold D. A., Sheinberg D. L. (1996), What is rivalling during binocular rivalry?, *Nature, 380, 621-4*

Shadlen M. N., Newsome W. T. (1996), Motion perception: seeing and deciding, *PNAS, 93, 628–633*

1997 **Amit** D. J., and Brunel N. (1997), Model of global spontaneuous activity and local structured activity during delay periods in the cerebral cortex, *Cerebral Cortex 7, 237-252*

Andrews T. J., and Purves D. (1997), Similarities in normal and binocularly rivalrous viewing, *PNAS, 94(18), 9905-9908*

Ditzinger T., Tuller B., Haken H., and Kelso J. A. S. (1997), A synergetic model for the verbal transformation effect, *Biological Cybernetics, 77, 31-40*

Kanwisher N., McDermott J., Chun M. M. (1997), The fusiform face area: a module in human extrastriate cortex specialized for face perception, *Journal of Neuroscience, 17, 4302-4311*

Ó Scalaidhe S. P., Wilson F. A. W., Goldman-Rakic P.S. (1997), Areal segregation of face-processing neurons in prefrontal cortex, *Science, 278, 5340, 1135-1138*

Sheinberg D. L., and Logothetis N. K. (1997), The role of temporal cortical areas in perceptual organization, *PNAS, 94, 3408-3413*

Treue S. (1997), License to See: for one eye only?, *Neuron, 19, 223-225*

1998 **Bradley** D. C., Chang G. C., Andersen R. A. (1998), Encoding the three-dimensional structure-from-motion by primate area MT neurons, *Nature 392, 714-717*

Crick F., and Koch C. (1998), Consciousness and neuroscience, *Cerebral Cortex, 8, 97-107*

Dayan P. (1998), A hierarchical model of binocular rivalry, *Neural Computation, 10, 1119-1135*

Gammaitoni L., Hanggi P., Jung P., and Marchesoni F. (1998), Stochastic resonance, *Review of Modern Physics, 70, 223-287*

Logothetis N. K. (1998), Single units and conscious vision, *Philosophical Transactions of the Royal Society of London, Series B, 353, 1801-1818*

Lumer E. D. (1998), A neural model of binocular integration and rivalry based on the coordination of action-potential timing in primary visual cortex, *Cerebral Cortex, 8, 553-61*

Lumer E. D., Friston K. J., and Rees G. (1998), Neural correlates of perceptual rivalry in the human brain, *Science, 280, 1930-1934*

Tong F., Nakayama K., Vaughan J. T., and Kanwisher N. (1998), *Neuron, 21, 4, 753-759*

Tononi G., Srinivasan R., Russell D. P., Edelman G. M. (1998), Investigating neural correlates of conscious perception by frequency-tagged neuromagnetic responses, *PNAS, 95, 3198-3203*

Wade N. J. (1998), A natural history of vision, *Cambridge, Ma, MIT Press*

1999 **Abbott** L. F., and Dayan P. (1999), The effect of correlated variability on the accuracy of a population code, *Neural Computation, 11, 91-101*

Kim J. N., Shadlen M. N. (1999), Neural correlates of a decision in the dorsolateral prefrontal cortex of the macaque, *Nature Neuroscience, 2, 176-185*

Lee S.-H., and Blake R. (1999), Rival ideas about binocular rivalry, *Vision Research, 39, 1447-1454*

Leopold D. A., and Logothetis N. K. (1999), Multistable phenomena: changing views in perception, *Trends in Cognitive Sciences 3(7), 254-264*

Logothetis N. K. (1999), Vision: A window on consciousness, *Scientific American, 281, 68-75*

Lumer E. D., and Rees G. (1999), Covariation of activity in visual and prefrontal cortex associated with subjective visual perception, *PNAS, 96, 1669-1673*

Ooi T. L., and He Z. J. (1999), Binocular rivalry and visual awareness: the role of attention, *Perception, 28(5), 551-574*

Srinivasan R., Russell D. P., Edelman G. M., Tononi G. (1999), Increased synchronization of neuromagnetic responses during conscious perception, *Journal of Neuroscience, 19, 5435-5448*

Taylor C. C. W. (1999), The Atomists: Leucippus and Democritus. Fragments, A Text and Translation with Commentary, *Toronto: University of Toronto Press*

2000 **Kalarickal** G., and Marshall J. (2000), Neural model of temporal and stochastic properties of binocular rivalry, *Neurocomputing, 32-33, 843–853*

Polonsky A., Blake R., Braun J., Heeger D. J. (2000), Neuronal activity in human primary visual cortex correlates with perception during binocular rivalry, *Nature Neuroscience, 3, 1153-1159*

Romo R., Hernández A., Zainos A., Brody C. D., and Lemus L. (2000), Sensing without touching: psychophysical performance based on cortical microstimulation, *Neuron, 26, 1, 273-278*

2001 **Bair** W., Zohary E., Newsome W. T. (2001), Correlated firing in macaque visual area MT: time scales and relationship to behavior, *Journal of Neuroscience, 21(5), 1676-1697*

Blake R. (2001), A primer on binocular rivalry, *Brain and Mind 2, 5-38*

Bonneh Y. S., Cooperman A., Sagi D. (2001), Motion induced blindness in normal observers, *Nature, 411, 798-801*

Brunel N, Chance F. S., Fourcaud N., and Abbott L. F. (2001), Effects of synaptic noise and filtering on the frequency response of spiking neurons, *Physical Review Letters, 86, 2186-2189*

Brunel N., and Wang X.-J. (2001), Effects of neuromodulation in a cortical network model of object working memory dominated by recurrent inhibition, *Journal of Computational Neuroscience, 11, 63-8*

Dodd J. V., Krug K., Cumming B. G., Parker A. J. (2001) Perceptually bistable three-dimensional figures evoke high choice probabilities in cortical area MT, *Journal of Neuroscience, 21, 4809-4821*

Downing P. E., Jiang Y., Shuman M., Kanwisher N. (2001), A cortical area selective for visual processing of the human body, *Science, 293, 2470-2473*

Leopold D. A., O'Toole A. J., Vetter T., and Blanz V. (2001), Prototype-referenced shape encoding revealed by high-level aftereffects, *Nature Neuroscience, 4, 89-94*

Liu Y. H., and Wang X.-J. (2001), Spike-frequency adaptation of a generalized leaky integrate-and-fire model neuron, *Journal of Computational Neuroscience, 10, 25-45*

Logothetis N. K., Pauls J., Augath M., Trinath T., and Oeltermann A. (2001), Neurophysiological investigation of the basis of the fMRI signal, *Nature 412(6843), 150-157*

Nguyen V. A., Freeman A. W., Wenderoth P. (2001), The depth and selectivity of suppressioin in binocular rivalry, *Perception & Psychophysics, 63(2), 348-360*

Salinas E., and Sejnowski T. J. (2001), Correlated neuronal activity and the flow of neural information, *Nature Reviews Neuroscience, 2, 539-550*

Shadlen M.N., Newsome W. T. (2001), Neural basis of a perceptual decision in the parietal cortex (area LIP) of the rhesus monkey, *Journal of Neurophysiology, 86, 1916-1936*

Sompolinsky H., Yoon H., Kang K., Shamir M. (2001), Population coding in neuronal systems with correlated noise, *Physical Reiew E Statistical, Nonlinear, Soft Matter Physics, 64, 051904*

Tong F., Engel S. A. (2001), Interocular rivalry revealed in the human cortical blind-spot representation, *Nature 411, 195-199*

2002 **Blake** R., and Logothetis N. K. (2002), Visual competition, *Nature Reviews Neuroscience, 3, 13-21*

Grunewald A., Bradley D. C., Andersen R. A. (2002), Neural correlates of structure-from-motion perception in macaque V1 and MT, *Journal of Neuroscience, 22, 6195–6207*

Fourcaud N., and Brunel N. (2002), Dynamics of the firing probability of noisy integrate-and-fire neurons, *Neural Computation, 14, 2057-2110*

Kreiman G., Fried I., Koch C. (2002), Single-neuron correlates of subjective vision in the human medial temporal lobe, *PNAS, 99, 8378-83*

Lago-Fernandez L., and Deco G. (2002), A model of binocular rivalry based on competition in IT, *Neurocomputing, 44, 503-507*

Laing C. R., and Chow C. (2002), A spiking neural model of binocular rivalry, *Journal of Computational Neuroscience, 12, 39-53*

Lee S. H., and Blake R. (2002), V1 activity is reduced during binocular rivalry, *Journal of Vision, 2, 618-626*

Leopold D. A., Wilke M., Maier A., and Logothetis N. K. (2002), Stable perception of visually ambiguous patterns, *Nature Neuroscience, 5, 6, 605-609*

Logothetis N. K. (2002), The neural basis of the blood-oxygen-level-dependent functional magnetic resonance imaging signal, *Philosophical Transasctions of the Royal Society B, 357(1424), 1003-1037*

Maier A., Leopold D. A., Logothetis N. K. (2002), Neural activity during stable perception of ambiguous displays in monkey visual cortex, *Poster presented at 32nd Annual Meeting of the Society for Neuroscience (Neuroscience 2002), Orlando, FL, USA.*

Mamassian P., Landy M., and Maloney L. T. (2002), Bayesian modelling of visual perception, *Eds Rao R. P. M., Olshausen B. A., Lewicki M. S., Probabilistic Models of the Brain: Perception and Neural Function, Cambridge, MA: MIT Press, pp 13-36*

Roitman J. D., Shadlen M. N. (2002), Response of neurons in the lateral intraparietal area during a combined visual discrimination reaction time task, *Journal of Neuroscience, 22, 9475-9489*

Sasaki H., and Gyoba J. (2002), Selective attention to stimulus features modulates interocular suppression, *Perception, 31(4), 409-419*

Sterzer P., Russ M. O., Preibisch C., and Kleinschmidt A. (2002), Neural correlates of spontaneous direction reversals in ambiguous apparent visual motion, *Neuroimage, 15(4), 908-16*

Wang X.-J. (2002), Probabilistic decision making by slow reverberation in cortical circuits, *Neuron, 36, 955-968*

Wilke S. D., and Eurich C. W. (2002), Representational accuracy of stochastic neural populations, *Neural Computation, 14, 155*

Xie X., Hahnloser R. H. R., and Seung H. S. (2002), Selectively grouping neurons in recurrent networks of lateral inhibition. *Neural Computation, 14, 2627–2646*

2003 **Camerer** C. F. (2003), Behavioral game theory: Experiments in strategic interaction, *Princeton Univ Press*

Crick F., and Koch C. (2003), A framework for consciousness, *Nature neuroscience, 6, 119-126*

Hasegawa H. (2003a), Dynamical mean-field theory of spiking neuron ensembles: Response to a single spike with independent noises, *Physical Review E, 67, 041903-19*

Hasegawa H. (2003b), Dynamical mean-field theory of noisy spiking neuron ensembles: Applications to the Hodgkin-Huxley model, *Physical Review E, 68, 041909-13*

Hock H. S., Schöner G., and Giese M. (2003), The dynamical foundations of motion pattern formation: Stability, selective adaptation, and perceptual continuity, *Perception & Psychophysics, 65(3), 429-457*

Hupé J.-M., and Rubin N. (2003), The dynamics of bi-stable alternation in ambiguous motion displays: a fresh look at plaids, *Vision Research, 43, 531-548*

Logothetis N. K. (2003), The underpinnings of the BOLD functional magnetic resonance imaging signal, *Journal of Neuroscience, 23(10), 3963-3971*

Maier A., Wilke M., Logothetis N. K., and Leopold D. A. (2003), Perception of temporally interleaved ambiguous patterns, *Current Biology, 13, 1076-1085*

Renart A., Brunel N., and Wang X.-J. (2003), Mean field theory of recurrent cortical networks: from irregularly spiking neurons to working memory, *Computational neuroscience: a comprehensive approach, (Feng, J. ed), Boca Raton, FL: CRC, pp 431-490*

Romo R., Salinas E. (2003), Flutter discrimination: neural codes, perception, memory and decision making, *Nature Reviews Neuroscience, 4, 203-218*

Romo R., Hernández A., Zainos A., and Salinas E. (2003), Correlated neuronal discharges that increase coding efficiency during perceptual discrimination, *Neuron, 38, 4, 649-657*

Salinas E. (2003), Background synaptic activity as a switch between dynamical states in a network, *Neural Computation, 15(7), 1439-1475*

Stollenwerk L., and Bode M. (2003), Lateral neural model of binocular rivalry, *Neural Computation, 15, 2863-2882*

van Ee R., Adams W. J., Mamassian P. (2003), Bayesian modeling of cue interaction: bistability in stereoscopic slant perception, *Journal of Optical Society of America A, 20, 7, 1398*

Wilke M., Logothetis N. K., Leopold D. A. (2003), Generalized flash suppression of salient visual targets, *Neuron, 39, 1043-1052*

Wilson H. R. (2003), Computational evidence for a rivalry hierarchy in vision, *PNAS, 100(24), 14499-14503*

2004 **Atmanspacher** H., Filk, Römer H. (2004), Quantum Zeno features of bistable perception, *Biological Cybernetics, 90, 33-40*

Chen X., and He S. (2004), Local factors determine the stabilization of monocular ambiguous and binocular rivalry stimuli, *Current Biology, 14, 11, 1013-1017*

Cosmelli D., David O., Lachaux J. P., Martinerie J., Garnero L., Renault B., Varela F. (2004), Waves of consciousness: ongoing cortical patterns during binocular rivalry, *Neuroimage, 23, 128-140*

Fürstenau N. (2004), A chaotic attractor model of cognitive multistability, *IEEE International Sonference on Systems, Man and Cybernetics, 853-859*

Gail A., Brinksmeyer H. J., and Reinhard E. (2004), Perception-related modulations of local field potential power and coherence in primary visual cortex of awake monkey during binocular rivalry, *Cerebral Cortex, 2004 14(3), 300-313*

Hasegawa H. (2004a), Augmented moment method for stochastic ensembles with delayed couplings. I. Langevin model, *Physical Review E, 70, 021911-11*

Hasegawa H. (2004b), Augmented moment method for stochastic ensembles with delayed couplings. II. FitzHugh-Nagumo model, *Physical Review E, 70, 021912-9*

Logothetis N. K., and Wandell B. A. (2004), Interpreting the BOLD signal, *Annual Review of Physiology, 66, 735-69*

Maier A., 2004, Monocular rivalry, *wikipedia*

Meng M., and Tong F. (2004), Can attention selectively bias bistable perception? Differences between binocular rivalry and ambiguous figures, *Journal of Vision, 4, 539-551*

Mitchell J. F., Stoner G. R., and Reynolds J. H. (2004), Object-based attention determines dominance in binocular rivalry, *Nature, 429, 410-413*

Pearson J., and Clifford C. W. G. (2004), Determinants of visual awareness following interruptions during rivalry, *Journal of Vision, 4, 196-202*

Rubin N., and Hupé J. M. (2004), Dynamics of perceptual bistability: plaids and binocular rivalry compared. *Binocular Rivalry, ed. Alais D. & Blake R., Cambridge, MA: MIT Press*

Smith P. L., Ratcliff R. (2004), Psychology and neurobiology of simple decisions, *Trends in Neurosciences, 27, 161-168*

Wang X.-J., Tegér J., Constantinidis C., and Goldman-Rakic P. S. (2004), Division of labor among distinct subtypes of inhibitory neurons in a cortical microcircuit of working memory, *PNAS, 101, 1368-1373*

Webster M. A., Kaping D., Mizokami Y., Duhamel P. (2004), Adaptation to natural facial categories, *Nature, 428, 557-561*

Zhou Y. H., Gao J. B., White K. D., Merk I., and Yao K. (2004), Perceptual dominance time distributions in multistable visual perception, *Biological Cybernetics, 90(4), 256-263*

2005 **Abbott** L. F., and Chance E. S. (2005), Drivers and modulators from push-pull and balanced synaptic inputs, *Progress in Brain Research 149, 147-155*

Brascamp J. W., van Ee R., Pestman W. R., and van Den Berg A. V. (2005), Distributions of alternation rates in various forms of bistable perception, *Journal of Vision, 5(4), 287-298*

Carter O. L., Presti D. E., Callistemon C., Ungerer Y., Liu G. B., and Pettigrew J. D. (2005), Meditation alters perceptual rivalry in Tibetan Buddhist monks, *Current biology, 15, 11, R412*

Chong S. C., Tadin D., and Blake R. (2005), Endogenous attention prolongs dominance durations in binocular rivalry, *Journal of Vision, 5, 1004-1012*

Deco G., and Rolls E. T. (2005), Neurodynamics of biased competition and cooperation for attention: a model with Spiking Neurons, *Journal of Neurophysiology, 94, 295-313*

Freeman A. W. (2005), Multistage model for binocular rivalry, *Journal of Neurophysiology, 94(6), 4412-20*

Haynes J. D., and Rees G. (2005), Predicting the stream of consciousness from activity in the human visual cortex, *Current Biology, 15, 1201-1207*

Haynes J. D., Deichmann R., Rees G. (2005), Eye-specific effects of binocular rivalry in the human lateral geniculate nucleus, *Nature, 438, 496-499*

Kohn A., and Smith M. A. (2005), Stimulus dependence of neuronal correlation in primary visual cortex of the macaque, *The Journal of Neuroscience, 25(14), 3661-3673*

Kornmeier J., and Bach M. (2005), The Necker cube – an ambiguous figure disambiguated in early visual processing, *Vision Research*, 45, 955-960

Mamassian P., and Goutcher R. (2005), Temporal dynamics in bistable perception, *Journal of Vision, 5, 361-375*

Moldakarimov S., Rollenhagen J. E., Olson C. R., and Chow C. C. (2005), Competitive dynamics in cortical responses to visual stimuli, *Journal of Neurophysiology, 94, 3388-3396*

Opris I., Bruce C. (2005), Neural circuitry of judgment and decision mechanisms, *Brain Research Reviews, 48:509-526*

Palmer J., Huk A. C., Shadlen M. N. (2005), The effect of stimulus strength on the speed and accuracy of a perceptual decision. *Journal of Vision, 5, 1*

Rubin N., and Hupé J.-M. (2005), Dynamics of perceptual bistability: Plaids and binocular rivalry compared, *Binocular rivalry, MIT Press, eds. Alais D. & Blake R., pp:137-154*

Stoner G. R., Mitchell J. F., Fallah M., and Reynolds J. H. (2005), Interacting competitive selection in attention and binocular rivalry, *Progress in Brain Research, 149, 227-234*

Tsuchiya N., and Koch C. (2005), Continuous flash suppression reduces negative afterimages, *Nature Neuroscience, 8, 8, 1096-1101*

van der Ven A. H. G. S., Gremmen F. M., and Smit J. C. (2005), A statistical model for binocular rivalry, *British Journal of Mathematical and Statistical Psychology, 58, 97-116*

van Ee R., van Dam L. C. J., and Brouwer G. J. (2005), Voluntary control and the dynamics of perceptual bi-stability, *Vision Research, 45, 1, 41-55*

Wills T. J., Lever C., Cacucci F., Burgess N., and O'Keefe J. (2005), Attractor dynamics in the hippocampal representation of the local environment, *Science, 308, 873-876*

2006 **Averbeck** B. B., and Lee D. (2006), Effects of noise correlations on information encoding and decoding, *Journal of Neurophysiology, 95, 3633-3644*

Averbeck B. B., Latham P. E., and Pouget A. (2006), Neural correlations, population coding and computation, *Nature Reviews Neuroscience, 7, 358-366*

Brascamp J. W., van Ee R., Noest J. A., Jacobs R. H. A. H., and van den Berg A. V. (2006), The time course of binocular rivalry reveals a fundamental role of noise, *Journal of vision, 6, 1244-1256*

Chong S. C., and Blake R. (2006), Exogenous attention and endogenous attention influence initial dominance in binocular rivalry, *Vision Research, 46, 11, 1794-1803*

Deco G., Rolls E. T. (2006), Decision-making and Weber's law: a neurophysiological model, *European Journal of Neuroscience, 24, 901-916*

Kim T. Y., Grabowecky M., and Suzuki S. (2006), Stochastic resonance in binocular rivalry, *Vision Research, 46(3), 392-406*

Logothetis N. K. (2006), Vision: A window on consciousness, *Scientific Amrican: Secrets of the senses; Special Editions, 1, 4-11*

Pressnitzer D., and Hupé J. M. (2006), Temporal dynamics of auditory and visual bistability reveal common principles of perceptual organization, *Current Biology, 16, 13, 1351-1357*

Soltani A., Lee D., and Wang X.-J. (2006), Neural mechanism for stochastic behaviour during a competitive game, *Neural Networks, 19, 1075-1090*

Wong K.-F., and Wang X.-J. (2006), A recurrent network mechanism of time integration in perceptual decisions, *Journal of Neuroscience, 26, 1314-1328*

Zheng M., and Ukai K. (2006), Intermittent stimuli increase alternations of ambiguous figures, *Journal of Physics: Conference Series, 31, 197-198*

2007 **Babiloni** F., Astolfi L., Cincotti F., Mattia D., Tocci A., Tarantino A., Marciani M. G., Salinari S., Gao S., Colosito A., and De Vico Fallan F. (2007), Cortical activity and connectivity of human brain during the prisoner's dilemma: an EEG hyperscanning study. *Proceedings of 29th Annual International Conference of the IEEE EMBS, Lyon France, 2007: 4953-4956*

Deco G., and Martí D. (2007a), Deterministic analysis of stochastic bifurcations in multi-stable neurodynamical systems, *Biological Cybernetics, 96, 487-496*

Deco G., and Martí D. (2007b), Extended method of moments for deterministic analysis of stochastic multistable neurodynamical systems, *Physical Review E, 75, 031913-7*

Fehr E., and Camerer C. F. (2007), Social neuroeconomics: the neural circuitry of social preferences, *TRENDS in Cognitive Sciences, 11(10), 419-427*

Gold J. I., Shadlen M. N. (2007), The neural basis of decision making, *The Annual Review of Neuroscience, 30:535–574*

Hancock S., and Andrews T. J. (2007), The role of voluntary and involuntary attention in selective perceptual dominance during binocular rivalry, *Perception, 36, 288-298*

Kornmeier J., Ehm W, Bigalke H., and Bach M. (2007), Discontinuous presentation of ambiguous figures: How interstimulus-interval durations affect reversal dynamics and ERPs, *Psychophysiology, 44, 552-560*

Lee S. H., Blake R., Heeger D. J. (2007), Hierarchy of cortical responses underlying binocular rivalry, *Nature Neuroscience, 10, 1048-1054*

Long G. M., Moran C. J. (2007), How to keep a reversible figure from reversing: teasing out top-down and bottom-up processes, *Perception, 36, 431-445*

Maier A., Logothetis N. K., Leopold D. A. (2007), Context dependent perceptual modulation of single neurons in primate visual cortex, *PNAS, 104, 5620-5625*

Moreno-Bote R., Rinzel J., and Rubin N. (2007), Noise-induced alternations in an attractor network model of perceptual bistability, *Journal of Neurophysiology, 98, 1125-1139*

Noest A. J., van Ee R., Nijs M. M., van Wezel R. J. A. (2007), Percept-choice sequences driven by interrupted ambiguous stimuli: A low-level neural model, *Journal of Vision, 7(8):10, 1-14*

Press W. H., Teukolsky S. A., Vetterling W. T., Flannery B. P. (2007), *Numerical recipes: the art of scientific computing, Ed 3. New York: Cambridge U2*

Shpiro A., Curtu R., Rinzel J., and Rubin N. (2007), Dynamical characteristics common to neuronal competition model, *Journal of Neurophysiology, 97, 462–473*

Sterzer P., and Kleinschmidt A. (2007), A neural basis for inference in perceptual ambiguity, *PNAS, 104(1), 323-8*

Wilson H. R. (2007), Minimal physiological conditions for binocular rivalry and rivalry memory, *Vision Research, 47, 2741-2750*

2008 **Brascamp** J. W., Knapen T. H. J., Kanai R., Noest A. J., van Ee R., van den Berg A. V. (2008), Multi-timescale perceptual history resolves visual ambiguity, *PLoS one, 1, e1497*

Carter O., Tonkle T., Wang Q., Hayward V., and Moore C. (2008), Tactile rivalry demonstrated with an ambiguous apparent-motion quartet, *Current Biology, 18, 1050-1054*

Cohen M. R., and Newsome W. T. (2008), Context-dependent changes in functional circuitry in visual area MT, *Neuron, 60, 1, 162-173*

Curtu R., Shpiro A., Rubin N., and Rinzel J. (2008), Mechanisms for Frequency Control in Neuronal Competition Models, *SIAM Journal of Applied Dynamical Systems, 7(2), 609–649*

Glimcher P. W., Fehr E., Rangel A., Camerer C. F., and Poldrack R. (2008), Neuroeconomics Decision making and the brain, *Academic Press Inc*

Goense J. B. M., and Logothetis N. K. (2008), Neurophysiology of the BOLD fMRI signal in awake monkeys, *Current Biology, 18(9), 631-40*

Grossberg S., Yazdanbakhsh A., Cao Y., and Swaminathan G. (2008), How does binocular rivalry emerge from cortical mechanisms of 3-D vision?, *Vision Research, 48, 2232-2250*

Gutnisky D. A., and Dragoi V. (2008), Adaptive coding of visual information in neural populations, *Nature, 452, 220-224*

Hasegawa H. (2008), Information conveyed by neuron populations: Firing rate, fluctuation and synchrony, *NeuroQuantology, 6, 2, 105-118*

Hohwy J., Roepstorff, and Friston K. (2008), Predictive coding explains binocular rivalry: An epistemonological review, *Cognition, 108, 3, 687-701*

Klink P. C., van Ee R., and van Wezel, R. J. A. (2008a), General validity of Levelt's propositions reveals common computacional mechanisms for visual rivalry, *PLoS one, 3(10), e3473*

Klink P. C., van Ee R., Nijs M. M., Brouwer G. J., Noest A. J. (2008b), Early interactions between neuronal adaptation and voluntary control determine perceptual choises in bistable vision, *Journal of vision, 8(5), 16, 1-18*

Lee D. (2008), Game theory and neural basis of social decision making, *Nature Neuroscience, 11 (4), 404-409*

Loxley P. N., and Robinson P. A. (2007), energy approach to rivalry dynamics, soliton stability, and pattern formation in neuronal networks, *Physical Review E, 76, 046224-9*

Martí D., Deco G., Mattia M., Gigante G., Del Guidice P. (2008), A fluctuationdriven mechanism for slow decision processes in reverberant networks, *PLoS one, 3, e2534*

Pastukhov A., and Braun J. (2008), A short-term memory of multi-stable perception, *Journal of Vision, 8(13):7, 1-14*

Pearson J., and Brascamp J. (2008), Sensory memory for ambiguous vision, *Trends in Cognitive Science, 12, 9, 334-341*

Poulet J. F., and Petersen C. C. (2008), Internal brain state regulates membrane potential synchrony in barrel cortex of behaving mice, *Nature, 454, 881-885*

Sterzer P., and Rees G. (2008), A neular basis for perceptual stabilization in binocular rivalry, *Journal of Cognitive Neuroscience, 20:3, 389-399*

Tsuchiya N., Maier A. V., Logothetis N. K., Leopold D. A. (2008), Decoding kinetic depth using only the temporal structure of spike trains from area MT, *Neuroscience Meeting Planner, Washington, DC: Society for Neuroscience, 2008, poster*

Wang X.-J. (2008), Decision making in recurrent neuronal circuits, *Neuron, 60, 215-234*

2009 **Braskamp** J. W., Pearson J., Blake R., and van den Berg A. V. (2009), Intermittent ambiguous stimuli: implicit memory causes periodic perceptual alternations, *Journal of Vision, 9(3):3, 1-23*

Britz J., Landis T., and Michel C. M. (2009), Right parietal brain activity precedes perceptual alternation of bistable stimuli, *Cerebral Cortex, 19, 1, 55-65*

Cohen M. R., and Maunsell J. H. R. (2009), Attention improves performance primarily by reducing interneuronal correlations, *Nature Neuroscience, 12, 1594-1600*

Deco G., Rolls E. T., Romo R. (2009), Stochastic dynamics as a principle of brain function, *Progress in Neurobiology, 88, 1-16*

Doesburg S. M., Green J. J., McDonald J. J., Ward L. M. (2009), Rhythms of consciousness: binocular rivalry reveals large-scale oscillatory network dynamics mediating visual perception, *PLoS one, 4, e6142*

Gaillard R., Dehaene S., Adam C., Clémenceau S., Hasboun D., Baulac M., Cohen L., Naccache L. (2009), Converging intracranial markers of conscious access, *PLoS Biology, 7, e61*

Gigante G., Mattia M., Braun J., Del Guidice P. (2009), Bistable perception modeled as competing stochastic integrations at two levels, *PLoS Computational Biology, 5, 7, e1000430*

Hasegawa H. (2009), Population rate codes carried by mean, fluctuation and synchrony of neuronal firings, *Physica A, 388, 499-513*

Klink P. C., Noest A. J., Holten V., van den Berg A. V., and van Wezel R. J. A. (2009), Occlusion-related lateral connections stabilize kinetic depth stimuli through perceptual coupling, *Journal of Vision, 9(10), 20, 1-20*

Loxley P. N., and Robinson P. A. (2009), Soliton Model of competitve neural dynamics during binocular rivalry, *Physical Review Letters, 102, 258701-4*

Libedinsky C., Savage T., and Livingstone M. (2009), Perceptual and physiological evidence for a role for early visual areas in motion-induced blindness, *Journal of Vision, 9, 14, 1-10*

Manousakis E. (2009), Quantum formalism to describe binocular rivalry, *BioSystems, 98, 57-66*

Mitchell J. F., Sundberg K. A. and Reynolds J. H. (2009), Spatial attention decorrelates intrinsic activity fluctuations in macaque area V4, *Neuron 63, 879-888*

Nordlie E., Gewaltig M. O., Plesser H. E. (2009), Towards reproducible descriptions of neuronal network models, *PLoS Computational Biology, 5, e1000456*

Poort J., and Roelfsema P. R. (2009), Noise correlations have little influence on the coding of selective attention in area V1, *Cerebral Cortex, 19, 543-53*

Quiroga R. Q., and Panzeri S. (2009), Extracting information from neuronal populations: information theory and decoding approaches, *Nature Reviews Neuroscience, 10, 173-185*

Shpiro A., Moreno-Bote R., Rubin N., and Rinzel J. (2009), Balance between noise and adaptation in competition models of perceptual bistabilty, *Journal of Computational Neuroscience, 27, 37-54*

Sterzer P., Kleinschmidt A., and Rees G. (2009), The neural basis of multistable perception, *Trends in Cognitive Science, 13,310-318*

Tsuchiya N., Maier A., Logothetis N. K., Leopold D. A. (2009), Neuronal activity in area MT during perceptual stabilization of ambiguous structure-from-motion. *Journal of Vision, 9, 8, 756*

van Ee R. (2009), Stochastic variations in sensory awareness are driven by noisy neuronal adaptation: evidence from serial correlations in perceptual bistability, *Journal of the Optical society of America A, 26, 12, 2612-2622*

Wilke M., Mueller K. M., Leopold D. A. (2009), Neural activity in the visual thalamus reflects perceptual suppression, *PNAS, 106, 9465-9470*

Wilson H. R. (2009), Requirements for conscious visual processing, *Cortical Mechanisms of Vision, Edited by M. Jenkins and L. Harris. Cambridge University Press, 399-417*

Zhou W., and Chen D. (2009), Binaral rivalry between the nostrils and in the cortex, *Current Biology, 19, 18, 1561-1565*

2010 **Ashwin** P., and Lavric A. (2010), A low-dimensional model of binocular rivalry using winnerless competition, *Physica D, 239, 529-536*

Braun J., Mattia M. (2010), Attractors and noise: two drivers of decisions and multistability, *NeuroImage, 52, 740-751*

Cafaro J., and Rieke F. (2010), Noise correlations improve response fidelity and stimulus encoding, *Nature, 468, 964-967*

Carmel D., Arcaro M., Kastner S., Hasson U. (2010a), How to Create and Use Binocular Rivalry, *Journal of Visualized Experiments, 45, e2030*

Carmel D., Walsh V., Lavie N., and Rees G. (2010b), Right parietal TMS shortens durations in binocular rivalry, *Current Biology, 20,18, R799-R800*

Curtu R. (2010), Singular Hopf bifurcations and mixed-mode oscillations in a two-cell inhibitory neural network, *Physica D, 239, 504-514*

Cziraki C., Greenlee M. W., Kovács G. (2010), Neural correlates of high-level adaptation-related aftereffects, *Journal of Neurophysiology, 103, 1410-1417*

Kanai R., Bahrami B., and Rees G. (2010), Human parietal cortex structure predicts individual differences in perceptual rivalry, Current Biology, 20, 1626-1630

Keliris G., Logothetis N. K, Tolias A. S. (2010), The role of the primary visual cortex in perceptual suppression of salient visual stimuli, *Journal of Neuroscience, 30, 12353-12365*

Kilpatrick Z., Bressloff P. (2010), Binocular rivalry in a competitive neural network with synaptic depression. *SIAM Applied Dynamical Systems 9(4), 1303–1347*

Komiyama T., Sato T. R., O'Connor D. H., Zhang Y.-X., Huber D., Hooks B. M., Gabitto M., and Svoboda K. (2010), Learning-related fine-scale specificity imaged in motor cortex circuits of behaving mice, *Nature, 464, 1182–1186*

Laing C. R., Frewen T., and Kevrekidis I. G. (2010), Reduced models for binocular rivalry, *Journal of Computational Neuroscience, 28, 459–476*

Lundqvist M., Compte A., and Lansner A. (2010), Bistable, Irregular Firing and Population Oscillations in a Modular Attractor Memory Network, *PLoS Computational Biology, 6(6), e1000803*

Moreno-Bote R., Shpiro A., Rinzel J., and Rubin N. (2010), Alternation rate in perceptual bistability is maximal at and symmetric around equi-dominance, *Journal of Vision, 10(11), 1-18*

Naber M., Gruenhage G., and Elnhäuser (2010), Tri-stable stimuli reveal interactions among subsequent percepts: Rivalry is biased by perceptual history, *Vision Research, 50,8, 818-828*

Tricomi E., Rangel A., Camerer C. F., O'Doherty J. P. (2010), Neural evidence for inequality-averse social preferences, *Nature, 46, 1089-1091*

Zaretskaya N., Thielscher A., Logothetis N. K., and Bartels A. (2010), Disrupting parietal function prolongs dominance durations in binocular rivalry, *Current Biology, 20, 2106-2111*

2011 **Abe** H., and Lee D. (2011), Distributed coding of actual and hypothetical outcomes in the orbital and dorsolater prefrontal cortex, *Neuron, 70, 731-741*

Blake R., and Wilson H. (2011), Binocular vision, *Vision Research, 51, 754-770*

Bressloff P., Webber M. (2011), Neural field model of binocular rivalry waves, *Journal of Computational Neuroscience, 1-20*

Cohen M. R., and Kohn A. (2011), Measuring and interpreting neuronal correlations, *Nature Neuroscience Review, 14, 811-819*

Dal Bo P., and Fréchette G. (2011), The evolution of cooperation in infinitely games: experimental evidence, *American Economic Review 101, 411-429*

Ecker A. S., Berens P., Tolias A. S., and Bethge M. (2011), The effect of noise correlations in populations of diversely tuned neurons, *The Journal of Neuroscience, 31(40), 14272-14283*

Gu Y., Liu S, Fetsch C. R., Yang Y., Fok S., Sunkara A., DeAngelis G. C., and Angelaki D. E. (2011), Perceptual learning reduced interneuronal correlations in macaque visual cortex, *Neuron, 71, 4, 750-761*

Hipp J. F., Engel A. K., Siegel M. (2011), Oscillatory synchronization in large scale networks predicts perception, *Neuron, 69, 387-396*

Kalisvaart J. P., Klaver I., and Goossens J. (2011), Motion discrimination under uncertainty and ambiguity, *Journal of Vision, 11(1), 20, 1-21*

Kang P., and Shevell S (2011), Multistable binocular feature-integrated percepts are frozen by intermittent presentation, *Journal of Vision, 11(1):5, 1-8*

Knapen T., Brascamp J., Pearson J., van Ee R., and Blake R. (2011),The role of frontal and parietal brain areas in bistable perception, *Journal of Neuroscience, 31(28), 10293-10301*

Lehky S. R. (2011), Unmixing binocular signals, *frontiers in Human Neuroscience, 5, 78, 1-7*

Martínez-Cancino R., and Sotero R.C. (2011), Dynamical Mean Filed approximation of a canonical cortical model for studying inter-population synchrony, *NaturePrecedings, doi: 10.1038/npre. 2011.5583.1*

Pastukhov A., and Braun J. (2011), Cumulative history quantifies the role of neural adaptation in multistable perceptio, *Journal of Vision, 21(6), 801-84*

Pitts M. A., and Britz J. (2011), Insights from intermittent binocular rivalry and EEG, *frontiers in Human Neuroscience, 5, 107, 1-6*

Seely J., and Chow C. C. (2011), Role of mutual inhibition in binocular rivalry, *Journal of Neurophysiology, 106, 2136-2150*

2012 **Alais** D. (2012), Binocular rivalry: competition and inhibition in visual perception, *WIREs Interdisciplinary Reviews: Cognitive Science, 3, 87-103*

de Jong M. C., Knapen T., and van Ee R. (2012), Opposite influence of perceptual memory on initial and prolonged perception of sensory ambiguity, *PLoS one, 7, 1, e30595*

Diekman C., Golubitsky M., McMillen T., and Wang Y. (2012), Reduction and dynamics of a generalized rivalry network with two learned patterns, *SIAM Journal of Applied Dynamical Systems, 11, 4, 1270-1309*

García-Rodriguez P. (2012), Noise-induced reversals in bistable visual perception, *Dissertation, Universitat Pompeu Fabra, Barcelona*

Huguet G., Hupé J.-M., and Rinzel J. (2012), A model for dynamical switching in tristable perception for visual plaids, *BMC Neuroscience, 13 (Suppl 1); P59*

Klink P. C., Oleksiak A., Lankheet M. J. M., van Wezel R. J. A. (2012), Intermittent stimulus presentation stabilizes neuronal responses in macaque area MT, *Journal of Neurophysiology, 108, 2101-2114*

Leopold D. A. (2012), Primary visual cortex: awareness and blindsight. *Annual Reviews Neuroscience, 35, 91-109*

Manousakis E. (2012), When perceptual time stands still: Long percept-memory in binocular rivalry, *BioSystems, 109, 115-125*

Noest A. J., and van Wezel R. J. A. (2012), Dynamics of temporally interleaved percept-choice sequences: interaction via adaptation in shared neural populations, *Journal of Computational Neuroscience, 32, 177-195*

Panagiotaropoulos T. I., Deco G., Kapoor V., and Logothetis N. K. (2012), Neuronal discharges and gamma oscillations explicitly reflect visual consciousness in the lateral prefrontal cortex, *Neuron 74, 924-935*

Schwartz J.-L., Grimault N., Hupé J.-M., Moore B. C. J., and Pressnitzer D. (2012), Multistability in perception: binding sensory modalitites, an overview, *Philosophical Transactions of The Royal society B, 367, 896-905*

Wang X.-J. (2012), Neural dynamics and circuit mechanisms of decision-making, *Current Opinion in Neurobiology, 22, 1039-1046*

Woldman W. (2012), Computational model on neuronal stabilization in perceptual choice dynamics, *Master Thesis, supervisors Meijer H. G. E., van Gils S. A., and van Wezel R. J. A., University of Twente*

2013 **Adibi** M., McDonald J. S., Clifford C. W. G., and Arabzadeh E. (2013), Adaptation improves neural coding efficiency despite increasing correlations in variability, *The Journal of Neuroscience, 33(5), 2108-2120*

Herrero J. L., Gieselmann M. A., Sanayei M., and Thiele A. (2013), Attention-induced variance and noise correlation reduction in macaque V1 is mediated by NMDA receptors, *Neuron, 78, 729-39*

Jeanne J. M., Sharpee T. O., and Gentner T. Q. (2013), Associative learning enchances population coding by inverting interneuronal correlation patterns, *Neuron, 78, 2, 352-363*

Panagiotaropoulos T. I., and Logothetis N. K. (2013), Multistable visual perception as a gateway to the neural correlates of phenomenal consciousness, *The scope and limits of neuroscientific analysis, The handbook of experimental phenomenology: visual perception of shape, space and appearance (ed. L Albertazzi), pp. 119-144. New York, NY: Wiley*

Panagiotaropoulos T. I., Kapoor V., Logothetis N. K., and Deco G. (2013), A common neurodynamical mechanism could mediate externally induced and intrinsically generated transitions in visual awareness, *PLoS one, 8, 1, e53833, 1-10*

Pastukhov A., Garcia-Rodriguez P. E., Haenicke J., Guillamon A., Deco G., and Braun J. (2013), Mutli-stable perception balances stability and sensitivity, *frontiers in Computational Neuroscience, 7, 17, 1-17*

Ponce-Alvarez A., Thiele A., Albright T. D., Stoner G. R., and Deco G. (2013), Stimulus-dependent variability and noise correlations in cortical MT neurons, *PNAS, 110, 32, 13162-13167*

Rankin J., Meso A. I., Masson G. S., Faugeras O., and Kornprobst P. (2013), Bifurcation study of a neural fields competition model with an application to perceptual switching in motion integration, *Journal of Computation Neuroscience, DOI 10.1007/s10827-013-0465-5*

Said C. P., and Heeger D. J. (2013), A model of binocular rivalry and cross-orientation suppression, *PLoS Computational Biology, 9, 3, e1002991*

van Loon A. M., Knapen T., Scholte H. S., John-Saaltink E. St., Donner T. H., and Lamme V. A. F. (2013), GABA shapes the dynamics of bistable perception, *Current Biology, 23, 823-827*

Wallis G., and Ringelhan S. (2013), The dynamics of perceptual rivalry in bistable and tristable perception, *Journal of vision, 13(2), 24, 1-21*

Wang M., Arteaga D., He B. J. (2013), Brain mechanisms for simple perception and bistable perception, *PNAS, E3350-E3359*

Zheng M., and Ukai K. (2013), How intermittent presentation affects conscious perceptual reversals of ambiguous figures, *SpringerPlus, 2, 180, 1-6*

2014 **Murphy** A. P., Leopold D. A., and Welchman A. E. (2014), Perceptual memory drives learning of retinotopic biases for bistable stimuli, *frontiers in Psychology, 5, 60, 1-11*

Panagiotaropoulos T. I., Kapoor V., and Logothetis N. K. (2014) Subjective visual perception: from local processing to emergent phenomena of brain activity, *Philosophical Transactions of the Royal Society B: Biological Sciences, in press*

List of Abbreviations

AHP - *after hyper polarization*
AMPA - *α amino 3 hydroxy 5 methyl 4 isoazoleproprionic acid*
AR - *auditory rivalry*
BFS - *binocular flash suppression*
BIF - *bifurcation*
BOLD - *blood oxygen level dependent*
BR - *binocular rivalry*
CV - *coefficient of variation*
DBS - *deep brain stimulation*
DTI - *diffusion tensor imaging*
ECoG - *electrocorticography*
EEG - *electroencephalography*
EPSC - *excitatory post synaptic current*
fMRI - *functional magnetic resonance imaging*
GABA - *γ aminobutyric acid*
GFS - *generalized flash suppression*
icPFC - *inferior convexity of prefrontal cortex*
IF - *integrate and fire*
IPSC - *inhibitory post synaptic current*
IT - *inferior temporal cortex*
LFP - *local field potential*
LGN - *lateral geniculate nucleus*
LIF – *leaky integrate and fire*
LPFC - *lateral prefrontal cortex*
MEG - *magnetoencephalography*
MIB - *motion induced blindness*
MP - *multistable perception*
MR - *monocular rivalry*
MRI - *magnetic resonance imaging*
MT - *middle temporal*
MTL - *medial temporal lobe*
MUA - *multi unit activity*
NMDA - *N methyl D aspartate acid*
OR - *olfactory rivalry*
PA - *physical alternation*
PFC - *prefrontal cortex*
PET - *positron emission tomography*
RS - *rotating sphere*
QD - *quartet dots*
SD - *standard deviation*

SFM - *structure from motion*
STS - *superior temporal sulcus*
SUA - *single unit activity*
TB - *tristable perception*
Td - *mean time dominance*
TMS - *transcranial magnetic stimulation*
TR - *tactile rivalry*
V1 - *primary visual cortex*
V4 - *intermidiate cortical visual area*
V5 - *middle temporal (MT)*

.. θες ν' αγγίξεις την αλήθεια,
για βγες απ' όξω απ' τη συνήθεια ..
Νικόλας Άσιμος [7]

[7] ".. if it's the truth you want to touch, it's the habit you'll have to scratch .."
Nikolas Asimos

burn.
fires in your eyes.
gates of your mind, mirrors of your sight.